Missouri S&T Library and Learning Resources

Scholars' Mine

Doctoral Dissertations | Student Theses and Dissertations

Summer 2021

Scaling, experiments, and simulations of condensation heat transfer for advanced nuclear reactors safety

Palash Kumar Bhowmik

Follow this and additional works at: https://scholarsmine.mst.edu/doctoral_dissertations

 Part of the Nuclear Engineering Commons

Department: Nuclear Engineering and Radiation Science

Recommended Citation

Bhowmik, Palash Kumar, "Scaling, experiments, and simulations of condensation heat transfer for advanced nuclear reactors safety" (2021). *Doctoral Dissertations*. 2999.
https://scholarsmine.mst.edu/doctoral_dissertations/2999

This thesis is brought to you by Scholars' Mine, a service of the Missouri S&T Library and Learning Resources. This work is protected by U. S. Copyright Law. Unauthorized use including reproduction for redistribution requires the permission of the copyright holder. For more information, please contact scholarsmine@mst.edu.

SCALING, EXPERIMENTS, AND SIMULATIONS OF CONDENSATION HEAT TRANSFER FOR ADVANCED NUCLEAR REACTORS SAFETY

by

PALASH KUMAR BHOWMIK

A DISSERTATION

Presented to the Graduate Faculty of the

MISSOURI UNIVERSITY OF SCIENCE AND TECHNOLOGY

In Partial Fulfillment of the Requirements for the Degree

DOCTOR OF PHILOSOPHY

in

NUCLEAR ENGINEERING

2021

Approved by

Joshua P. Schlegel, Advisor
Shoaib Usman
Hyoung K. Lee
Ayodeji B. Alajo
Muthanna H. Al-Dahhan

Copyright 2021

PALASH KUMAR BHOWMIK

All Rights Reserved

ABSTRACT

The purpose of this research was to perform scaled experiments and simulations to validate computational fluid dynamics (CFD) and empirical models of condensation heat transfer (CHT) for the passive containment cooling system (PCCS) of Small Modular Reactors (SMRs). SMRs are the futuristic candidates for clean, economic, and safe energy generation; however, reactor licensing requires safety system evaluations, such as PCCS. The knowledge in the reviewed relevant literature showed a gap in experimental data for scaling SMR's safety systems and validating computational models. The previously available test data were inconsistent due to unscaled geometric and varying physics conditions. These inconsistencies lead to inadequate test data benchmarking. This study developed three scaled (different diameters) test sections with annular cooling for scale testing and analysis to fill this research gap. First, tests were performed for pure steam and steam with non-condensable gases (NCGs), like nitrogen and helium, at different mass fractions, inlet mass flow rates, and pressure ranges. Second, detailed CFD simulations and validations were performed using STAR-CCM+ software with scaled geometries and experimental parameters (e.g., flow rate, pressure, and steam-NCG mixtures), thus mimicking reactor accident cases. The multi-component gases, multiphase mixtures, and fluid film condensation models were applied, verified, and optimized in the CFD simulations with associated turbulence models. Third, the physics-based and data-driven condensation models and empirical correlations were assessed to quantify the scaling distortions. Finally, the experiments, simulations, and modeling results were evaluated for critical insights into the physics conditions, scaling effects, and multi-component gas mixture parameters. This study supported improvements to nuclear reactor safety systems' modeling capabilities irrespective of size (small or big), and findings were equally applicable to other non-nuclear energy applications.

ACKNOWLEDGMENTS

At first, I would like to thank Almighty. Then, I thank my parents, family members, teachers, friends, and well-wishers, who helped me shape my life and reach to this stage.

I will forever be grateful to my advisor, Professor Dr. Joshua P. Schlegel, for guiding me through my doctoral journey. I sincerely thank him for his insights, constant encouragement, advice, feedback, and overall patience. I feel fortunate working with him. I also express my heartfelt gratitude to Dr. Shoaib Usman, Dr. Hyoung K. Lee, Dr. Ayodeji B. Alajo, and Dr. Muthanna H. Al-Dahhan their continuous support and advice. I also thank Dr. Syed Alam and Dr. Graham for their valuable input.

I am grateful to my faculty, office staff, colleagues, and lab mates. Special thanks to my friends: Galib, Chandller, Varun, Sungje, Murat, Bader, Camila, and Saud, from the nuclear engineering department to make my life easier and enjoyable. Also, thanks to Bangladeshi students, who made my stay here home away from home.

I want to thank the Small Modular Reactor Research and Education Consortium to complete this task. I appreciate the CASL (Consortium of Advanced Simulation of Light-water-reactor) for providing me professional training on reactor simulation.

I am carrying some sweet memories working with the Council of Graduate Students (CGS). I thank our former interim chancellor Dr. Chris Maples and our current UM system president, Dr. Mun Choi, for their support and cooperation during working with the CGS. I also thank our present chancellor, Dr. Mohammad Dehghani and campus community, for being supportive of the graduate students during the COVID-19 outbreak.

I am eternally indebted to my parents and family members for their unconditional love and continuous encouragement. An extraordinary thanks to my son Rudranil and my wife, Tithi. They are true blessings in my life.

I dedicate this dissertation to my parents, my son, wife, and all well-wisher.

TABLE OF CONTENTS

Page

LIST OF ILLUSTRATIONS

LIST OF TABLES

NOMENCLATURE

Acronyms

BLM Boundary Layer Model

CASL Consortium for Advanced Simulation of Light Water Reactors

CFD Computational Fluid Dynamics

CHT Condensation Heat Transfer

CV Containment Vessel

DD Design and Development

DAQ Data Acquisition

DF Degradation Factor

DLM Diffusion Layer Model

DP Differential Pressure

GW Gigawatt

HE Heat Exchanger

HTC Heat Transfer Coefficient

HTMA Heat and Mass Transfer Aalogy

IAEA International Atomic Energy Agency

ID Inner Diameter

LOCA Loss of Coolant Accident

LWR Light Water Reactor

Mtoe Million tonnes of oil equivalent

NCG Noncondesable Gas

NEAMS Nuclear Energy Advanced Modeling and Simulation

NPT National Pipe Thread

NRC Nuclear Regulatory Commission

NTU Number of Transfer Units

OD Outer Diameter

PCCS Passive Containment Cooling System

PDE Partial differential equations

PRIS Power Reactor Information System

PWR Pressurized Water Reactor

RSM Reynolds Stress Model

RTD Resistance Temperature Detector

SCH Pipe Schedule

SMR Small Modular Reactor

SST Shear Stress Transport

TS Test Section

TWh Trillion Watt hour

VOF Volume of Fluid

W-SMR Westinghouse SMR

Symbol

u x component of velocity [m/s]

v y component of velocity [m/s]

w z component of velocity [m/s]

q or q" Heat flux [W/m^2]

A Area [m^2]

D Diameter [m]

H Height [m]

h Heat transfer coefficient [W/m^2 K]

M Mole fraction

m" Condensation mass flux

P Pressure [N/m^2]

T Temperature [K]

Ta Coolant adiabatic wall temperature [ºC or K]

Tcl or Tc Steam-mixture central line temperature [ºC or K]

Ts Vapor-liquid interfacial surface temperature [ºC or K]

Tsat Steam-mixture central line temperature [ºC or K]

Twi Condenser tube inner wall temperature [ºC or K]

Two Condenser tube outer wall temperature [ºC or K]

U Overall heat transfer coefficient [W/m^2 K]

W or $\dot{m}$ Mass flow rate [kg/s]

z Axial position from condenser inlet to outlet [m]

Greek

β_f Momentum transfer blowing parameter

δ Film thickness

Γ Liquid flow per unit perimeter

μ Dynamic viscosity [N·s/m^2]

ν Kinematic viscosity [m^2/s]

ω Mass fraction

ψ General scale ratio

ρ Density [kg/m^3]

τ_i Interfacial shear stress

D Diffusion coefficient

E Energy per unit mass

j Species

k Thermal conductivity [W m^{-1} K^{-1}]

S Source (mass, momentum or energy)

t Time

Non-Dimensional Numbers

Nu	Nusselt number
Pr	Prandtl number
Re	Reynolds number
Sh	Sherwood number

Subscript or Superscript

i, j, k	tensor index for x, y, z
z	Axial location
b	bulk
con	condensation
cw	cooling water
exp	experiment
i, o	inner, outer
in, out	inlet, outlet
p	prototype
s	scaled
sat	saturated
st	steam
v, l	vapor, liquid
w	wall

1. INTRODUCTION

This section gives an overview of the motivation and review of the condensation heat transfer (CHT) study for the small modular reactor (SMR). The world's energy and electricity data clearly state that the energy demand will increase faster than the current value in the next decade and would impact the environment severely due to the high dependency on fossil fuels. Therefore, focus should be given to emission-free energies like renewable and nuclear. But due to geographical and weather reliance, renewable energy sources are not suitable for all regions. In such cases, nuclear energy will be a better option. However, the giant nuclear reactors require a high capital investment and a larger electric grid (about 10 times higher capacity than the plant capacity), which is not easy for many countries and regions. To overcome this challenge, SMRs should be considered. Again, SMR's safety features like the passive containment cooling (PCCS) lack enough test data for details study and licensing. This study intends to fulfill these gaps. This section covers the background and motivation for the SMR PCCS study, followed by scope, objectives, and thesis overview.

Keywords: Motivation, Scope, Objective, Problem statement, and Overview

1.1. BACKGROUND AND MOTIVATION

1.1.1. World Energy Goals (UN, 2019). The United Nations (UN) declared affordable clean energy as one of the seventeen sustainable development goals (SDG). It states to ensure access to affordable, reliable, and modern energy for all worldwide by 2030. Currently, 11% of the global population does not have access to electricity, and most of them live in rural areas. A billion people lack clean cooking fuels, which caused 4.3 million deaths in 2012 (UN, 2019). Moreover, this fossil energy that comes from coal, oil and gas contributes approximately 60% of the total greenhouse gas emissions.

1.1.2. World Energy Status and Prospects (IEA, 2019). The International Energy Agency (IEA) reported that the global energy demand rose by 2.3% in 2018 and became 14,301 Mtoe. This growth rate is about twice the average rate of growth since 2010, and it resulted in a sharp record-breaking increase of CO_2 emissions by 1.7% of 33.1 Gt. Fossil fuels like coal, oil, gas, and biomass-waste contributes 90% of the total demand. Likewise, the electricity generated in 2018 was about 26.6 billion MWh, with a growth rate of 4%. In the forms of electricity generated, fossil fuel-fired contributed 64%. Whereas, nuclear energy contributed 10%, and the rest were the renewable energy sources. According to IEA, to stem climate change, 40% of the world's total electricity should come from emissions-free sources like renewables and nuclear.

These statistics clearly exemplify that worldwide energy and electricity demands are rising and will continue growing with a higher percentage. The more use of fossil fuel will devastate the environment. In this regard, emphasis should be given to emission-free energy sources, such as renewables and nuclear. Renewable sources like solar, wind, geothermal, and others mostly depend on geographical locations and weather conditions. As a consequence, nuclear reactors compatible with small to medium electric grid are preferable.

1.1.3. Nuclear Energy History and Present Status. In the 1930s, physicist Enrico Fermi first introduced the idea of nuclear energy by splitting atoms with the neutron. Then, with his team in 1942, he achieved the first nuclear chain reaction at the University of Chicago. This was followed by the success of the first usable electric power from atomic energy at Idaho's Experimental Breeder Reactor-1 in 1951, the first nuclear power plant (NPP) of 5 MW in the city of Obninsk, USSR in 1954 and the first commercial NPP in Shippingport, Pennsylvania, in 1957. From that day on, the total number of NPRs in operation throughout the world has increased to 450 as of 2019 with a net installed capacity of 398 GWe (PRIS, 2019).

The USA is the most significant contributor to nuclear energy, with 98 nuclear power reactors (NPRs) across 59 sites, support 475 thousand jobs, save consumers an average 6% on electricity bills, in total adds $60 billion to the country's GDP, as reported in July 2015 (NEI, March 2019). From the electric utility report, the total generating cost is only $31.83 per MWh, which includes $6.14, $5.98, and $19.71 as capital, fuel, and operation costs, respectively.

1.1.4. Prospect of Nuclear Energy to Combat Climate Change. World communities have acknowledged the utilization of nuclear energy for socio-economic development combined with environmental consideration like reducing greenhouse gases, and they should continue to support it (IAE, 2015). The U.S. Environmental Protection Agency reported in 2019 that nuclear alone avoided 528 metric tons of carbon emissions each year, which prevent the emission of NOX and SO_2, valued at $28.1 billion annually (NEI, March 2019).

As of March 2019, nuclear generated energy was higher than ever before in the USA: 19.3% of total electricity generation and 55.2% of emission-free electricity, with a capacity factor of 92.3% (NEI, March 2019). Worldwide 53 new NPRs with a net installed capacity of 54GWe are under construction and the world reactor's years of operation totals approximately 18303. During this long operation, nuclear power has faced fewer accidents resulting in fewer casualties than any other power source, including renewables. However, accidents like Three Mile Island, Chernobyl, and the latest Fukushima accident, have raised the concern for increased safety.

1.1.5. Motivation for Small Modular Reactor (SMR). The large capacity reactors (unit capacity > 600 MWe) of generation II and III have been dominating the nuclear industry for decades. Despite that, with the rising concern for safety and environment, the adoption of the additional safety features for the large reactors is very costly. This challenge make the Small Modular Reactors (SMRs), with a capacity equal or less than 300 MWe (IAEA, 2018), preferable for the near future. SMRs by design inherent passive safety systems and are developing from the current reactors as shown in Figure 1.1(a) (András Cserháti,

2017). The large reactors have the benefit of economic scale factors, which can be achieved by SMRs using several other factors like multiple units, faster learning, construction time, modularization, and design considerations (Carelli *et al.*, 2007; Rosner and Goldberg, 2011), as presented in Figure 1.1(b).

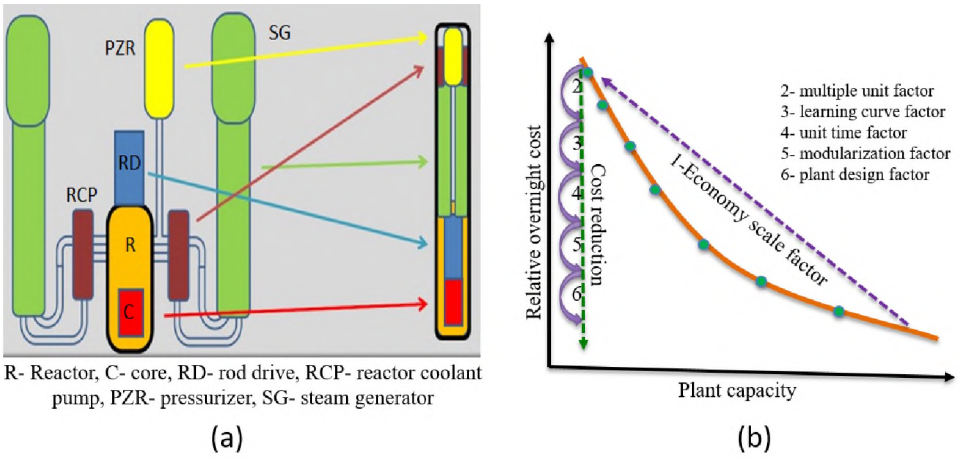

Figure 1.1. Overview of the SMR development and economics: (a) Schematics, (b) Plant capacity vs overnight cost for different cost factors

The big capacity reactors can not be synchronized to a smaller size grid. For that reason, big reactors are not an option at all for many countries. An electric grid cannot withstand power variations more than 10% of its total capacity (Carelli *et al.*, 2007). For example, a large reactor of 1000 MWe requires a grid capacity of more than of 10,000 MWe. The remote and isolated places prefer smaller grids to avoid high transmission loss. Therefore, SMRs are preferable for small (e.g. within 1000 MWe) to mid-size (e.g. between 1000 to 6000 MWe) power grids.

Nuclear industry have deep concern on initial cost, safety, economy, and proliferation, which give priority to the SMRs when compared to current commercial reactors. SMRs design vendors offers benefits of off-site fabrication, i.e., factory-built, lower capital cost, enhance safety, modular design, and operational flexibility. They also offers flexible power generation and co-generation, like process heating, hydrogen production, and water

desalination that make it possible for replacing aging fossil-fired plants for higher safety margins and better economies (Bhowmik, 2016; IAEA, 2018). Currently, more than 50 SMR designs are under the development phase, and among them, CAREM, HTR-PM and KLT40s are in the construction stage. SMRs design varies based on coolant types like water, gas, liquid-metal, sodium, and molten salt. The most common design types are water-cooled SMRs, as shown in Figure 1.2 (IAEA, 2018).

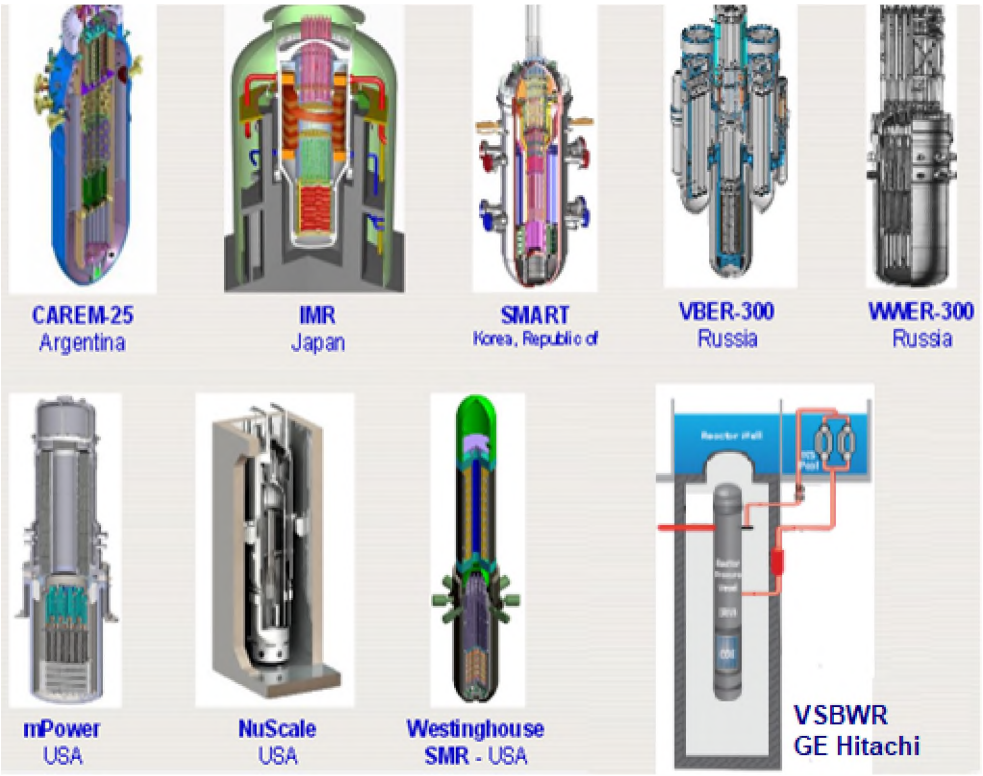

Figure 1.2. Schematics of few Water-cooled SMRs (IAEA, 2018)

Though there have been significant advancements in SMR development, some technical issues need further studies (Alam *et al.*, 2019; Bhowmik *et al.*, 2021d; Bhowmik and Suh, 2021; IAEA, 2018). For example, reactor licensing requires safety systems analysis like PCCS, which is facing challenges due to a lack of enough test data.

1.1.6. Passive Safety and PCCS of SMR. The advanced water-cooled SMRs design has adopted passive safety systems with built-in pressurizer, reactor pressure vessel (RPV), containment vessel (CV), and water pools, as shown in Figure 1.3 (Smith and Wright, June 2012). The reactor core consists of fuel rod assemblies arranged in the lower plenum of the RPV, which is filled with water and placed inside the CV. An automatic depressurization system (ADS) is used during accidents to vent steam to the CV. Then the steam is mixed with the non-condensable gas like air and hydrogen that are present in the CV. Next, the steam is condensed at the containment wall, which is again cooled by the outside containment water pool. This process is termed passive containment cooling system or PCCS. Finally, the condensate is fed back through the injection line to the reactor core.

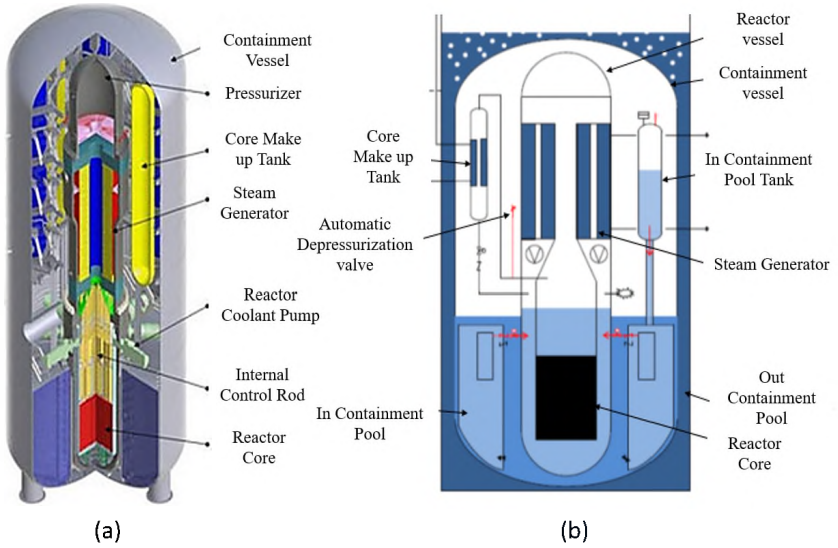

Figure 1.3. Schematics of Westinghouse: (a) SMR, (b) SMR's PCCS

In the Westinghouse SMR (W-SMR), there are coolant tanks for core makeup and an in-containment water pool to support cooling, before the initiation of the ADS and to keep the PCCS active for seven days without an external water source (Smith and Wright, June 2012). In the Nuscale SMR, PCCS includes three vents and two recirculation valves. It actuates when at least two vents and one recirculation valves are open (NuScale, 2019).

1.2. SCOPE OF THE STUDY

This study focused on PCCS analysis of SMR and it is applicable to other engineering applications in nuclear and other industries. Two such applications are: fluid heating or cooling by solid(s), and the other one is separating fluid flows with a solid wall. These research exhibited direct applications in once-through steam generator of pressurized water reactor (PWR) (Tanrikut and Yesin, 2000), PCCS of AP1000 (Schulz, 2006), and isolation condenser (IC) of simplified boiling water reactor (SBWR) (Sato and Kojima, 2007).

1.2.1. Problem Statement and Project Overview. In advanced reactor designs, steam condensation at the containment during an accident plays a vital role in removing decay heat from the containment atmosphere (Kataoka, 2013; Shulyak, 2011). It becomes more critical for integral SMRs because they consist of small containment vessel (Bhowmik *et al.*, 2021c). During an accident transient, high-pressure steam is released from the reactor vessel, and condensation occurs on the containment vessel wall. This condensation process depends on steam mass flow rate, pressure, temperature, noncondensable gas (NCG) present, and outside containment cooling, requiring in-depth research and analysis (Bhowmik *et al.*, 2021a,b; Yadav *et al.*, 2016). Moreover, previous studies on condensation for the passive containment cooling system were limited to smaller pipe sizes, and there was a lack of scaling data. Hence, the earlier data, models, and correlations had to be validated for SMR containment with scaled tests data. Scaled experiments, simulations, and evaluation of physics-based and empirical models motivated this study.

The project overview is shown in Figure 1.4. SMR schematics provided an overview of the problem statement: how steam released and condense in SMR containment. The schematics of the condensation represented the wall condensation in the presence of non-condensable gas. The scaled test picture shows the test sections (same height, but different diameters).

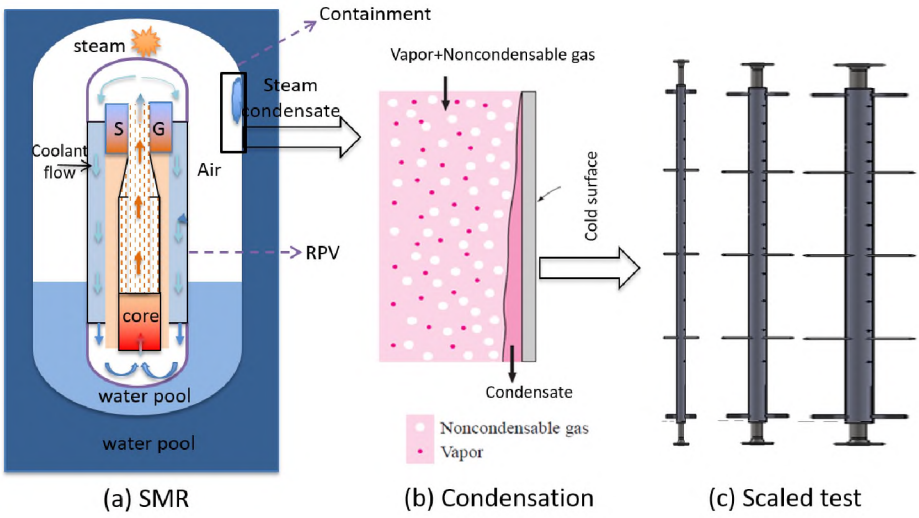

Figure 1.4. Overview of the research project: (a) SMR schematics, (b) Filmwise condensation, and (c) Scale test sections for experimentation

1.2.2. Approximations and Considerations. In this study, the following physics and boundary conditions were considered:

1. *Scaled test facility:* Three different diameters and the same height test sections were designed, developed and installed in a modular test facility for scale experiments. The test sections were counter-current concentric tube condensers in which vapor and cooling water flowed in opposite directions through a the condenser tube and the jacket annulus, respectively

2. *Flow dynamics:* Only the film condensation on the condensing wall was considered, neglecting the mist formation. It was approximated that both the vapor and water fully-developed, steady-state, and turbulent flow; whereas, the liquid film had laminar flow. The effects of interfacial shear stress on vapor and flim were not identical.

3. *Fluid properties and heat transfer:* Inlet boundary conditions for both the vapor-NCG and cooling water were known. Only radial heat transfer was considered, starting with vapor to liquid film and then to the coolant through tube surfaces. The jacket tube wall was insulated, and condensate-NCG mixture drained at ambient pressure.

1.2.3. Objectives and Goals. The objectives of this research were to study the CHT of a PCCS. The specific goals were as follows:

1. Review the available theory, models, tests, and simulated data for film CHT.
2. Design and develop scale test facility, and perform experiments for pure steam and with different percentages of NCGs for various mass flow and pressure conditions.
3. Simulate and validate CFD models using the test data to check the scalability performances inside vertical pipe geometries.
4. Evaluate CHT models to verify scaling performances for SMR's systems.

1.3. DISSERTATION OVERVIEW

The dissertation was organized as follows:

1. *Introduction and Literature Review:* Section 1 covered the background and motivation for SMR as a future reliable emission-free energy source with an overview of the scope and the objectives of this study. In Section 2, relevant studies on in-tube condensation experiments, simulations, models, and empirical correlations with physics descriptions, findings, and limitations were reviewed.
2. *Facility Design and Construction:* In this section, the detailed design overview of the scaled modular CHT test facility was presented. This was followed by the lessons learned from earlier studies, thereby identifying the design parameters and necessary equations. The learning was used in this study to calculate steps, facility design, construction, instrumentation, and safety analysis.

3. *Method and Experiment:* This section covered the physics phenomena of in-tube vertical downward flow film condensations, data reduction methods, scale parameters, tests, calibrations, and uncertainty analyse. Then test data were collected and processed for different inlet, outlet, and physics conditions.

4. *Simulation and Modeling:* In Section 5, numerical studies were presented using simplified geometries and experimental conditions as the boundary conditions to validate CFD software and provide an overview on system code. In Section 6, using the physics-based modeling and other significant correlations, the film condensation models were evaluated.

5. *Results and Conclusion:* In Section 7, results from scaled experiments, scaled CFD simulations, and models evaluations were presented; the critical findings and correlating with the associated physics phenomena were the focus. Results were evaluated for different inlet and physics conditions. Then key parameters for scaling of the film condensation were presented. In Section 8, the impacts of this study with associated findings, limitations, and future research were discussed.

2. LITERATURE REVIEW AND STATE OF THE ART

This section is a literature review of previous condensation heat transfer studies. It covers theoretical, semi-theoretical, experimental, and numerical studies with a brief overview of associated test facilities, models, correlations, CFD, and system codes simulations. The basic condensation theory, the analytical approach, and models are presented with the developed mass, energy, and momentum balance equations. Previous test facilities and numerical analyses are reviewed, and related design, tests, and simulation parameters are listed. The well-cited models, such as degradation factor (DF), heat and mass transfer analogy (HMTA), boundary layer, are presented with the proposed correlations.

Keywords: CHT, theory, models, correlations, experiment and numerical studies

2.1. BACKGROUND AND SECTION OUTLINE

In the simplest form, condensation is defined as a process of changing a vapor to a liquid on a cold wall through heat transfer (Whalley, 1987). In this process, vapor first comes in contact with a cold surface. Then, it releases its latent energy by releasing heat to the cold surface. This heat transfer eventually reduces vapor temperature to saturation temperature, and finally, the vapor is transformed into a liquid, i.e., condensate (Incropera *et al.*, 2007). This condensate forms resistance between hot vapor on the cold wall and reduces the heat transfer performance. There are two types of condensation: film-wise and drop-wise condensation, as shown in Figure 2.1. Film-wise condensation occurs on a clean surface; whereas, drop-wise condensation occurs on a coated surface, which inhibits wetting. In film-wise, condensate film covers the surface and flows due to shear or gravitational forces. However, in drop-wise condensation, drops form in surface cavities.

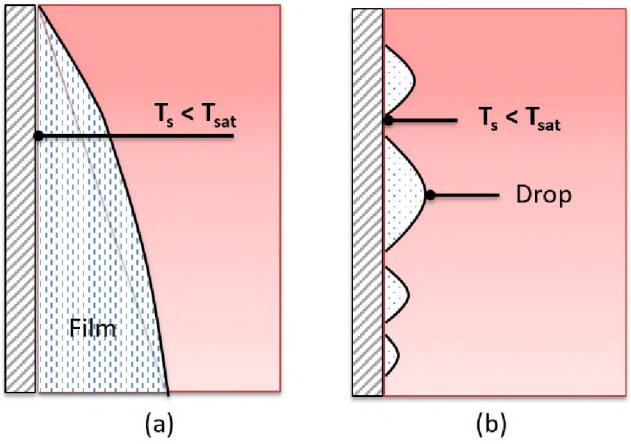

Figure 2.1. Condensation schematics: (a) Filmwise and (b) dropwise

The presence of NCGs during a CHT scenario, as presented in Figure 2.2, shows that steam flows radially (towards the cold wall) and carriages the NCG. Hence, the NCGs gather between the condensate and saturated steam. Eventually, a steam-NCG diffusion layer is formed, through which steam has to diffuse. This layer intensely reduces heat transfer. Approximately 1% air, by mass, can reduce heat flux by more than half.

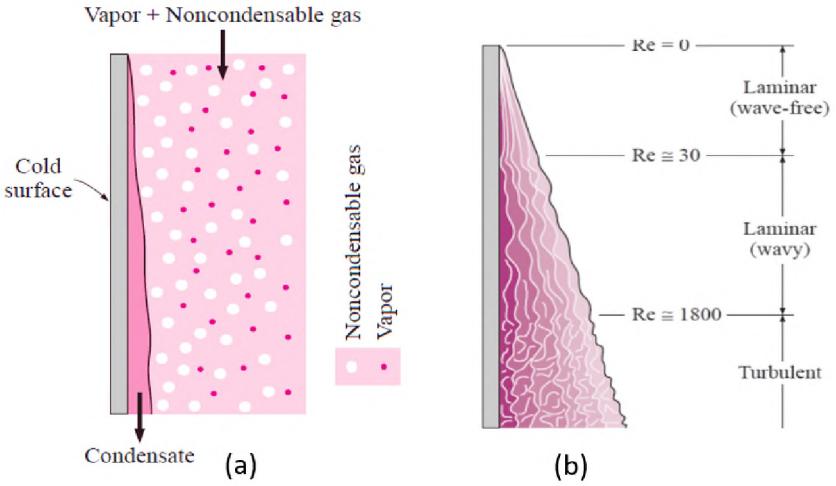

Figure 2.2. Condensation schematics: (a) steam-NCGs mixture and (b) condensate flow regime as per Re

The CHT of reactor systems for decay heat removal is mainly in-vessel or inside the reactor vessel and in-containment during a normal shutdown, refueling, and under hypothetical accident conditions. Again, the CHT scenarios for the reactor systems categorized as condensation in reflux flow, in-tube vertical downflow, in-tube bundle flow, in-large water pools, and in vertical walls. Figure 2.3 illustrates the basic condensation scenarios (Vierow, 2008). This section will focus on review of in–tube vertical downflow and filmwise wall condensation studies in Figures. 2.3 (b) and (c).

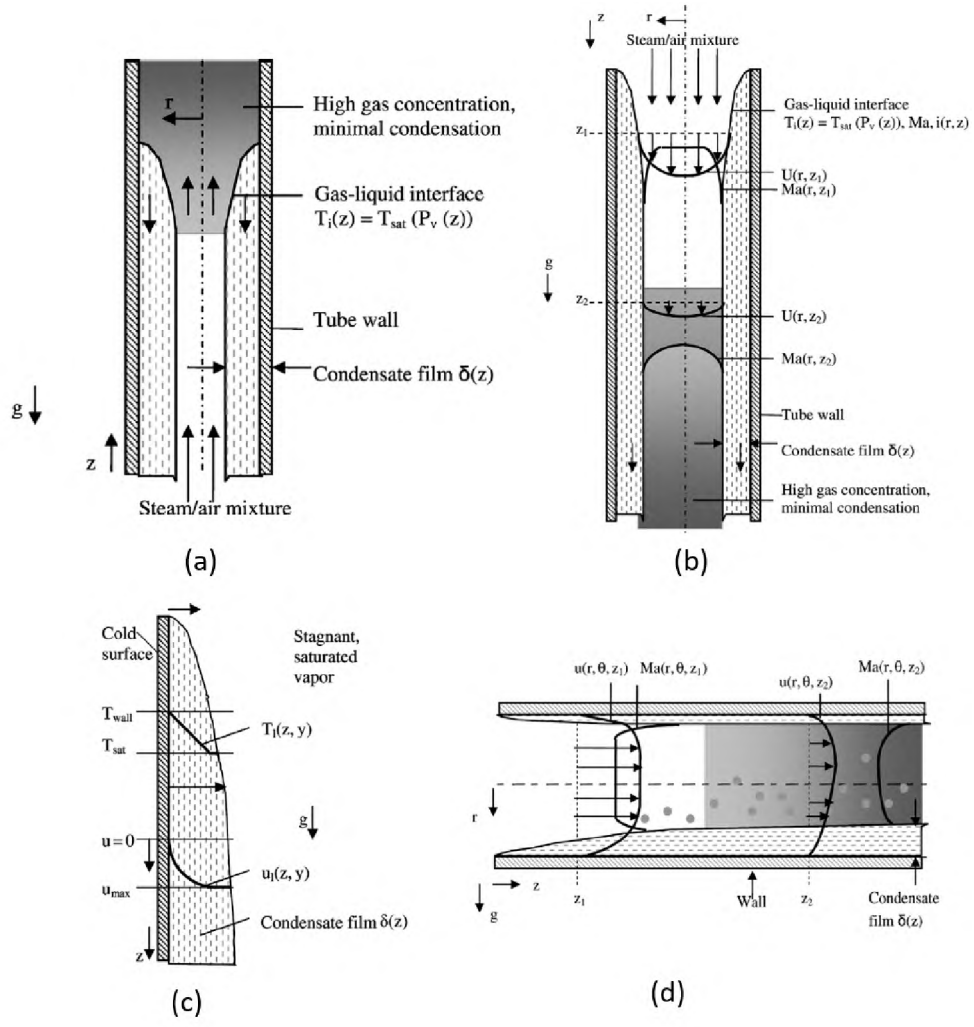

Figure 2.3. Condensation scenarios: (a) in–tube reflux flow, (b) in–tube vertical downflow, (c) vertical plate flow, and (d) in–tube horizontal flow (Vierow, 2008)

2.2. OVERVIEW OF PREVIOUS FILM CONDENSATION STUDIES

The previous works of CHT are grouped into theoretical, experimental, and numerical studies. The experimental studies are sub-grouped into separate and integral effect tests with wide ranges of differing geometric, physics, fluids, and operating conditions. Similarly, the theoretical and numerical studies are sub-grouped as conceptual modeling, simulations, and multiphysics-CFD softwares, and system codes. Many of the earlier studies for the reactor in containment condensation considered the effect of NCGs like air, nitrogen, hydrogen, and helium.

Nusselt (1916) developed the first film condensation model analytically for a vertical plate. He considered laminar falling film flow due to gravity, and he derived a relation for local film thickness and CHT coefficient. Then, Colburn (1951) extended the Nusselt's analysis for turbulent film by introducing vapor shear force as the dominant force, instead of gravity. Subsequently, Rohsenow (1956) considered the effects of interfacial shear stress for liquid film and vapor in tube geometry. Next, Goodykoontz and Dorsch (1966) and Goodykoontz and Dorsch (1967) performed steam CHT tests inside vertical tube condensers and observed that axial pressure depended on vapor flow and heat flux. After that, Soliman *et al.* (1968) modified the earlier Colburn's model for annular flow. They compared the results with Goodykoontz's test data and identified the effects of wall shear stress between vapor and film. Later, Soliman's proposed correlation was found valid only for mist conditions. Finally, Shah (1979) developed a similar, but useful, correlation for the CHT using a wide range of test data sets for different fluids and physical conditions.

The NCG reduces condensation was first addressed by Othmer (1929). Similar studies on this topic were conducted by Sparrow and Eckert (1961). Over time, several researchers studied the PCCS behavior analysis. Kim (2000), and Oh (2006) studied the steam-air mixture with a secondary side pool boiling at a constant saturated temperature in a vertical tube test section. Their test results showed a strong pressure dependence with the linear trend on the CHT coefficient. Siddique (1992) and Kuhn (1995) performed tests

on the vertical heat exchanger. Kuhn (1995) improved his test section to reduced turbulence perturbation and flow entrance effects, then obtained results close to the theoretical estimation. Later, Lee and Kim (2008) did experiments with nitrogen gas.

The review of CHT studies related to the present study, covering film condensation, in vertical tube downward vapor flow with NCG, and for reactor systems were performed by several researchers (Dalkilic and Wongwises, 2009; De la Rosa *et al.*, 2009; Ganguli *et al.*, 2013; Huang *et al.*, 2015; Kataoka, 2013; Slaughterbeck, 1970; Su *et al.*, 2016; Yadav *et al.*, 2016). These previous studies were reviewed in this study.

2.3. REVIEW OF EXPERIMENTAL STUDIES

From the film CHT literature, the major separate effect tests and the integral effect tests–CVTR, HDR, TOSQAN, MISTRA, ThAI, PANDA, PHEBUS, and NUPEC facilities (De la Rosa *et al.*, 2009; Yadav *et al.*, 2016)–were reviewed.

2.3.1. Major CHT SET Tests. A brief review of the important CHT separate effects tests are presented:

2.3.1.1. Uchida et al. and Tagami CHT tests. Uchida *et al.* (1964) and Tagami (1965) carried out steam condensation tests with NCGs under natural convection conditions inside a steel containment (height 0.3 m high and ID 0.2 m) at pressure and temperature ranges approximately 1 bar and 322 K, respectively. Uchida *et al.* (1964) used a vertical plate (height 1.4 cm and width 3 cm); whereas, Tagami (1965) used a cylindrical surface. They developed empirical correlations that are widely used in LWR thermal-hydraulic codes for licensing. These correlations used estimated HTC and mass fractions of NCGs and steam. Later, Peterson's (1996) theoretical studies showed that Uchida *et al.* (1964) test data could also be represented as a ratio of gas to vapor bulk density. The estimated HTC showed low dependency on wall temperature and high variation for bulk gas pressure.

2.3.1.2. Vierow CHT test. Vierow (1990) proposed a degradation factor method correlating the computed HTC with the Nusselt HTC by two factors, f_1 and f_2, using CHT test data from a condenser tube (length 2.1 m and 0.022 m ID) for a pressure range of 30 to 450 kPa. The factor f_1 related to Re; whereas, factor f_2 related to the NCG mass fraction of 0 to 14%, and it suggested to use both factors together. For pure vapor, factor f_2 became unity. The degradation factor method is the simplest, but also useful, in applications.

2.3.1.3. Dehbi CHT tests. Dehbi (1991) conducted steam condensation tests to check the effects of NCG for turbulent natural convection in a vertical and internally cooled condenser tube (3.5 m long, 38 mm ID, and copper) placed inside a vessel (5 m long, 450 mm ID, and stainless steel), as shown in Figure 2.4. In his study, steam was produced in a container and mixed with a known amount of NCG (air or air-helium mixture). Three sets of tests were performed for the steam-air and steam-air-helium mixture with the wall subcooling temperature of 15 to 50 °C, mixture Re < 1500, and Grashof number of 10^{11}. In the steam-air experiments, 25% to 90% air mass fractions for pressure 1.5, 3, and 4.5 atm were considered. Though, for the steam-air-helium tests, an additional helium mass fraction of 1.7%, 4.7%, and 8.3% for pressure 3 atm were used.

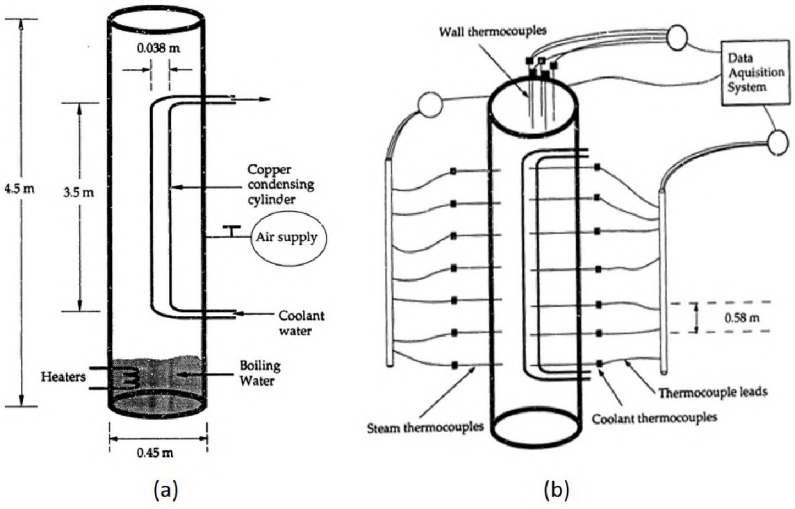

Figure 2.4. Test facility schematic: Dehbi (1991)

Results showed that the HTC decreased slowly with subcooling, increased mildly with high pressure, and increased significantly with low pressure. At low pressure, the developed correlation predicted similar heat transfer rates to Uchida *et al.* (1964). Again, compared with Huhtiniemi and Corradini (1993), it was observed that significant flow was induced due to natural circulation.

2.3.1.4. Siddique CHT tests. Siddique (1992) conducted steam condensation tests with NCG (air and helium) under forced convective conditions in a vertical condenser tube (2.5 m long and 46 mm ID) with a jacket cooling tube, as shown in Figure 2.6. This study was focused on the isolation condenser of a proposed Simplified Boiling Water Reactor. The test data were collected for inlet mixture temperatures of 100, 200, and 140 °C, mixture inlet Re (air 5000 to 22,700 and helium 5000 to 11,400), and different mass fractions of NCGs (air 10% to 35% and helium 2% to 10%). The local HTC varied from 100 to 25,000 $Wm^{-2}K^{-1}$. The results showed that for the same mass fraction, helium had more inhibiting effects on CHT than that of air; whereas, for the same molar ratio, the air was dominate. It was observed that film waviness had a negligible effect on HTC for low Schmidt number fluids, like steam with air, hydrogen, or helium mixtures.

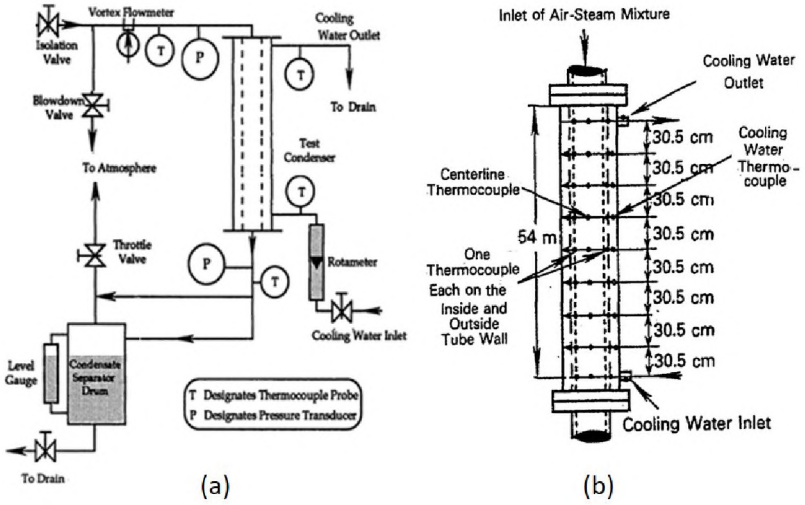

Figure 2.5. Test facility schematic: Siddique (1992)

2.3.1.5. Kuhn CHT tests. Kuhn (1995) performed steam condensation tests in a vertical condenser tube (3.37 m long, 47.5 mm ID, and 1.65 mm thickness) with jacket cooling, as shown in Figure 2.6. The test section was a simple counter-current heat exchanger in which the steam-NCG mixture flowed downward in the condenser tube, and the cooling water moved upwards. The maintained cooling water flow was low to get a broader span temperature profile. The temperatures at different axial positions of the condenser tube outer wall and the cooling tube inner wall were measured. Then, using the turbulent model of Yuann *et al.* (1995), the temperature shape factor and the local bulk temperatures were estimated. After that, using the coolant bulk temperature, the condensing wall temperature and heat flux were calculated. Repetitive tests were conducted for pure steam, steam-air, and steam-helium mixtures. The test data were recorded for pressure 1–5 bar, steam mass flow, 30–60 kg/h, and different mass fraction of NCGs (air 1% to 40% and helium 0.3% to 15%). Results showed that the local heat flux estimation method was more accurate than others. Finally, three different CHT correlations were proposed based on degradation factors, diffusion layer theory, and mass transfer conductance-based models.

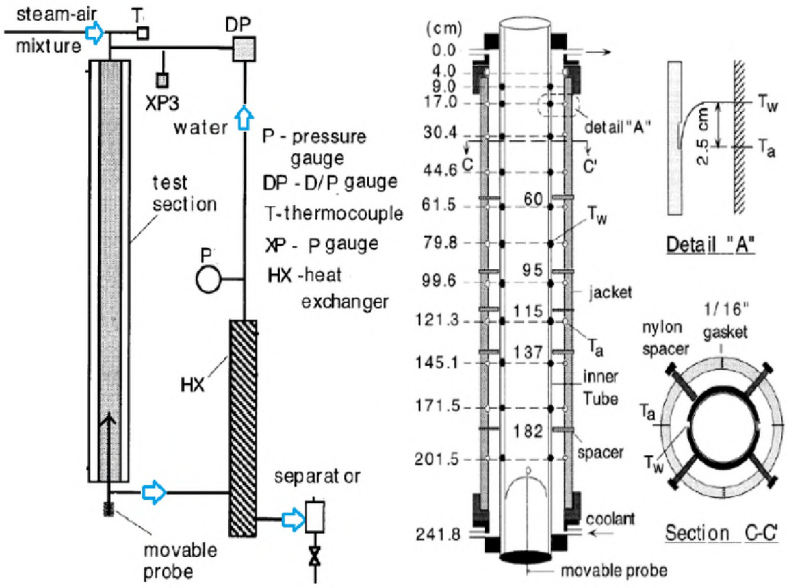

Figure 2.6. Test facility schematic: Kuhn (1995)

2.3.1.6. Anderson et al. CHT tests. Anderson *et al.* (1998) performed steam condensation experiments with air and helium to investigate the dependence of essential parameters. They used a 1:12 scaled facility (2.8 m tall, 1.7 m wide, and 0.32 m depth) of AP600, as shown in Figure 2.7. The test facility consisted of atmospheric and pressurized test sections, which were made of transparent polycarbonate and stainless steel, respectively. Two condensers (0.91m long each) were placed horizontally and vertically in the top-right corner of the atmospheric section, and test data was collected at atm pressure. The pressurized section was designed for 4 bar (absolute) pressure. They used seven aluminum plates (0.3 m wide and 38 mm thickness) placed at various angles to simulate a 2:1 scaled semi-elliptical dome structure for condensation accident scenarios at the containment. The test data were recorded at 1 to 3 bar pressure, 60 to120 °C bulk temperature, 25 to100 °C wall temperature and 0.4 to 4 mole-fraction of NGS/steam. The experimental HTC varied between 50 to 800 $Wm^{-2}K^{-1}$. It was observed that for lighter gas, like He <35 mol.%, it had a negligible effect; however, stratification occured at the upper part of the dome at a mass fraction of over 30%, and the local HTC decreased to half value.

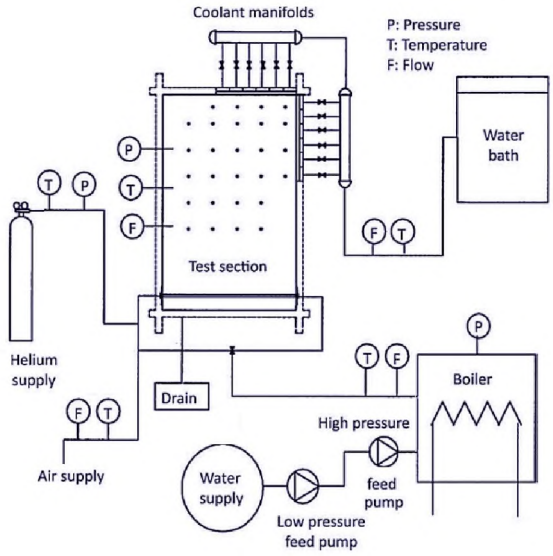

Figure 2.7. Test facility schematic: Anderson *et al.* (1998)

2.3.1.7. Park and No CHT tests. Park and No (1999b) investigated the parametric effects on the steam condensation with NCG (air) in a vertical condenser tube (2.4 m long and 47.5 mm ID) for the PCCS of CP-1300, as presented in Figure 2.8.

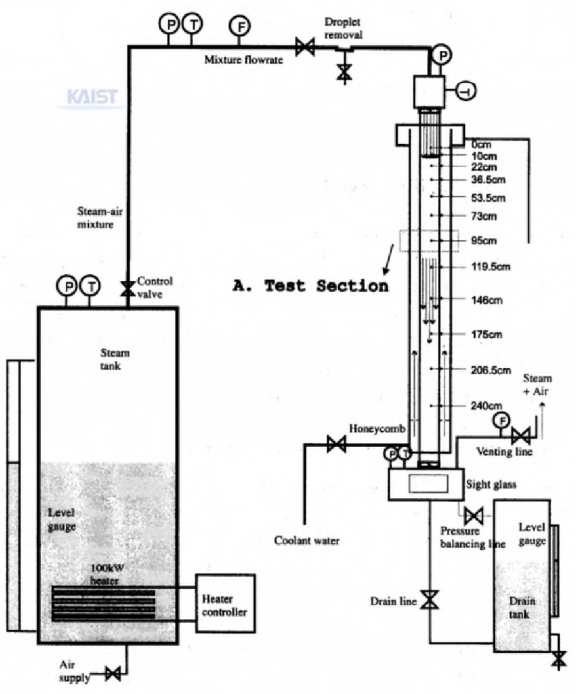

Figure 2.8. Test facility schematic: Park and No (1999b)

They compared the local HTC with three different conditions, i.e., inlet air mass fractions, inlet saturated steam temperatures, and inlet mixture Re. Results showed that the HTC increased with a decrease of the inlet air mass fraction, as well as inlet saturated steam temperature. Also, results showed a low dependency on the inlet mixture Re. An empirical correlation was developed that showed 22.3% standard deviation with test data. Again, the test HTC data were compared with the simulated data of RELAP5/MOD3.2 using the two wall film condensation models, the default, and the alternative. The results confirmed that the default model of RELAP5/MOD3.2 under-predicted the HTC, and the alternative model over-predicted them.

2.3.1.8. Liu et al. CHT tests. Liu *et al.* (2000) conducted condensation experiments in a smooth vertical tube (2.54 cm ID) with NCG (air and helium) to evaluate the heat removal capacity in a post-accident containment, as shown in Figure 2.9. Test data were collected for total pressures of 2.48 to 4.55 bar and air mass fractions of 0.30 to 0.65. An empirical correlation was developed for HTC. This correlation covered test data points within 20% and satisfied the diffusion layer model with suction effects. Their correlations estimates were approximately 2.2 times the amount of HTC than the Uchida *et al.* (1964) correlation. Again, they performed experiments with a restriction on radial flow and reduced the HTC by a factor of approximately 0.6. Test data for helium (simulating hydrogen) of 15%, 30%, and 60% mole fraction, showed reduced condensation HTC. Also, a gas stratification was observed for the helium mole fraction over 60%.

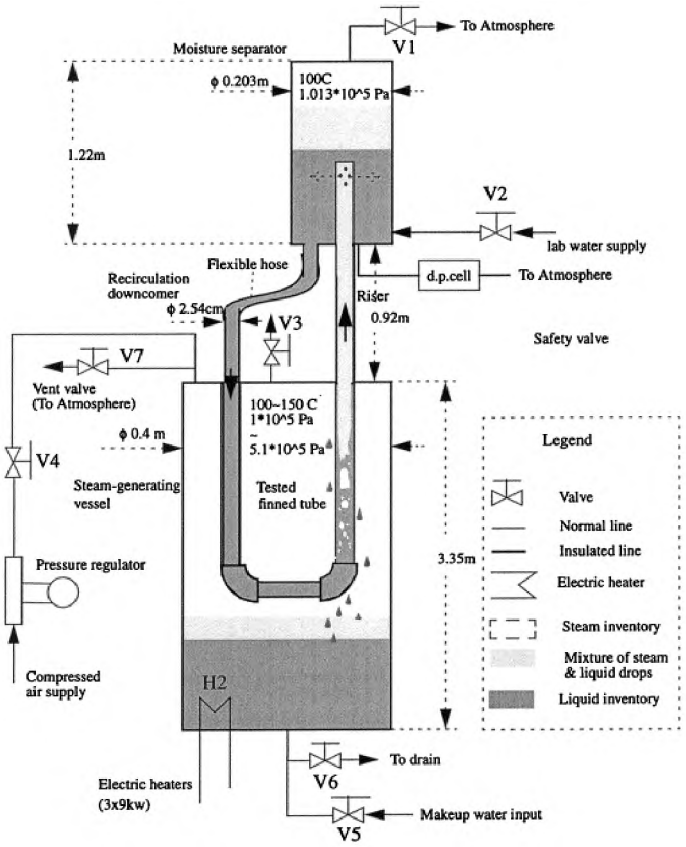

Figure 2.9. Test facility schematic: Liu *et al.* (2000)

2.3.1.9. Lee and Park CHT tests. Lee and Park (2002) experimentally studied the local hydrogen behavior in a cylindrical multi-subcompartment mixing chamber, a 1:11 scaled facility (1 m height and 178 m ID) of the safety injection tank of Young Gwang Nuclear (known as Hanbit Unit 3 and 4), as presented in Figure 2.10. The chamber was designed with two compartment layers and a substantial cylindrical column (115 m height and 0.25 m ID) at the center, as shown in Figure 2.10 (a). Helium was used as the test fluid, instead of hydrogen, and data was collected for various conditions (such as complete mixing, with steam injection, and obstacles in the gas pathway) and injection locations. Results of helium concentrations showed that local test data differed from the widely used lumped compartment analysis.

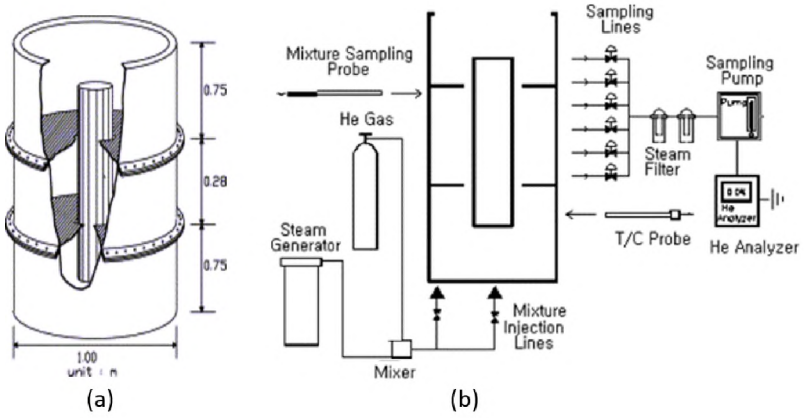

Figure 2.10. Test facility schematic: Lee and Park (2002)

2.3.1.10. Oh and Revankar CHT tests. Oh (2006) performed steam CHT experiments inside a vertical tube submerged in a pool of water for test conditions of complete condensation, cyclic venting, and through-flow modes, as shown in Figure 2.11. The primary condensing tube (26.6 mm ID, 3.38 mm thickness, 2.4 m long) and the secondary boiling tube (161 mm ID) were made of type 304 stainless steel. Tests were performed for

pressures ranging from 0.1 to 0.4 MPa, and it was observed that the CHT increased, but HTC decreased, with the system pressure. Test data showed a similar trend, but it had a 15% higher value with the Nusselt solution.

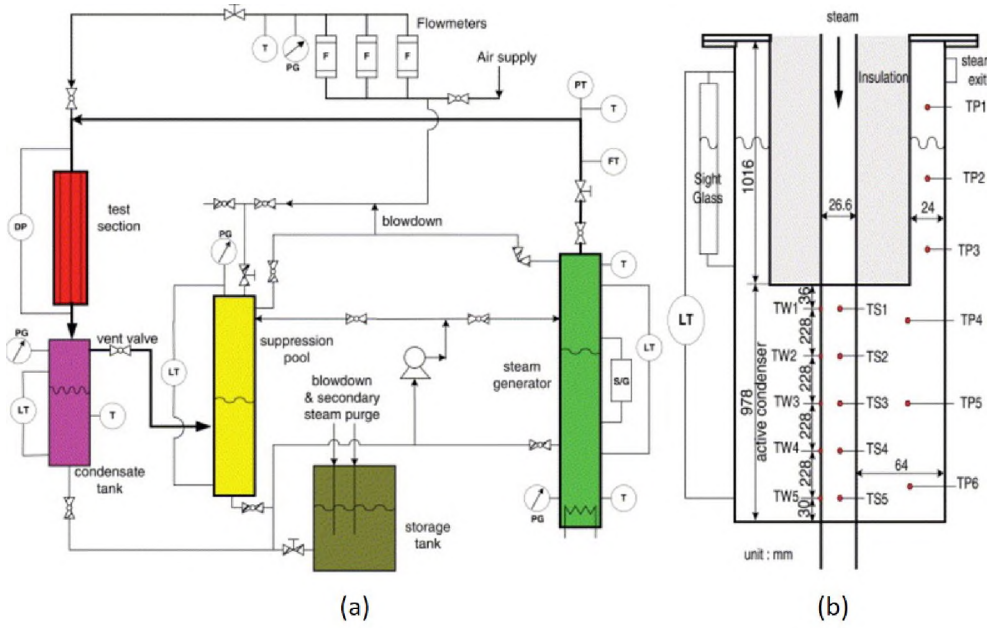

Figure 2.11. Test facility schematic: Oh (2006)

2.3.1.11. Lee and Kim CHT tests. Lee and Kim (2008) conducted steam CHT tests for inlet steam flow rates of 6.5 to 28.2 kg/h with up to 40% nitrogen (as NCG) inside a vertical condenser tube (3 m long, 13 mm ID, and 2.5 mm thickness) made of stainless steel, as presented in Figure 2.12. Thirteen K-type thermocouples were soldered to the outer surface of the condenser tube at different axial locations. Another set of thermocouples were placed at the half radial position of the jacket coolant to measure coolant bulk temperature. They used air bubbles in the cooling water jacket, like Siddique (1992), to produce turbulence and proper mixing to get the bulk temperature. Moreover, the transparency of the acrylic tube helped to see and maintain the desired flow mixing. Their test conditions were pure

steam, mixture bypass, and NCG accumulation at atmospheric pressure. The pure steam test data agreed with Shah (1979) correlation with an under-prediction of the HTC near the condenser tube inlet.

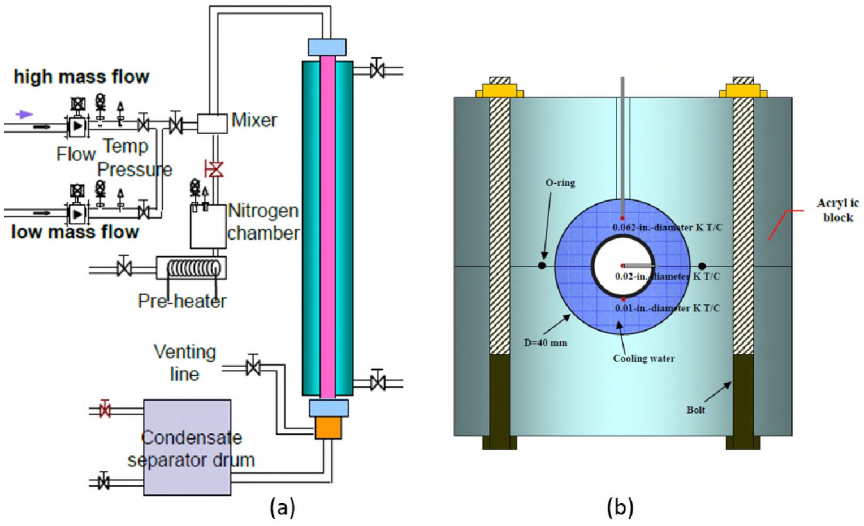

Figure 2.12. Test facility schematic: Lee and Kim (2008)

This under-prediction was due to the developing flow and suction effects caused by high mass transfer. In their mixture bypass tests, the mass fraction of nitrogen increased rapidly, due to steam condensation, causing the vapor partial pressure and saturation temperature to decrease. Eventually, this acted as a substantial thermal resistance to the heat transfer. In their NCG accumulation tests, nitrogen gas volume factions were maintained at 20% to 80%. The test data showed that the local HTC increased with an increase of inlet steam flow rate and a decrease of NCG mass fraction; however, they observed that NCG had only a weak influence on steam condensation in the small-diameter condenser. A new correlation was developed for steam condensation with NCG with a standard deviation of 17.5%. This correlation was independent of the condenser tube diameter (for the range 0.5 inches to 2 inches).

2.3.1.12. Aglar and Tanrikut CHT tests. Ağlar and Tanrikut (2008) performed steam CHT tests in vertical condenser tubes (length 0.033 m and 2.158 m ID) for inlet pressures from 1.8 to 5.5 bar, air mass fractions from 0 to 0.52, and inlet mixtures Re from 45000 to 94000, as presented in Figure 2.13. They used Kuhn's data reduction method and data-fitted by the Marquardt-Levenberg's nonlinear method.

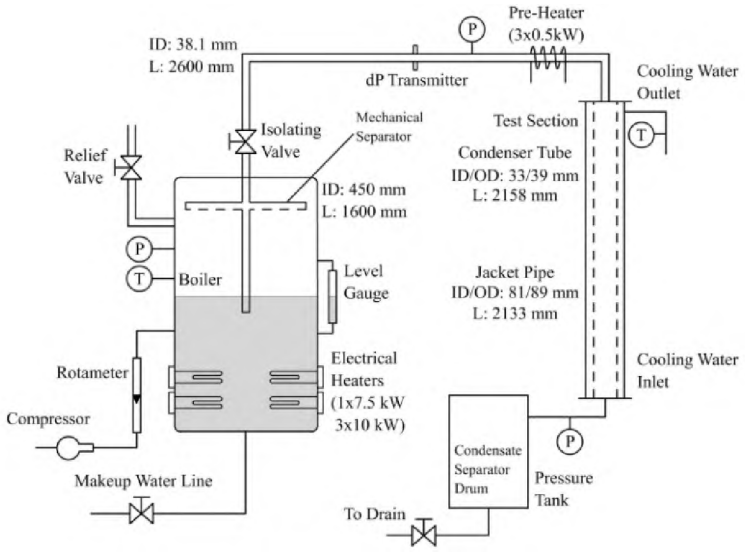

Figure 2.13. Test facility schematic: Ağlar and Tanrikut (2008)

Their developed degradation factor correlation with Re for both the condensate and the steam-air mixture had a 19.4% deviation from the test data. In their studies, they did not consider the film waviness, as the Schmidt-number of the air-vapor mixture was small, which created a thicker concentration layer than the hydrodynamic layer.

2.3.2. List of Notable Separate Effect Tests. A brief summary of notable previous steam CHT with NCG tests in a vertical tube is listed in Table 2.1 for various geometric, fluid, flow, and pressure conditions. It was found that most of the previous CHT tests were performed with a one or two-inch condenser tube. The most common NCG was air. The second common NCG was helium. During an accident condition with fuel failure, hydrogen gas produced, released, mixed, and accumulated with containment air. In spite

of that, using hydrogen in the test is not safe due to its self-igniting properties. Instead of hydrogen, a non-reacting inert gas, helium was widely used. The flow and pressure range for most of the previous tests were limited to 6 to 60 kg/hr and 0.1 to 0.5 MPa, respectively.

Table 2.1. List of CHT experiments in vertical tube inside

Authors	**D:L** (mm)	**NCGs** (%)	**Flow** (kg/hr)	**Pressure** (MPa)	**HTC** ($Wm^{-2}K^{-1}$)
Vierow and Schrock (1991)	22:2100	Air (0-14)	5.9-25	0.03-0.45	0-1600
Siddique (1992)	46:2540	Air/He (10-35)	7.9-32	0.1-0.5	100-2500
Kuhn (1995)	47.5:2400	Air/He (0-40)	30-60	0.1-0.5	500-13000
Araki *et al.* (1995)	49.5:2000	Air (0-24)	9-58	0.15-0.25	–
Park and No (1999b)	47.5:2400	Air (10-40)	7.6-40	0.17-0.5	100-7000
Kim (2000)	46.2:1800	Air (0-30)	–	0.35-7.5	4000-74000
Oh (2006)	26.6:984	Air (0-10)	9.0-20	0.1-0.4	3500-6500
Lee and Park (2002)	10.9:1000	Air (0-0.22)	–	40-100	
Lee and Kim (2008)	13:2800	N (0-40)	6.5-28	0.1-0.13	300-27900

2.3.3. Brief Review of Integral Effect Tests. The integral tests facilities are used to investigate plant system-level performances. The important integral effects CHT test facilities were COPAIN, CONAN, MISTRA, TOSQAN, and ThAI, as presented by several review studies (Ambrosini *et al.*, 2006; Cheng *et al.*, 2001; Yadav *et al.*, 2016). COPAIN CHT tests a vertical condensing surface (height 2 m, duct size 600 mm $\times$ 500 mm) used in a rectangular duct for steam with NCG (air and helium) flow (0.1 to 0.3 m/s) for pressure 0.1 MPa (Cheng *et al.*, 2001). The CONAN facility consists of a condensing surface (height 2 m, duct size 340 mm $\times$ 340 mm), allowing steam-air downward flow and upward flow in the coolant (water) channel (Ambrosini *et al.*, 2006). Results showed the suction effects, especially at relatively high steam mass fractions. Likewise, CHT tests were performed under the International Standard Problem (ISP-47) program to assess the capabilities of the lumped parameter (LP) and to validate CFD using three integral test facilities: MISTRA, TOSQAN, and ThAI (Yadav *et al.*, 2016).

2.4. REVIEW OF THE NUMERICAL STUDIES

Several researchers performed numerical studies of CHT of PCCS, as mentioned in the previous section. These numerical studies are grouped into mainly CFD studies, using commercially available software and system codes like RELAP and GOTHIC.

The multiphysics CFD analysis for CHT were performed by several researchers using Fluent (Dehbi *et al.*, 2013; Fu *et al.*, 2016; Li, 2013; Ravva *et al.*, 2014; Su *et al.*, 2014), CFX (Houkema *et al.*, 2008; Jiang *et al.*, 2013; Martín *et al.*, 2005; Zschaeck *et al.*, 2014), STAR CCM+ (Bian *et al.*, 2017), CFD ACE+ (Sharma *et al.*, 2012), and other softwares. Some of them used experimental correlations, and others used diffusion boundary layer models for simulation. Then they validated the results with different CHT test data parameters, like: HTC, heat flux, condensation rate, temperature, pressure, mass fraction and other local phenomena.

2.4.1. Review of CFD Studies. In the CHT-CFD analysis, researchers generally used commercial multi-physics software and tried to validate their simulations with test data. Some of the commonly cited CHT-CFD studies were reviewed in this section.

2.4.1.1. Fu et al. CHT CFD studies. Fu *et al.* (2016) performed CFD analysis of steam condensation in vertical tubes with NCG (He and air) using ANSYS Fluent 2D axisymmetric model for Kuhn geometry and test conditions, as shown in Figure 2.14. Simulations were carried out for steady-state with source terms for each species in the conservation equations, so source terms were also used at the wall adjacent cells, instead of modeling condensate film in the fluid domain. Remeshing was done to maintain near-wall y+ <1. Mass flow inlet, pressure outlet, and polynomial fit temperature from test data were used as the boundary conditions for inlet, outlet, and vapor-film interface, respectively. These interface temperatures were estimated from the inner wall temperatures, heat flux, film thickness, and thermal conductivity. Results were validated with Kuhn test data and showed general agreement, as illustrated in Figure 2.14.

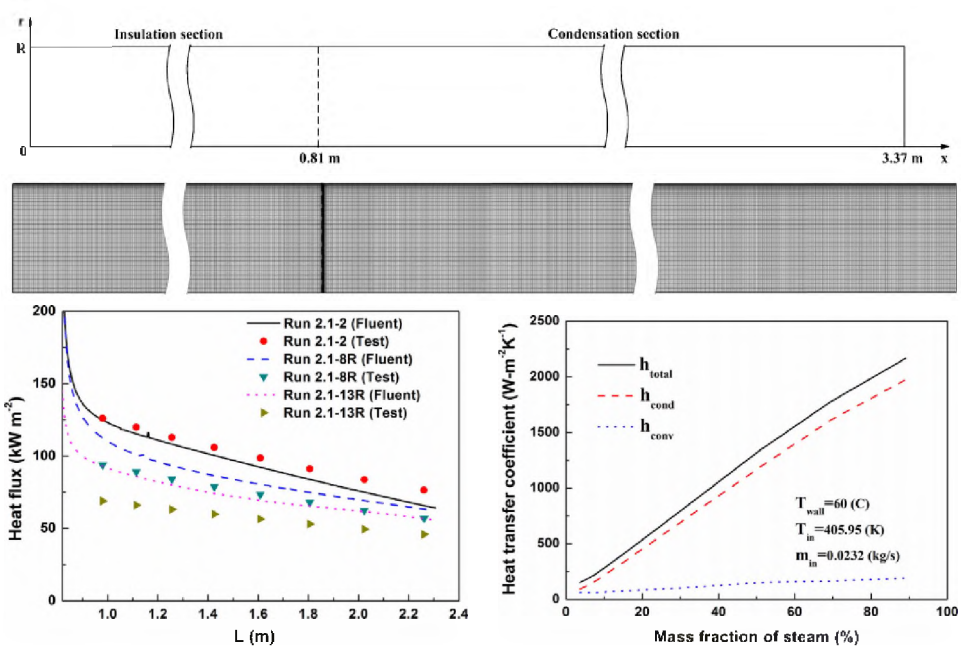

Figure 2.14. Geometry, mesh, and sample results of Fu *et al.* (2016) CFD study

Simulated results showed that the condensation HTC dominated over convection HTC for the high steam mass fraction. Though the heat flux increased with the reduction of film-gas interface temperature, the mixture HTC reduced due to enhanced the temperatures between mixture bulk and film-mixture interface. The simulation showed that due to the suction effect, there was a significant radial velocity. This suction effect increased with steam mass flow rate, but it stayed constant for the increase of Re. Condensate mass transfer was higher in the steam-He than the steam-air, as steam diffuses quicker in helium than air. However, this mass transfer was constant for both mixtures for high steam content (> 90%).

2.4.1.2. Punetha and Khandekar CHT CFD studies. Punetha and Khandekar (2017) studied a CFD-based steam condensation modeling approach with NCGs in ANSYS CFX, as presented in Figure 2.15. The results were validated for the test facilities of CONAN, Kuhn, Su et al., and TOSQAN. This study considered natural fluid flow with buoyancy effects of the involved species to mimic the accumulation and diffusion of hydrogen in the

containment during a LOCA. Simplified boundary layer equations were used with a wall condensation model (WCM) and a multi-component gas model (MCM) with a condensate sink term. The WCM worked for the higher mass fraction of NCG (> 6-8%).

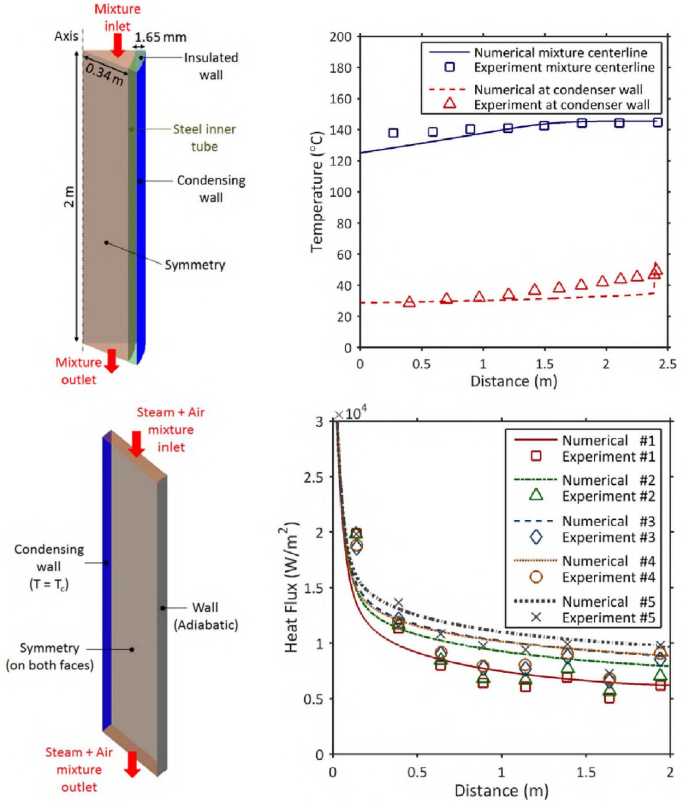

Figure 2.15. Sample geometry and results of Punetha and Khandekar (2017) CFD study

The diffusion of the denser species was more dominant than the bouncy force in the mixing and diffusion dynamics. Additionally, the stratification of higher species dies over time for both small and large scale tests. Except for low NCG (up to 6%), the simulated results matched well with the test data.

2.4.1.3. Li CHT CFD studies. Li (2013) performed a CFD analysis of steam CHT with NCG for the Kuhn's test condition using ANSYS Fluent software. Instead of applying wall constant temperature and heat flux, it used the turbulent flow of the annular coolant for the conjugate heat transfer. However, independent simulations for the condenser and cooling

jacket sections were performed to avoid the software limitation of a single mixture material for a domain. Thus, two simulations were solved iteratively and asynchronous coupled, i.e., one acting as input for the other and run until required convergence reached. The Nusselt approach, ideal gas assumption, and Boussinesq approximation were adopted to model the condensing film, steam-air mixture, and the cooling jacket, respectively. Simulations covered for the air mass fraction of 66% to 98%, variable fluid properties and temperature, per Kuhn's test.

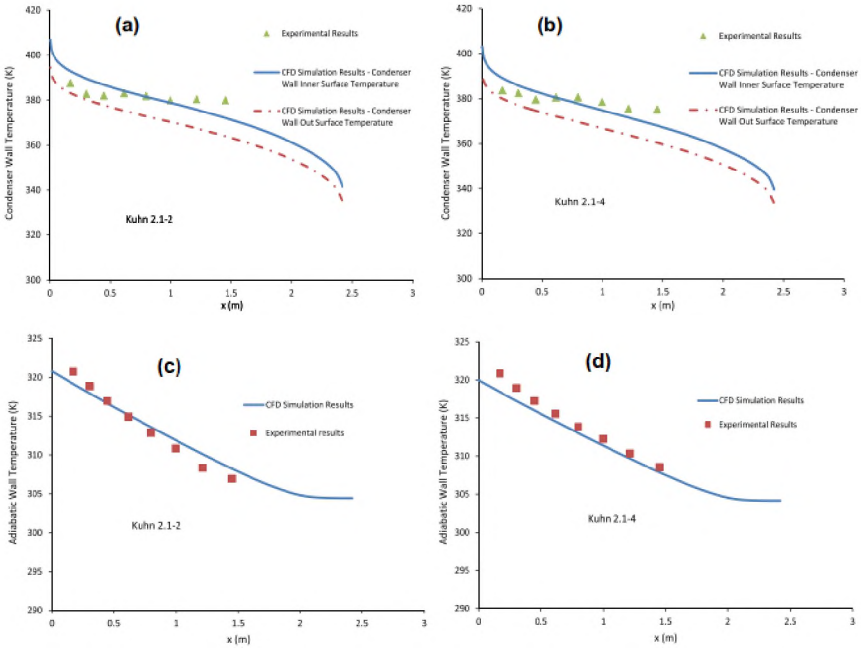

Figure 2.16. Sample results of (Li, 2013) CFD study for Kuhn's test

Results showed that the vapor-mixture centerline and adiabatic wall temperatures at axial locations were in general agreement, but heat flux varied with the Kuhn data, as shown in Figure 2.16. It was observed that the average axial velocity declined rapidly as the steam condensed, while the vapor-mixture density increased both axially and radially along the condenser tube.

2.4.1.4. Zschaeck et al. CHT CFD studies. Zschaeck *et al.* (2014) conducted a CFD analysis of steam wall condensation with NCG using ANSYS CFX for square and cylindrical ducts. They used their proposed mathematical model and validated the results with two sets of Kuhn's test data, as shown in Figure 2.17. In their model to simulate condensation, they considered mass sinks, multi-component gas, wall boundaries, and conjugate heat transfer interfaces. Their study lacked the details of liquid film modeling, condensation accumulation phenomena, and assumed that solid material absorbs the latent heat. The model geometry was simplified to 90-degree symmetry, as shown in Figure 2.17. Both two and three-dimensional studies with mesh sensitivity analyses were performed to identify the spatial discretization error.

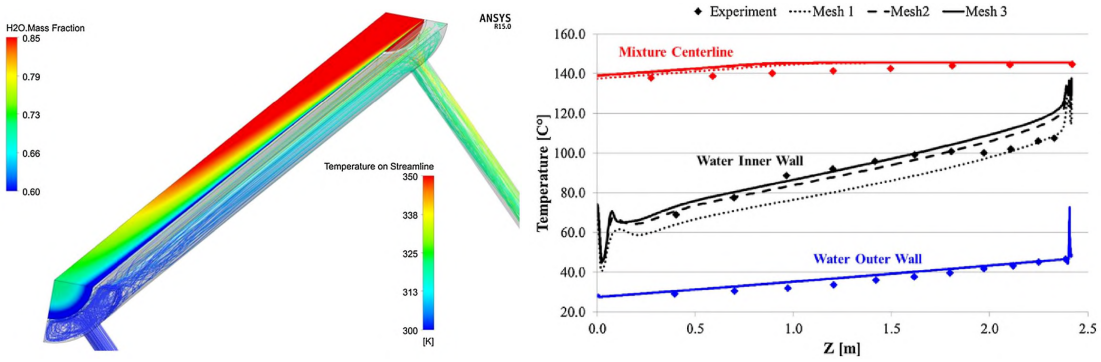

Figure 2.17. Sample results of (Zschaeck *et al.*, 2014) CFD study for Kuhn's test

Results of the vapor centerline temperature showed over-prediction compared to the test temperature data. This mismatch was attributed to the lack of recommended value for turbulent intensity and viscosity ratio. They observed that the temperature distribution results of 3D mesh provided better predictions than 2D mesh at the inner wall and cooling jacket. Though, for Z > 1.8 m, there was a deviation, which was reported due to uncounted heat loss.

2.4.1.5. Lee et al. CHT CFD studies. Lee *et al.* (2015) investigated steam condensation using a vertical downflow in a circular condenser tube with 2D axisymmetric geometry, as shown in Figure 2.18, to check the axial variation of the wall heat flux and temperature. The F-32 was used as the working fluid and as the volume-of-fluid (VOF) model in the Fluent. Their study provided detailed construction of the model, numerical method, interfacial change sub-model. The simulated temperature profile exhibited a steep gradient near the liquid film interface, similar to the profile of eddy diffusivity.

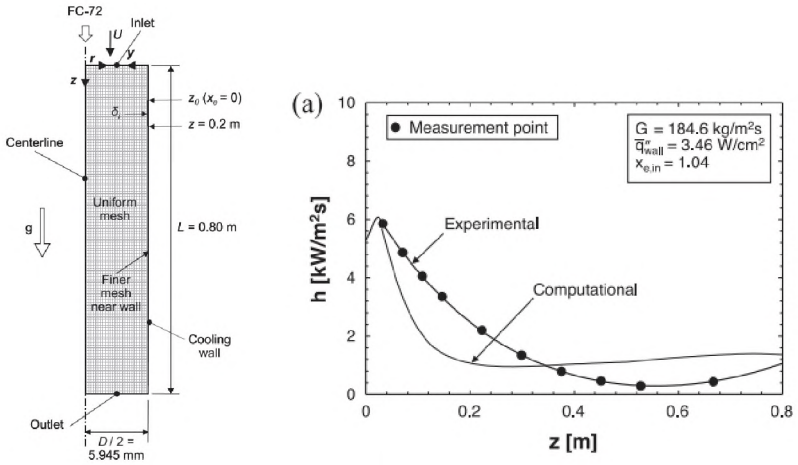

Figure 2.18. Computational domain and sample results of Lee *et al.* (2015) study

This study used a mass transfer intensity factor (ri) with a recommended value of 10,000 for estimating condensation HTC and interfacial temperature. As it was observed, the value of ri was related to temperature and HTC. A low ri value resulted in a lower interfacial temperature than the saturation and wall temperatures. It also resulted in low wall temperature and condensate HTC. On the contrary, a high ri value induced high interface disturbances and weak convergence. They reported that there was no eddy diffusivity of momentum at the film-mixture interface and condensing surface due to turbulence reduction by the surface tension. A similar profile of the temperature was also obtained with a sharp slope near the wall and interface. The void fraction profile showed disturbed film-interface

due to droplets. The results exhibited that the vapor velocity and shear reduction caused with the axial flow direction at the interface. This study highly recommended high-resolution test data of liquid-film, flow velocity, and temperature distribution.

2.4.1.6. Ambrosini et al. CHT CFD studies. Ambrosini *et al.* (2014) performed a steam wall condensation benchmarked study with different international organization. They used different models, phenomena, test data, and CFD tools. Their studies addressed the importance of the CFD model and benchmarking. They used a simplified idealized CONAN test facility as a simulation domain, and the results were validated and benchmarked with the test data for lower mixture velocity, the lower flow rate for several blind exercises for the members. They used the same geometry and similar operating conditions and the benchmarked quality improved, as illustrated in Figure 2.19. This study showed the challenges of CFD codes for predicting the PCCS of a real reactor system. Continuing studies using lumped parameters and fundamental approaches in CFD models was recommended.

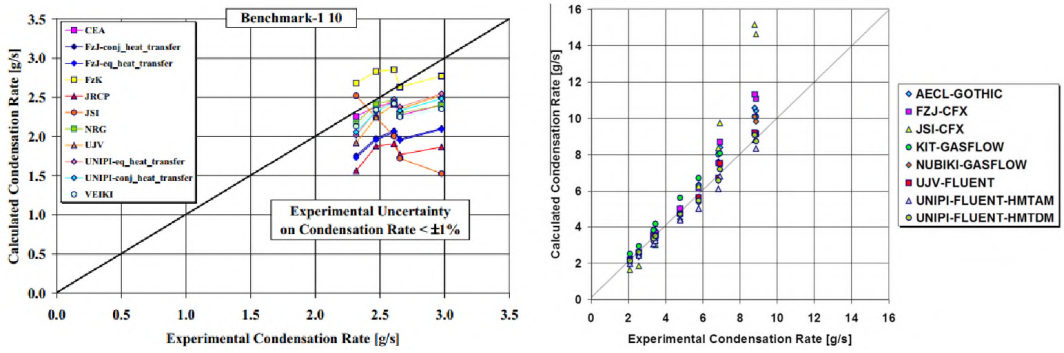

Figure 2.19. Sample results of SARNET benchmark study

2.4.1.7. Wang et al. CHT CFD studies. Wang *et al.* (2016) investigated the influence of film waviness effects on steam CHT with NCGs. Several wavy-solid-surfaces with different wave heights and lengths with and without moving velocities were used in ANSYS Fluent with the k-e turbulence model, as illustrated in Figure 2.20. A gas-phase condensation model was used as a source term to the contagion condensing wall.

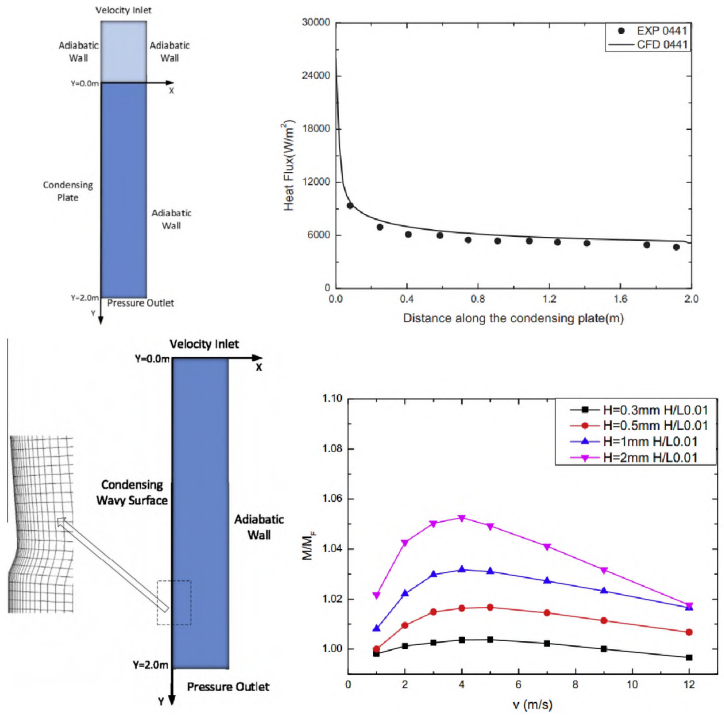

Figure 2.20. Sample geometry and results of Wang *et al.* (2016) CFD study

Results showed that the wave structure enhanced the condensation rate (up to 10%), and it required wavy effect multiplication factors for high Re. The realizable k-e model was used, as it agreed well and increased the condensation rate due to an increase in condensing area and altering flow structure. The maximum increase observed at the gas velocity of 4 m/s, but the rise was no more than 10% for all cases, as shown in Figure 2.20. These results exhibited a second-order effect and confirmed the requirement of a modification factor for film waviness. The wave influence considered for high film Re (up to 2000) in a large containment. The limitation of this study originated from the consideration of using simplified 2D-wave effects and treating the liquid phase as a solid surface. This study recommended using the volume-of-fluid model to improve the simulation performance of the interaction between two phases.

2.4.1.8. List of notable CFD studies. Including the previous CFD studies, there were other notable CHT studies available in literature (Bian *et al.*, 2017; Dehbi *et al.*, 2013; Houkema *et al.*, 2008; Jiang *et al.*, 2013; Martín *et al.*, 2005; Ravva *et al.*, 2014; Revankar *et al.*, 2008; Sharma *et al.*, 2012; Su *et al.*, 2014). A brief of these studies are presented in Table 2.2.

Table 2.2. Review of CHT using Multiphysics CFD Bian *et al.* (2018)

Authors	**Software**	**Model**	**Test facility**	**Scope and focus**
Martín *et al.* (2005)	CFX	Exp	Dehbi, Anderson	HTC
Houkema *et al.* (2008)	CFX	DBM	Kuhn, PHEBUS	Con. rate
Sharma *et al.* (2012)	CFD ACE+	Exp	COPAIN	Heat flux
Li (2013)	Fluent	DBM	Kuhn	T, Heat flux
Jiang *et al.* (2013)	CFX	DBM	COPAIN	HF, Con. rate
Dehbi *et al.* (2013)	Fluent	DBM	Uchida, Tagami, COPAIN, Dehbi	HTC, Heat flux
Ravva *et al.* (2014)	Fluent	DBM	TOSQAN	P, T, V, Ma
Su *et al.* (2014)	Fluent	Exp	Su et al.	HTC
Zschaeck *et al.* (2014)	ANSYS CFD	Exp	CONAN, Kuhn	using math model
Ambrosini *et al.* (2014)	CFD tools	Exp	CONAN	Benchmarking
Lee *et al.* (2015)	Fluent	Exp	Wang et al.	VOF, 2D, FC-72
Wang *et al.* (2016)	Fluent	Exp	COPAIN	Wavy-surface
Fu *et al.* (2016)	Fluent	Exp	Kuhn	Suction effect
Bian *et al.* (2017)	STAR–CCM+	DBM	COPAIN, Su	Local phenomena

Note: Here, Exp-experiment, VOF- Volume-Of-Fluid, DBM-diffusion boundary layer model
Con.-condensation, T-temperature, P-pressure, V-velocity, HF-heat flux, and Ma-mass fraction,

2.4.2. System Code and Software. Several system codes like RELAP5/MOD3.3, GOTHIC, CONTAIN, COMPACT, and MELCOR were used for CTH analysis using lumped solution approach. George and Singh (1996), Papini *et al.* (2011), Lin *et al.* (2013), Bocanegra *et al.* (2016) utilized GOTHIC for containment analysis. Previous research to assess the RELAP5 condensation models and correlations related to single and in-tube condensation by, Hassan and Raja (1993), Banerjee and Hassman (1993), Shumway (1995), Boyer *et al.* (1995), Choi *et al.* (1998), Park and No (1999a), Moon *et al.* (2000), Ağlar and Tanrikut (2008), Moghanaki and Rahgoshay (2013), Ağlar (2013), Zhou *et al.* (2013), Nguyen and Trinh (2014), Brooks *et al.* (2015), Fu *et al.* (2015), Park (2015), Fullmer *et al.* (2016).

2.5. SEMI EMPIRICAL AND EXPERIMENTAL CORRELATIONS

Using the analytical and test data and the semi-empirical correlations, the degradation factor (f), which was the ratio of experimental and Nusselt's HTC, was developed by Vierow (1990), Kuhn *et al.* (1996), Park and No (1999b) and Lee and Kim (2008). For condensing falling film, Chun and Seban (1971), Shmerler and Mudawwar (1988), Chun and Seban (1971), and Labuntsov (1957) developed empirical correlations without shear effects; whereas, Blangetti *et al.* (1982), Butterworth (1983), and Araki *et al.* (1995)'s correlations considered the shear effects. Additionally, Traviss et al. (1973) and Shah (1979) developed correlations with broader ranges of test data for the annular flow. A brief review of these experimental correlations was discussed in the **later sections**.

2.5.1. Degradation Factor Method. The ratio of experimental and Nusselt's local HTC defined as degradation factor (DF, f).

2.5.1.1. Vierow (1990). Kuhn *et al.* (1996) modified the Vierow (1990) f with f_1, including the effect of interfacial shear (δ_{shear}) and surface waviness to improve the film heat transfer as:

$$f = \frac{h_{exp}}{h_{Nu}} = f_1 \cdot f_2 = \left(1 + a\,Re_{mix}^{d}\right) \cdot \left(1 - bM_{NCGs}^{c}\right) \tag{2.1}$$

2.5.1.2. Kuhn *et al.* (1996). Kuhn *et al.* (1996) modified the Vierow (1990) f with f_1, including the effect of interfacial shear (δ_{shear}) and surface waviness to improve the film heat transfer as:

$$f = \frac{h_{exp}}{h_{Nu}} = f_1 \cdot f_2 = f_{1,\,shear} \cdot f_{1,\,other} \cdot f_2 = \frac{\delta_{shear}}{\delta_{Nu}} \cdot \left(1 + a\,(Re_f/4)^{d}\right) \cdot \left(1 - bM_{NCGs}^{c}\right) \tag{2.2}$$

The parameters of the Vierow (1990) and Kuhn *et al.* (1996) are listed in Table 2.3.

Table 2.3. Parameters of f in different DF correlations

Authors	**Parameters**				**for/where**
	a	b	c	d	
Vierow *et al.*	2.88E-5	10	1	1.18	$M_{NCGs} < 0.063$
	2.88E-5	0.938	0.13	1.18	$0.063 < M_{NCGs} < 0.6$
	2.88E-5	1	0.22	1.18	$0.6 < M_{NCGs}$
Kuhn *et al.*	7.32E-4	2.601	0.708	1	$M_{air} < 0.1$
	7.32E-4	1	0.292	1	$0.1 < M_{air}$
	7.32E-4	35.81	1.074	1	$0.003 < M_{He} < 0.01$
	7.32E-4	2.09	0.137	1	$M_{He} > 0.1$

2.5.1.3. Park and No (1999b). Park and No (1999b) considered low dependence of steam-NCGs mixture Re and Prandtl number, Pr on CHT and developed DF, f using gas mass fraction, Jacob number, Ja and liquid film Re as:

$$f = \frac{h_{tot}}{h_f} = 0.0012 W_{nc}^{-1.4} Ja^{-0.63} Re_f^{0.24} \tag{2.3}$$

for $1715 < Re_g < 21670$, $0.83 < Pr_g < 1.04$, $0.111 < M_{air} < 0.836$, $0.01654 < Ja < 0.07351$, and $12.4 < Re_f < 633.6$.

2.5.1.4. Lee and Kim (2008). Lee and Kim (2008) developed degradation factor (f) for steam-NCGs mixture in a U tube in a reflux condensation, using gas mass fraction and shear force of the mixture. Their test data showed the CHT coefficient decrease with increase tube diameter.

$$f = \tau_g^{*0.3124} \left(1 - 0.964 M_a^{0.402}\right) \tag{2.4}$$

$$\text{for } 0.06 < \tau_g^* < 46.65, \quad 0.038 < M_{air} < 0.814$$

2.5.2. Other Experimental Correlations. A number of correlations have been developed for turbulent film CHT with and without considering interfacial shear for in/outer-tube wall or annular two-phase flow condition.

2.5.2.1. Correlations without shear effect. Chun and Seban (1971) proposed a empirical correlation for local Nu from an evaporating falling water film at outer wall of a vertical tube for $Re_f = \Gamma/\mu$ up to 5250.

$$Nu_f = 3.8 \times 10^{-3} \, (4Re_f)^{0.4} \, Pr^{0.65} \tag{2.5}$$

Shmerler and Mudawwar (1988) also proposed correlations like Chun and Seban (1971), from evaporating falling film for Re range 1,250-9,400 and Pr range 1.75-5.4).

$$Nu_f = 3.8 \times 10^{-3} \, (4Re_f)^{0.35} \, Pr^{0.95} \tag{2.6}$$

Likewise, Labuntsov (1957) proposed another correlation based on the data from steam condensing falling film on vertical surfaces.

$$Nu_f = 0.023 \, (4Re_f)^{0.25} \, Pr^{0.5} \tag{2.7}$$

2.5.2.2. Correlations with shear effect. Blangetti *et al.* (1982) modeled turbulent film flow heat transfer using an integral analysis in the following form, with listed parameters in Table 2.4. They used water and methoxi-isopropanol-water (MWA) in a vertical tube condenser at atmospheric pressure with steam: vapor Re_v from 7100 to 25,500 for Pr equal 1.73, and MWA: gas Re_g from 7100 to 25,500 for Pr equal 19.3 and film Re_f < 3,500.

$$Nu_f = a \, Re_f^b \, Pr^c \left(1 + e\tau_i^{*f}\right) \tag{2.8}$$

Butterworth (1983) proposed a model with weighted contributions combining his semi-empirical correlation for shear-dominated film with Labuntsov (1957) correlation for gravity-dominated films as:

Table 2.4. Parameters for Blangetti et al. (1982) correlations

	$\tau_l^* = 0$	$0 < \tau_l^* < 5$	$5 < \tau_l^* < 10$	$10 < \tau_l^* < 40$
a	0.008663	0.008663	0.027	0.04294
b	0.382	0.382	0.2071	0.09617
c	0.5689	0.5689	0.5	0.4578
e		0.145	0.407	0.6469
f		0.541	0.42	0.473

$$\mathrm{Nu_f} = \left(\mathrm{Nu}_{\tau_i}^{*\,2} + \mathrm{Nu_g}^2\right)^{1/2} \tag{2.9}$$

where, $\mathrm{Nu}_{\tau_i^*} = \left[\left(\frac{1.41}{(4\,\mathrm{Re_f})^{0.5}}\right)^m + \left(\frac{0.071\mathrm{Pr}^{1/2}}{(4\mathrm{Re_f})^{1/24}}\right)^m\right]^{1/m} {\tau_i^*}^{1/2}$ was for share-dominated flow and $\mathrm{Nu_g}$ used Labuntsov's correlation for gravitation-dominated flow.

Chen *et al.* (1987) used a similar model like Butterworth (1983) for film condensation of quiescent vapor by adopting correlations from Chun and Seban (1971) for laminar-wavy flow, Blangetti and Schlunder's integral balance (1978) for turbulent flow, and Soliman *et al.* (1968) for shear-dominated flow as:

$$\mathrm{Nu_f} = \left(\mathrm{Nu}_{\tau_i}^{*\,2} + \mathrm{Nu_g}^2\right)^{1/2} = \left[\left(0.31\,(4\mathrm{Re_f})^{-1.32} + \frac{(4\mathrm{Re_f})^{2.4}\,\mathrm{Pr}^{3.9}}{2.37\times10^{14}}\right)^{1/3} + \frac{\mathrm{Pr}^{1.3}}{771.6}\tau_i^*\right]^{1/2} \tag{2.10}$$

where, $\mathrm{Nu_g} = \left(\mathrm{Nu_{la}^6} + \mathrm{Nu_{tu}^6}\right)^{1/6}$ with $\mathrm{Nu_{la}} = 0.823\,(4\mathrm{Re_f})^{-0.22}$ from Chun's (1971) and $\mathrm{Nu_{tu}} = 0.00402\,(4\mathrm{Re_r})^{0.4}\,\mathrm{Pr}^{0.65}$ from Schlunder's integral balance (1978), and $\mathrm{Nu}_{\tau_i^*} = 0.036\mathrm{Pr}^{0.65}{\tau_i^*}^{1/2}$ from Soliman's (1968).

Araki *et al.* (1995) developed correlations for CHT coefficients in laminar and turbulent regime as a function of mixture Re and air partial pressure ratios, $\frac{\mathrm{P_{nc}}}{\mathrm{P_{tot}}}$.

$$h_c = \begin{cases} 0.33\left(\frac{\mathrm{P_{nc}}}{\mathrm{P_{tot}}}\right)^{-0.67} & \text{for } 650 < \mathrm{Re_{mix}} < 2,300 \\ 2.11\times10^{-4}\mathrm{Re_{mix}^{0.8}}\left(\frac{\mathrm{P_{nc}}}{\mathrm{P_{tot}}}\right)^{-0.99} & \text{for } 2,300 < \mathrm{Re_{mix}} < 21,000 \end{cases} \tag{2.11}$$

2.5.2.3. Correlations for annular flow. Traviss et al. (1973) used velocity profile F_T (which was also related to temperature profile) of Von Karnam and Martinelli's pressure drop parameter ϕ_l to form the following correlations.

$$\frac{hd}{k_l} = \frac{Pr_l \left(4\,Re_f\right)^{0.9}}{F_T}\phi_l = \frac{0.15 Pr_l \left(4Re_f\right)^{0.9}}{F_T}\left[\frac{1}{X_{tt}} + \frac{2.85}{X_{tt}^{0.476}}\right] \tag{2.12}$$

where, F_T and X_{tt} is presented by-

$$F_T = 5Pr_l + 5\ln\left(1 + 5Pr_l\right) + 2.5\ln\left[0.0031\left(4Re_f\right)^{0.812}\right] \tag{2.13}$$

$$X_{th} = \left(\frac{1-x}{x}\right)\left(\frac{\rho_v}{\rho_l}\right)^{0.5}\left(\frac{\mu_l}{\mu_g}\right)^{0.1} \tag{2.14}$$

Shah (1979) developed a correlation with a wide range of test data for both laminar and turbulent flow. He used 10 different fluids in 21 test conditions from horizontal to vertical upflow and downflow with vapor quality 0–100%, liquid Re from 25 to 15,800 and the absolute local and the critical pressures ratio P/P_{cr} from 0.002 to 0.44.

$$\frac{h}{h_l} = 1 + \frac{3.8}{\Psi^{0.95}} \tag{2.15}$$

where, h and h_l were HTC for local two phase flow and superficial liquid phase, respectively. h_l was defined as $h_l = h_{l0}(1-x)^{0.8}$ and evaluated from the Dittus-Boelter equation: $h_{l0} = 0.023\left(\frac{k_l}{d}\right)\left(\frac{Gd}{\mu_l}\right)^{0.8} Pr_l^{0.4}$. Also, the phase paramter Ψ was defined as $\Psi = \left(\frac{1}{x} - 1\right)^{0.8}\left(\frac{p}{p_{cr}}\right)^{0.4}$. Finally, the overall correlation was presented as:

$$\frac{h}{h_{l0}} = (1-x)^{0.8} + \frac{3.8x^{0.76}(1-x)^{0.04}}{\left(P/P_{cr}\right)^{0.38}} \tag{2.16}$$

2.5.2.4. Correlations for reactor containment. Uchida *et al.* (1964) and Tagami (1965) developed CHT correlations for reactor containment, which were later used in GOTHIC code. In the Uchida test, air-steam mixture was used for pressure 0.1 to 0.28 MPa, and it developed the following relationship:

$$h_{\text{Uchida}} = 380\left(\frac{W_{n/c}}{1 - W_{n/c}}\right)^{-0.7} \tag{2.17}$$

where, $W_{n/c}$ NCG (air) mass fractions. Likewise, Tagami performed CHT test for both forced and natural convection, in which the forced convection test was to represent the initial stages of a LBLOCA, and developed the following transient (time-dependent) correlations:

$$h_{tot} = h_{tot\_\max}\left(\frac{t}{t_A}\right)^{0.5}, \text{ where } h_{tot\_\max} = 426\left(\frac{E_A}{t_A V_c}\right)^{0.6} \tag{2.18}$$

where E_A, V_c, and t_A are dimensional energy group, containment volume, and total time.

The correlations of film thickness developed by researchers in theoretical modeling and experiments for laminar and turbulent flow conditions in varying geometric conditions are listed in Table 2.5.

Table 2.5. Correlations for vertical downward flow film thickness Padmanaban (2006)

Authors	**Geo.**	**Flow, Re**	**Methods**	**Film thickness**
Dukler & Bergelin (1952)	Both	>270	Theory	$\left(3.0 + 2.5\ln\bar{\delta}^{+}\right)\bar{\delta}^{+} = \text{Re} + 64$
Brauer (1956)	Pipe-o	20-1800	Probe	$\bar{\delta} = 0.302\left(3\nu^2/\text{g}\right)^{1/3}\text{Re}^{8/15}$
Kapitza (1949)	Plate	<100	Both	$\delta = \left(2.4\nu^2\,\text{Re}/g\right)^{1/3}$
Brotz (1954)	Pipe	100 – 4300	Exp	$\bar{\delta} = 0.112\left(3\nu^2/\text{g}\right)^{1/3}\text{Re}^{2/3}$
Fiend (1960)	Pipe	Laminar	Exp	$\bar{\delta} = 0.369\left(3\nu^2/\text{g}\right)^{1/3}\text{Re}^{1/2}$
Zhivaikin & Volgin (1961)	Pipe	150–3500	Exp	$\bar{\delta} = 0.141\left(\text{v}^2/g\right)^{1/3}(4\text{Re})^{7/12}$
Takahama & Kato (1980)	Pipe	150–2000	Exp	$\bar{\delta} = 0.473\left(\text{v}^2/\text{g}\right)^{1/3}\text{Re}^{0.526}$
Brauner (1987)	Plate	Turbulent	Theory	$\bar{\delta} = 0.104\left(\nu^2/\text{g}\right)^{1/3}\text{Re}^{7/12}$
Karapantsios et al. (1989)	Pipe	126 – 3275	Exp	$\bar{\delta} = 0.451\left(\nu^2/\text{g}\right)^{1/3}\text{Re}^{0.538}$

Note: Here, Geo. for geometry, Exp for experiment, pipe and pipe-o for pipe inside and outside.

2.6. LIMITATION OF PREVIOUS WELL-CITED CHT STUDIES

To simulate the reactor containment physical condition, most of the CHT studies focused on NCG and naturally driven cases. The most cited work by Uchida *et al.* (1964) and Tagami (1965), which were adopted in many system codes, like GOTHIC, as the models of simplicity. Uchida *et al.* (1964) and Tagami (1965) used the same test chamber (6.4m height and 3.4 m diameter), three internally cooled tubes (0.3m height and 0.2m diameter) and surface condenser with steam and air (mass fraction 0.1 to 0.95), but the details of their test conditions and velocity field measurements were not published (Mullin, 2015). Therefore, their test data can not be reproduced or compared with other tests (Corradini, 1997).

Vierow (1990), Ogg (1991), and Siddique (1992) conducted in-tube CHT tests for GE's reactor systems using steam-NCG (air) with jacket cooling. Their test data lacked consistency due to the variation in test facility designs. Akaki *et al.* (1995) CHT test data showed a standard deviation of 29% to 34% for HTC, depending on the inlet Reynolds number. Later, Kuhn (1995) at UCB designed and developed (D&D) a similar, but standard, CHT test facility that reduced the test data error for the steam-NCG (air and He) mixture. Again, Kuhn's (1995) test facility was limited to a fixed geometry.

Oh (2006) addressed the limitation of using the annular jacket water as it may reach saturated states, i.e., a constant temperature boundary conditions during a reactor accident case and failure to estimate condensation rate accurately. They designed and developed (D&D) a scaled CHT test section with half scaled length and a diameter for steam-NCG mixture and pool boiling condition, but the reported test data error was approximately 11%.

Similarly, Lee and Park (2002) performed the CHT test to check the local hydrogen behavior with steam-helium in a 1:11 scaled facility of Safety Injection (SI) tank of Young Gwang nuclear power plant. However, local test data widely differed from the lumped compartment analysis. Lee and Kim (2008) used a transparent 13 mm condenser tube for the steam-nitrogen mixture and conducted tests at atmospheric conditions, which differs

from the containment system pressure (3.5 MPa). They used a surge tank, a preheater for NCG (nitrogen), and a separate condensate system with a drum before and after the test sections, which made the facility unnecessarily complicated.

Dehbi (1991) conducted CHT tests with steam-NCG (air) in a vertical and internally cooled condenser (38mm ID). Similarly, Jang *et al.* (2015) performed a CHT test with a tube of 40mm ID, used a CCD camera, and observed filmwise, as well as dropwise, condensation with mist formation. They found deviation in HTC with Dehbi's (1991) test data, which they reported that due to the smaller size of the test chamber, the non-uniform gas mixture inside the condensing chamber, and a significant axial temperature gradient along the tube in Dehbi's (1991) studies. Jang *et al.* (2015) developed a new correlation that showed a standard deviation (STD) of ±13% for Nu but a STD of ±20% for Dehbi (1991) test data.

In short, the well cited CHT experimental studies that used unscaled test facilities. These studies were not comparable to the PCCS of SMRs due to dissimilar geometric and physics conditions. Moreover, most the these studies did not consider entrance and heat loss effects.

Likewise, the earlier steam condensation CFD studies used smaller tubes and different test conditions, and the results were inconsistent due to unscaled geometry. Additionally, previous CFD-CHT studies were limited to 2D geometry or 3D simplified geometry. Most of them used heat flux or temperature boundary conditions from the test data or asynchronously coupled heat transfer between condensing and coolant flow domain. These simplifications and approximations showed improvement in their results, but it deviated from reality and brought higher uncertainty in scaling. A CFD validation study with scale geometries and test condition is much needed for the PCCS. This study focused on bridging this research gap by using scaled vertical condensing geometries (1", 2", and 4" ID). In addition, this study used 3D computation domains, implicit unsteady solver, conjugate heat transfer interface, fluid film, and multi-component gas models and validated with Kuhn's and S&T's tests.

3. SCALED MODULAR TEST FACILITY DESIGN AND CONSTRUCTION

This section focused on the state-of-the-art novel modular integral test facility design for CHT scaled testing. Saturated steam was chosen as the working fluid with NCGs (N, He, and air) in different mass fractions. This facility adopted a pre-cooler unit for inlet steam conditioning and a post-cooler unit for condensate-cooling. The scaled test sections are vertical concentric tube heat-exchangers with three different diameters. Next, high fidelity sensors, instruments, and data acquisition systems were installed and calibrated to set up the modular facility. Lastly, facility safety analysis and shakedown tests were performed.

Keywords: Condensation heat transfer, scaled design, and facility safety analysis

3.1. BACKGROUND AND SECTION OUTLINE

The estimation of the steam condensation rate depends on how accurately the local heat fluxes were assessed using condenser cooling surface temperatures and fluid bulk temperatures. Again, the local bulk temperature was estimated using surface temperatures and fluid mass-energy balances. Also, the heat loss to the environment is approximated as zero. Thus estimations and approximations lead to high variance in condensation rate assessments. Studies also reported high variance in estimated condensation rates for both laminar and turbulent cases, with and without non-condensable gases (NCGs) (Kim, 2000; Oh, 2006; Othmer, 1929; Sparrow and Eckert, 1961). The cause of this variation was due to diverse test facility designs, operating conditions, and various data reduction methods used (Kuhn, 1995; Lee, 2007; Park, 1999; Revankar *et al.*, 2008; Siddique, 1992; Yadav *et al.*, 2016).

In most facilities, the steam-NCG mixtures enter the steam-condensation units in vertical or horizontal geometry, inside or outside the tube, and the steam condenses to liquid water in an open-loop or closed-loop configuration (De la Rosa *et al.*, 2009; Su

et al., 2016; Yadav *et al.*, 2016). Next, NCG and the steam-condensate mixtures were collected in gas separation tanks to separate NCG (Revankar *et al.*, 2008). Finally, the steam-condensate needs to cool for safe discharge in the open-loop systems or be reused in closed-loop systems (Huang *et al.*, 2015; Kuhn, 1995). Cooling water flowed in concurrent or countercurrent directions. A countercurrent annulus jacket water flow was prefered for higher heat transfer performance, safer operation, and ease of fabrication (Lee, 2007). In nuclear applications, conservative estimates were required in the design parameter selection and estimation (Dehbi, 1991; Siddique, 1992) and thus required all the limiting conditions to be addressed.

3.2. OBJECTIVES AND TASKS

This section aimed to design a modular scaled facility to study steam condensation with NCGs. An experimental facility was constructed in the THEMES Laboratory at Missouri S&T. Some key features, objectives, and tasks of this study were:

- *Review the facility design criteria* such as operating conditions, geometric scale, material selection, measuring parameters, instrumentation, and data acquisition
- *Design and fabricate the test sections,* i.e. concentric tube heat-exchangers, the pre-cooler, and condensate-cooling heat exchangers
- *Develop the facility,* instrumentation, and facility safety analysis.

3.3. LESSON LEARNED FROM EARLIER CHT TEST FACILITIES

In Section 2, major earlier experimental facilities for steam-condensation studies were reviewed. This review showed the following steps and modifications were required to develop a standard novel test facility-

3.3.1. Conditioned Inlet Steam with Embedded Pre-cooler. The test fluid steam was received from a boiler or steam generator to the test section in saturated or superheated conditions depending on pressure and temperature. A standard modular test facility should add a pre-cooler unit to control the inlet condition effectively.

3.3.2. Steam-NCGs Homogeneous Mixture. A separate NCG supply unit is required to premix a specific mass or volume fraction of NCG with the steam. Mass flow rate, temperate, and pressure for mixing fluids, and the mixture, needs to be measured independently. This mixing was required to prepare a homogeneous mixture. Standard electronic smart mass flowmeters with high-sampling time-averaged techniques should be used to get steady-state low-variance test data.

3.3.3. Instrumented Steam-condenser Design Challenges. The downward steam flow was preferred for hydrodynamic stability and to avoid back pressure disturbances. The condenser section should be adequately insulated to prevent heat losses, to approximate an adiabatic boundary condition and safe-touch surface. Temperature sensors were mounted on tube walls to estimate local heat fluxes. The temperature sensor should place such a way to minimize uncertainty.

3.3.4. Condensate Cooling and Integral Energy Balance. The open-loop was preferable becasue it reduce the accumulation and backpressure disturbances. By contrast, a closed-loop for condensation cooling was preferable to avoid coolant losses. Again, the process parameters at condensate and the cooling sides need to be measured for integral analysis.

3.4. STANDARD FACILITY DESIGN OVERVIEW

Figure 3.1 represents an overview of the test facility design process. The overall process was categorized into three major stages- design parameters identification, process flow design, and data acquisition system as follows:

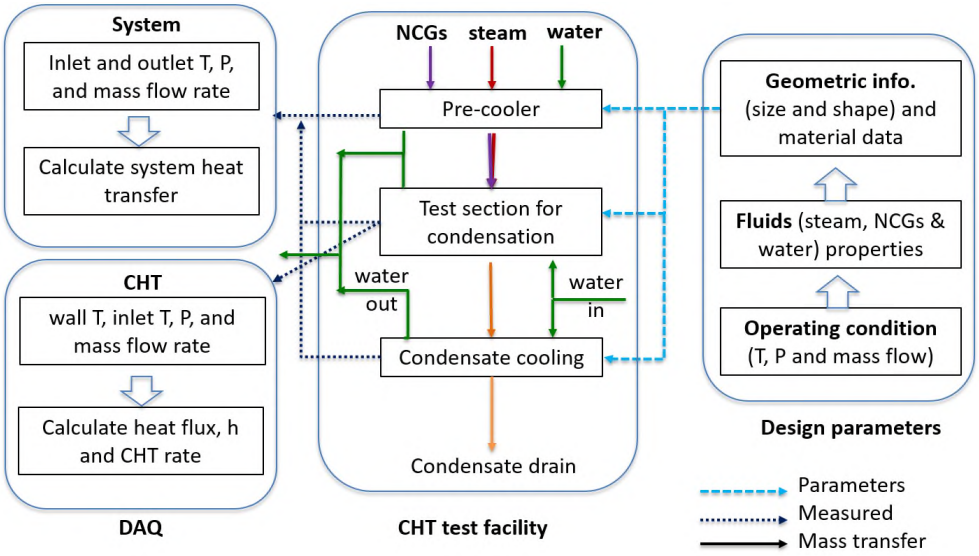

Figure 3.1. Overview of the test facility design

3.4.1. Design Parameters Identification. Initially, all the design parameters need to be listed and categorized, such as geometric information, fluid properties, and operating conditions. Geometric information includes test section pre-design geometric data and facility geometric limitations, i.e., size, shape, and materials. Then the suitable test fluids, as well as the operating conditions/ranges, need to be estimated.

3.4.2. Process Flow and System Design. After assigning all the design parameters, the fluid systems of the test facility need to be developed. The process consisted of a primary system- steam-NCGs mixture and a secondary system- cooling water, as shown in Figure 3.1. In the process flow, NCGs and the steam mixture were conditioned in the pre-cooler unit, then condensed.

3.4.3. Measurement and DAQ. In the third stage, the process parameters like temperature, pressure, and mass flow rate needed to be measured in the test sections, inlet-outlet, and system regions. A retardant temperatures measurement options were preferred at the radial symmetry (180 deg) along the axial locations in the test section.

3.5. TEST FACILITY DESIGN DESCRIPTION (PRE-DESIGN)

Initially, a simplified test facility was designed with a single test section, which was then modified by integrating all three test sections, as presented in Figure 3.2. This modular facility reduced overall construction and operation time. The steam from the steam supply was throttled and then mixed with small amount of non-condensable gas (NCG). Next, the mixture ran through a pre-cooler to condition the mix to a saturated state, and then the steam condensed in the test section, and finally drained after post-cooling.

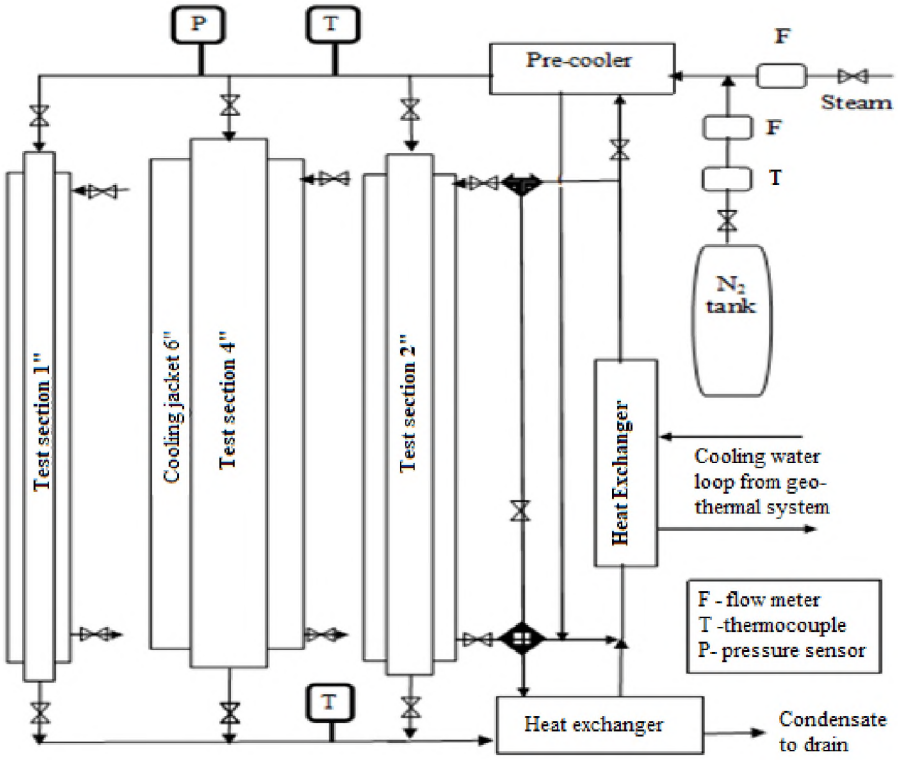

Figure 3.2. Modular test facility flow schematic Bhowmik *et al.* (2021c)

The modular facility was modified to form the final design, as in Figure 3.3, with additional NCGs and isolation valves. The measuring points included all the process parameters, like temperature (T), pressure (P), differential pressure (DP), and mass flow

rate (m). The test facility consisted of mainly three systems/units- steam and NCGs supply system, three scaled condensers (test sections), and a cooling water system. The details of the test facility were:

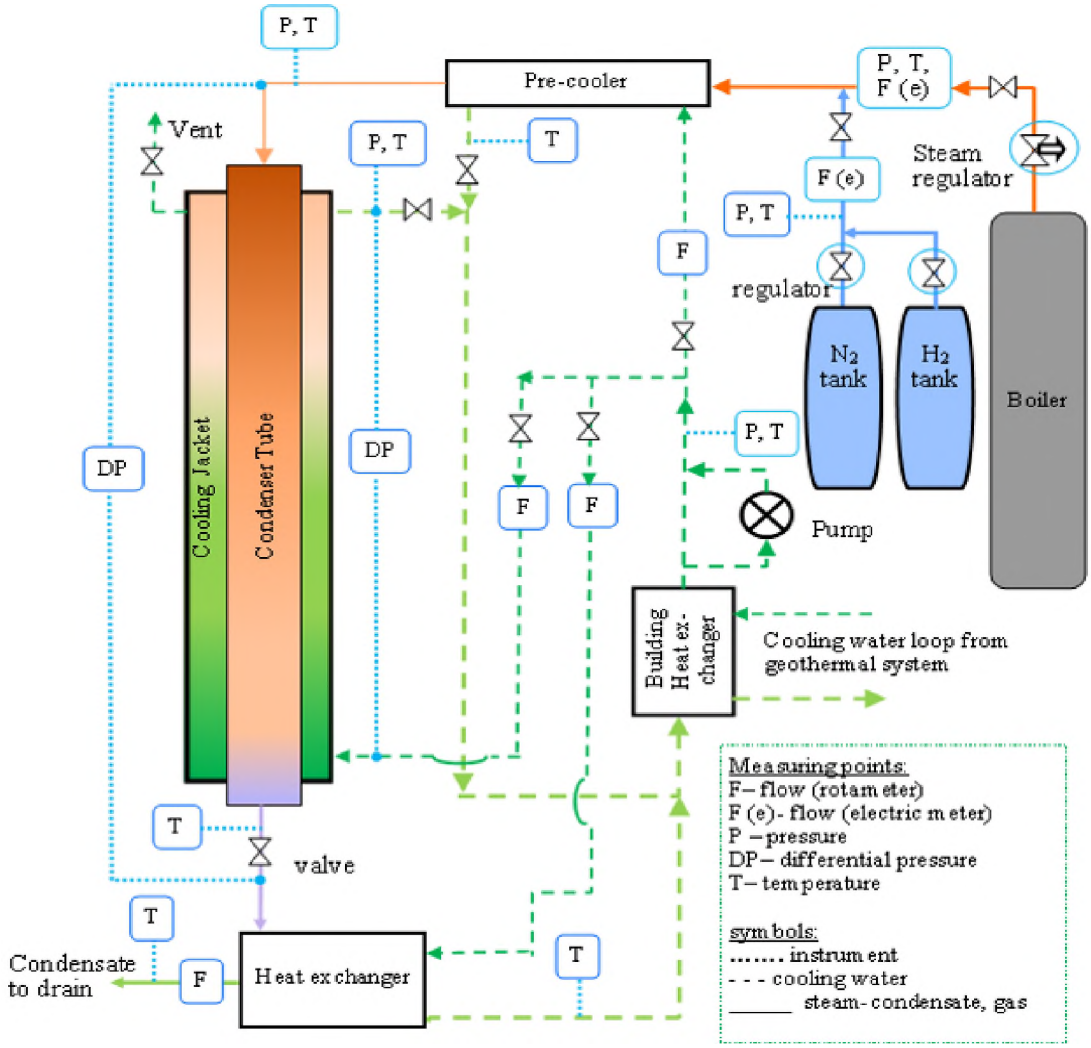

Figure 3.3. Instrument and control schematic Bhowmik *et al.* (2021c)

3.5.1. Steam and NCGs Supply System. For this study, steam was used from the in-house boiler's steam supply system. The design pressure of this boiler was 10 bar though, the maximum operating pressure was 6 bar. Thus, the boiler system supplies steam at a nominal pressure of 100 psi, and the maximum steam mass flow rate was 0.0675 kg/s. The steam flow was controlled and isolated by a throttle valve. Before the throttle valve, a

condensation drain line was installed with a separate isolation valve to remove condensation from the steam supply line. After the throttle valve, two independent pressure regulators reduced and maintained the steam pressure for the experiment. The operating ranges of the two regulators were 75 psi and 15 psi. An electronic mass flow meter measures the steam flow rate. This meter also measures steam temperature, pressure, density, and viscosity.

In another circuit, NCGs (nitrogen, helium, and air) storage cylinders were installed with built-in regulators, pressure indicators, and isolation valves. Then, the cylinder's supply line was connected to the steam line to the test section. An electronic laminar flow element was used to measure the gas mass flow rate. Finally, the mixture of steam and NCGs enters the pre-cooler unit, which conditioned the steam-NCGs homogeneous mixture to saturated state before entering the test section. The mixture pressure and temperature at the entrance of the test sections were measured. Finally, the steam condenses within the test facility.

3.5.2. Instrumented Condensing Test Section. The test section is a concentric pipe system that was used to condense the saturated steam from the boiler, as shown in Figure 3.3. The outer jacket had cooling water flowing through it to remove heat from the steam. Thermocouples were placed at multiple locations to measure the temperature increase in the cooling water and the wall temperature to calculate the condensation heat transfer rates and heat transfer coefficients.

3.5.3. Cooling Water and Condensate-cooling System. The test facility used a building-geothermal cooling water supply at about 10 psi. The cooling water loop comprised of incoming and return headers. A pump with a bypass line was set in between the two headers to increase the operating pressure to 30 psi for a high mass flow rate. The cooling water system consisted of three test-sections, a jacket water cooling loop, a pre-cooler, and a condensate post-cooling heat-exchanger. The building heat-exchanger was used to sink heat from the closed cooling water system and maintain a fixed operating temperature range.

3.6. DESIGN CALCULATIONS

The design of the CHT test section and the facility consists of the following:

3.6.1. Heat Exchanger Design Principles. This study used three concentric tubes or double pipe heat exchanger geometries. The fluid temperature distribution for parallel and counter flow arrangements and a special case of condensing vapor displayed in Figure 3.4. In this study, the LMTD (log mean temperature difference) and the effectiveness-NTU (number of transfer units) were used.

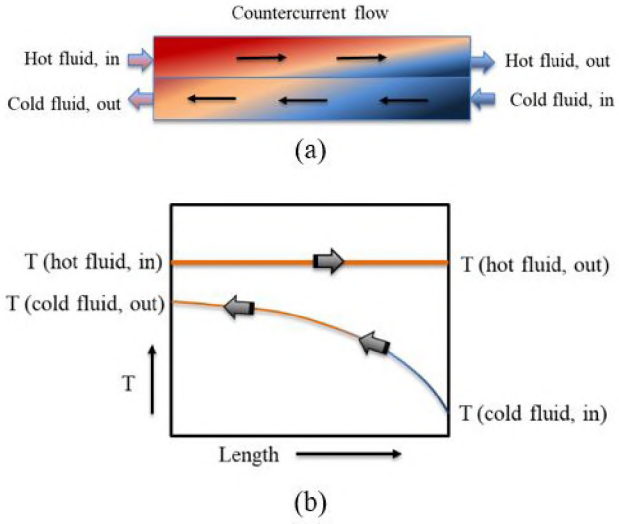

Figure 3.4. Counter-flow HE: (a) flow schematics, (b) T distribution (condensing case)

LMTD method requires specified inlet temperature (T_{in}), and outlet temperature (T_{out}). The necessary equations for LMTD method are:

$$q = UA\Delta T_{lm} = UA\frac{\Delta T_2 - \Delta T_1}{\ln(\Delta T_2/\Delta T_1)} \tag{3.1}$$

$$UA = \frac{1}{R} = \left[\frac{1}{(hA)_c} + R_{cmad} + \frac{1}{(hA)_h}\right]^{-1} \tag{3.2}$$

where, q is the heat flux (kW/m^2), A is the heat transfer surface area, R is the equivalent resistance. U and h are overall, and convective heat transfer coefficients.

The effectiveness-NTU i.e. $\varepsilon - \text{NTU}$ method is preferable when only T_{in} is known. In this method, the design case can be two types, as shown in Figure 3.5. The $\varepsilon - \text{NTU}$ method has two design cases:

- Analyze existing design to find T and q for given inlet conditions
- HE designs to determine type and size to match the required flow and T.

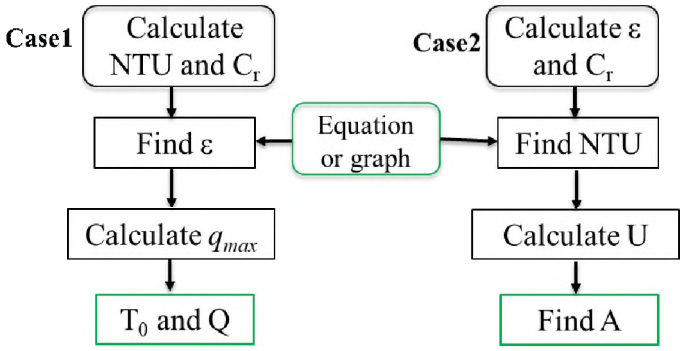

Figure 3.5. HE design steps with NTU methods

The equations used for the $\varepsilon - \text{NTU}$ method were:

$$\varepsilon = \frac{q}{q_{\max}} = \frac{q}{C_{\min}\left(T_{h,i} - T_{c,i}\right)} = f\left(\text{NTU}, \frac{C_{\min}}{C_{\max}}\right) \tag{3.3}$$

$$\text{NTU} = f\left(\varepsilon, C_r\right) = \frac{UA}{C_{\min}} \tag{3.4}$$

Where, $C_{\min}$ and $C_{\max}$ are the maximum and minimum of the heat capacity. For condensation case the ratio of heat capacity, $C_r = 0$ and hence, the effectiveness is:

$$\epsilon = 1 - \exp^{-\text{NTU}} \tag{3.5}$$

3.6.2. Conservative Design Criteria. In this study, conservative design principles are adopted to ensure facility safety and integration. The primary design requirements are present in Table 3.1. The necessary design steps are- (a) calculate steam flow rate for pressure range 15-150 psi, (b) calculate coolant mass flow rate and pipe size, T measurement points, and (c) design the rest of the system (pre-cooler, cond HE, gas flow, and piping).

Table 3.1. Primary design requirement

Design Parameter	Design Requirement
Jacket water T inlet/outlet	20 °C/80 °C
Test section steam condition	15 to 150 psi, 100 to 180 °C
Pre-cooler outlet	Saturated steam

3.6.3. Scaled Test Section Design. The test section is a concentric pipe system designed to condense the saturated steam from the boiler. The final design geometries are as Table 3.2, considering the primary design requirement and the conservative approach.

Table 3.2. Scaled design geometries

Test Section	Steam tube SS304	Water Jacket SS304
1	1" SCH 10	2" SCH 40
2	2" SCH 10	4" SCH 40
3	4" SCH 10	6" SCH 40

The test sections presented in Figure 3.6, with the thermocouple marked, was made of stainless steel material. The steam and water tube schedule are 10 and 40, respectively. This design allowed jacket water flows at 15-35 psi to maintain inlet/outlet temperature at approximately 20/80 °C.

Steam and water tubes were welded with cover-plates and flanges, as shown in Figure 3.7. Twelve threaded Teflon rods (¼"-20 NPT) were placed in the axial location to keep the steam tube appropriately aligned.

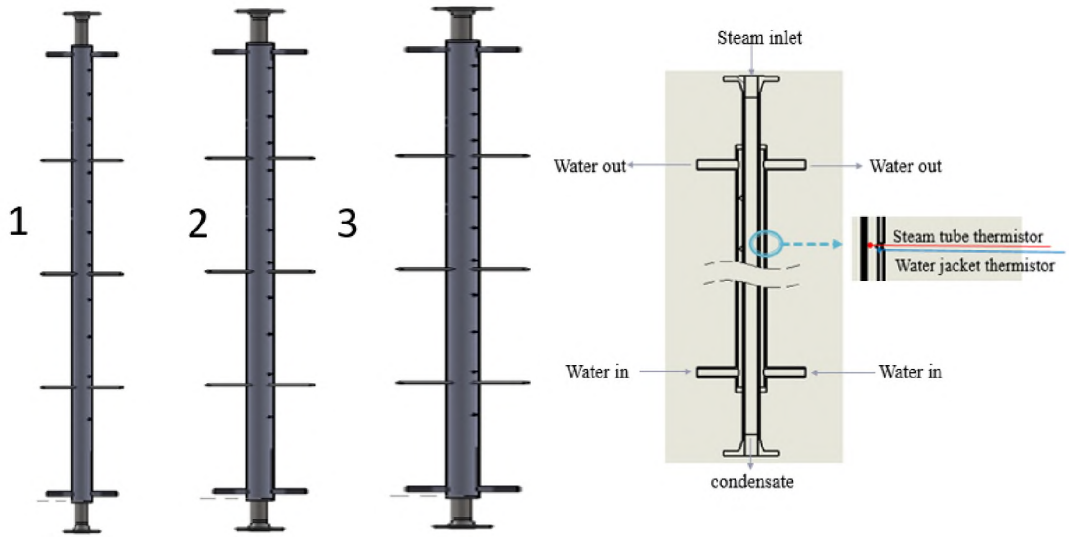

Figure 3.6. Test section: (a) Scaled design and (b) cut-view

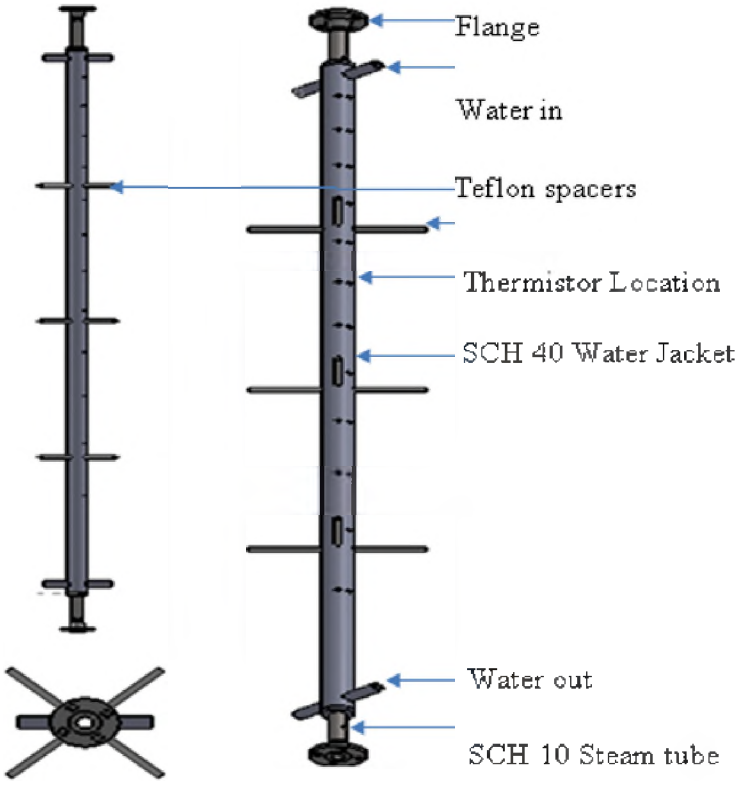

Figure 3.7. Top, front and Isometric View of Test Facility

3.6.4. Placement of the RTDs in the Test Sections. The axial placement of the thermocouples is calculated to minimize measurement uncertainty as per thermocouples factory tolerance (±0.2 °C) using mass and energy balance equations. Then by solving the balance equation, the temperature to the axial distance was calculated.

$$dq = mc_p d\mathrm{T(z)} = UAd\mathrm{T(r)} \tag{3.6}$$

$$\mathrm{T_z} = \mathrm{T_{in}} - (\mathrm{T_{sat}} - \mathrm{T_{in}})\exp^{(-\alpha z)} \tag{3.7}$$

where, α was a constant, which depends on the fluid properties and geometry of the system. The specific heat, heat transfer surface area, and overall heat transfer coefficient were c_p, A, and U, respectively. The overall heat transfer coefficient, U was obtained from the convective and conductive resistances of the steam and tube. In total, 44 RTDs measured the temperature of the steam tube outer wall ($\mathrm{T_{wo}}$) and cooing jacket tube inner wall ($\mathrm{T_a}$) at different axial locations, as shown in Figure 3.8.

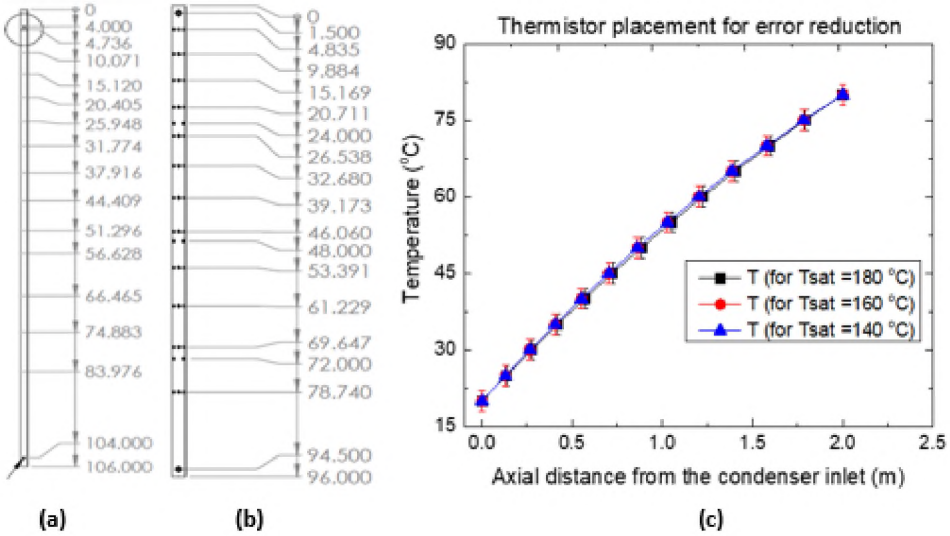

Figure 3.8. RTD location in (a) inner tube, (b) outer tube and (c) axial T distribution

To measure the outer wall temperature, T_{wo} accurately, the contact between RTD and the tube wall is very significant. To ensuring a good connection, twenty-two small indentations are prepared, and contact filled up with a high conductive gel.

3.6.5. Fabrication and Facility Construction. Fabrication work was done in a regular machine workshop. Dye penetration tests and a hydro test confirmed the integrity of the welding. The test sections were mounted on the test bench with piping and valves. The test bench was a steel frame structure that supports the test section. The pipeline, fittings, and isolation valves were chosen with consideration to the operating pressure and temperature. A fixed diameter section was used before each flowmeter to get a fully developed flow. Finally, all the instruments and sensors were installed. Figure 3.9 presents the test facility before insulation.

Figure 3.9. Constructed test facility before insulation

3.7. ADVANCED INSTRUMENTATION

The following instruments, sensors, and data acquisition systems were used-

3.7.1. Thermistors. The temperature sensors (model: PR-25 CUD-3-100-A-1/4-0600-M12) were chosen to operate in a wide range of temperatures -50 to 250 ºC with *pm* 0.2 ºC tolerance. The model sensor had a straight sheath with 1⁄4 NPT mounting, Class A, 100 Ω, 1/4 " diameter, 6" long, and M12 male connector. These thermistor sensors were suitable for steady-state operation with a response time of 14 seconds and operating current of 12μA. A total of 44 of these thermistors were placed in the test section at the different axial locations to measure temperature by measuring the differential resistance.

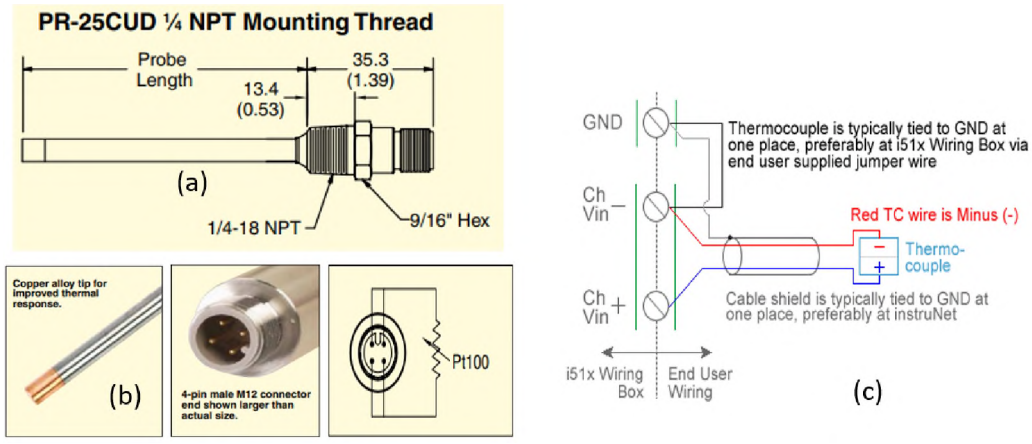

Figure 3.10. RTD (a) Dimentions, (b) tip-cable configuration, and (c) interface circuit

3.7.2. Pressure Transducers. Differential pressure transducers ST3000 920 E1H-0000-5-D7E9F Yamakate were used to measure the differential pressure along the length of a pipe or test section. This transducer has a working temperature range of -40 ºC to 180 ºC and a working pressure range of 2kPa to 21MPa with a measuring span of 0.75kPa to 100kPa. The uncertainty for this varies inversely with pressure, and it is about 0.1%.

3.7.3. Laminar Flow Element for NCGs. Aalborg GFMS-015178 is a laminar flow element gas flow meter. It was installed to measure the NCGs flow rate. The flow meter was factory-calibrated for atmospheric pressure. At higher pressure than the atmospheric pressure, it can be re-calibrated by correcting the flow rate, as follow:

$$Q_p \mu_p = Q_{atm} \mu_{atm} \tag{3.8}$$

Where, Q_{atm} and μ_{atm} are the flow rate and viscosity of nitrogen at atmospheric pressure. Q_p and μ_p the flow rate and viscosity of nitrogen at a higher pressure.

3.7.4. Steam Mass Flow Totalizer. The mass flowmeter (model: InnovaMass 240i/241i iSeries was used. It offered mass or volumetric flow monitoring of gases, liquid and steam with additional three more process variables: density, pressure and temperature. It used 2 inch pipe and vortex principle. The alternating vortices created by the buffle body flex the piezoelectric sensor and they produce a frequency output that is directly proportional to the flow rate. The measurement accuracy up to 0.7% of reading; maximum temperature and pressure range are 200 ℃ and 750 psig, respectively. It is equipped with configurable 4-20 mA output with HART, Modbus and USB and RS-232.

3.8. FACILITY SAFETY ANALYSIS AND MODIFICATIONS

A process hazard analysis (PHA) scrutinizes each process component to determine potential deviations from a regular operation that leads to various monetary, environmental, and personal damages (Crawley and Tyler, 2015; Kletz, 1999). A PHA for CHT facility was performed on March 11-15, 2019, using HAZOP. The full facility was divided into five nodes. Table 3.3 exemplifies the nodes that were tied to the item numbers in each priority ranking.

Table 3.3. Sections considered during PHA

Node	Equipment/system	Design Intent
1	*Steam supply system*: regulators, valve, and flowmeter	To get regulated steam supply and to measure: mass flow, pressure and temperature
2	*Gas supply system*: regulators, valves, and flowmeter	To get regulated NCG flow and to measure: mass flow, pressure and temperature
3	*Cooling loop*: pre-cooler and building heat exchanger	To get saturated steam by cooling water with a pump
4	*Condensing test section*	To measure CHT rate of steam with NCGs
5	*Condensate cooler*	To cool condensate to safe discharge

The review of the HAZOP (hazard and operability study) showed ranked hazards from high priority- A, to very low priority- D (Dunjó *et al.*, 2010). All hazards/risk-rated A should be addressed immediately, either through drastic design change or control logic (Kletz, 1997). B Ranks should be treated by implementing design changes, if necessary. The C rated risks need to be addressed by standard operating procedures or proper control. D tagged risks should be kept in mind as the potential risk (Kletz, 1999). For example, failure or deviation of operation that creates high, low, or no flow/pressure conditions, should be priority ranked. Each deviation linked with potential causes, engineering, and administrative controls. Next was to evaluation of the deviation consequences and recommended reduction of the possible damages (Crawley and Tyler, 2015). Several design modifications were implemented to ensure safe operation. Also, the team followed the general recommendations like providing proper training, developing standard operating procedures (SOP), and using fail-safe components, control logic, and process. Finally, a shakedown test was performed to check possible leaks and system integrity.

4. DATA REDUCTION METHOD AND EXPERIMENT

A data reduction method developed to perform the test data analysis was the main focus of this section. To accomplish this, a novel standard- scaled test facility designed and constructed with three different diameter vertical concentric tubes test sections. Saturated steam was used as the working fluid with NCGs (such as nitrogen, helium and air) and water was used as the coolant. Repetitive tests and calibrations were performed to ensure test data reproducibility. A time-averaged data was used to represent steady state condition, uncertainties quantified and presented.

Keywords: Condensation heat transfer, scaled test, and data reduction method

4.1. BACKGROUND AND CONDENSATION PHYSICAL PHENOMENA

The data reduction method was utilized to obtain high resolution test data with low uncertainty. Two sets of thermocouples were placed to get the condensing-tube-outer surface and the cooling-tube-inner surface temperatures with symmetric positions. Test data were recorded for a wide range of steam mass flow rates and pressure drops. The test facility system parameters like, pressure, temperature and flow were recorded for integral test analysis for energy balance.

Physics phenomena is very important for data reduction method development. Figure 4.1 represents the schematics for the physical process of steam condensation inside a vertical tube with a jacket water annular cooling. The steam flows downward and the coolant flows upward. It is a simple counter current heat exchanger. A symmetry half is illustrated starting from the axisymmetric pipe center line to adiabatic (insulated) wall.

Steam-NCGs mixture enters the condensation test section at a uniform velocity, $u(z)$ at $z = 0$. The inlet temperature, pressure, and gas mass fraction are T_{inlet}, P_{inlet}, and mg, respectively. Thus, the mixture is cooled by the annular cooling water flow. Heat transfer

from the hot mixture to the coolant occurrs through the tube wall, as shown by the heat flux, q″. The condensing tube thickness, surface roughness, and material properties, such as thermal conductivity (k), affects the fluid flows and heat transfer performances. The schematics of the flow and temperature profile are illustrated in the Figure 4.1. Mixture temperature, $T^s_\infty(z)$, and velocity, v, are the maximum at the center line, and their profile decrease radially.

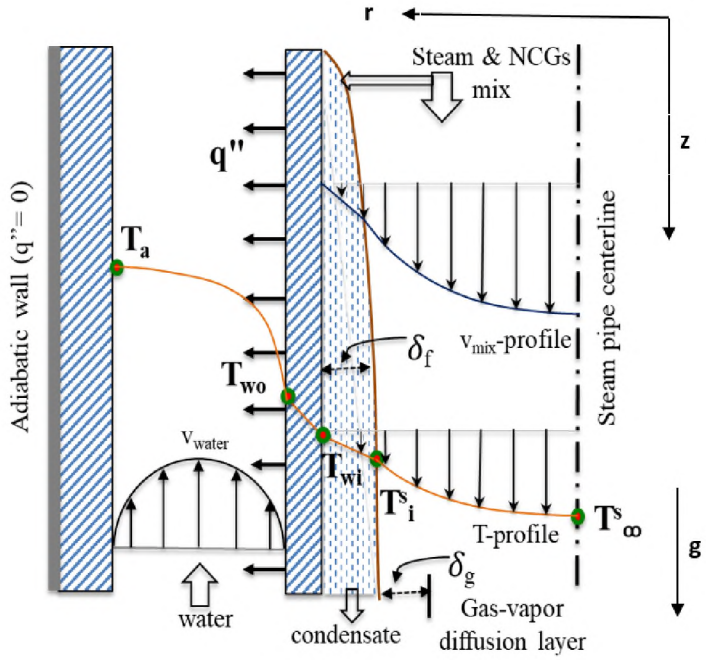

Figure 4.1. CHT physical phenomena schematic

At the tube wall surface, steam velocity is zero as no-slip condition and steam come in contact with the tube inner wall (at T_{wi}) and cooled, condensed, and formed liquid film. The film temperature, T_f is always below the steam saturation temperature, $T^s(z)$. The film thickness, δ, develops axially and formes downward flow. The liquid film has lower heat transfer coefficient, h_f, than that of pure steam, h_s, and acts as the main heat transfer resistance for pure steam condensation.

The NCGs can not penetrate the liquid film, and hence, it accumulates in the film and vapor interfaces. As the NCGs has lower heat transfer coefficient, h_g, than that of steam, h_s, and liquid film, h_f, it reduces the interface saturation temperature, $T_i^s(z)$, and the overall heat transfer performance, h. Besides, $T_i^s(z)$ depends on interface vapor partial pressure, P_{vi}. The accumulation of the NCGs at the film-vapor interface also depends on the gas mass fraction and condensation rates. The temperature at the inner tube outer wall, the bulk coolant, and the outer tube inner wall are T_{wo}, T_{bulk}, and T_a, respectively.

4.2. METHODS AND DATA REDUCTION TECHNIQUES

Figure 4.2 presents the flowchart of the CHT data reduction method. The overall process can be grouped into (a) estimating coolant bulk temperature and local heat flux, (b) determining the local parameters such as experimental heat transfer coefficient, blowing parameter, and film thickness, and (c) using the dimensionless parameter and scaling, and calculating Reynolds number and Nusselt number.

4.2.1. Estimating Coolant Bulk Temperature and Local Heat Flux. The heat transfer between the mixture and coolant occurred through the tube wall. The local heat flux in the inner and outer surfaces of the condensing tube was identical and in the opposite direction. To estimate the local heat flux (q''), axial distribution of the coolant balk temperature, T_b, needed to be calculated. The T_b can be calculated from the measure coolant mass flow rate (W_c), and the numerically calculated temperature shape factor, F. The F was estimated using the tube wall temperatures, T_{wo} and T_a. The T_{wo} is the inner tube outer surface, and T_a is the outer tube inner surface temperature.

The energy balance equation was used to determine local heat flux. At first, the jacket water cooling temperature, T_a, instead of axial coolant bulk temperature, T_b, was used to approximate the heat flux, $q''_{wi}(z)_{approx.}$

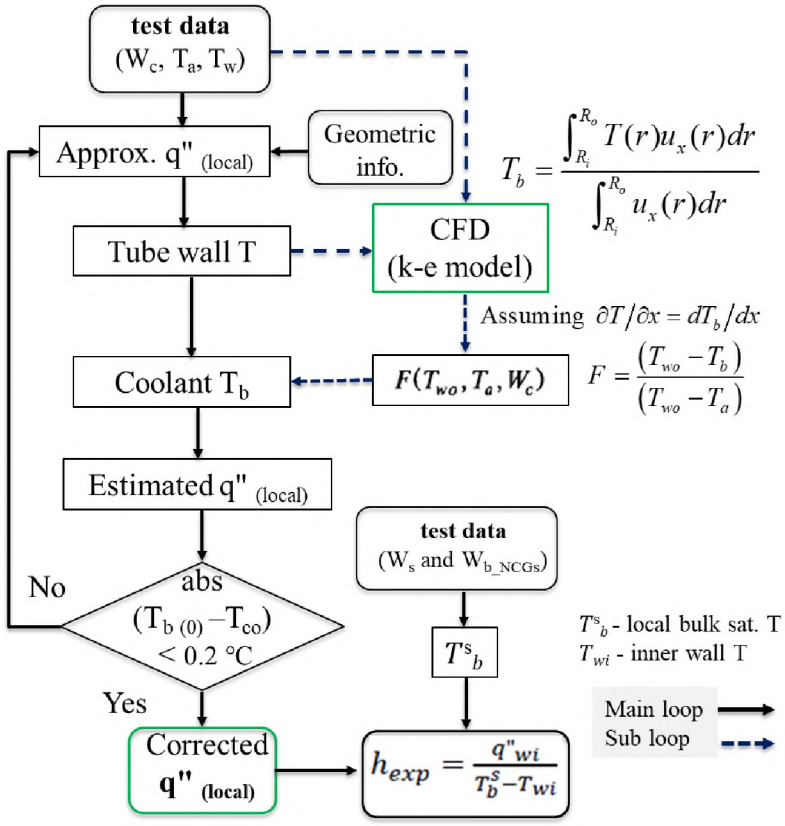

Figure 4.2. Local heat flux and heat transfer coefficient estimation

$$q''_{wi}(z)_{approx.} = -\frac{W_c c_p}{\pi d_i}\frac{dT_a(z)}{dz} \tag{4.1}$$

Then, using the approximated heat flux, the temperature at the inner and the outer wall of the condensing tube were calculated using

$$T_{wi} = T_{wo} + \frac{r_i q''_{wi}(z)\ln\left(\frac{d_o}{d_i}\right)}{k_w} \tag{4.2}$$

Next, T_{wo} and T_a were used as the boundary conditions (B.C.) for estimating the axial temperature distribution of bulk coolant, T_b. For a strong mixing, as a result of turbulent flow, the variable boundary conditions had only a minor effect on temperature profile. The axial T_b for coolant is presented as fllows:

$$T_b = \frac{\int_{R_i}^{R_o} T(r)u_z(r)dr}{\int_{R_i}^{R_o} u_z(r)dr} \tag{4.3}$$

Several researchers estimated the bulk temperature numerically using the mass, energy, and momentum balance equations and modeling turbulences. In this study, it was estimated using the CFD analysis with $k-\varepsilon$ turbulence model. Considering a fully developed flow i.e., assuming $\partial T/\partial z = dT_b/dz$, the normalized temperature distribution, the temperature profile factor, F, is calculated for different mass flow rates and wall temperatures.

$$F = \frac{(T_{wo} - T_b)}{(T_{wo} - T_a)} \tag{4.4}$$

Finally, the coolant mass flow rate (W_c) and axial bulk temperate to estimate the actual heat flux, $q''_{wi}(z)$ as:

$$q''_{wi}(z) = -\frac{W_c c_p}{\pi d_i}\frac{dT_{b,c}(z)}{dz} \tag{4.5}$$

This presented data reduction method provides a strong estimation of the axial T_b and F. However, at the entrance, flow was not fully developed, and at the exit, there were flow disturbances due to rapid flow area and direction change. To avoid the uncertainties, test data were taken from certain distances from the entrance and exit.

4.2.2. The Local HTC, Blowing Parameter, Film Thickness. In this study, saturated steam and NCGs mixture were used as the working fluid. The inlet steam temperature is equal to the bulk saturated temperature, $T^s_\infty(z)$ or $T^s_b(z)$. The estimated heat flux, $q''_{wi}(z)$, and condensing wall temperature, T_{wi}, were used to estimate local HTC, h_{exp}.

$$h_{exp} = \frac{q''_{wi}}{T^S_b - T_{wi}} \tag{4.6}$$

where T_b^s and T_{wi} are the vapor bulk saturation temperature and tube inner wall temperature, respectively. A smooth laminar film thickness and condensing film flow per unit perimeter as per equation 4.7 was calculated from the hydrodynamic analysis.

$$\Gamma = \frac{g}{\mu}\rho_1 \left(\rho_1 - \rho_m\right) \frac{\delta_f^3}{3} + \frac{\rho_1 \tau_i \delta_f^2}{2\mu_1} \tag{4.7}$$

Interfacial shear stress τ_i considering condensation suction effect is as follows:

$$\tau_i = 0.5 f_{io} \rho_m \left(u_m - u_i\right)^2 \frac{\beta_f}{\exp\left(\beta_f\right) - 1} \tag{4.8}$$

where u_m is the bulk steam–gas mixture velocity, u_i the interface velocity, and the blowing parameter, β_f, for momentum transfer is presented as

$$\beta_f = \frac{m''}{\rho_m u_m f_{io}/2} \tag{4.9}$$

where $m^{"}$ has a negative value of condensation mass flux. The laminar film thickness from equation equation 4.7 at $\tau_i = 0$ reduces to Nusselt's analysis as follows:

$$\delta_{fo} = \left(\frac{3\mu_1 \Gamma}{g\rho_1 \left(\rho_1 - \rho_m\right)}\right)^{1/3} \tag{4.10}$$

4.2.3. Dimensionless Parameters: Re and Nu. The laminar film thickness presented in Equation 4.7 was represented in a dimensionless form using dimensionless parameters, $Re_f = \Gamma/u_1, \delta_f^* = \delta_f/L, \tau_i^* = \tau_i/(\rho g l)$, and $L = \left(v_1^2/g\right)^{1/3}$.

$$\frac{Re_f}{1 - \left(\rho_m/\rho_1\right)} = \frac{\delta_f^{*3}}{3} + \frac{\tau_i^* \delta_f^{*2}}{2} \tag{4.11}$$

Finally, the film Nusselt number was presented with the characteristic length L.

$$Nu_f = \frac{h_f L}{k_f} = \left(Nu_{f,h}^4 + Nu_{f,tu}^4\right)^{1/4} \tag{4.12}$$

where $Nu_{f,la}$ and $Nu_{f,tu}$ were local laminar and turbulent Nusselt number, respectively. They are calculated as

$$Nu_{f,la} = \frac{1}{\delta_f^*} \tag{4.13}$$

$$Nu_{f,tu} = a\,Re_f^b\,Pr^c\left(1 + e\tau_i^{*f}\right) \tag{4.14}$$

4.3. EXPERIMENTAL PROCEDURE

A standard operating procedure (SOP) of S&T-CHT was developed, which consisted of shakedowns and final experiments.

In the shakedown test, the responses of the measuring sensors and instrument like thermocouples, flow, and pressure measuring devices at specific operating conditions were recorded and analyzed. Then, the fixed bias errors and uncertainty were primarily quantified, and necessary modification was adopted for data reduction and analysis. Also, the heat loss and integral energy balance calculations were performed within the safe operating ranges and conditions.

The second stage was the experimentation and data recording using different test sections, steam-NCGs flow, and pressure ranges. In the final stage, using the above discussed data reduction method, the test data were analyzed. For a safe start-up, operation, and shutdown, there were recommended start-up checklists and SOP.

4.3.1. Pre Start-up Checklist. The following checklists were used during pre start-up: (a) clean the work area and confirm that no safety concern for the experiment, (b) check the steam supply from the boiler at the main header, (b) confirm valves were in safe-fail mode, and no leakage in the steam, water, and NCG circuit, (e) confirm the data acquisition (DAQ) system working to monitor and record the process parameters.

4.3.2. Start-up Procedure. After confirming the pre-start-up checklist, then opening the main steam throttle valve, and dumping steam before entering the test section. The steam charge heats up and cleans the associated piping. Next, fill up the cooling water

loop by venting air adequately. The DAQ should monitor same temperature from all the thermocouples, as the cooling water loop was in an isothermal state. Then, run the water pump and increased the loop pressure to check any leakage. Finally, charge steam in the test section. Steam condensed in the test section, and then, it was cooled and drained. The flow control valve used to regulate flows of steam, water, and NCGs.

4.3.3. Steady-state Operation and Data Collection. The control of the steady-state conditions were performed by monitoring the system parameters on a computer via a DAQ. Data were recorded at intervals of one-third of a second and for about two minutes after the desired steady-state operating condition was reached and sustained for a short time.

In this study, the steam condensation performance and scaling analysis required a wide range of test data for different steam mass flow rate, weight percents of NCGs, and inlet pressures range. Therefore, the mass flow rates for the steam, cooling water, and NCGs have to be controled to get specific test conditions by adjusting inlet and outlet flow control valves (controlling the valve opening manually).

One of main challenges in CHT scale tests was to maintaining the same test conditions in the different test sections. The test data from different test sections needed to be comparable to keep the dimensionless process parameter, like Re and Pr, within the same range. Therefore, a wide range of tests data were recorded.

4.3.4. Safe Shutdown Procedure. Like a start-up, the closure should follow gradual reduction in the inlet steam flow to avoid unnecessary rapid temperate and pressure changes. The safe shutdown principle like shutting down the heat source (e.g. steam flow) first, and later, the heat sink (e.g. cooling water flow), need to be followed. The safe shutdown procedure were: (a) shutting the steam supply, (b) then, shutting the NCGs supply, (c) next draining the vapor-condensate-gas mixture, (d) finally, shutting the cooling water pump and draining the water from the loop.

4.3.5. Post Shutdown Checklist. The following checklist were maintained after shutdown: (a) no leakage, (b) safe-touch temperature of the pipe-fittings, (c) clean work place, (d) valves in a fail-safe mode, (e) recorded tests data and backup storage.

4.4. SYSTEM CHECK AND QUALITY ASSURANCE

4.4.1. Calibration. Calibration tests data showed that the measured temperature values had some fixed bias error. This source of the fixed bias error was from the thermistor input circuit and the shunt resistor. Experiments were conducted with low steam flow conditions to check the condensation performance calibration and data reduction program development. The fixed bias errors were removed. Temperature distribution (condenser tube walls, outer tube inner surface) at the condenser tube axial position is presented in Figure 4.3.

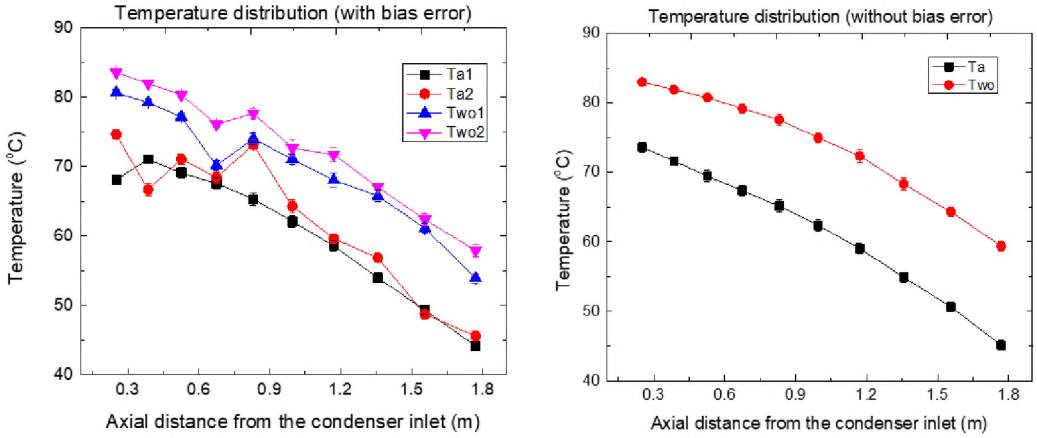

Figure 4.3. Axial T distribution: (a) before calibration, (b) after calibration

4.4.2. Quality Assurance and Uncertainty Quantification. The primary process parameters were mass flow rate, inlet-outlet temperature, and pressure of steam and water. They can be varied to check the heat transfer and condensation performance independently

and mutually. At the entrance region, the flow were not fully developed, and at the exit, there was some flow disturbance due to rapid flow area and direction changes. To avoid uncertainties, test data were taken from a certain distance from the entrance and exit.

The test data analysis was performed with standard error propagation methods. In this method, the total error σ_F of a function F and the relative error $\frac{\sigma_F}{F}$ were calculated by estimating error from independent measured variables $(x_1, x_2, x_3, \ldots\ldots x_n)$ as follows:

$$\sigma_F = \left[\left(\frac{\partial f}{\partial x_1}\sigma_{x_1}\right)^2 + \left(\frac{\partial f}{\partial x_2}\sigma_{x_2}\right)^2 + \ldots\ldots\ldots \left(\frac{\partial f}{\partial x_n}\sigma_{x_n}\right)^2\right]^{1/2} \tag{4.15}$$

$$\frac{\sigma_F}{F} = \left[\left(\frac{\sigma_{x_1}}{x_1}\right)^2 + \left(\frac{\sigma_{x_2}}{x_2}\right)^2 + \ldots\ldots \left(\frac{\sigma_{x_n}}{x_n}\right)^2\right]^{1/2} \tag{4.16}$$

In this study, the key parameter of interest were the experimental heat transfer coefficient, $h_{exp}(z)$, and the degradation factor, f, are presented as:

$$h_{exp}(z) = -\frac{W_{cw}c_p}{\pi d_i\,(T_{sat}(z) - T_{wi}(z))}\frac{dT_{cw}(z)}{dz} \tag{4.17}$$

$$f = \frac{h_{exp}(z)}{h_{Nu}(z)} \tag{4.18}$$

Finally, the relative error of $h_{exp}(z)$ and f were estimated using the relative propagation error definition as follows:

$$\frac{\sigma_{exp}}{h_{exp}} = \left[\left(\frac{\sigma_{w_{cw}}}{W_{cw}}\right)^2 + \left(\frac{\sigma_{c_p}}{c_p}\right)^2 + \left(\frac{\sigma_{d_i}}{d_i}\right)^2 + \left(\frac{\sigma_{(T_c - T_w)}}{(T_{sat} - T_{wi})}\right)^2 + \left(\frac{\sigma_{(cw/dz)}}{dT_{cw}/dz}\right)^2\right]^{1/2} \tag{4.19}$$

$$\frac{\sigma_f}{f} = \left[\left(\frac{\sigma_{h_{exp}}}{h_{exp}}\right)^2 + \left(\frac{\sigma_{h_{Nu}}}{h_{Nu}}\right)^2\right]^{1/2} \tag{4.20}$$

5. CFD AND SYSTEM CODE SIMULATION

A CFD study was performed to validate the STARCCM+ software for scaling of steam CHT with NCGs. The boundary and appropriate physics conditions from the test data were used. The condensation process was modeled by using the condensation-seed parameter as a source term for mass, momentum, and energy conservation equations. The multi-component gas model was used to define the steam-NCG, mixture and the implicit-unsteady numerical solver was chosen for better numerical stability. The mesh and time steps sensitivity analysis confirmed the optimum mesh size and time step. Simulations were conducted for various mass flow rates and NCG mass fraction. Finally, bulk fluid, inner and outer wall temperatures, and condensation HTC were compared with the test data to evaluate the scalability performance of CHT models.

Keywords: SMR, PCCS, condensation heat transfer, scaled test, CFD validation

5.1. BACKGROUND AND SECTION OUTLINE

This CHT study focused on the PCCS of SMRs. SMRs became popular for simplified modular construction with enhanced safety features. Similar to other nuclear reactors, SMRs design analysis for licensing is time-consuming and costly. Proper scale-test analysis and CFD validations can partly reduce this. Some initiatives were previously taken, like CASL and NEAMS, to develop a simulation toolkit and address technical issues of the reactor's performance and safety. However, the literature review showed a lack of proper validation of CFD for the scaling of PCCS. The previous simulation results were inconsistent due to unscaled geometric, fluid, and physics conditions. To bridge the research gap, three scaled vertical-concentric tube heat-exchangers were used (1", 2", and 4" diameter). Likewise, a half symmetry of the tube geometries were used to reduce computation time.

The governing equations for fluid flow and heat transfer are partial differential equations (PDE). Typically, these PDE's are not suitable for easy analytical solutions. To address this, the physics domain was divided into smaller subdomains, and the governing equations were discretized for each subdomain in different methods like finite volumes, finite elements, or finite differences. These discretizations converted PDE to simple algebraic equations, which were easy to solve for approximate solutions. Continuity of this approximate solution across the interfaces of neighboring subdomains was necessary to get the full solution for the entire domain. The subdomains were termed as elements or cells, and the total physical domain was called mesh or grid.

The CFD study followed some general steps, as shown in Figure 5.1. First, the geometry (2D or 3D) and mesh preparation. The meshing of computational domains played a pivotal role by discretizing the partial differential equations to a system of algebraic equations (Ahmed *et al.*, 2021; Tusar *et al.*, 2021). Then, physics and regions were selected and paired with associated boundary conditions. After that, the selection of necessary computational algorithms, discretization methods, and convergence criteria occurred.

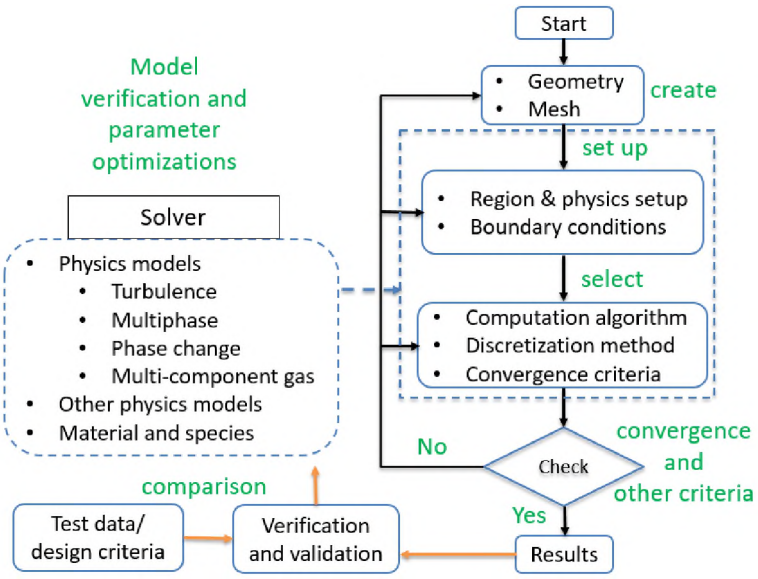

Figure 5.1. CHT CFD general steps

The physics and computation method required physical models and material properties. In the CHT CFD study, the necessary physics models were turbulence models, multiphysics models, phase change (condensation), multi-component gas models, and fluid films. These physics models maintain the conservation laws with their solver parameter settings (Shamim *et al.*, 2016). These settings required adjustment to verify the model and parameter optimizations. Next, a repetitive adjustment was required to get a proper physics and solution set up, which generated the solution within the convergence limit. Finally, the CFD results were visualized, verified, and validated with corresponding experimental data.

5.2. MULTIPHYSICS CFD SIMULATION

The multiphysics CFD studies used governing equations, appropriate turbulence models, physics models, precise geometries, and optimized meshes. These models and meshes were pivotal for CFD simulation to avoid inaccurate simulation results and solution error due to instability. Therefore, it was essential to use optimized mesh. To prepare optimized meshes, the basic strategies were: (a) using simplified but clean geometry, (b) maintaining an overall grid size, (c) using mesh refinement at critical areas and boundary layers, (d) assigning proper Y+ value and mesh convergence study.

5.2.1. Governing Equations. The conservation equations of mass, momentum, energy, and species were applied with the finite volume method in STAR-CCM+ software. The conservation transport equations in integral and differential forms were:

$$\underbrace{\frac{\partial}{\partial t}\int_V \rho\phi dV}_{\text{unsteady}} + \underbrace{\oint_A \rho\phi\mathbf{v}\cdot d\mathbf{A}}_{\text{convection}} = \underbrace{\oint_A \Gamma\nabla\phi\cdot d\mathbf{A}}_{\text{diffusion}} + \underbrace{\int_V \mathcal{S}_\phi dV}_{\text{generation}} \tag{5.1}$$

$$\underbrace{\frac{\partial\rho\phi}{\partial t}}_{\text{unsteady}} + \underbrace{\nabla\cdot(\rho\phi\mathbf{v})}_{\text{convection}} = \underbrace{\nabla\cdot(\Gamma\nabla\phi)}_{\text{diffusion}} + \underbrace{\mathcal{S}_\phi}_{\text{generation}} \tag{5.2}$$

The conservation equations of mass, momentum, and energy with species conservation, as presented below, applied the finite volume method in STAR-CCM+ software. In these equations, the symbols and subscripts are ρ for the density (mass per unit volume), v (velocity), S for the source (mass, momentum or energy per volume), t for time, the transport parameter, ϕ. The value of ϕ for continuity, momentum, energy, and species equations were: 1, **v**, e (energy per unit mass), and ω (mass fraction), respectively.

Other parameters like, P (pressure), f (body force), T (temperature), j (species), and D (diffusivity) came from the details of the momentum, energy and species equations.

$$\text{Continuity}: \quad \frac{\partial \rho}{\partial t} + \nabla \cdot (\rho \mathbf{v}) = S_m \tag{5.3}$$

$$\text{Momentum}: \quad \frac{\partial (\rho \mathbf{v})}{\partial t} + \nabla \cdot (\rho \mathbf{v}\mathbf{v}) = \nabla \cdot P + \rho f + S_{\rho v} \tag{5.4}$$

$$\text{Energy}: \quad \frac{\partial (\rho e)}{\partial t} + \nabla \cdot (\rho \mathbf{v} e) = \rho f \cdot \mathbf{v} + \nabla \cdot (P \cdot \mathbf{v}) + \nabla \cdot \left(k_{eff} \nabla T\right) + S_h \tag{5.5}$$

$$\text{Species conservation}: \quad \frac{\partial \left(\rho \omega_j\right)}{\partial t} + \nabla \cdot \left(\rho \mathbf{v} \omega_j\right) = \nabla \cdot \left(\rho D_j \nabla \omega_j\right) + m_j \tag{5.6}$$

5.2.2. Turbulence Modeling. The previous studies showed that the realizable $k-\varepsilon$ turbulence model with two-layer y+ treatment performed better than $k-\omega$ and RSM turbulence models for CHT modeling and analysis (Bian *et al.*, 2017). The $k-\varepsilon$ model satisfied the mathematical limitations of the Reynolds stress model with a new formulation for the turbulent viscosity and turbulence dissipation rate, ε; however, the standard $k-\varepsilon$ and RNG (Re-Normalisation Group) $k-\varepsilon$ were not realizable models. Thus, governing equations for the realizable $k-\varepsilon$ model used were:

$$\frac{\partial (\rho k)}{\partial t} + \frac{\partial \left(\rho \mathbf{w}_j k\right)}{\partial x_j} = \frac{\partial}{\partial x_j}\left[\left(\mu + \frac{\mu_t}{\mathrm{Pr}_k}\right)\frac{\partial k}{\partial x_j}\right] + P_k + G_b - \rho\varepsilon - Y_M \tag{5.7}$$

$$\frac{\partial (\rho \varepsilon)}{\partial t} + \frac{\partial \left(\rho \mathbf{w}_j \varepsilon\right)}{\partial x_j} = \frac{\partial}{\partial x_j}\left[\left(\mu + \frac{\mu_t}{\mathrm{Pr}_\varepsilon}\right)\frac{\partial \varepsilon}{\partial x_j}\right] + \rho C_1 \bar{S}\varepsilon - C_2 \rho \frac{\varepsilon^2}{k + \sqrt{v\varepsilon}} + C_{\varepsilon 1}\frac{\varepsilon}{k} C_{\varepsilon 3} G_b \tag{5.8}$$

Where, $C_1 = \max\left[0.43, \frac{\eta}{\eta+5}\right], \eta = S\frac{k}{\epsilon}, S = \sqrt{2S_{ij}S_{ij}}, C_{1\epsilon} = 1.44, C_2 = 1.9,$ and$\sigma_k = 1, \sigma_\epsilon = 1.2$. These equations represented the k or ε formulation in such a way that the rate of change in time and the transport by advection was equal to transport by diffusion with the rate of change (production-destruction). In these equations, the symbols and subscripts were: k (turbulence kinetic energy), ε (turbulence dissipation rate), G_b (generation term of k due to buoyancy), Y_M (fluctuating dilatation on ε), w (velocity), P (pressure), Pr (Prandtl number), S (source term), μ (dynamic viscosity), and ν (kinematic viscosity).

5.2.3. Condensation Theory and Model. The Star-ccm+ software used a fluid film model for steam condensation. The physics phenomena in the fluid film modeled a vapor region that condensed on a cold surface and increased the film thickness. This fluid-film model required the creation of a 2D shell region in the vapor-wall condensing interfaces and activation of the evaporation and condensation model. Therefore, the shell region interacted between gas and solid wall interfaces. In the fluid film model, the mass flux of each species was conserved at the region and interfaces as:

$$\rho_{g_s} Y_{g_{s,i}} \left(v_{g_s} - h\right) - \rho_{g_s} D_{g_{s,i}} \left.\frac{dY_i}{dy}\right|_{g_s} = \rho_{l_s} Y_{l_{s,i}} \left(v_{l_s} - h\right) - \rho_{l_s} D_{l_{s,i}} \left.\frac{dY_i}{dy}\right|_{l_s} \tag{5.9}$$

Where, subscript g, l, i, and s referred to the gas, liquid, interface, and surface, respectively. Similarly, the ρ, Y, v, h, and D represented phase density, mass fraction, velocity (normal component), film thickness, and molecular diffusion coefficient, respectively. The mass conservation in the interfaces was represented as: $\rho_{g_s}\left(v_{g_s} - h\right)$equal$\rho_{l_s}\left(v_{l_s} - h\right)$ with evaporation (or condensation as a negative value) rate as $m_v = -\rho_{l_s} h$. The evaporation and heat flux (for $Q_v = \Sigma_i^{N_v} \Delta H_i^{vap} m_{v,i}$) were:

$$m_{v,i} = Y_{g_{s,i}} m_v - \rho_{g_s} D_{g_{s,i}} \left.\frac{dY_i}{dy}\right|_{g_s} \tag{5.10}$$

$$k_g \left.\frac{dT}{dy}\right|_{g_s} - k_l \left.\frac{dT}{dy}\right|_{l_s} - Q_v = 0 \tag{5.11}$$

Where, k was the thermal conductivity, and N_v was the number of interacting components. In this software, both hydrodynamically limited and thermally limited approaches for modeling condensation were available, in which condensation occured below or at the saturation temperature, T_{sat}, respectively. For condensation below T_{sat}, the interfacial temperature, T_s calculated iteratively using the secant iterative method, as per following equations, in which n ranges from 3 to N_{it}.

$$f(T_s) = k_g \left.\frac{dT}{dy}\right|_{g_s} - k_l \left.\frac{dT}{dy}\right|_{l_s} - Q_v(T_s) \tag{5.12}$$

$$T_{s,n} = T_{s,n-1} - f_{n-1}\left(\frac{T_{s,n-1} - T_{s,n-2}}{f_{n-1} - f_{n-2}}\right) \tag{5.13}$$

Where, $T_{s,0}$ was the actual T_s at the optimizer entrance and $T_{s,1}$ was taken to be 5% below $T_{s,0}$ and T_{sat} limits the calculation of T_s for condensation, as addressed earlier. The saturation state was reached by any of the two conditions, $\Sigma_i^{N_v} Y_{g_{s,j}} = 1$ and $\Sigma_i^{N_v} Y_{g_{ooj}} = 1$ were fulfilled. The first condition stated that the T_s were equal to the boiling temperature. By contrast, the second condition indicated that for a pure vapor, only a quasi-steady equilibrium could be reached at the interface, as Ts reached the T_{sat}.

Finally, the film HTC was estimated by Equation 5.12, with an adoption of a dropwise condensation model's multiplying factor, $f_A = 2\pi N R_{eff}^2$, (only when $f_A < 1$), which was similar to the hydrodynamically limited model.

$$k_l \left.\frac{dT}{dy}\right|_{l_s} \approx \frac{2k_f}{h}\left(T_{l,c} - T_s\right) \tag{5.14}$$

Where k_f, h, N, and R represented the film thermal conductivity, film thickness, number of droplet seeds on the wall, and minimum seed radius, correspondingly. The model geometries were simple vertical condenser tubes, where the steam-NCG mixture flow downward, and annuls jacket water flowed upward. The condenser tubes (made of stainless steel) were equal length of 2.56 m, but different diameters.

5.2.4. Simulation Setup. The CFD simulation setup consisted of steps: geometry preparation, meshing, region, and physics setup with associated boundary conditions, as:

5.2.4.1. Geometry. In this study, three model geometries and Kuhn's test conditions were used for validating STAR-CCM+ CFD simulations, as shown in Figure 5.2. Half-sliced circumferentially symmetric model geometries, as shown in Figure 5.2 (a), were prepared in SOLID-WORKS and then imported to STAR-CCM+ for meshing. The half-geometries were used to reduce the simulation time and cost. The information of the reference, scaled-up and scaled-down geometries were listed in Table 5.1.

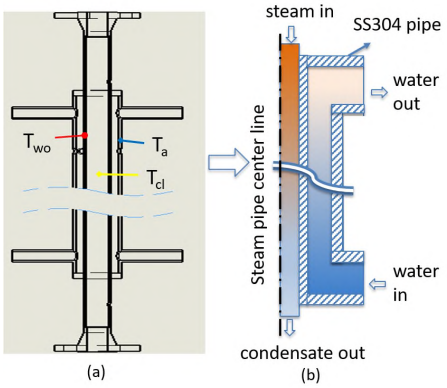

Figure 5.2. CHT CFD geometry setup: (a) full schematics (b) half geometry

Simulation was carried out for particular tests condition, as presented in Figure 5.3, using the scaled geometries. Results of the simulations for the scaled geometries and tests condition were used to identify the condenser tube diameter scaling effect.

Table 5.1. Model geometric information

Parameter	Scaled-down	Reference	Scaled-up
Steam tube			
ID (mm)	27.86	47.5	106.68
Thickness (mm)	2.77	1.65	3.05
Height (m)	2.56	2.56	2.56
Annular cooling tube			
OD (mm)	52.5	73.66	154.05

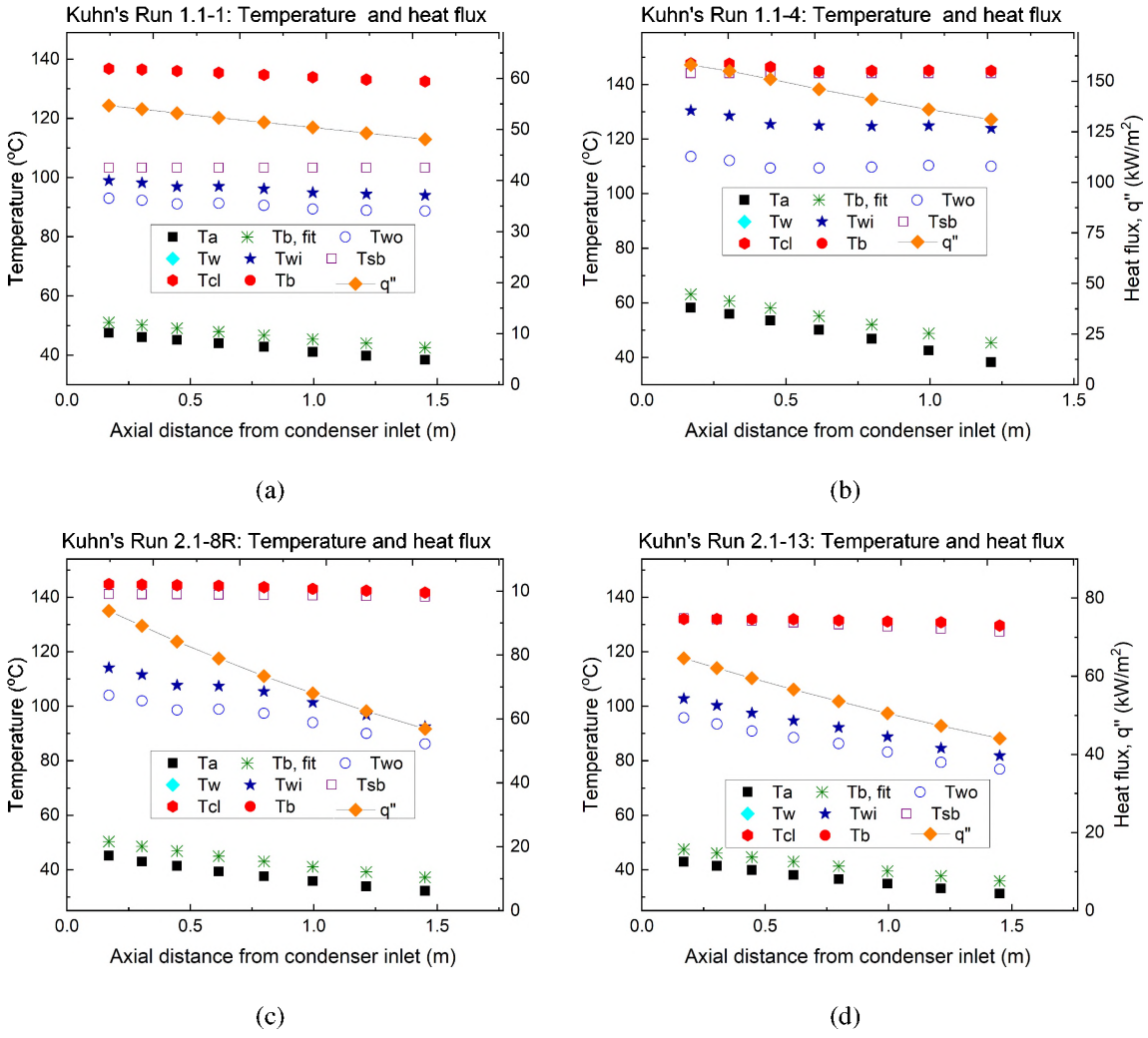

Figure 5.3. Test conditions (Temperature and heat flux): (a) run 1.1-1, (b) run 1.1-1, (c) run 2.1-8R, (b) run 2.1-13

The physics domain was separated in to an adiabatic entrance and a condensing section. The vapor flow developed thought the entrance section. Therefore, a fully developed flow was obtained at the condensing section. The test databases were reported for specific axial locations for pure steam and steam-helium/nitrogen/air mixture. The simulation studies were carried out for a particular test condition, as presented in Table 5.2.

Table 5.2. Kuhn's geometry and test cases info. Kuhn (1995)

Test cases	**Steam and Air**					**Water**		
	Steam flow	Air flow	Pin	Tin	Air (%)	Flow	T_in	T_out
run 1.1-1	60.2	0	113.9	138.8	0	999.8	31.5	52
run 1.1-4	60.2	0	405.2	148.8	0	1086	33.4	66.2
run 2.1-8R	51.2	8.87	413	145.3	14.8	925	27.5	52.5
run 2.1-8R	51.2	8.87	413	145.3	14.8	925	27.5	52.5

Note: Flow (kg/hr), temperature (C), pressure (kpa)

5.2.4.2. Meshing. Meshing plays a pivotal role in CFD analysis. Creating appropriate meshes was critical, as this study used a computational domain consisting of two fluid streams (counter-current flow) separated by a solid body. Moreover, there were two-phase flow (bulk mixture and condensate) in the steam region. Proper meshing to form cells and interface was essential, which allowed adequate transfer of mass, energy, momentum, and species.

All the physics domains were assigned regions to create a 3D volume mesh. In this process of region-based meshing, the following mesh models were applied: polyhedral mesh, prism layer mesh, surface remesh, and embedded thin mesh models.

The polyhedral mesh performed better than the simple square and triangular meshes, as reported by several researchers [ref]. The prism layer mesh worked well in simulating the boundary layer wall behavior. Thus, the polyhedral mesh was used for bulk steam and cooling water regions; whereas, embedded thin mesh was used for steel tube section. The surface remesher and prism layer mesh were used to improve fluid-solid interface mesh quality.

The domain parts were imported from CAD geometry and then assigned regions to create 3D volume mesh with associated continuum models in STAR-CCM+, as shown in Figure 5.2. Meshing continuum models were used: polyhedral mesh, prism layer mesh, surface re-mesh, and embedded thin mesh were used. In the steam and water regions, the polyhedral mesh model was used as base mesh; whereas, the prism layer mesh model was used for the wall treatment. In the steel tube region, the same mesh size of the interface was used, to confirm mesh quality and continuous interface preparation.

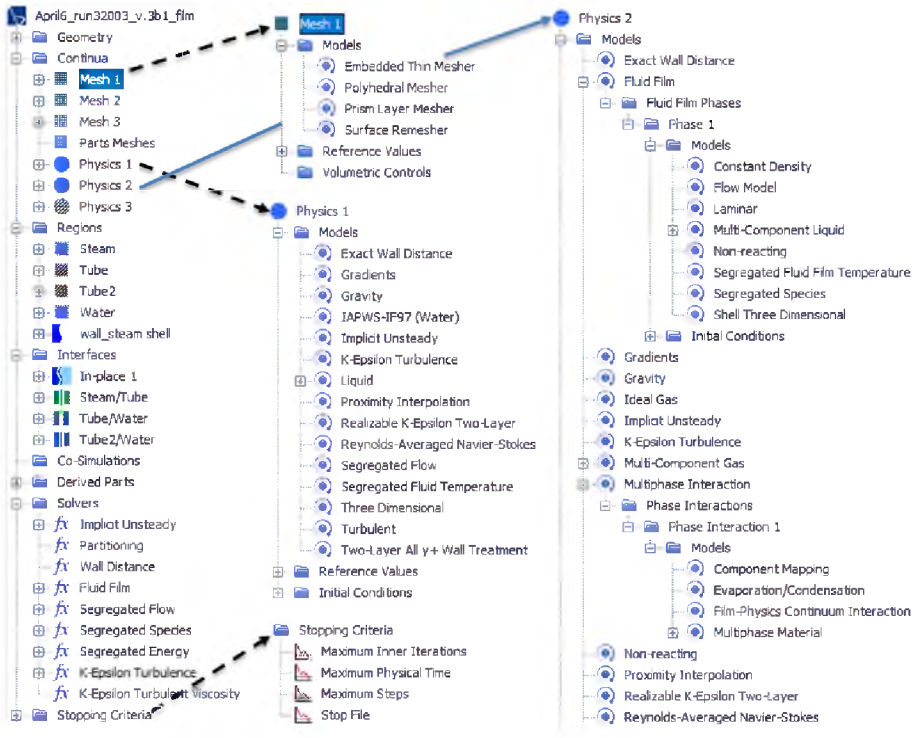

Figure 5.4. CHT CFD mesh and physics setup

The following steps were followed to prepare a high-quality mesh. First, a clean and defect-free geometry was used with no abnormal features, such as intersections or sharp outcroppings. Then, importance was given to select a suitable general mesh size from the previous studies, in which maintaining a lower skewness ratio was a key. Next, mesh refinement was performed at critical areas to balance computational time, cost, and accuracy.

After that, the boundary layer refinement or inflation was adopted, and it maintained a proper dimensionless wall distance value, or Y+, for the chosen turbulence model. Finally, detailed mesh convergence studies were conducted for selecting a optimized mesh size. This was done by repeating the previous steps and by increasing mesh fineness.

5.2.4.3. Region and physics setup. In this study, different applicable physics models were assigned to the steam, tube material, and the coolant regions. These models were adopted from previous studies to simulate the CHT Kuhn's test condition. This study considered the implicit unsteady state, as the physics properties of steam-condensate flow exhibited unsteady behavior. The available models, such as the fluid film model, the multi-component gas model, and the multiphase interaction model of the STAR-CCM+, were adopted. These models represented condensate film and the effect due to the presence of non-condensable gas. For turbulent flow modeling, the realizable $k - \epsilon$ model was used. The segregated solid energy and constant density models were used in the solid region; whereas, segregated flow, species and temperature models were used in the fluid regions. In addition to the two-layer, all y+ and exact wall distances were applied to the fluid regions. In the coolant water region, the IAPWS-IF97 material database was used. To apply the film model, a shell region was created for the steam-tube interface and condensate properties inserted manually, as an initial condition. The model mesh-geometry was divided into several regions with associated boundary conditions, as shown in Figure 5.5.

5.2.4.4. Boundary conditions. Inlet boundary conditions were set to mass flux in the water and steam regions, as per Kuhn's test data (inlet temperatures and pressure), and the outlet boundary condition was set to pressure outlet. For scaled geometries, the inlet velocities were scaled for the pipe diameters by keeping the same inlet Re because the test HTC depended on it.

Figure 5.5. CHT CFD region and solver setup

5.2.4.5. Other setup. The reference and initial values were taken from the Kuhn's tests to get a prompt simulation and avoid simulation instability. In the solver settings, the control parameters- the under-relaxation factors for the film velocity, film thickness, turbulence, and segregated energy- were adjusted to achieve convergence with stability.

5.2.5. Verification of the CFD Simulation. Mesh and models sensitivity tests were performed with different mesh sizes, prism layers, condensation models, and condensation seed parameters. Different time steps size, physical time, and number of inner iterations were used to check the solutions stability and convergence. These optimized parameters are presented in Table 5.3.

5.2.5.1. Mesh independence test. Mesh sensitivity tests were performed using different sizes of base meshes with varying prism layers (10% of the base). The strategy of mesh arrangement was devised to keep the smaller meshes to the adjacent wall area, and the bigger meshes to the tube center region, as shown in Figure 5.6 (b). This technique ensured low y+ value (within 1) and confirmed an appropriate boundary layer modeled

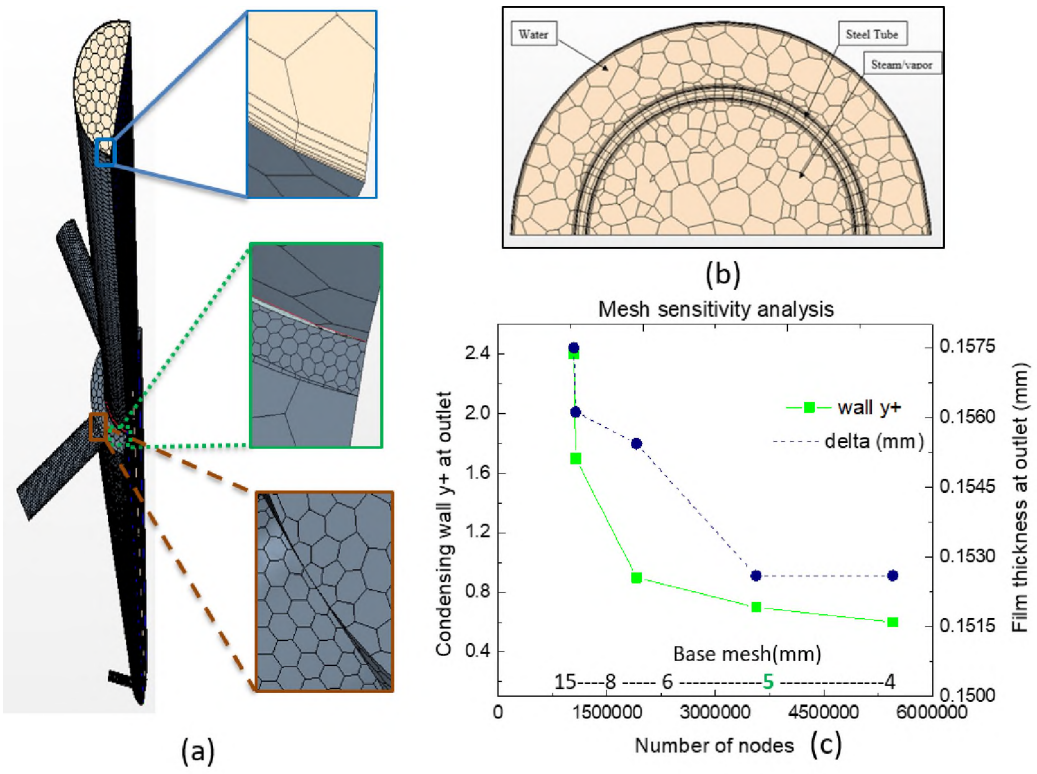

Figure 5.6. Meshing: (a) setup, (b) mesh-geometry front view, and (c) mesh sensitivity result of y+ and outlet condensate film thickness for different number of nodes (mesh sizes)

Table 5.3. Simulations mesh and model matrix

	Mesh		**Diffusivity Models**	**Iterations**
Model	Base Size (mm)	Prism layers (% of base)	Molecular diffusivity Kinetic theory	Inner iterations: 5, 10, 20
Kuhn's Test 2.18R	6.75, 6.5, 6, 5, 4, 3, 2	3, 5, 10, 12 (10, 20, 24)	Binary diffusion coeff., Schmidt number	Time steps: 0.5, 0.25, 0.2, 0.1 Time (min): 5, 10, 15, 30

in the near-wall region. The mesh sensitivity study presented in Figure 5.6 (c) indicated that for smaller mesh the variation of the condensate film thickness and y+ value also smaller. These were the key parameters representing the condensation rates and near-wall boundary viscous sub-layer. Therefore, the optimized mesh showed a strong match with other parameters, as shown in Figure 5.7.

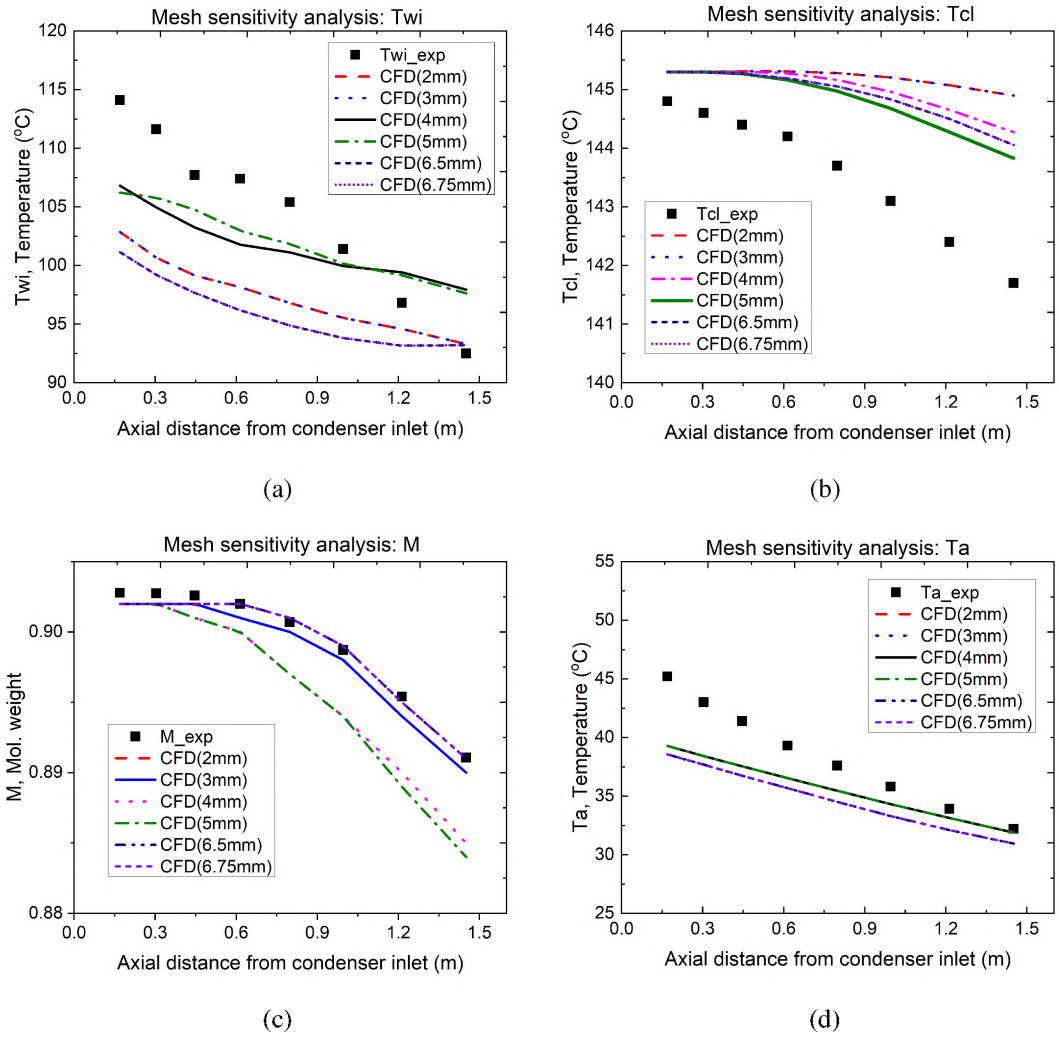

Figure 5.7. Mesh sensitivity result with test data of: (a) Ta, (b) Twi, (c) Tcl and (d) M, mole fraction

For the steam, water, and tube regions different optimized mesh sizes were utilized as listed in Table 5.4.

Table 5.4. Simulations optimized mesh size matrix

	Base mesh size (mm)			**Prism layer**
Geometry	*Vapor-mixture*	Tube (solid)	Water (coolant)	Number (% of base)
Scale-down	3	1	2	10 (25%)
Ref and scale-up	4	1	3	10 (25%)

5.2.5.2. Run time sensitivity test. In the study, an implicit solver was used to ensure stability of the CFD simulation irrespective of the time step size. However, time step, inner iteration number, and time were important parameters to obtain allowable convergence with limited computation time. The change in the mesh size was related to the time steps, as per CFL (Courant–Friedrichs–Lewy) condition (to keep CFL within 1). The CFL number was proportional to the fluid velocity multiplied by the ratio of time step size and mesh size, as per Equations. 5.15. This study verified the run time stability, while keeping the same CFL number, as presented in Figure 5.8.

$$C = \frac{\mathbf{u}\Delta t}{\Delta x} + \frac{\mathbf{v}\Delta t}{\Delta y} + \frac{\mathbf{w}\Delta t}{\Delta z} \leq C_{\max} \tag{5.15}$$

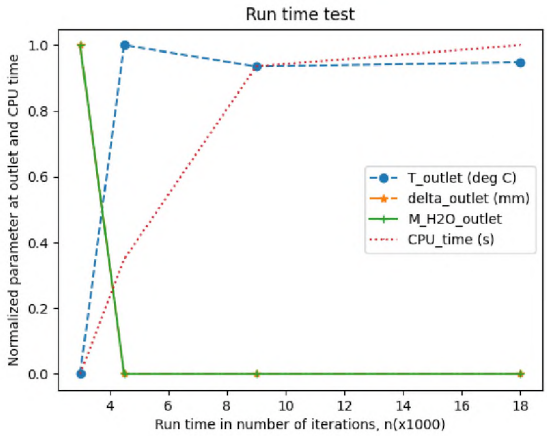

Figure 5.8. Run time sensitivity test of normalized parameter at condenser outlet (bulk T, M, and delta), and total CPU time

5.2.5.3. Verification of diffusivity models. The diffusivity of the molecules, or species, plays an important role in the condensation study. There are several methods and models for estimating the diffusivity in the STAR-CCM+ software, like molecular diffusivity, kinetic theory, binary diffusion coefficient, and Schmidt number. Simulation resutls using these models are presented in Figure 5.9, which shows that binary diffusivity model predicted better than other models, and therefore it was used in this study.

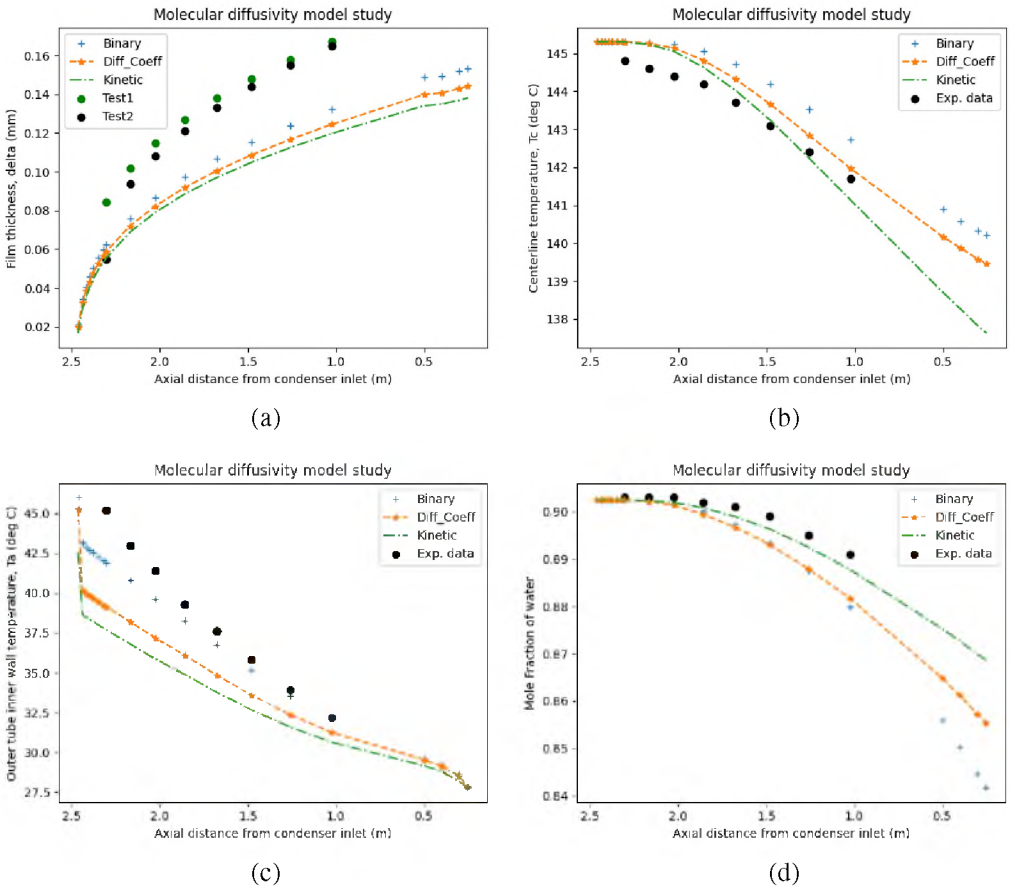

Figure 5.9. Molecular diffusivity models: (a) film thickness, (b) Tc, (c) Ta, (d) M

5.2.5.4. Seed parameter optimization test. The STAR-CCM+ software used a seed density as the source parameter for the wall condensation model. However, there was no recommended value for it in previous studies. Moreover, this parameter was not available in experimental studies, an assessment of the allowable range of seed parameters to initiate the condensation simulation was very critical. A parametric study was performed with different seed numbers from 1 to 100,000, and the fluid film thickness and steam-mixture centerline temperature from the CFD simulation were compared to Kuhn's test data, as presented in Figure 5.10.

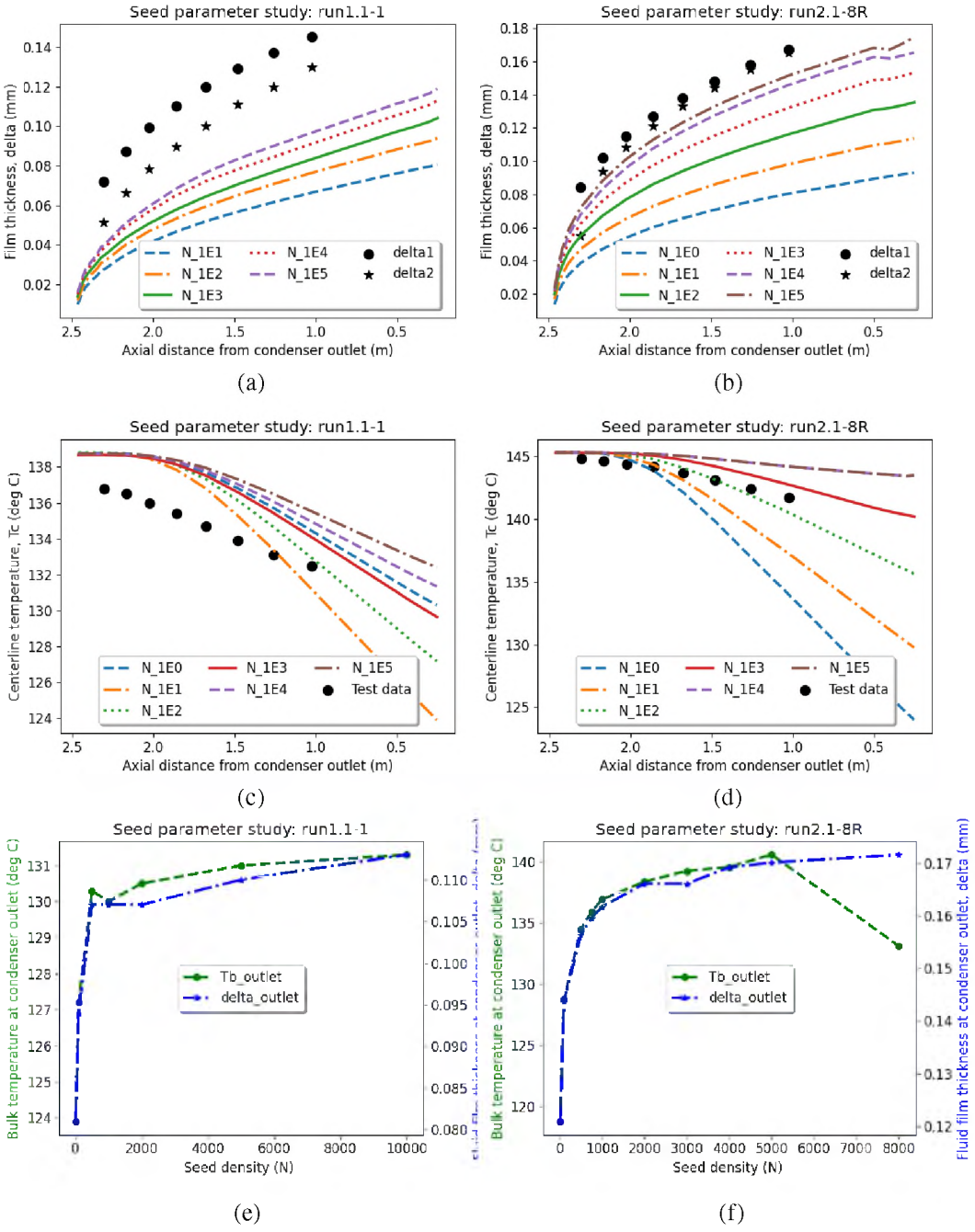

Figure 5.10. Seed parameter optimization: (a) film thickness, (b) centerline temperature, (c) condenser outlet centerline temperature and film thickness

Plots of fluid film thickness showed that it increased with the seed number. However, the experimental film thickness was higher than that of the CFD values. The Test1 data was considered with interfacial shear stress, but Test2 data did not. The higher seed numbers, 10,000 and 100,000, incurred low residual accuracy and high fluctuations. They also showed a high variation of the film thickness at the outlet region of the condenser section, as in Figure 5.10 (a)-(b). The centerline temperature data illustrated that seed values up to 100 deviated toward the condenser outlet, and seed values above 5,000 produced high simulation residuals and abrupt fluctuation, as in Figure 5.10 (c)-(d). Finally, a seed value range from 1000 to 5000 was optimum, considering both film thickness and centerline temperature data, as presented in Figure 5.10 (e)-(f). A seed value of 1000 was used in this study, as a conservative approach.

5.2.5.5. Verification turbulence models. Three turbulence models: $k-\varepsilon$, $k-\omega$, and the Reynolds stress model (RSM) were verified in the cooling water region to examine the temperature distribution, heat flux, and film thickness, as illustrated in Figure 5.11.

The temperature distribution plot, as shown in Figure 5.11 (a), for the three turbulence models showed: (a) the steam-NGS centerline temperatures were identical, (b) the condenser tube wall (outer) temperatures had higher variations than the annular tube adjacent coolant temperatures, and (c) overall, $k-\omega$ model predicted better than the $k-\varepsilon$ and RSM models; however, at the condenser entrance region, and for steam-air case the tube wall temperature prediction by $k-\varepsilon$ was better than other two models.

The heat flux distribution and film thickness on the condenser tube surface plot presents that the RSM predicted better than the other two models. The previous CFD studies used simplified geometries to avoid the inlet and outlet piping for the coolant regions; however, this study did not simplify the coolant flow geometries. Therefore, coolant flow incurred: anisotropic, streamline curvature, recirculation, and cross-flow, in which the RSM model was preferable (Mishra and Girimaji, 2013).

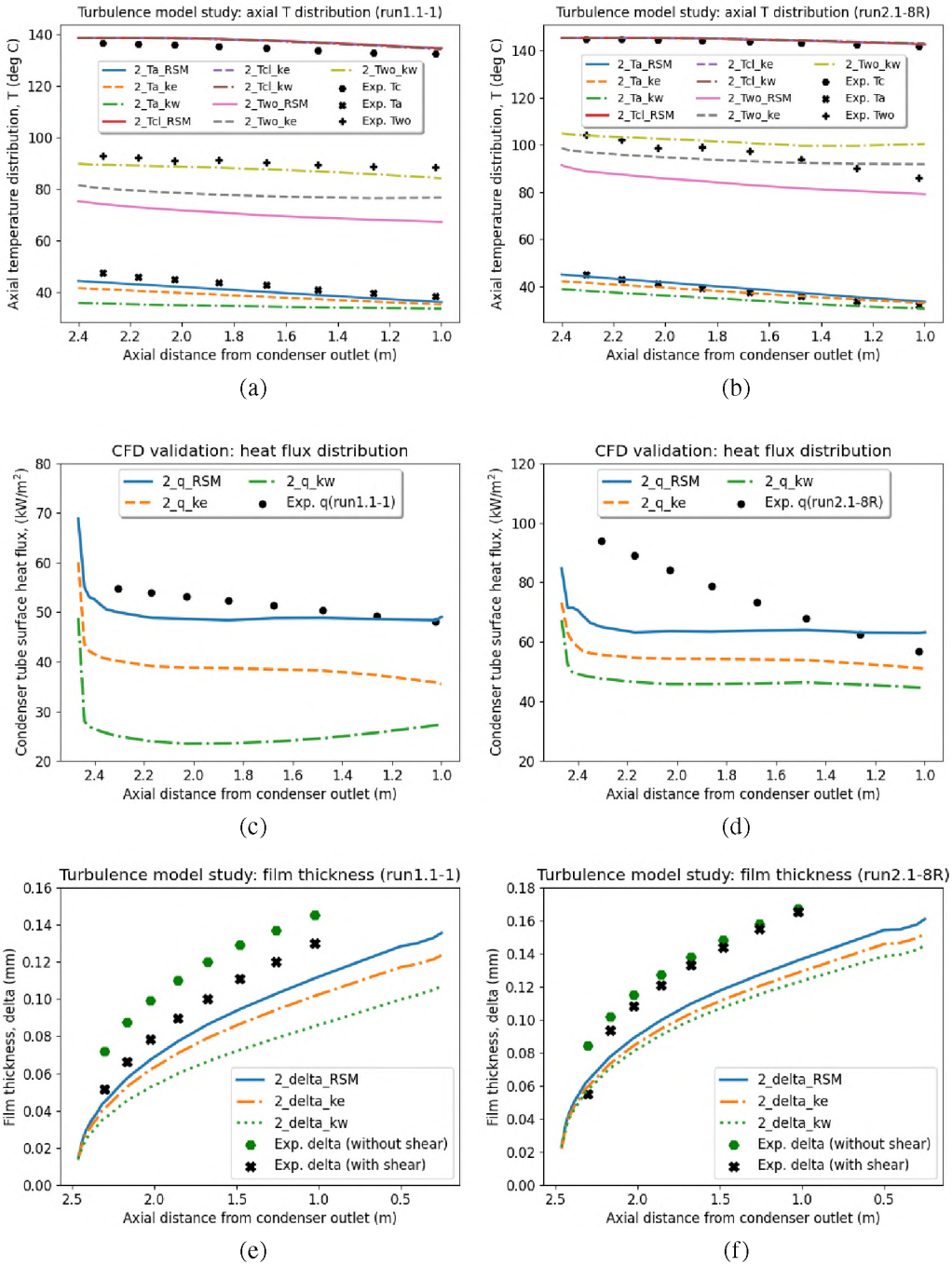

Figure 5.11. Turbulence model verification: (a)-(b) temperature, (c)-(d) heat flux, and (e)-(f) film thickness

5.2.5.6. Verification of velocity and temperature distribution. The velocity and temperature distribution within the CFD computational domain carried critical information, which could not be visualized in the experimental data. These velocities and temperature distribution profiles were used to verify the flow conditions, i.e., laminar, turbulent, or a transition between the laminar and turbulent regions. The axial velocity distributions and radial temperature distribution of the steam and coolant (water) regions at four axial positions (condenser tube height: 0.5 m, 1 m, 1.5 m, and 2 m) were presented in Figure 5.12 and Figure 5.13, respectively.

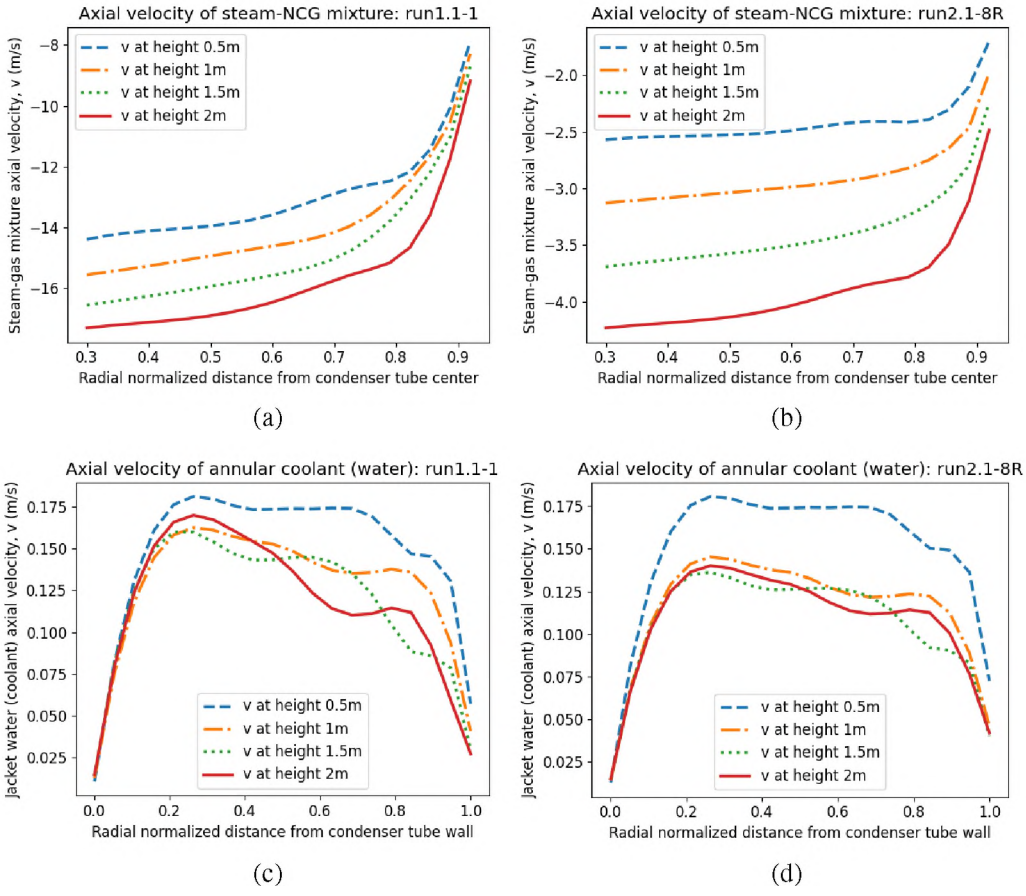

Figure 5.12. Velocity and temperature distributions: (a)-(b) axial velocity (steam), (c)-(d) axial velocity (water)

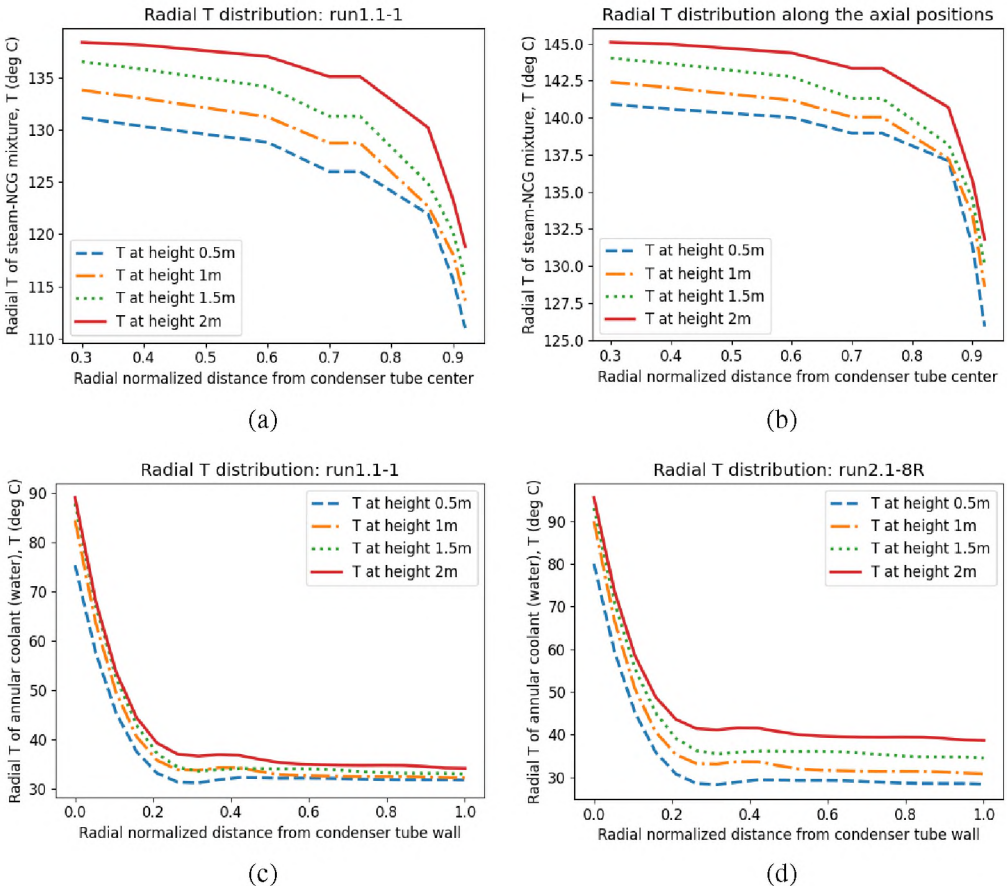

Figure 5.13. Temperature distributions: (a)-(b) radial temperature (steam), and (c)-(d) radial temperature (water)

The axial velocity of steam was downward, whereas the axial velocity of water was upward. However, both axial velocity plots were presented in the same direction. The steam axial velocities, as Figure 5.12 (a)-(b), plotted from the tube center to the tube wall in the normalized x-axis, showed that velocity magnitudes gradually decreased along with the axial positions, but velocity sharply decreased at a radial position adjacent to the condensing wall. This sharp decline in the velocity was due to the formation of the condensing liquid film, and at the condensing wall, the velocity was zero due to the wall no-slip condition. The axial velocity of the water region plotted from the condenser tube to the annular tube normalized positions in the x-axis, as Figure 5.12 (c)-(d), showed that velocity profiles

unchanged for axial position 1 m and above, which confirmed the fully developed flow. The velocity profiles had a parabolic shape with a peak near the heated surface due to the temperature-induced flow.

The steam and water region's radial temperature distribution plots, as shown in Figure 5.13 (a)-(b) and (c)-(d), represented the bulk temperature distributions as steady, except when adjacent to the condenser tube walls (within the normalized values: 0.8 to 1 for steam and 0 to 0.2 for water). Radial temperature near the condensing wall sharply declined due to the formation of liquid film and heat transfer to the coolant through the condenser tube. The coolant region's temperature distribution showed the opposite trend, sharply increasing temperature near the heated wall. These temperature distributions were vital because they were used to estimate the bulk temperatures and heat fluxes.

Figure 5.14 presents the distribution of air mole fraction at the radial position, which followed a similar trend with the temperature distribution but with a moderate gradient. The mole fraction adjacent to the liquid film was the maximum, which reassured the physics phenomena–the non-condensable gas accumulate (got trapped) at the steam-film interface–reduce the heat transfer and condensation.The air mole fraction distribution followed a similar profiles even the values varied for the two test cases: run2.1-8R (M of 14.8%) and run2.1-13 (M of 39.6%).

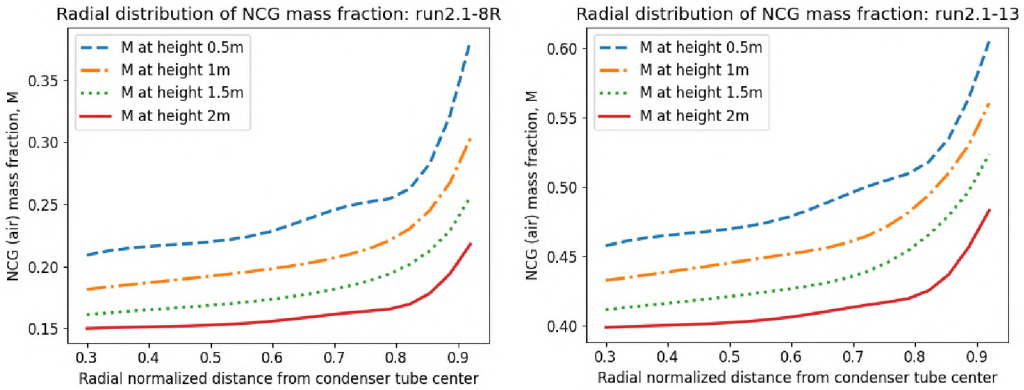

Figure 5.14. Radial distribution of air mass fraction: (a) run2.1-8R and (b) run2.1-13

5.3. REVIEW OF SYSTEM CODE CAPABILITIES

Several system codes, like RELAP5/MOD3.3, GOTHIC, CONTAIN, COMPACT, and MELCOR, were used for CTH analysis using lumped solution approach. Several researchers utilized GOTHIC for containment analysis (Bocanegra *et al.*, 2016; George and Singh, 1996; Lin *et al.*, 2013; Papini *et al.*, 2011). Among the many system codes, the widely used RELAP5 code for the CHT analysis was reviewed. RELAP5 condensation models and correlations for in-tube condensation was studied by several researchers (Ağlar and Tanrikut, 2008; Fullmer *et al.*, 2016; Hassan and Raja, 1993; Moghanaki and Rahgoshay, 2013; Moon *et al.*, 2000; Nguyen and Trinh, 2014; Park and No, 1999a; Park, 2015; Zhou *et al.*, 2013).

5.3.1. RELAP–3D Condensation Theory and Model. RELAP5-3D originated from RELAP5/MOD3 and is the most commonly used system code. It was developed by INL for modeling and simulating multi-dimensional reactor thermal-hydraulic and kinetic characteristics of LWRs during a laminar film in vertical, inclined, and horizontal wall surfaces with the following assumptions. First, the wall temperature, T_w, should be lower than the vapor bulk saturation temperature, $Tb_{,sat}$ and the liquid film temperatures, T_f. Second, for liquid volume fraction, less than 0.1 the condensation model switches to forced convection. Finally, the quality of NCGs should be less than 0.999 and the pressures must be below the critical pressure limit. The condensation HTC, h_c calculated from total heat flux, q_t'' and heat flux to the liquid film, q_f'' as:

$$q_t'' = h_c \, (T_w - T_{sat}) \tag{5.16}$$

$$q_f'' = h_c \, (T_w - T_f) \tag{5.17}$$

The Colburn-Hougen model was used in RELAP5 to calculate the film CHT of steam with NCG. The original Colburn-Hougen model used energy conservation law to calculate the CHT through the film-mixture gas interface. However, it did not included the sensible heat transfer between the gas and interface. The modified RELAP's CHT model prediction was improved, which was addressed by Jehee Lee (2019).

$$q'' = h_m \left(h_{g,sat} - h_{f,sat}\right) \left(\frac{\rho_{vb}}{x_{vb}}\right) \ln\left(\frac{P - P_{vi}}{P - P_{vb}}\right) \tag{5.18}$$

Where, j_v, h_m, ρ_{vb}, P, P_{vi}, P_{vb} are vapor mass flux $\left(kg/m^2 \cdot s\right)$, mass transfer coefficient (m/s), saturation vapor density at P_{vb} $\left(kg/m^3\right)$, total pressure (Pa), partial pressure of steam at liquid/gas/vapor interface (Pa) and at bulk stream (Pa).

Nusselt's and Shah's correlations were used for laminar and turbulent flow:

$$h_{nusselt} = \frac{k_f}{\delta} \tag{5.19}$$

$$h_{shah} = h_{sf}\left(1 + \frac{3.8}{z^{0.95}}\right) \tag{5.20}$$

Where, δ, k_f and h_{sf}, represents film thickness, film thermal conductivity, and superficial HTC. The details of it is discussed in impirical correlations subsections. In Shah's correlation, $Z = \left(\frac{1}{X} - 1\right)^{0.8} P_{red}^{0.4}$ and $h_{sf} = h_l(1 - X)^{0.8}$.

The X was the ratio of vapor-NCG mass to the total fluid mass, including condensate film. The reduced bulk pressure, P_{red} was defined as the ratio of bulk pressure to the critical pressure. The HTC, h_l, was defined per Dittus-Boelter correlation as:

$$h_l = 0.023\left(\frac{k_l}{D_h}\right) Re_l^{0.8} Pr_l^{0.4} \tag{5.21}$$

Where, h_l is the Dittus-Boelter coefficient which is defined in terms of hydraulic diameter D_h, thermal conductivity k_l, Reynolds Re_l and Prandtl number Pr_l.

Finally, code computes the maximum of h_{shah} and $h_{nusselt}$ as the condensation HTC.

5.3.2. GOTHIC and Other System Codes Model. GOTHIC code was developed for general purpose thermal-hydraulic analysis with specific features for nuclear power plant modeling and analysis by EPRI in 1993. GOTHIC was widely used for the reactor containment analysis, and it was selected for the safety analysis of NuScale, the first licensed US small modular reactor. In the GOTHIC condensation model the NCG effects was adopted by diffusion layer, Uchida, and Tagami models. Figure 5.15 presents the CHT prediction capabilities and benchmark with test dataset.

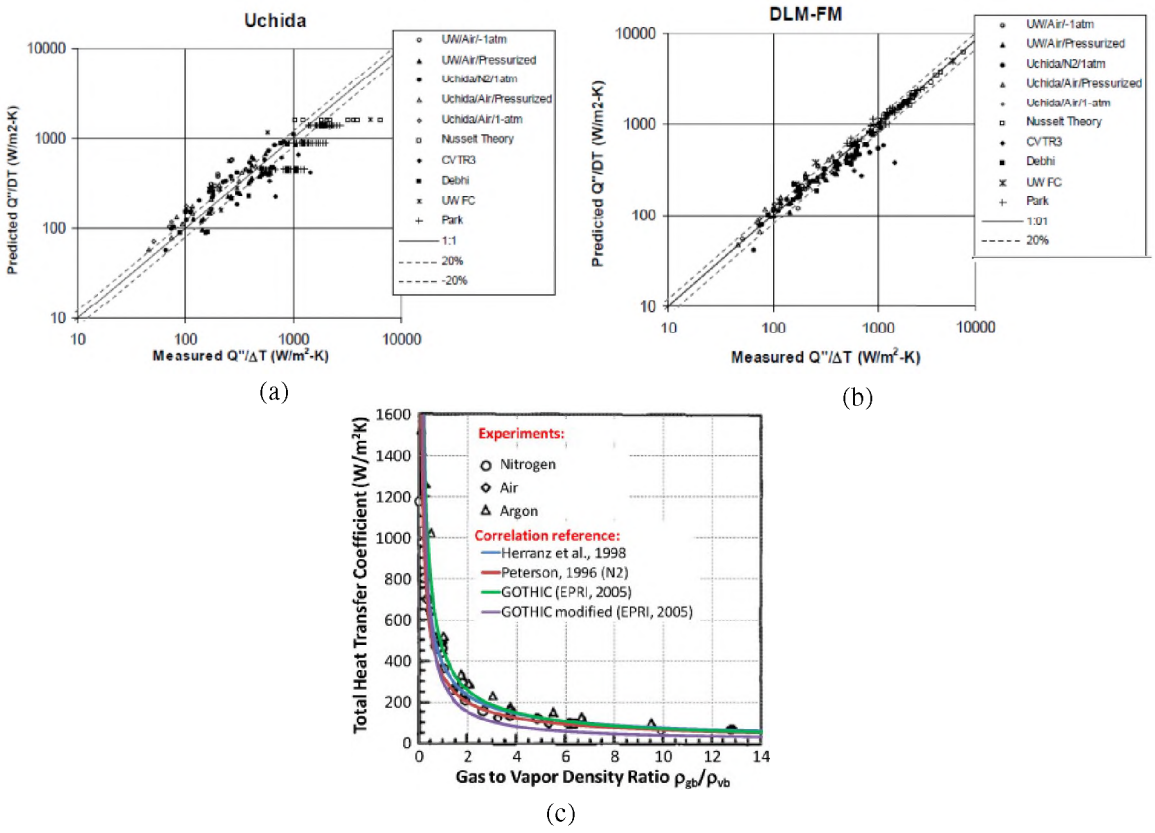

Figure 5.15. GOTHIC condensation model benchmark with test dataset: (a) diffusion layer model, (b) Uchida correlation, (c) overall HTC for different NCG Papini *et al.* (2011)

6. MODELING AND CORRELATION

This section focused on the assessment and modeling of the condensation heat transfer (CHT) models for the passive safety of small modular reactors (SMR). This study covered the review of the theoretical and semi-theoretical CHT models and correlations. The well-cited models, such as degradation factor, heat and mass transfer analogy, and boundary layer were reviewed. The previous CHT models were developed for small tube geometries, which differs from the containment of SMR. This study examined the scaled relations of the CHT models. Both theoretical and semi-theoretical models were adopted. However, this study emphasized on the fundamental physics-based analysis for laminar and turbulent film condensation downward flow conditions inside scaled tube geometries.

Keywords: Condensation, heat transfer, theory, models, scaling, analysis

6.1. BACKGROUND AND CHT MODELING APPROACH

The CHT models were grouped into theoretical, semi-theoretical, and empirical categories. These models were further categorized into boundary layer models, diffusion layer models, heat and mass transfer analogy (HMTA), and fluid film models. Minkowycz and Sparrow (1966), Fillo (1985), Dehbi *et al.* (1991), and Oh and Revankar (2005) analyzed CHT by developing boundary layer models; whereas, Colburn and Hougen (1934), Kim and Corradini (1990), and Peterson *et al.* (1993) used HTMA.

Nusselt's study analysed the laminar film condensation for a quiescent vapor on a vertical flat plate, as shown in Figure 6.1. It was the first closed-form physics-based solution. Many other theoretical correlations were developed based on Nusselt's studies, including the effects of subcooling, surface waviness, interfacial shear stress, and turbulence. The details derived from Nusselt's analysis was presented in Appendix A.

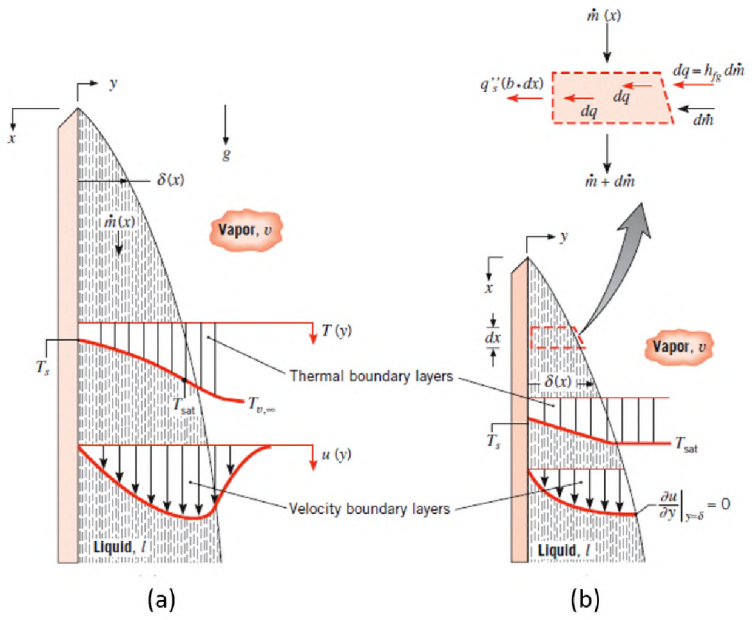

Figure 6.1. Film condensation schematics (a) without and (b) with Nusselt's approximations (Incropera *et al.*, 2007)

Likewise, other researchers developed CHT models and correlations presented in this section. The CHT analytical studies for vertical tube geometries were studied by several researchers (Dehbi and Guentay, 1997; Ghiaasiaan *et al.*, 1995; Munoz-Cobo *et al.*, 1996; Siddique *et al.*, 1994; Wang and Tu, 1988; Yuann *et al.*, 1995), which were similar to the reactor passive cooling applications. Many of these developed correlations showed agreement for vertical tube geometries with lower wall curvature effects on film thickness and heat transfer coefficient. It was observed that some correlations were straightforward with low accuracy; whereas, others had high accuracy but required few details for the iterative process.

Moreover, there was no correlation for the scaling of tube geometry effects. To fill this gap, this section reviewed the well-developed CHT models. Two fundamental physics-based analysis models and four semi-empirical models were assessed to check the model scaling performance. Focus was given to the downward laminar and turbulent vapor

film condensation in a vertical condenser tube. The resulting solutions were checked with the input parameters, like the tube radius, axial locations, wall temperature, inlet Re, and saturation temperature and pressure.

6.1.1. Focus Area of CHT Models. The focus areas for the CHT models inside tubes with NCG were: interfacial shear stress, NCG concentration, waviness of film, and mist and droplet formation. These focus areas and related CHT models were briefly discussed in this subsection.

6.1.1.1. Interfacial shear stress. The share stress was high for high Re (i.e. turbulent flow) in the vapor-gas mixture. The effects became dominant for higher relative velocity between the mixture and the condensing film.

6.1.1.2. Non-condesable gas concentration. The NCGs concentration effects were important for the steam downflow in CHT. The NCGs accumulated in the mix-film interface, and their concentration became the driving force for the gas diffusion. Then, a small waviness of the liquid film produced a significant change in the CHT coefficient, even at low film Re.

6.1.1.3. Mist and droplet effects. The last focus areas were mist and droplet formation effects, which showed high impact on CHT by increasing the sensible HTC through the diffusion boundary layer in condensate film.

These CHT models were briefly discussed:

6.1.2. Boundary Layer Model. As the CHT rate was greatly affected by the presence of NCG, the boundary layer model (BLM) was developed. This model solved the mass, momentum, and energy for the liquid film and steam-NCG mixtures. Researchers developed the BLM with different approaches. Minkowycz and Sparrow (1966) first used the boundary layer model of condensation film for an isothermal plate with stream functions and similarity transformation. Their studies covered laminar forced and free condensation regimes. They also considered the effects of superheating, thermal diffusion, interfacial shear, and changing fluid properties. Then, Fillo (1985) proposed a condensation model

with NCG for forced and natural convection by using the turbulent gas-vapor boundary layer. Dehbi *et al.* (1991) modeled CHT with NCG for turbulent-free convection over vertical surfaces. In their turbulent modeling, they used the turbulent kinetic energy method and empirical constants from the steam-air test data. Also, by using the independent variable transformation suggested by Minkowycz and Sparrow (1966), this solution agreed with the test data. Ghiaasiaan *et al.* (1995) and Yuann *et al.* (1995) developed models keeping the shear stress and film-waviness roughness effects for fully-developed flow conditions. Ghiaasiaan *et al.* (1995) models also covered droplet effects, which were not considered in Yuann *et al.* (1995) model. Oh and Revankar (2005) proposed a filmwise CHT model for a vertical tube with NCG using the heat and mass transport parameters such as interfacial friction, Nu, and Sh. Results compared with tests data and correlations agreed with the Prandlt mixing length type model.

6.1.3. Heat and Mass Transfer Analogy (HMTA). Another approach for CHT modeling is HMTA using the thermal resistance analogy, and it was first introduced by Colburn and Hougen (1934). They defined the mass concentration gradient controls and the heat transfer process through the NCG layer. Later, Corradini (1984) added a correction factor that accounted for the suction effect at high mass transfer rates across the liquid-gas interface. Next, Kim and Corradini (1990) used this approach, adding force and natural convection CHT with NCG, and they analyzed the effect of the film waviness. Then Wang and Tu (1988), and later Dehbi and Guentay (1997), developed models with shear stress and suction effects for fully-developed flow conditions. Additionally, Siddique *et al.* (1994) and Munoz-Cobo *et al.* (1996) proposed models considering the suction effect and film-waviness roughness effects for developing flow conditions. Munoz-Cobo *et al.* (1996) model also covered shear stress and droplets effects, which were not available in Siddique et al.'s model. Subsequently, Peterson *et al.* (1993) introduced a diffusion layer model, as shown in Figure 6.2, which presents the heat transfer as a combination of condensation and convection.

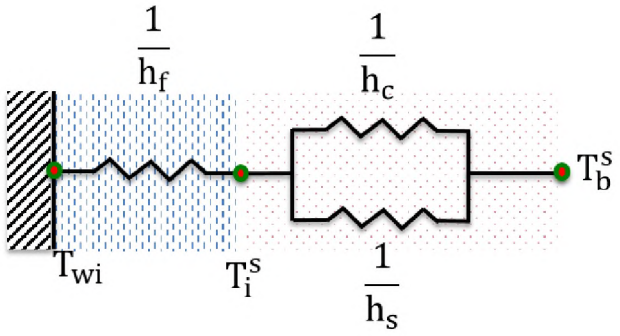

Figure 6.2. Diffusion layer model

Kuhn (1995) developed a mass transfer conduction model using the estimated suction parameters and sensible HTC from the Couette-flow model. Later, using this model and test data, an empirical correlation was developed, which showed that the total HTC had a standard deviation of 3.24% for the steam-helium mixtures and 6.38% for the seam-air mixtures.

Table 6.1 and Table 6.2 presented a summary of the well-cited filmwise CHT models with different (semi-theoretical and theoretical) modeling approaches. These summaries showed that the HMTA, Boundary layer models were used with shear, suction, and film-wavyness for fully-developed, as well as developing flow.

Table 6.1. Summary of the analytical models for vertical tubes

Model	**Methodology**	**Shear Stress**	**Suction Effect**	**Drops**	**Waviness Roughness**	**Flow**
Wang and Tu (1988)	HMT analogy	✓	✓	x	x	FD
Siddique *et al.* (1994)	HMT analogy	x	✓	x	✓	DF
Ghiaasiaan *et al.* (1995)	Boundary Layer	✓	x	✓	✓	FD
Munoz-Cobo *et al.* (1996)	HMT analogy	✓	✓	✓	✓	DF
Yuann *et al.* (1995)	Boundary Layer	✓	x	x	✓	FD
Dehbi and Guentay (1997)	HMT analogy	✓	✓	x	x	FD

Note: HMT for 'Heat & Mass Transfer', FD for 'Fully developed', and DF for 'Developing flow'

Table 6.2. Summary of filmwise condensation models

	Semi-theoretical models		Theoretical models	
Model	DF	HMTA	BL	DL
Method	DF = h_{exp}/h_{Nu}	Mass, momentum and energy	Coupled film & mixture region	Mass transfer by diffusion
By	K. M. Vierow	Colburn-Hougen	Sparrow-Minkowycz	Colburn-Hougen

Note: DF- Degradation factor, BL- Boundary layer, DL- Diffusion layer

6.1.4. CHT Empirical Models. The analytics and test data were used to develop the semi-empirical correlations, i.e., the degradation factor (f), which was the ratio of experimental and Nusselt's HTC, and it was first proposed by Vierow (1990) and then developed by Kuhn *et al.* (1996), Park and No (1999b), and Lee and Kim (2008). Likewise, researchers developed empirical correlations for condensing falling film without the shear effects (Chun and Seban, 1971; Labuntsov, 1957; Shmerler and Mudawwar, 1988) and with the shear effects (Araki *et al.*, 1995; Blangetti *et al.*, 1982; Butterworth, 1983). A broader range of test data for the annular flow with correlations was developed by Traviss et al. (1973) and Shah (1979).

6.1.5. CHT Models used in System Code and CFD Tools. Table 6.3 presented the associated CHT models used in system codes and CFD tools. The review showed that most of the system codes used lumped parameter approach and empirical correlations; whereas, the CFD tools utilized field equations, fluid film, and HMTA models.

Table 6.3. Different CHT Computer Codes

Code/software	**Type, nature**	**Models/correlations**
GOTHIC	code, lumped	Uchida & Tagami or Boundary layer
RELAP5/MOD3.3	code, lumped	Uchida or HMTA
Fluent	software, field eqns.	User defined
Star ccm+	software, field eqns.	Fluid film
CONTAIN & MELCOR	code, lumped	HMTA
COMPACT	code, lumped	Uchida & Tagami

Note: HMTA for Heat and Mass Transfer Analogy

6.2. ASSESSMENT OF SELECTED CHT MODELS

Several analytical and empirical CHT models were assessed to check the impact of NCG on the HTC in SMR's containment. The developed model was validated with scaled tests data for different diameter condensing tubes. These assessments were intended to develop a new scaled correlation for different NCG mixture percentages, including the effects of the film roughness, suction, flow entrance, and exit using Nu, Re, and Sh.

6.2.1. Degradation Factor (DF, f) Method. The ratio of experimental and Nusselt's local HTC defined as the degradation factor (DF, f) for CHT analysis. This factor, f, is related to the steam-NCGs mixture (Re) and NCGs bulk mass fraction

Table 6.4. Degradation Factor Method

Authors	**Semi-empirical models/correlations**
Vierow (1990)	$f = \frac{h_{exp}}{h_{Nu}} = f_1 \cdot f_2 = \left(1 + a\,Re_{mix}^{d}\right) \cdot \left(1 - bM_{NCGs}^{c}\right)$
Kuhn *et al.* (1996)	$f = \frac{h_{exp}}{h_{Nu}} = \frac{\delta_{shear}}{\delta_{Nu}} \cdot \left(1 + a\,(Re_f/4)^{d}\right) \cdot \left(1 - bM_{NCGs}^{c}\right)$
Park and No (1999b)	$f = \frac{h_{tot}}{h_f} = 0.0012 W_{nc}^{-1.4} Ja^{-0.63} Re_f^{0.24}$
Lee and Kim (2008)	$f = \tau_g^{*0.3124}\left(1 - 0.964 M_a^{0.402}\right)$

6.2.2. Other Experimental Correlations. This study assessed the scaling distortion effect of a selected number of empirical correlations, which were developed for turbulent film CHT, with and without considering interfacial shear at the tube wall, and the annular flow.

6.2.3. Correlations for Reactor Containment. Compared to the numerous empirical correlations for general application of CHT, there were a few developed correlations were available for reactor applications. Uchida *et al.* (1964), Tagami (1965), and Kataoka et al. (1992) were the first few researchers who performed CHT experimental studies

Table 6.5. Models and correlations for film CHT

Authors	**Empirical models/correlations**
Nusselt (1916)	$\mathrm{h(x)} = \frac{\mathrm{k_l}}{\delta} = \left[\frac{\mathrm{g}\rho_\mathrm{l}(\rho_\mathrm{l}-\rho_\mathrm{v})\mathrm{k_l^3 h'_{fg}}}{4\mu(\mathrm{T_{sat}}-\mathrm{T_w})\mathrm{x}}\right]^{1/4}$ and $\delta(\mathrm{x}) = \left[\frac{4\mathrm{k_l}\mu_\mathrm{l}(\mathrm{T_{sat}}-\mathrm{T_s})\mathrm{x}}{\mathrm{g}\rho_\mathrm{l}(\rho_\mathrm{l}-\rho_\mathrm{v})\mathrm{h_{fg}}}\right]^{1/4}$
Rohsenow (1956)	$h'_{fg} = h_{fg}\left[1 + 0.68\frac{C_{p,f}(T_i - T_w)}{h_{fg}}\right]$ improved Nusselt's analysis with a non-linear T distribution
Kutateladze (1982)	$\bar{h} = \frac{k_f}{\left(v_f^2/g\right)^{1/3}} \frac{\mathrm{Re}_{\delta\delta}}{1.08\,\mathrm{Re}_\delta^{12} - 5.2}, 30 \le \mathrm{Re}_\delta \le 1800$ the mean h on a vertical plate with interfacial wave effects
Chen *et al.* (1987)	$\mathrm{Nu_f} = \left(\mathrm{Nu}_{\tau_\mathrm{i}}^{*2} + \mathrm{Nu_g^2}\right)^{1/2}$, where $\mathrm{Nu_g} = \left(\mathrm{Nu_{la}^6} + \mathrm{Nu_{tu}^6}\right)^{1/6}$ with $\mathrm{Nu_{la}} = 0.823\,(4\mathrm{Re_f})^{-0.22}$ for film CHT of quiescent vapor
Shah (1979)	$\frac{\mathrm{h}}{\mathrm{h_{10}}} = (1-\mathrm{x})^{0.8} + \frac{3.8\mathrm{x}^{0.76}(1-\mathrm{x})^{0.04}}{(\mathrm{P/P_{cr}})^{0.38}}$ for $25 < \mathrm{Re} < 15{,}800$ and $\mathrm{P/P_{cr}}$ from 0.002 to 0.44.

and developed CHT correlations focusing reactor containment. Later, Dehbi *et al.* (1991) developed scaled empirical correlations. These developed correlations are presented in Table 6.6.

Table 6.6. Empirical correlations for CHT of reactor containment

Authors	**Developed correlations**
Uchida *et al.* (1964)	$h_{\mathrm{Uchida}} = 380\left(\frac{W_{n/c}}{1-W_{n/c}}\right)^{-0.7}$ used in GOTHIC code where $\mathrm{W_{n/c}}$ NCG (air) mass fraction
Tagami (1965)	$h_{\mathrm{Tagami}} = 11.4 + 284\left(\frac{1-W_{n/c}}{W_{n/c}}\right)$ for LBLOCA and natural convention test
Kataoka et al. (1992)	$h_{\mathrm{Kataoka}} = 430\left(\frac{W_{n/c}}{1-W_{n/c}}\right)^{-0.8}$ for a flat vertical plate between two pools
Dehbi *et al.* (1991)	$h_{\mathrm{Dehbi}} = \frac{L^{0.05}\left[(3.7+28.7P)-(2438+458.3P)\log W_{n/c}\right]}{T_b - T_w}$ for pressure of 0.15 to 0.45 MPa

6.2.4. CHT Models for SMR. Researchers developed various CHT models and correlations based on applications. The CHT models for reactor systems also varied for reactor system types and physics phenomena. The suitable CHT models for SMR were annular; vertical in-tube and flat plate downflow depended on flow type, flow channel, and condensing surface, as presented in Figure 6.3.

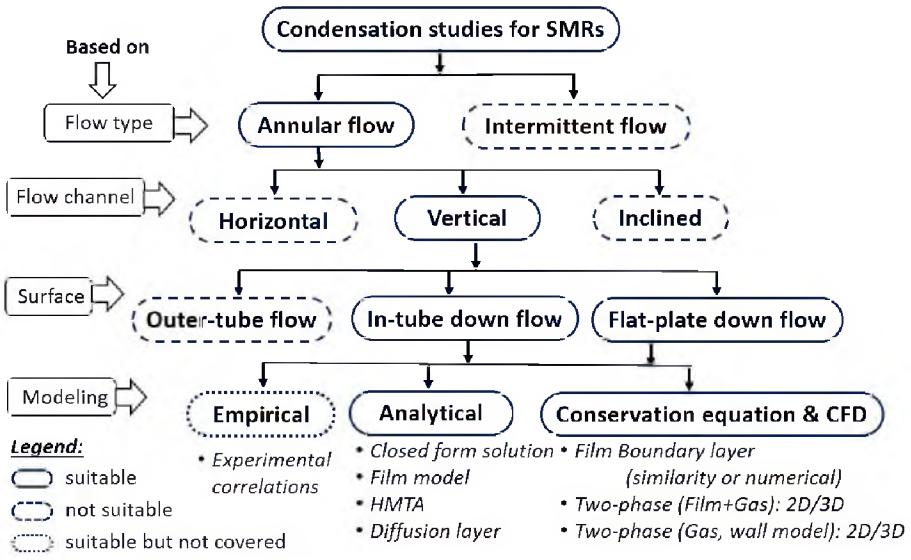

Figure 6.3. Overview of condensation studies for SMRs

The general approaches to CHT modeling for SMR are empirical, analytical, CFD or conservative equation solutions. The empirical models and correlations were developed using test data from large-scale integral effects tests (IET) or small-scale separate effect tests (SET). The analytical CHT models were closed-form solution, film model, HMTA, and diffusion layer. Likewise, the CHT models developed by solving conservation equations and using CFD modeling were filmed with boundary layer(similarity or numerical), two-phase 2D/3D models. In short, model of condensation that could be applicable to SMR phenomena included: (a) vertical plate (quiescent mixture or downward mixture flow), (b) vertical tube (downward mixture flow).

6.2.5. Le (2012) Physics Based Model. Nusselt's analysis was used as the starting point for the development of a physics-based CHT model in cylindrical coordinates. This modeling approach consisted of a laminar film CHT quiescent vapor and was followed by laminar and turbulent mixed convection film CHT, as shown in Figure 6.4. The Le (2012) model analysis are summarized in Table 6.7.

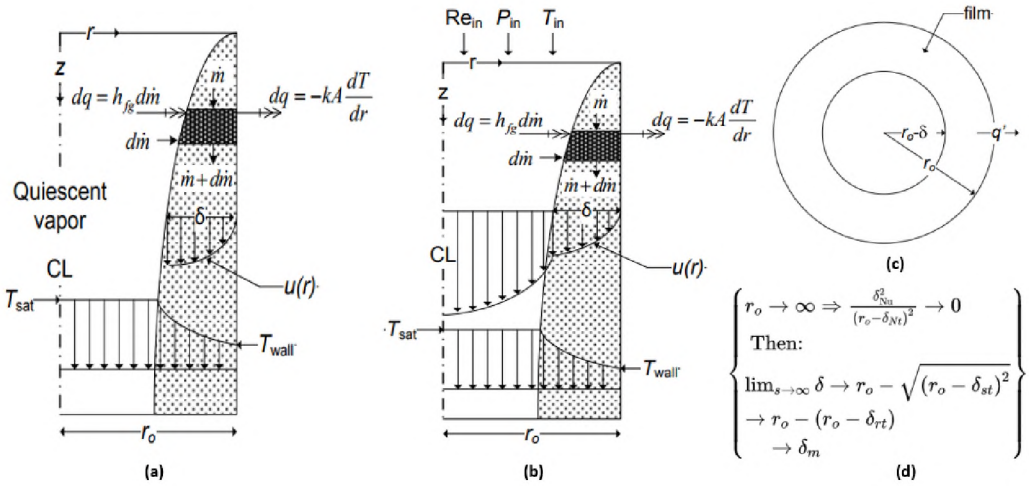

Figure 6.4. Le's (2012) CHT model schematics: (a) laminar film and quiescent vapor, (b) laminar film and non-quiescent vapor, (c) tube to wall model, (d) film thickness relation

6.2.5.1. Laminar film CHT for quiescent vapor. In this model, the following approximations were considered: vapor was pure, saturate, and quiescent with a uniform temperature. Then consider constant wall temperature, fluid properties, and laminar condensate flow. Next, the model was simplified with an only axial pressure gradient, $\frac{dP}{dz} = \rho_v g$, and no shear stress at the liquid-vapor interface. The film region approximated with only radial conduction heat transfer but no axial advection and diffusion of momentum.

6.2.5.2. Laminar and turbulent mixed-convection CHT. The laminar mixed-convection model used the laminar vapor flow with a shear force at the liquid-vapor interface. The liquid and the interface velocity separated by the forced and natural convection (fc and nc). However, turbulent model used the turbulent flow of vapor and condensate.

Table 6.7. Le(2012) Physics based CHT models

Physics condition	**Condensation models**
Film: Laminar Vapor: Quiescent	Approx.: Vapor (pure) at T_{sat}, constant: T_{wall}, fluid properties. B.C.: $\left.\frac{\partial u_L}{\partial r}\right\|_{r=r_0-\delta} = 0$, $u_L\|_{r=r_o} = 0$, $T_L\|_{r=r_o} = T_{\text{wall}}$, and $T_L\|_{r=r_o-\delta} = T_{\text{sat}}$ Film velocity: $u_L = \frac{g(\rho_L-\rho_V)}{4\mu_L}\left(2(r_o-\delta)^2 \ln\left(\frac{r}{r_o}\right) + \left(r_o^2 - r^2\right)\right)$ Film radial temperature: $T_L = T_{\text{mall}} + \frac{T_{\text{sat}}-T_{\text{wall}}}{\ln\left(\frac{r_o-\delta}{r_o}\right)} \ln\left(\frac{r}{r_o}\right)$ Condensate flow: $\dot{m}(z) = \frac{\pi g \rho_L(\rho_L-\rho_V)}{8\mu_L} r_o^4 \left(1 - 4\delta_+ + 3\delta_+^2 - 2\delta_+^2 \ln \delta_+\right)$ Film Nusselt number: $\text{Nu} = \frac{h2r_o}{k_L} = -\frac{2k_L}{r_o \ln \delta_+}\frac{2r_o}{k_L} = -\frac{4}{\ln \delta_+}$ Approx. solution: $\delta^* = 1 - \sqrt{1 - 2\delta^*_{Nu}}$, Or $X^4 - C = 0$ for, $X = \left(\frac{1-\delta_+}{2}\right)$, $\delta_+ = \left(\frac{r_o-\delta}{r_o}\right)^2$, $C = \delta^*_{Nu} = \frac{\delta_{Nu}}{r_o} = \frac{1}{r_o}.\left(\frac{4\mu_L k_L \Delta T z}{h_{fg} g \rho_L(\rho_L-\rho_V)}\right)^{1/4}$ With annular cooling, T_{wall} varies, $\Delta T = T_{sat} - T_{wall}$ is as follows- $\Delta T(z) = a_0 + a_1 z + a_2 z^2 + \cdots = \sum_{i=0}^{n} a_i z^i$ Here, properties: vapor constant at T_{sat}, film at $T_{flim} = T_{wall} + 0.31\Delta T$
Film: Laminar Vapor: Laminar	Approx.: Vapor is pure at saturate T, constant: T_{wall}, fluid properties. B.C.: $\left.\frac{\partial u_V}{\partial r}\right\|_{r=0} = 0$, $u_L\|_{r=r_o} = 0$, $u_L\|_{r=r_o-\delta} = u_V\|_{r=r_o-\delta}$, and $\tau_i = -\mu_V \left.\frac{\partial u_V}{\partial r}\right\|_{r=r_o-\delta} = -\mu_L \left.\frac{\partial u_L}{\partial r}\right\|_{r=r_o-\delta}$ Film velocity: $u_L = u_{L,f_c} + u_{L,nc}$ $= -\frac{\rho_+ g}{4\mu_L}\left(r_o^2 - r^2\right) + \frac{g(\rho_L-\rho_V)}{4\mu_L}\left(\left(r_o^2 - r^2\right) + 2(r_o-\delta)^2 \ln\left(\frac{r}{r_o}\right)\right)$ Interface velocity: $u_i = u_{i,f_c} + u_{i,nc}$ $= -\frac{\rho_+ g \delta(2r_o-\delta)}{4\mu_L} + \frac{g(\rho_L-\rho_V)}{4\mu_L}\left(\delta(2r_o-\delta) + 2(r_o-\delta)^2 \ln\left(\frac{r_o-\delta}{r_o}\right)\right)$ Approx. solution: $X^4 + BX^3 - C = 0$ where, $X = \left(\frac{1-\delta_+}{2}\right)$, $B = \frac{M}{\beta} = \frac{2\mu_L\mu_V \text{Re}_{in}}{g\rho_L(\rho_L-\rho_V)r_o^3}\frac{\rho_L\mu_V}{\rho_V\mu_L} = \frac{2\mu_V\mu_V \text{Re}_{in}}{g(\rho_L-\rho_V)\rho_V r_o^3}$
Film: Laminar Vapor: Turbulent	For $\mu_{V,eff} = \mu_V + \mu_V^t$, $\mu_{L,eff} = \mu_L + \mu_L^t$, and $k_{L,eff} = k_L + \mu_L^t C_{P,L}$ Approx. solution: $X^4 + BX^3 - C = 0$ where, $X = \frac{\delta}{r_o} - \frac{1}{2}\left(\frac{\delta}{r_o}\right)^2$ and $B = \frac{2\mu_{V,eff}\mu_V \text{Re}_{\text{in}}}{g(\rho_L-\rho_V)\rho_V r_o^3}$. For constant T_{wall}: $C = \frac{4\mu_{L,eff} k_{L,eff} \Delta T z}{g h_{fg} \rho_L(\rho_L-\rho_V) r_o^4}$ For varying T_{wall}: $C = \frac{4\mu_{L,eff} k_{L,eff}}{r_o^4 h_{fg} g \rho_L(\rho_L-\rho_V)} \sum_{i=0}^{n} a_i \frac{z^{i+1}}{i+1}$

6.2.6. Lee (2007) Theoretical Model. In this model (as presented in Figure 6.5), the following approximations and assumptions were considered: film was laminar, vapor at saturated temperature (T_{sat}), and condensing wall temperature, T_w was lower than the T_{sat}. The film wall condensation thickness was δ for vapor-NCG mixture temperature T_b. The film-gas interface temperature, Ti, and the NCG mass fraction Wnc was calculated using the energy balance between the film and mixture (vapor-NCG) and the secondary cooling regions, considering the sensible, latent and convection heat transfer. Lee's (2007) theoretical model analysis are summarized in Table 6.5.

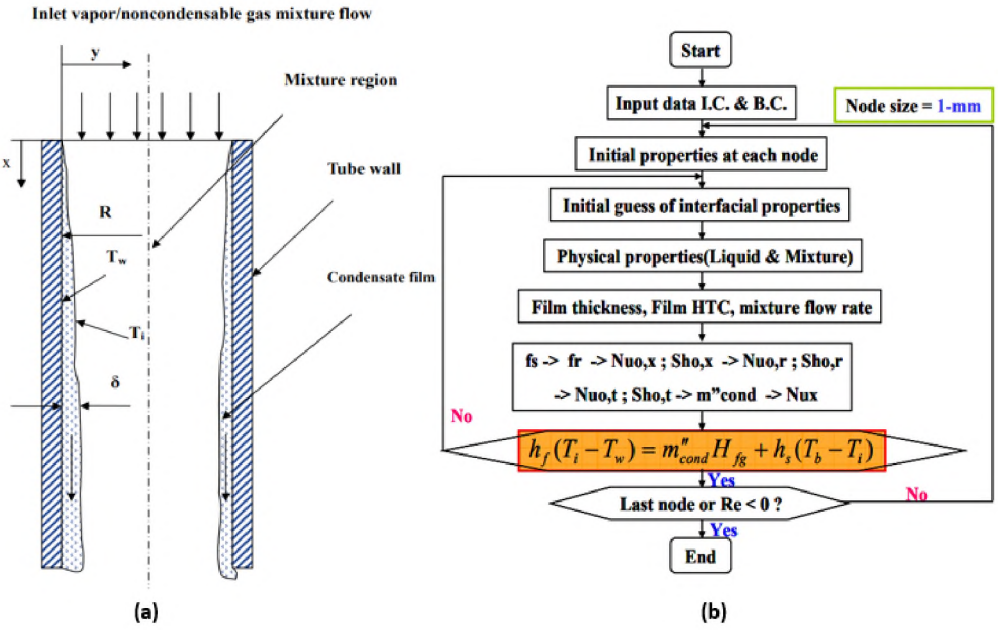

Figure 6.5. Lee (2007) Physics base CHT model's: (a) schematics, (b) calculation steps

The full model was sub-grouped by condensate flow, vapor-NCG mixture flow, and secondary cooling pool. A non-iterative approach was used with the correlations of McAdams (1942) for film HTC, Blangetti *et al.* (1982), and Peterson (1996) for Nu estimation of film and laminar-wavy film, respectively. HMTA was used in the mixture flow model with the suction effect used to calculate the mass flux, HTC, and Nu. The Rohsenow (1951) heat transfer model was utilized for secondary pool heat transfer analysis.

Table 6.8. Lee(2007) Physics based CHT models

Physics condition	**Condensation models**
Film: Laminar Vapor at T_{sat}	Approx.: $T_w < T_{sat}$, T_b and $W_{nc,b}$ depends on P, unknown: T_i and $W_{nc,i}$ HTC: film (h_f), condensation (h_c), (h_s), and total h_{tot} $h_f\,(T_i - T_w) = (h_c + h_s)\,(T_b - T_i)$ and $h_{tot} = \left[\frac{1}{h_f} + \frac{1}{h_c+h_s}\right]^{-1}$
Condensate flow	Film: $\delta = \frac{1.259\delta_N^{*4/3}}{\left[\delta_p\left(a_1+a_2x+a_3x^2\right)+l_i\left(b_1+b_2x+b_3x^2+b_4x^3\right)+m_i\delta_p\left(c_1+c_2x\right)\right]^{1/3}}$ where δ_N from Nusselt, $x = 2\delta_n/d$, $a_l = 2, a_2 = -28/15, a_3 = -1/3$, $b_l = 4/3, \quad b_2 = -2, \quad b_3 = 8/15, \quad b_4 = 1/3; \quad c_l = 1/2, \quad c_2 = -8/15$ Approx.(no interface shear): $\delta_p = \delta_N \frac{1.189}{\left(1-\frac{4}{5}x_N-\frac{1}{3}x_N^2\right)^{1/4}}$, where $x_N = 2\delta_N/d$ Interface (with shear): $m_i = \frac{360 f_{mix}\rho_{mix}(u_{mix}-u_i)^2}{(\rho_I-\rho_{mix})gd}$, $l_i = \frac{2\tau_i}{(\rho_l-\rho_{mix})g}$ Film HTC: $h = \frac{k_l}{\delta}$ McAdams:$h_f = \beta\frac{k_l}{\delta(x)}$, where β is 1.28 Blangetti(1982): $Nu_f = \frac{h_f L}{k_l} = \left(Nu_{x,la}^4 + Nu_{x,tu}^4\right)^{1/4}$, where $L = \left(\mu_l^2/\rho_l^2 g\right)^{1/3}$ Peterson et al. (1997) for Laminar-wavy-film: $\frac{Nu_{f,la}}{Nu(=1/\delta^*)} = 0.06\delta^* + 0.95$
Mixture flow	HMTA is used for Vapor/NCG Mixture Flow $h_s = Nu_{mix}\frac{k_{mix}}{d_i}$ and $h_c = \frac{m''_{cond} i_{fg}}{(T_b-T_i)}$ $m''_{cond} = h_m\frac{(W_{v,b}-W_{v,i})}{(1-W_{v,d})}$, where h_m is the mass transfer coeff. Without interface roughness: $Sh_{mix} = \frac{m_{cond}d}{\rho D}\frac{W_{nc,i}}{(W_{nc,i}-W_{nc,b})}$ Suction effect: $\frac{St}{St_o} = \ln\left(\frac{1+B_h}{B_h}\right)$, where $B_h = \frac{m''_{cond}}{G^\infty St}$ is suction parameter Modified: $m''_{cond} = \frac{G^\infty Sh_{o,x}}{Re_x\,Sc}\left[\ln\left\{1 + \frac{Re_x\,ScD\rho(1-\omega)}{G^\infty d}\right\}\right]$ where ω is the ratio of mass fraction of bulk and at interface mixture Developing flow: $Nu_{o,t} = Nu_o\left[1 + \frac{0.8\left(1+7\times10^4 Re^{-3/2}\right)}{x/d}\right]$ and $Sh_{o,t} = Sh_o\left[1 + \frac{0.8\left(1+7\times10^4 Re^{-3/2}\right)}{x/d}\right]$
Secondary Pool Rohsenow(1962)	$\frac{q''}{\mu_l i_{fg}}\left[\frac{\sigma}{g(\rho_l-\rho_v)}\right]^{1/2} = \left(\frac{1}{C_{sf}}\right)^{1/r} Pr_l^{-s/r}\left\{\frac{Cp_l\left[T_{w,o}-T_{sat}(P_l)\right]}{i_{fg}}\right\}^{1/r}$ where $r = 0.33, s = 1.0$, and $C_{sf} = 0.0132$

6.3. SCALING ANALYSIS FOR FILM CONDENSATION

The scaling analysis for CHT could be based on experimental data or on theoretical models. A brief overview of the both approaches were presented:

6.3.1. Scaling Based on Empirical Correlation. Dehbi *et al.* (1991) proposed simple empirical correations for the film CHT model scaling between a model to the prototypic system. This correlated the overall condensation HTC with the bulk vapor temperature Tb, wall surface temperature Tw, system pressure P, NCG mass fraction W, and the condensation plate length L.

$$h_{\text{Dehbi. R}} = \frac{(h_{\text{Dehbi}})_{\text{model}}}{(h_{\text{Dehbi}})_{\text{prototype}}} = \gamma^{0.05} \tag{6.1}$$

$$h_{\text{Dehbi}} = \frac{L^{0.05}[(3.7 + 28.7P) - (2438 + 458.3P)\log W]}{T_b - T_w} \tag{6.2}$$

where, γ was the length ratio, with power 0.05 it was expected that there was a very low difference in HTC between model and the prototype system.

6.3.2. Scaling Based on Diffusion Layer Model. Using the diffusion layer model, the ratio of the total HTC as per Wu and Corradini (2016) could be expressed as:

$$h_{T,R} = \frac{(h_T)_{\text{model}}}{(h_T)_{\text{prototype}}} = \frac{(\bar{h}_{\text{film,R}}) \cdot (h_{\text{con,R}})}{(\bar{h}_{\text{film}} + h_{\text{con}})_R} \tag{6.3}$$

where, the $h_{\text{con,R}}$ was one for the same thermodynamic properties. The $h_{\text{film,R}}$ was as:

$$\bar{h}_{\text{film,R}} = \gamma^{-1/4}\left[\frac{(L + 4.8/A)_{\text{model}}}{(L + 4.8/A)_{\text{prototype}}}\right]^{0.0338} \tag{6.4}$$

Hence, the total HTC was rearranged to the final form, as:

$$h_{T,R} = \left[\gamma^{-1/4}\left[\frac{(L + 4.8/A)_{\text{model}}}{(L + 4.8/A)_{\text{prototype}}}\right]^{0.0328}\right]\left[\frac{\bar{h}_{\text{film, R}} + (h_{\text{con}}/\bar{h}_{\text{film}})_R}{1 + (h_{\text{con}}/\bar{h}_{\text{film}})_{\text{prototype}}}\right]^{-1} \tag{6.5}$$

6.3.3. Evaluation of CHT Model. Le's (2012) physics-based CHT model was evaluated using Kuhn (1995) experimental data for pure steam, as shown in Figure 6.6 and Figure 6.7. For the model assessment, two test cases were used: a low pressure case (run1.1-1), and a moderate pressure case (run 1.3-2R2). Similar to the Le (2012) model, experimental temperature differences with four physics phenomena were investigated for vapor mixtures and condensate films using constant and curve fit experiments.

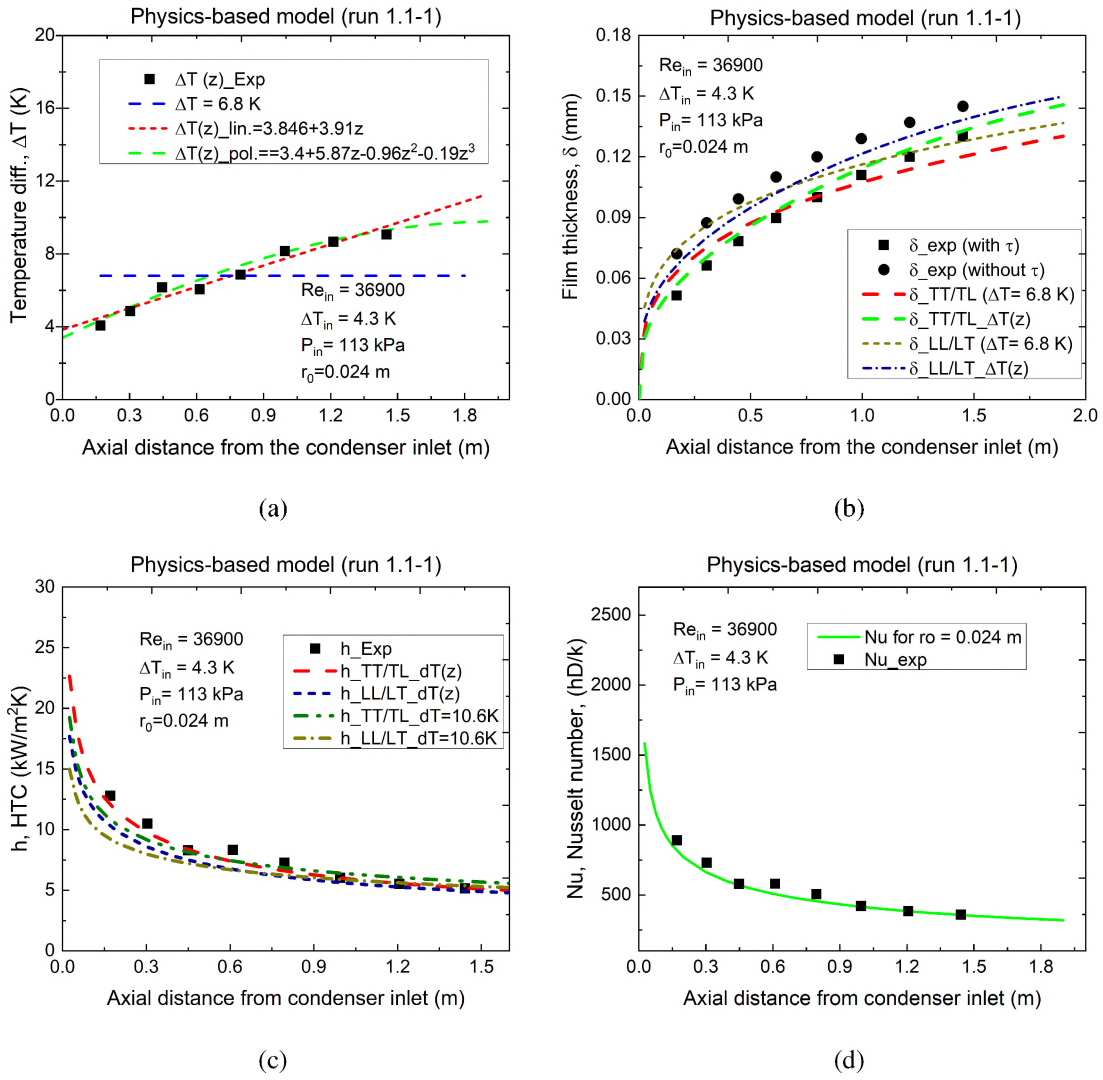

Figure 6.6. Le (2012) model's verification results using UCB Kuhn's test (run1.1-1) data: (a) ΔT, (b) δ, for constant and variable ΔT_{in}, (c) h, and (d) local Nu

The physics phenomena were TT, TL, LT, and LL, where T and L represent turbulent and laminar flow modes, respectively. The first flow mode was for vapor-mixture and second flow mode was for condensate film. The constant temperature difference method was straightforward to implement because it did not need experimental condensing wall temperature data. Neither of these temperature differences were the same, as presented in Figure 6.6 (a) and Figure 6.7 (a).

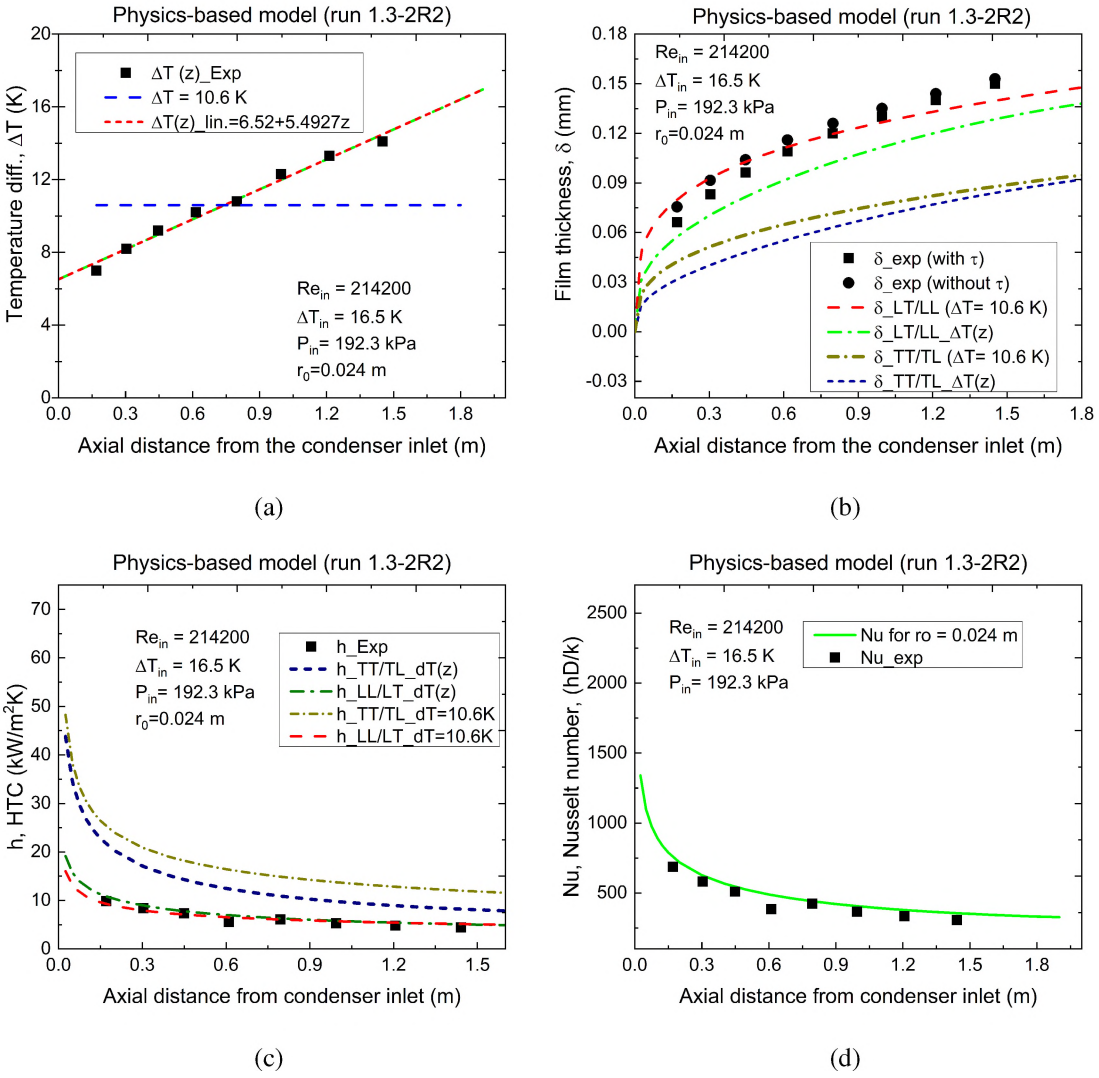

Figure 6.7. Le (2012) model's verification results using UCB Kuhn's test (run1.3-2R2) data: (a) ΔT, (b) δ, for constant and variable ΔT_{in}, (c) h, and (d) local Nu

For run1.1-1, model predicted film thickness and HTC values for temperature differences and flow mode cases were within a standard deviation of 10%. Nu values were validated for TT and TL cases because those cases produced better predictions than the others. Validation results of Nu were satisfactory, showing a standard deviation within 5 %.

The TT and TL cases showed deviation, and film thickness was under-predicted, but HTC was over-predicted by a factor of approximately 2. However, LL and LT cases estimated HTC and film thickness within 5% and 15% deviation of the test data. Thus, Nu values were validated for TT and TL cases and predicted within 5% deviation.

A review and evaluation of the models revealed that multiple approaches could be applied to model CHT, and predictability depended on the physics layout, test conditions, and boundary values. The degradation factor method used the closed-form analytical model and empirical solutions. HMTA with thermal resistance, heat, and mass transfer analogy was widely used by researchers with HTC prediction capabilities ad it had a standard deviation of 3.24 % for steam-helium mixtures and 6.38 % for seam-air mixtures (Kuhn, 1995).

The condensation modeling approach also used BLM to solve mass, momentum, and energy for the liquid films and steam-NCG mixtures. System codes, such as RELAP5 3D, GOTHIC, and MELCOR were used primarily in empirical correlations and HMTA; they were required by regulatory agencies for reactor design licensing and evaluations.

The first closed-form CHT solution was a physics-based approach, and Le's (2012) physics-based models demonstrated abilities to predict with an error margin but subjected to test and physics conditions. The scaling effects were evaluated using physics-based model and semi-empirical degradation factor method and results were presented in Section 7. Scaled test datasets supported investigation of the CHT modeling capabilities for the safety of SMR systems.

7. RESULTS AND DISCUSSION

This section presented the scaled experimental and CFD simulation results of the scaled PCCS with NCGs. Test data were presented for varying pressures, mass flows, cooling levels, and operating conditions. Results of the experimental data were discussed with the critical findings and observations. Simulation results were validated with test data, results were discussed to investigate the physics phenomena. A parametric simulation study conducted to simulate the real reactor accident case and identify the parameters of importance. Physics-based theoretical model was evaluated for scaling effects. Results showed dependency on the physics and test conditions that need to be evaluated for elevated pressures and mass flow rates for a full-scale PCCS of SMRs.

7.1. EXPERIMENTAL RESULTS

The experiments were conducted in two steps. The preliminary tests were conducted with pure steam at low flow rates and high coolant (water) flow rates. The heat flux of the condensing tube wall was estimated using the axial coolant bulk temperatures distributions. The preliminary test results were used to identify the optimized test conditions for the final tests. In addition, the CFD simulation results provided critical insights about the multi-phase flow and multi-component gas distribution to conduct the experiments and prepare a quality test dataset for further research.

7.1.1. Preliminary Measurements with Pure Steam. The preliminary tests were conducted using 4" steam tube test sections to check the performance of the newly developed CHT test facility for this study. Figure 7.2 represents the axial temperature distribution of the bulk steam, bulk coolant, condenser tube inner, and outer wall surface. The inlet and outlet of the steam and coolant (water) are presented as independent points, which represent the maximum and minimum temperature ranges in a test condition.

The temperature distribution indicated that the test section had a counter flow arrangement. For CHT test run number 1-M, 1-Q, 1-F, and 1-I, the steam mass flow ranged from 5.27 g/s (18.97 kg/hr) to 16.34 g/s (58.82 kg/hr), whereas coolant (water) mass flow ranged from 0.126 kg/s (453.6 kg/hr) to 0.158 kg/s (568.8 kg/hr). Test data showed that the axial temperature profile was uniformly increased if the difference in temperatures between the condensate outlet and the coolant inlet stayed high. The sample CHT tests data are presented in Figures. 7.1 to 7.3. Condensation test results were influenced by the temperature distributions and mass flow rates, according to preliminary data.

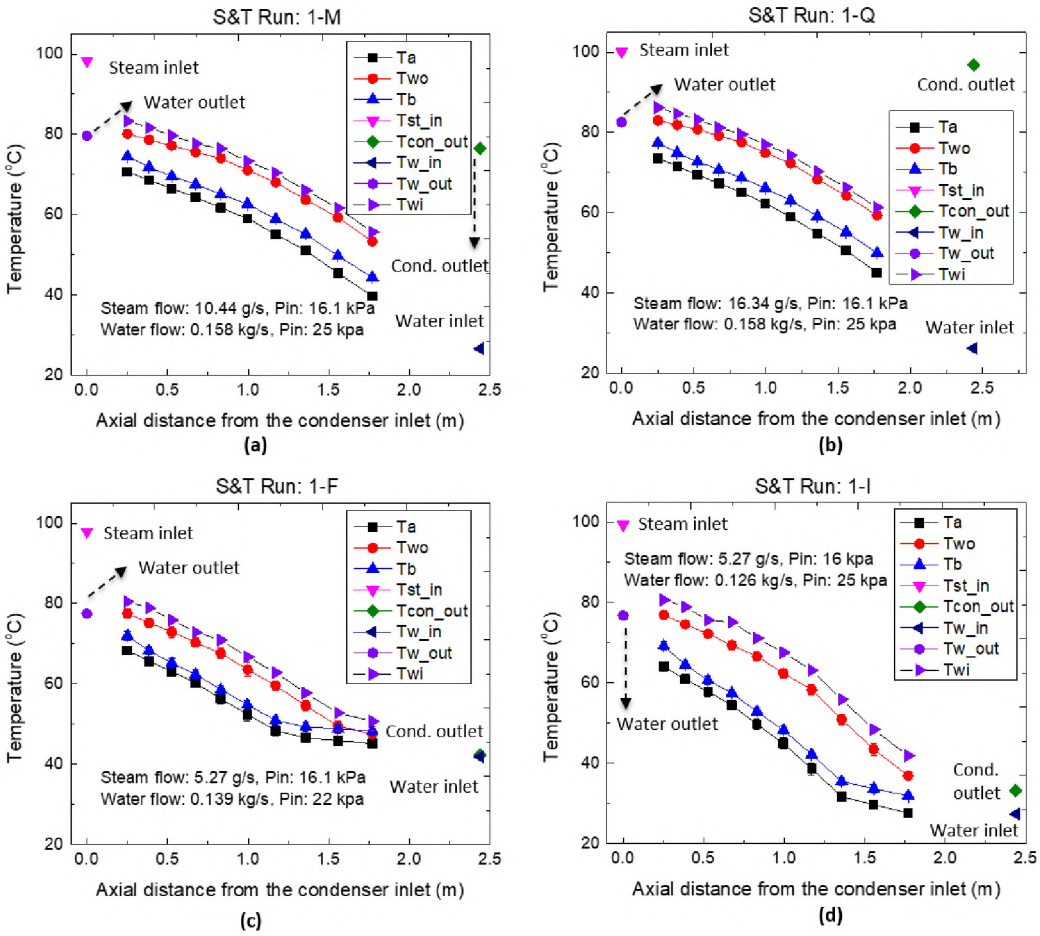

Figure 7.1. Test data (1): (a)-(d) axial T distribution for different steam mass flow rate

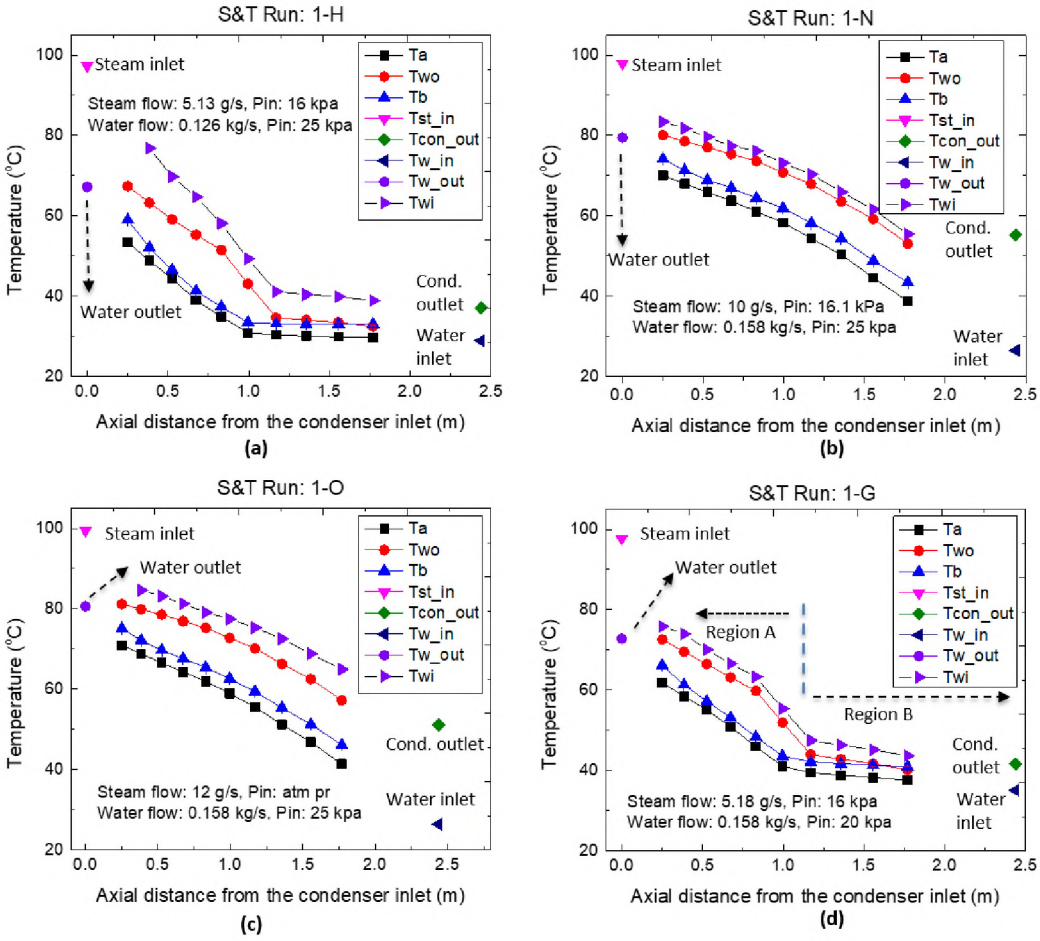

Figure 7.2. Test data (2): (a)-(d) axial T distribution for different steam mass flow rate

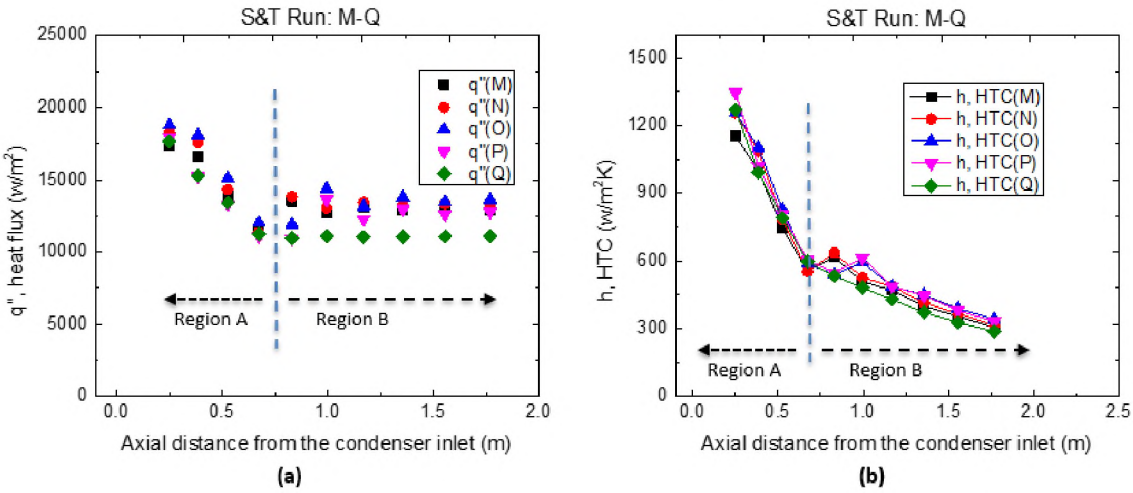

Figure 7.3. Test data: axial (a) heat flux, q'' and (b) HTC distribution

Results showed that a low steam mass flow and a high coolant mass flow could lead to complete condensation, as illustrated in region B of Figure 7.2 (d). The separated regions caused errors in the heat flux estimation and HTC calculation. It was necessary to keep the coolant flow as low as possible to achieve a sharp axial temperature distribution of the coolant. Low coolant flow, by contrast raised the coolant outlet temperature and if it was close to saturation, it caused cavitation at the coolant pump outlet. As a result, the design limit for the test section was set to keep the inlet and outlet temperatures of the jacket water between 20 ºC and 80 ºC.

The test facility had no option to measure the center-line temperature of saturate steam. According to Figure 7.2 (c) and (d), the temperature distribution was categorized as A and B in the presence of low steam flow and high coolant flow. In region A, there was data for estimating the CHT rate, while in region B, there was increased error and measurement uncertainty. The change can also be seen in the axial heat flux and HTC distribution in Figure 7.3. HTC and heat flux in region A were both higher than those in region B. As the condensate film grew and increased axially, the interfacing gas-mixture layer turbulence effected the induced film waviness of the condensate film.

The brief results demonstrate that the developed CHT facility worked as intended. The preliminary results were consistent with previous studies. The measured data's accuracy indicated a high dependency on steam and coolant flow rates and measurement techniques. The test data results exhibited different regions with varying levels of measurement uncertainty. Therefore, collecting test data within a low error band was vital.

The preliminary test data measurement error analysis showed standard errors of 2%, 3%, 11%, and 19% for the temperature, T (°C); mass flow rate, $\dot{m}$ (kg/s), heat flux, q (W/m^2); and HTC, h (W/m^2 K); respectively. In light of the preliminary test results, a standard testing procedure and testing conditions were derived, and then applied to the final experiments and analysis.

7.1.2. Final Measurements with Steam and NCG. Scaled experiments were conducted using steam and steam-NCG mixtures in three test sections. Nitrogen and helium gases were used as the NCG. Test data were collected for varying mixture mass fractions, mass flow rates, and coolant flow rates. The sample final test dataset are presented in Figure 7.4 to 7.10.

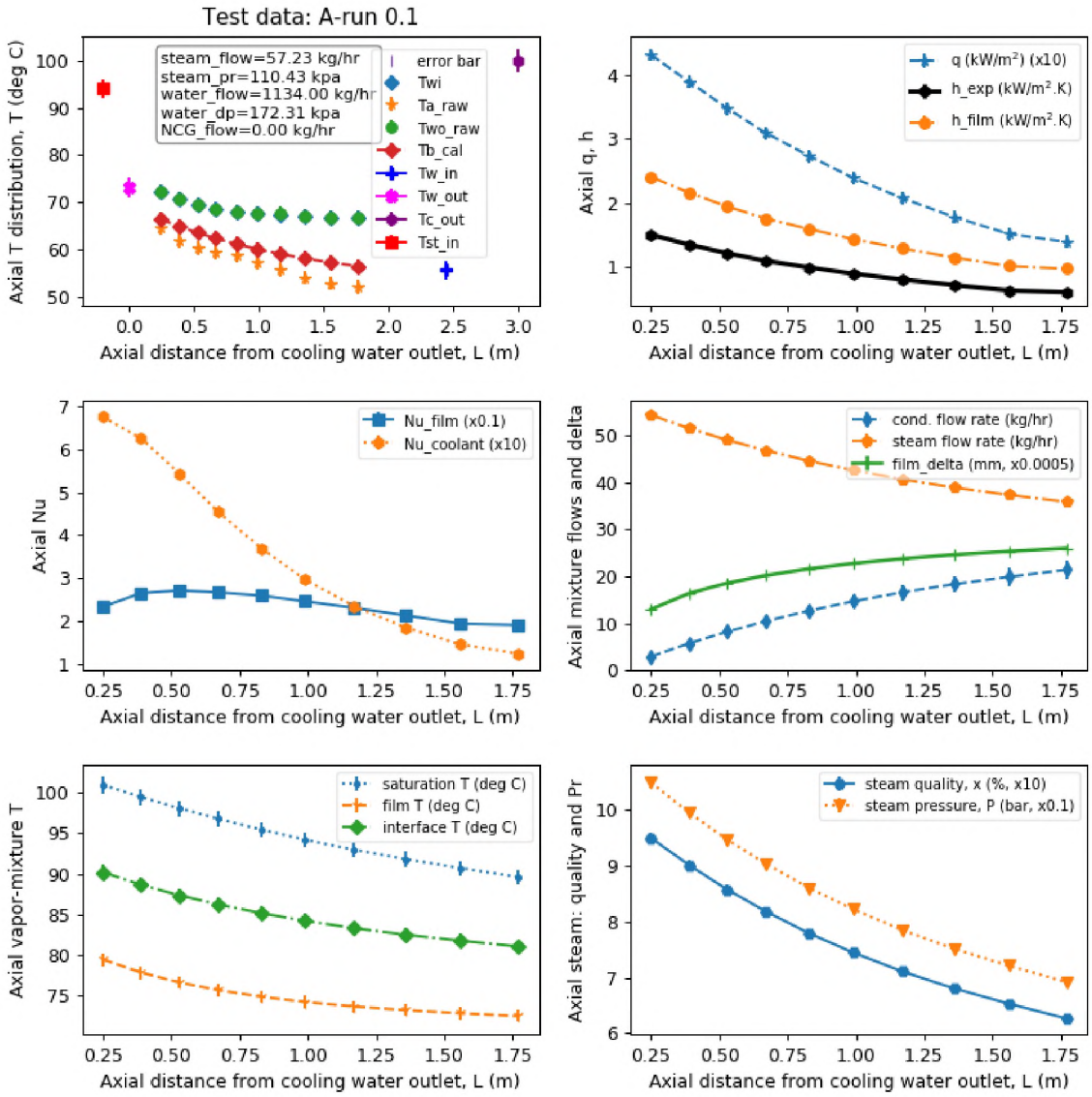

Figure 7.4. Test data: A-run0.1 (4in-test-section, pure steam)

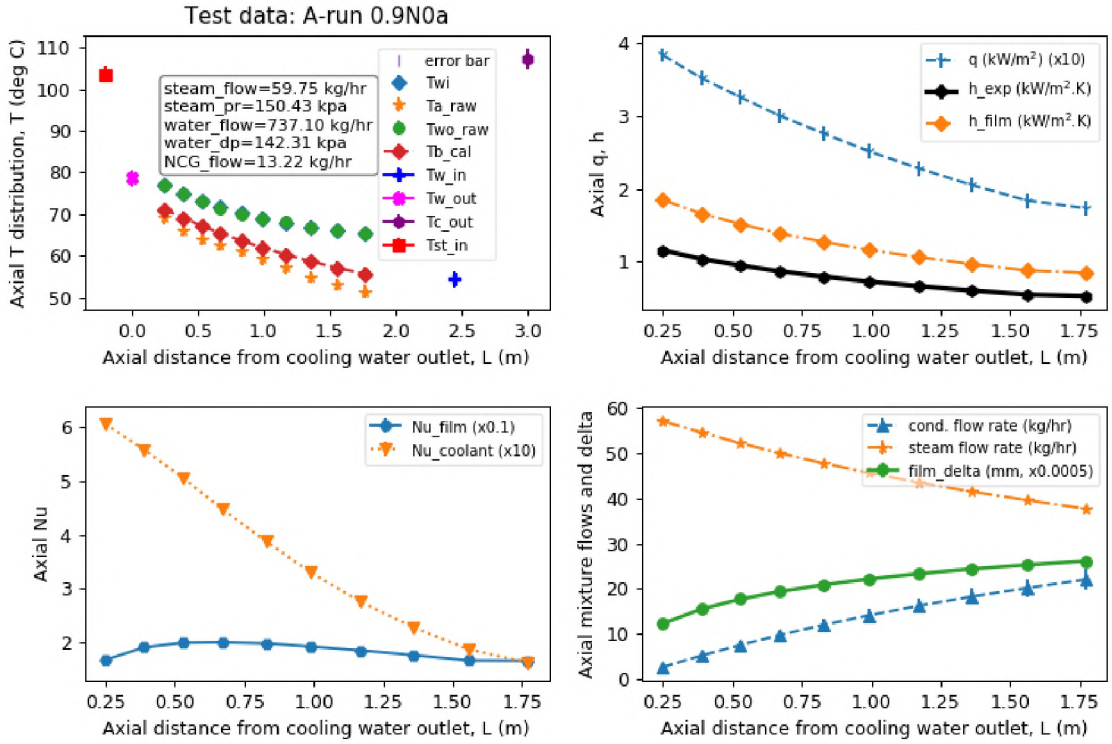

Figure 7.5. Test data: A-run0.9N0a (4in-test-section, NCG: N2, high flow)

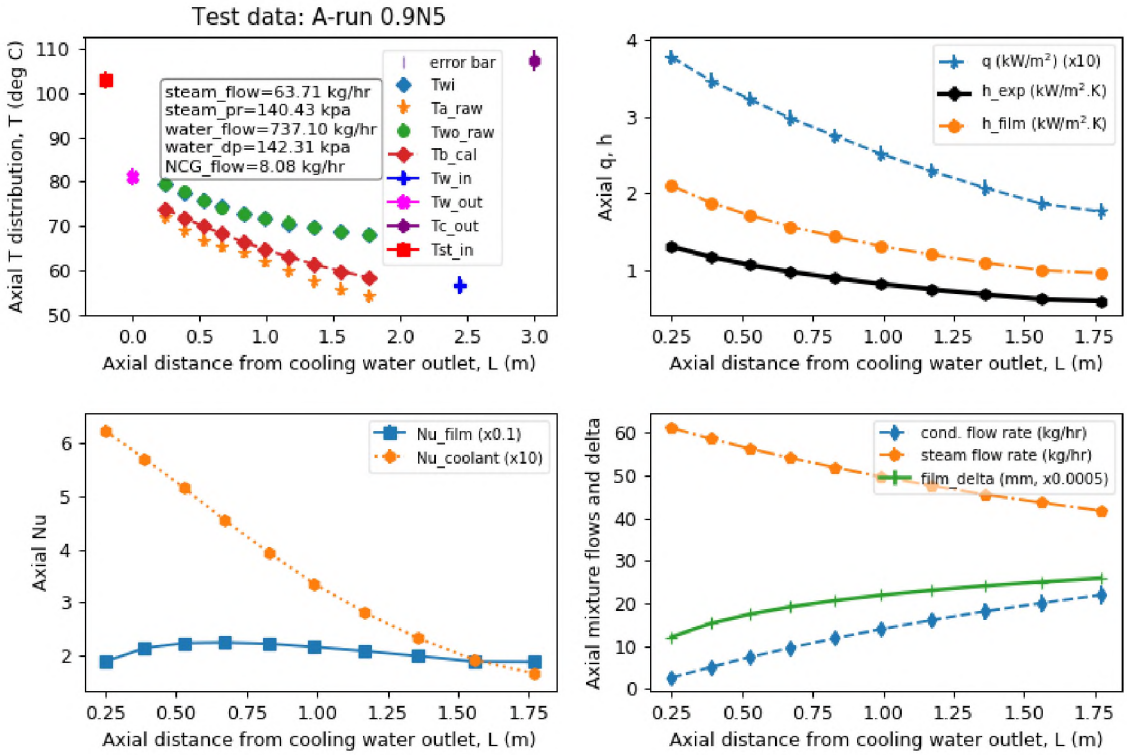

Figure 7.6. Test data: A-run0.9N5 (4in-test-section, NCG: N2, medium flow)

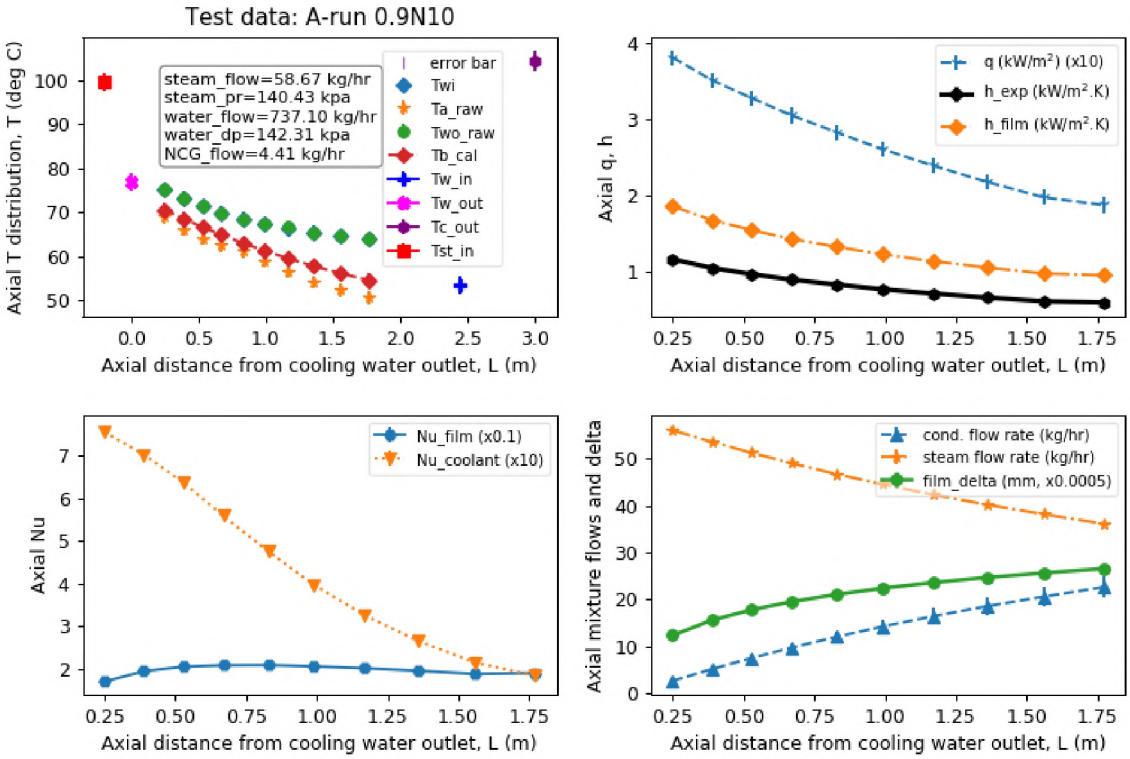

Figure 7.7. Test data: A-run0.9N10 (4in-test-section, NCG: N2, low flow)

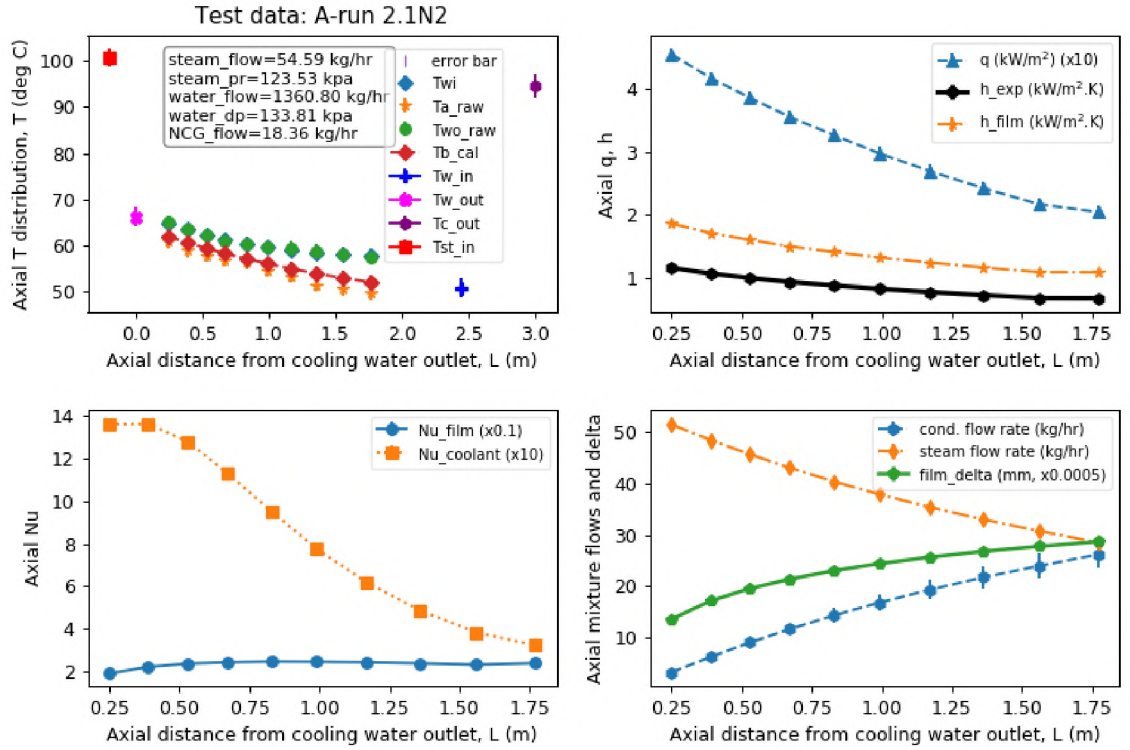

Figure 7.8. Test data: A-run2.1N2 (4in-test-section, NCG: He, high flow)

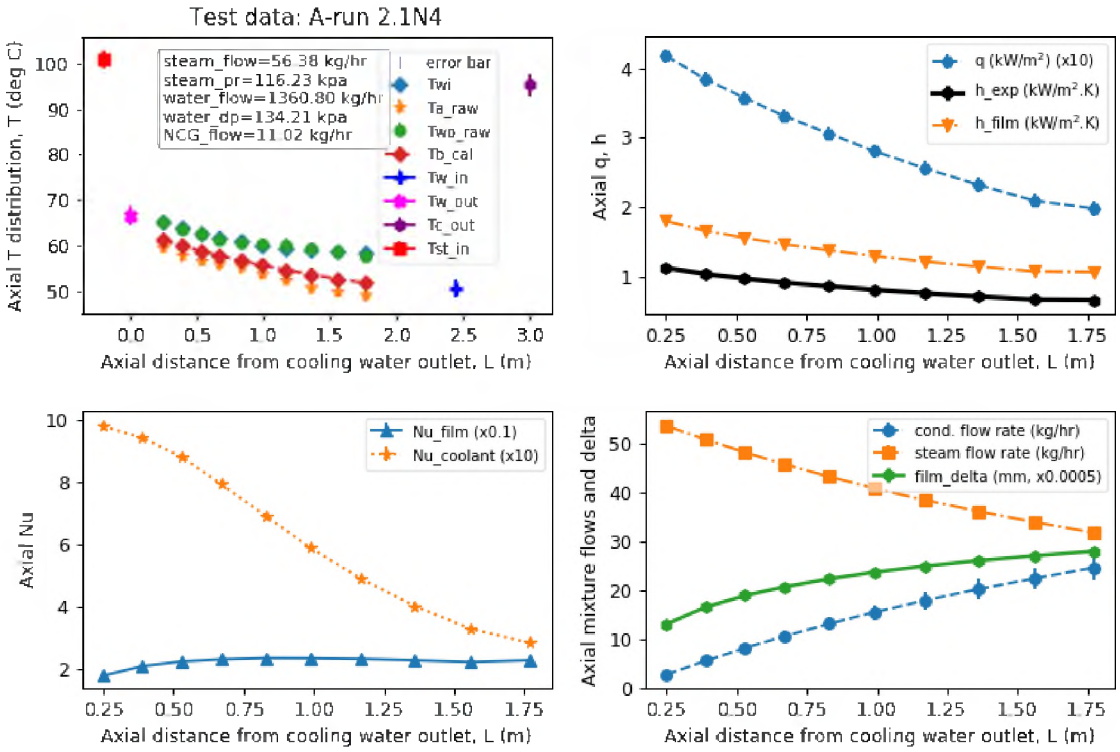

Figure 7.9. Test data: A-run2.1N4 (4in-test-section, NCG: He, medium flow)

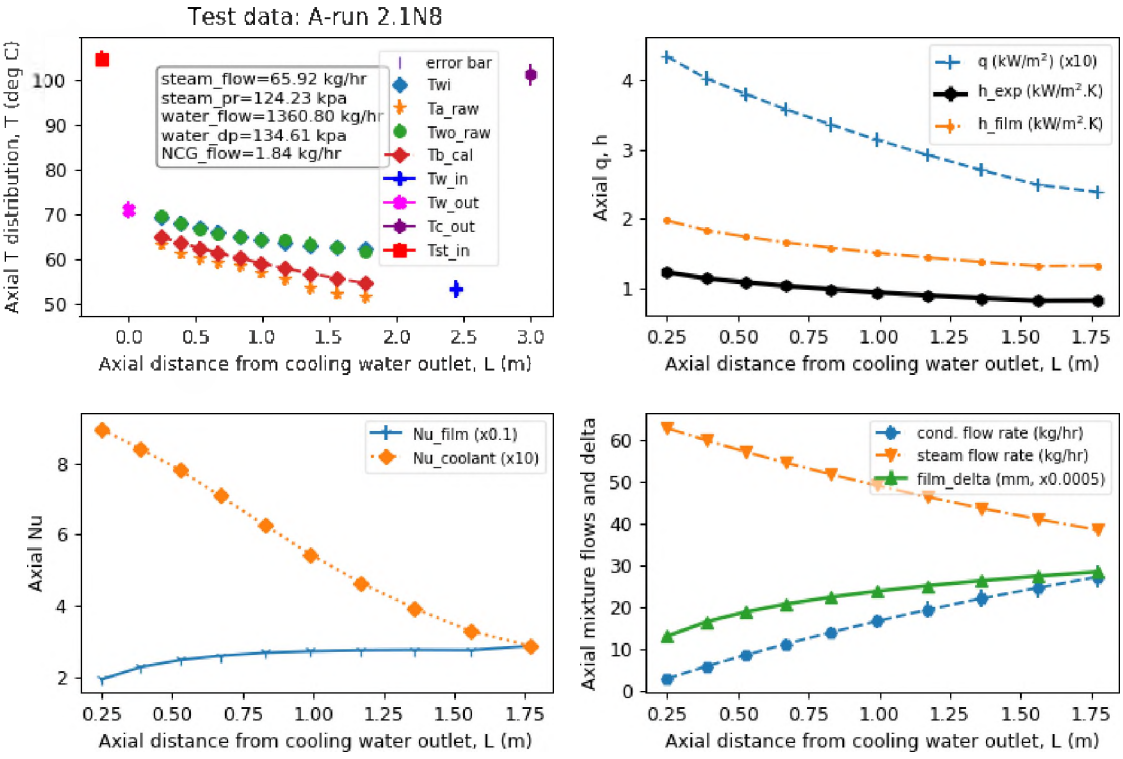

Figure 7.10. Test data: A-run2.1N8 (4in-test-section, NCG: He, low flow)

In the first subplot, the axial temperature distributions for the steam, gas, and coolant regions are shown. Other subplots represent calculated parameters, such as heat flux, HTC, Nu, mixture flow rate, and film thickness. The test results of varying NCG flow showed consistency for heat flux, HTC, and film thickness, as shown in Figure 7.11. The additional estimated parameters, such as steam saturation, film and interface temperatures, steam quality, and pressure are presented in the last two subplots of Figure 7.4 and exhibit the consistency.

The helium and nitrogen flow varied 3-15% and 4-8%, respectively, for the presented test data, as shown in Figure 7.11. Results showed that the effect of nitrogen was more dominant than that of helium. The test results showed low deviations and low effects of NCG. The tests were conducted under saturated steam conditions at approximate atmospheric pressure with ambient discharge. As a result, there was no option for gas accumulation. Moreover, NCG flowed from elevated pressure and forced the steam-condensate mixture to leave the test section, thus increasing flow turbulence with forced convection. SMRs had smaller diameters but longer containment vessels than large commercial power reactors, therefore these test results support scale testing and system analysis.

7.1.2.1. Effects of varying the steam flow rate i.e. Re. Steam flow adjustments were compared using the main throttle valve. Next, similar experiments were performed for different steam mass flow rates in three test sections. Three sample tests for steam high and moderate flow rates are in Figure 7.12 and Figure 7.13.

The condensate temperature at the outlet of the test section for low steam flow test case (A-run 0.2) was approximately 45°C, as shown in Figure 7.13, it exhibited a fully steam condensation case.

7.1.2.2. Effect of varying the steam pressure. Preliminary tests were performed to investigate the effects of varying the steam pressure on CHT. Inlet steam supply pressure regulators were used to adjust steam supply pressure. However, the outlet of the test section had to be pressurized, which resulted in backflow and altered the axial flow pattern. To keep

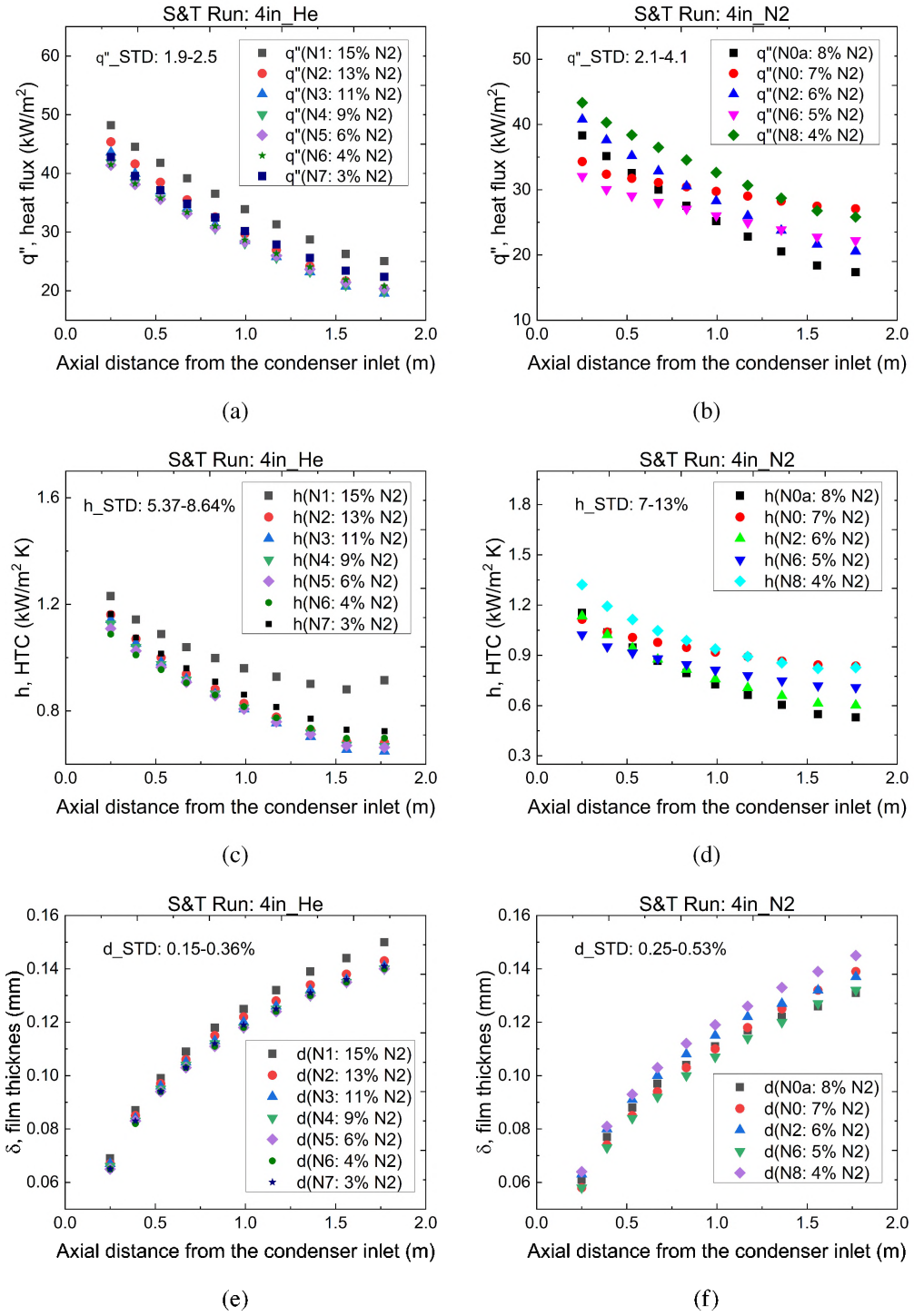

Figure 7.11. Test results for varying NCG: (a)-(b) q, (c)-(d) h, (e)-(f) film thickness

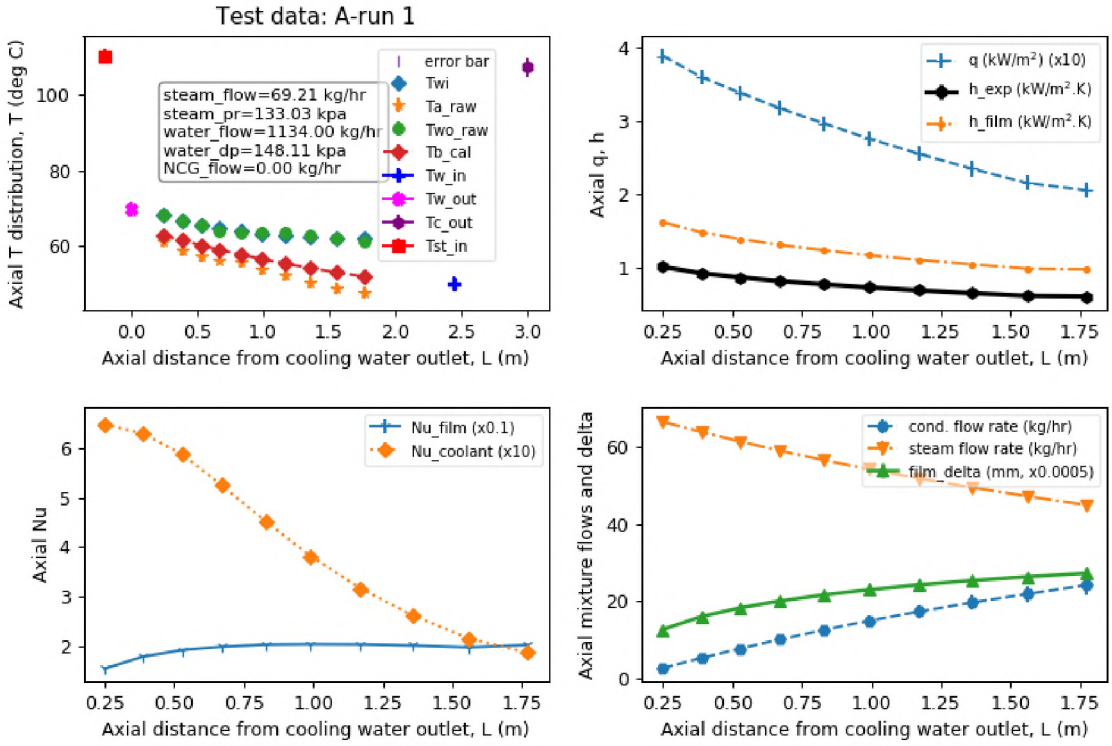

Figure 7.12. Test data: A-run1 (4in-test-section, steam, high flow)

test data consistancy with less distortion in temperatures and flow for scale effect analysis, the elevated pressure test data were not included in this study. Review showed that heat transfer reduced with decreased steam pressure.

7.1.2.3. Effect of reducing the coolant flow. The subcooling of the condenser tube was varied by adjusting the jacket water flow and by using the cooling water pump bypass line. Test data were collected for a limited set of subcoolings. This limitation was due to the increasing temperature spans between the jacket cooling inlet and the outlet temperatures. A wider temperature span yielded better temperature profiles for heat flux estimation. However, due to the closed-loop cooling system operating at high temperatures (above 90 ºC), cavitation and pressure fluctuations were observed at the pump outlets.

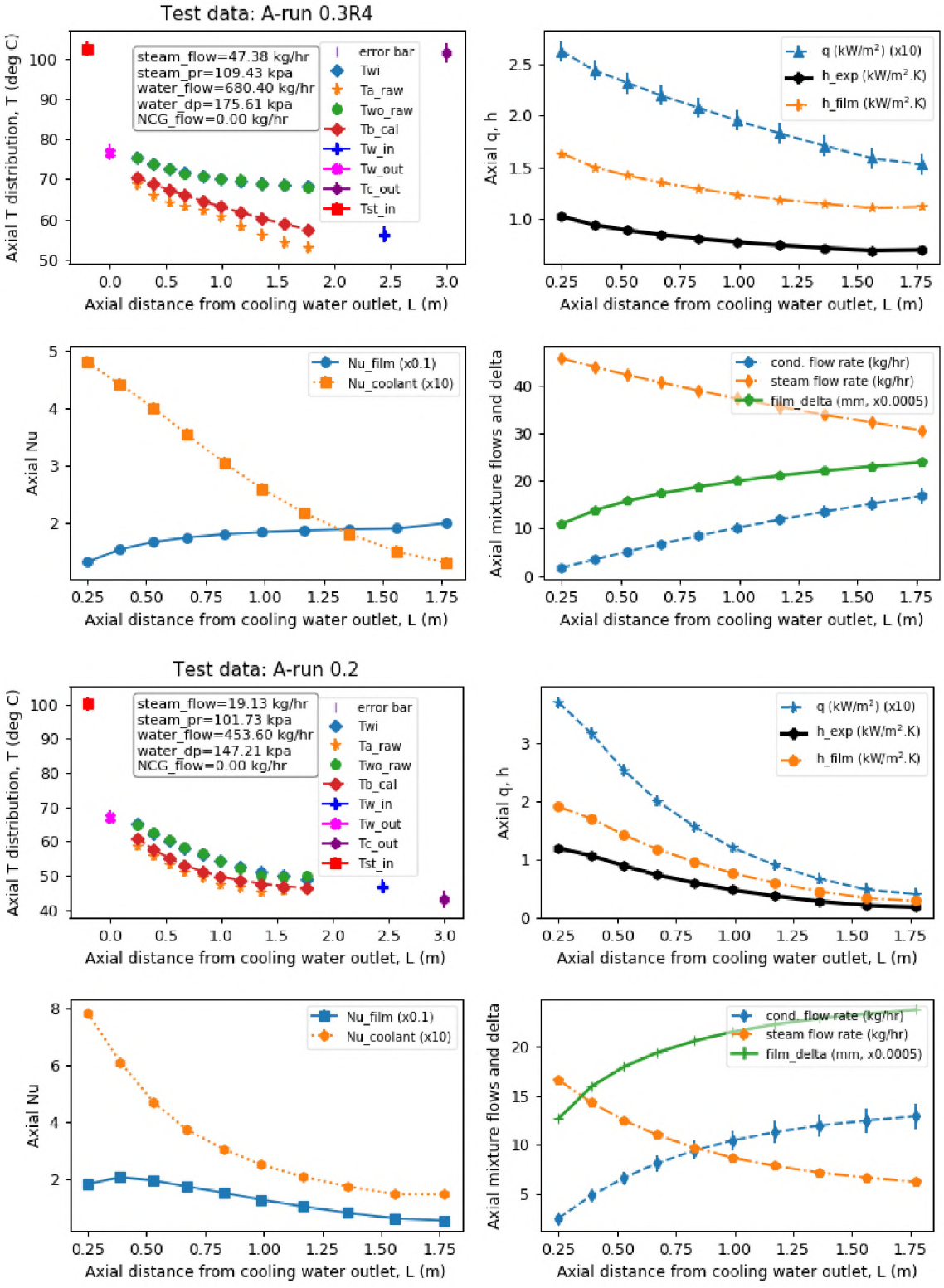

Figure 7.13. Test data: A-run2.1N4 and A-run2.1N8 (steam moderate flow)

7.1.3. Evaluating degradation factors. Final test data were used to estimate the degradation factor (DF), which was the ratio between experimental HTC and HTC from Nusselt analytical solution. DF values are shown in Figures 7.14 and 7.15 for pure steam, steam-helium, and steam-nitrogen mixtures for sample final scaled test. Results showed that for the selected tests (4in test section) the DF value ranged 0.08 to 0.19 for pure-steam, 0.08 to 0.2 for steam-helium and 0.08 to 0.22 for steam-nitrogen mixtures experiments. Test results of 1in and 2in test sections showed consistency in the data trend with DF ranged approximately 0.1 to 0.6.

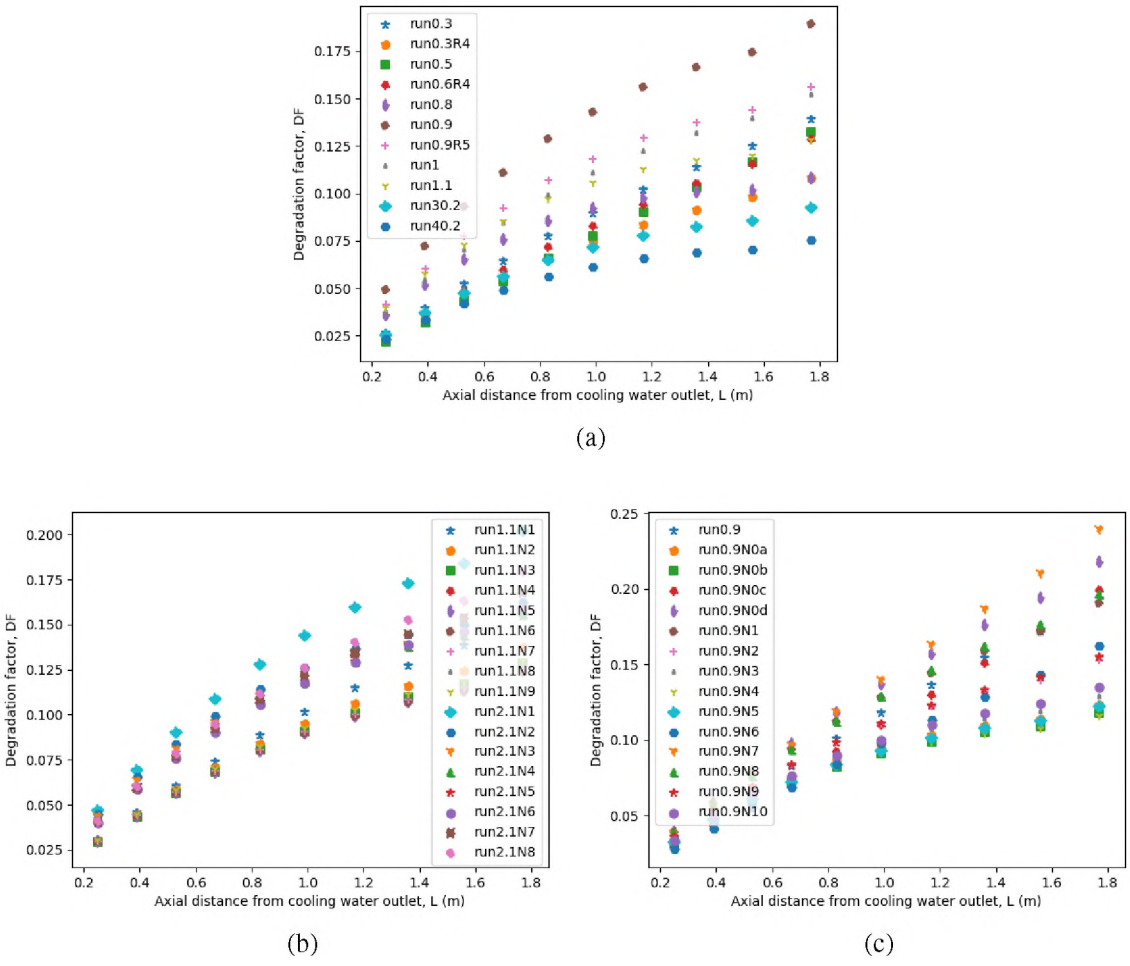

Figure 7.14. DF for 4-inch test-section: (a) pure steam, (b) steam-He, (c) steam-N2

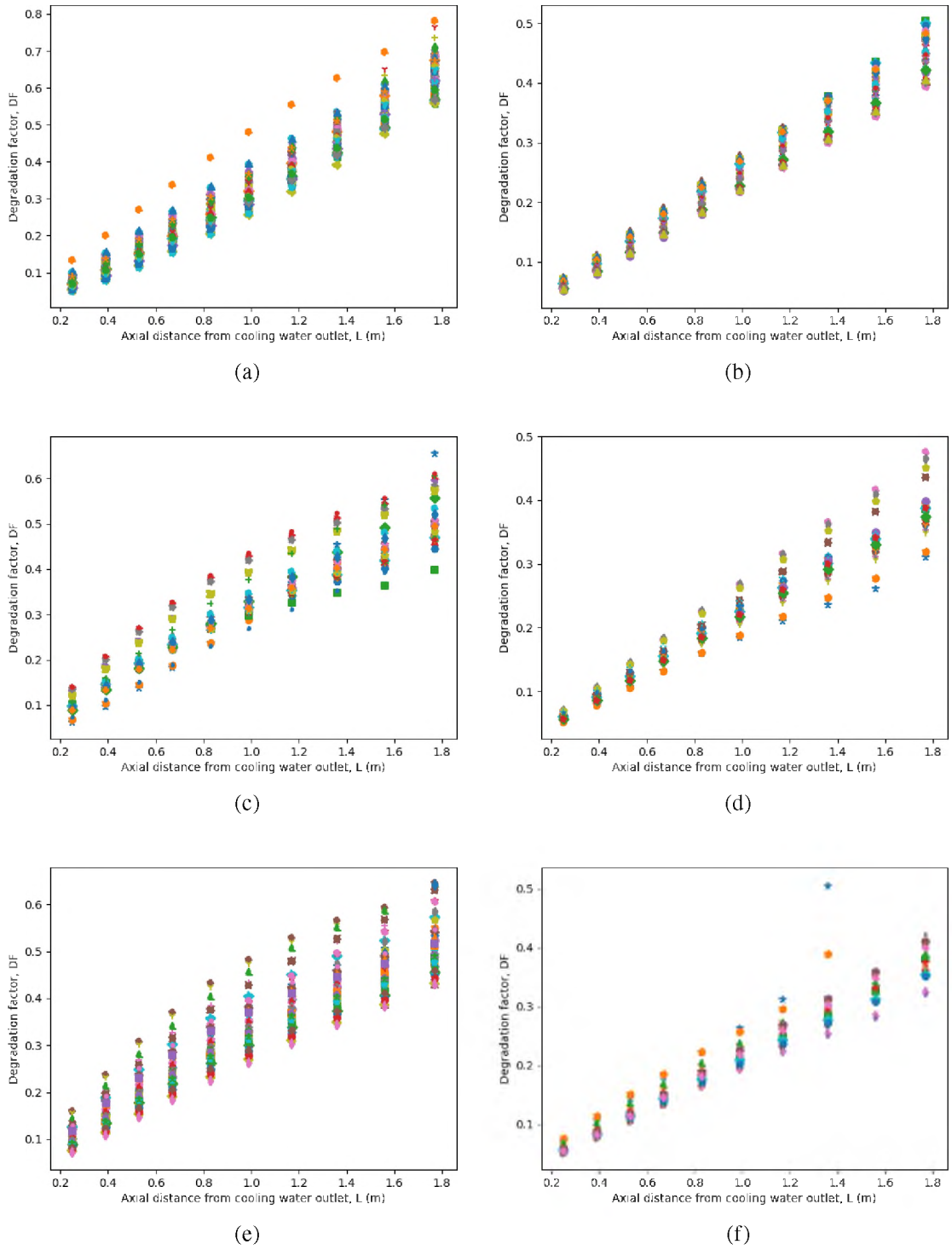

Figure 7.15. DF for 1-inch (1") and 2-inch (2") test sections: (a) pure steam (1"), (b) pure steam (2"), (c) steam-He (1"), (d) steam-He (2"), (e) steam-N2 (1"), (f) steam-N2 (2")

7.1.3.1. Discussion on test results. A scaled modular test facility addressing the concerns identified from the earlier experimental facilities with specific limitations was developed. To determine the wall heat flux value, a 4-wire thermocouple was used to provide accurate temperature readings. Repeated tests were performed to confirm the reproducibility of the test data for varying steam mass flow rates, and NCG mass fractions.

Test data showed that with increased in NCGs, the CHT, HTC, and condensation rate decreased. In contrast, these values decreased as the steam mass flow increased; however, with the rise of system pressure, the CHT value increased and the HTC value decreased. Nevertheless, the large-scale down induced dominance effects because of the dynamics of the entrance flow. In Nusselt's analysis, the facility with a reduced length showed a higher condensation HTC than the prototype, which was expected.

A detailed assessment of CHT with NCGs was performed. The previously developed physics-based model and semi-empirical correlations were evaluated compared with the comprehensive test data set. This correlation was valid for a range of boundary conditions, which needed to be tested for elevated pressure.

7.1.3.2. Other supportive tests and physics conditions. Steam release to a reactor containment is a transient phenomenon. Even though the developed correlations from the separate effect tests focused on steady-state conditions, transient test data to simulate the accident condition would be supportive for scaling effect analysis. In addition, the vapor-NCG mixture in the reactor containment also formed natural convective flows. As a result, these physics phenomena and associated test data were necessary to investigate scaling effects. The SMR reactor containment wall cooled by an outside water pool. Therefore, the pool boiling heat transfer scenarios were also necessary to evaluate the scaling effect. The developed scaled test facility at Missouri S&T was designed for separate effect tests, and preliminary tests for transient, natural convection, and pool boiling conditions were conducted. In this report, these test results and physics were not discussed. However, it would be worthwhile to continue research using these test data in the future.

7.2. CFD SIMULATION RESULTS

CFD simulations were performed with varying steam mass fractions using NCG to get temperatures, velocities, and species distributions. The coolant axial temperatures distribution and mass flow rates were used to calculate heat flux, HTC, and Nusselts number; Nu was used for the vapor-mixture and film regions. The simulated film thickness, δ calculated the film Nu. The combined simulated results agreed with Kuhn's test data for centerline temperature and wall temperature, which ensured the physics models' validation.

7.2.1. Validation of the CFD Simulation. The steam, tube-solid, and water regions' conjugate heat transfer were simulated together using Kuhn's tests: pure steam (run1.1-1 and run1.1-4) at 114 kPa pressure and 405 kPa pressure; and steam-air (run2.1.8R and 2.1-13)–low air mixture (15%) with steam and high air mixture (40%) with steam were considered. However, in the pure steam simulation, 1% air presence was considered as an impurity in the test section. Simulation results contours are presented in Figure 7.16.

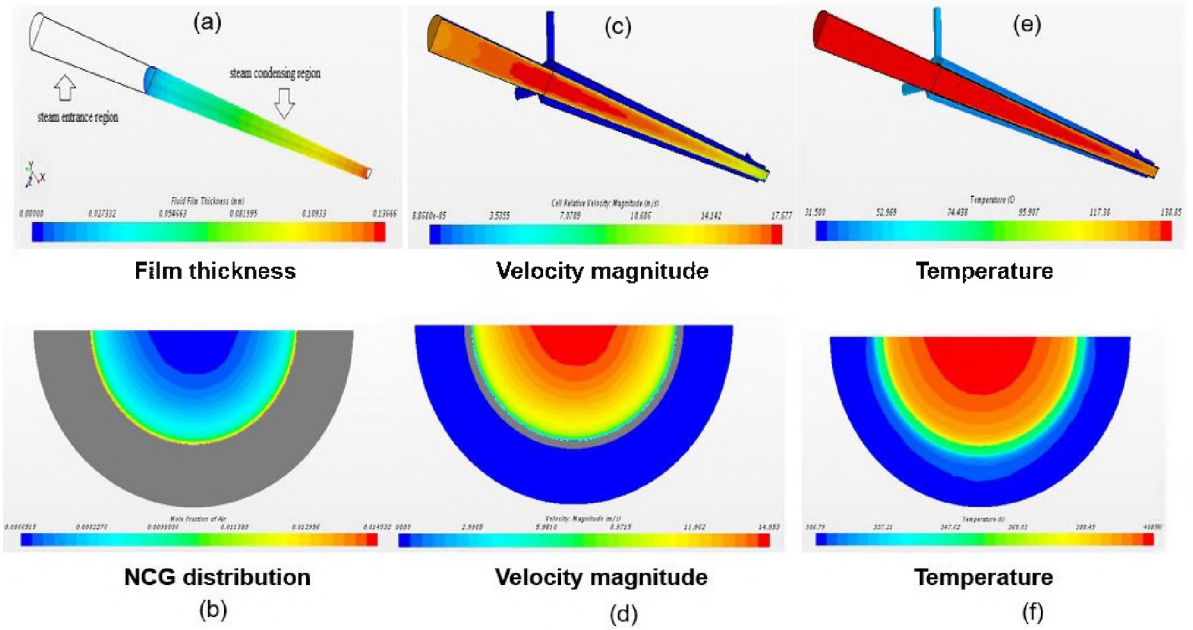

Figure 7.16. Result contour: (a) film, (b) NCG, (c)-(d) velocity, (e)-(f) temperature

The simulation results were validated against the tests data: centerline temperatures, wall temperatures, coolant temperatures, heat fluxes, and heat transfer coefficients, and Nusselt numbers, as presented in Figure 7.17, Figure 7.18, and Figure 7.19.

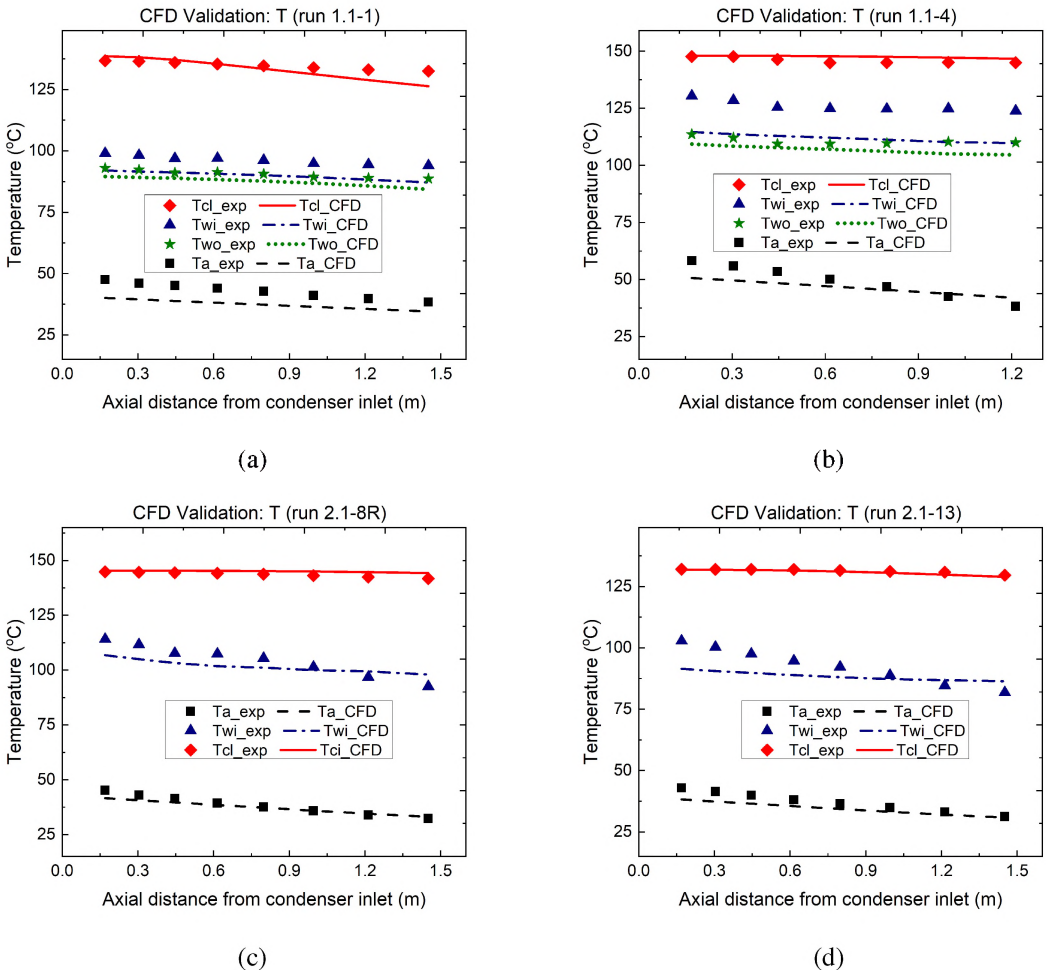

Figure 7.17. CFD validation: temperature distributions (a) run 1.1-1, (b) run 1.1-4, (c) run 2.1-8R, and (d) run 2.1-13

The simulated temperature distribution followed a trend similar to the test data. However, simulation results underestimated the condenser tube's inner wall temperatures by the standard errors of 6.5% (for run1.1-1), and 10.5% (for run1.1-4) more than the test data derived from the heat flux and outer wall temperatures. These deviations were within

±5 % for the steam-air test cases (run2.1-8R and run2.1-13). Simulated jacket tube walls temperatures and steam centerline temperatures agreed with the test data and had a STD within ±1-3 %, thus ensuring the physics models' validation.

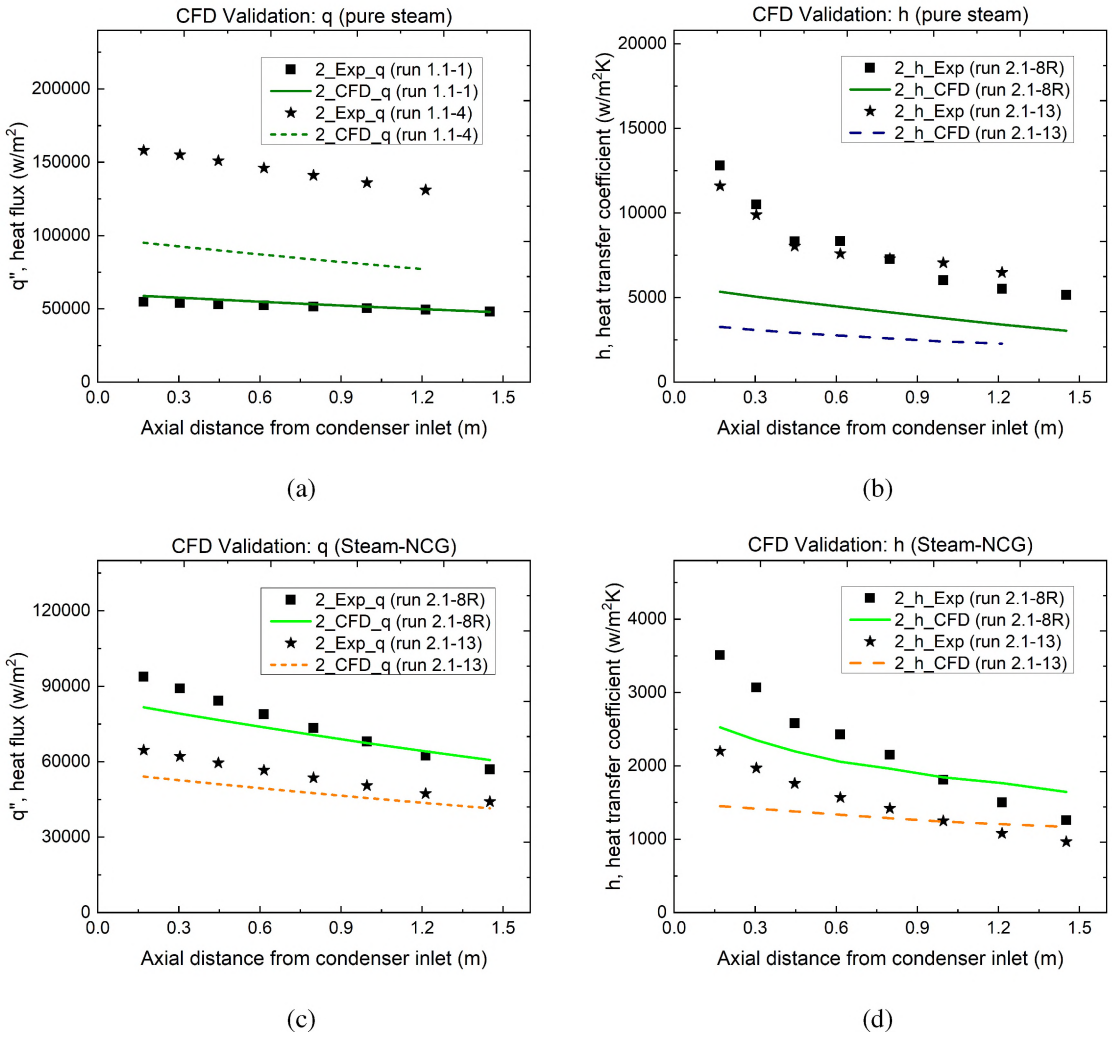

Figure 7.18. CFD validation: (a)-(b) heat flux, q, (c)-(d) HTC,h

At the condenser tube wall, the heat flux from the steam to the coolant was calculated using the coolant bulk temperatures, which were similar to the experimental heat flux calculations. The bulk temperature (Tb) was the mass averaged fluid temperature. Kuhn's used a k-e turbulence analytical model developed by Yuann (1993) to estimate the coolant Tb using the test parameters, like mass flow rates and wall temperatures.

Figure 7.20 presents the errors of the CFD simulations compared to the test data. Errors were propagated from the directly measured parameters (e.g., coolant temperature and mass flow rate) to the computed parameters (e.g., heat flux, heat transfer coefficient).

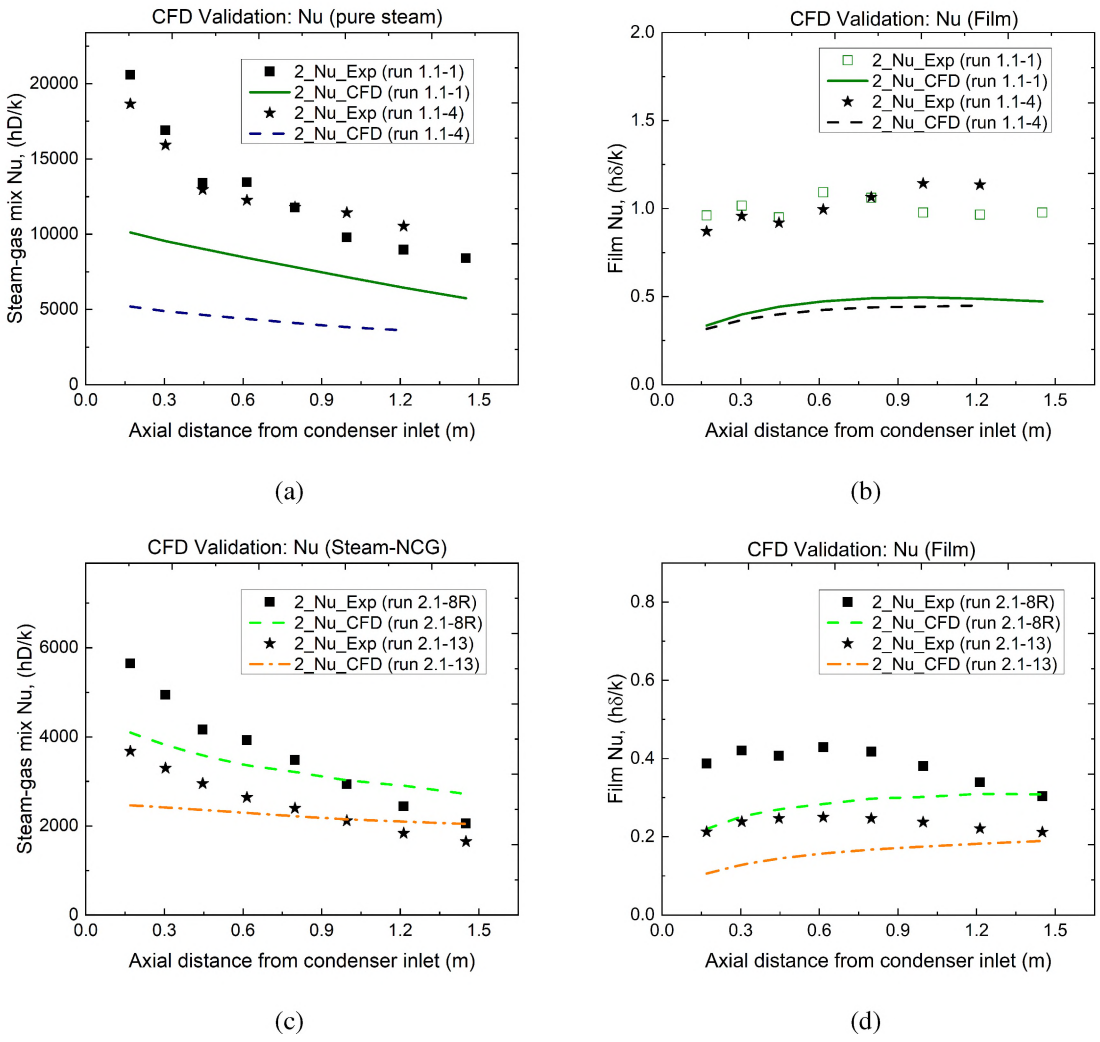

Figure 7.19. CFD validation: (a)-(b) vapor-NCG mixtur Nu, (c)-(d) condensate film Nu

The CFD heat flux results matched (by a standard error of 4.5%) the low-pressure (at 114 kPa) steam test data but underpredicted (by a standard error of 38%) for the high-pressure (at 405 kPa) steam test data. These heat flux deviations (under-prediction in an average) for the steam-air test cases were within 10%.

The increased heat flux errors came from the increased bulk temperature errors. The simulated bulk temperature results showed a standard error range of 8-9 % for pure-steam and 1-5 % for steam-air test cases. However, these errors were dominant (about 12%) at the condenser tube axial top half part then the errors (about 3-7%) of the bottom half part. Results showed that simulated data had a similar error trend to the experimental error. At the entrance and exit regions of the condenser sections, it incurred higher errors than the middle section. This difference in error distribution was due to the flow development and multi-dimensional inlet and outlet geometries.

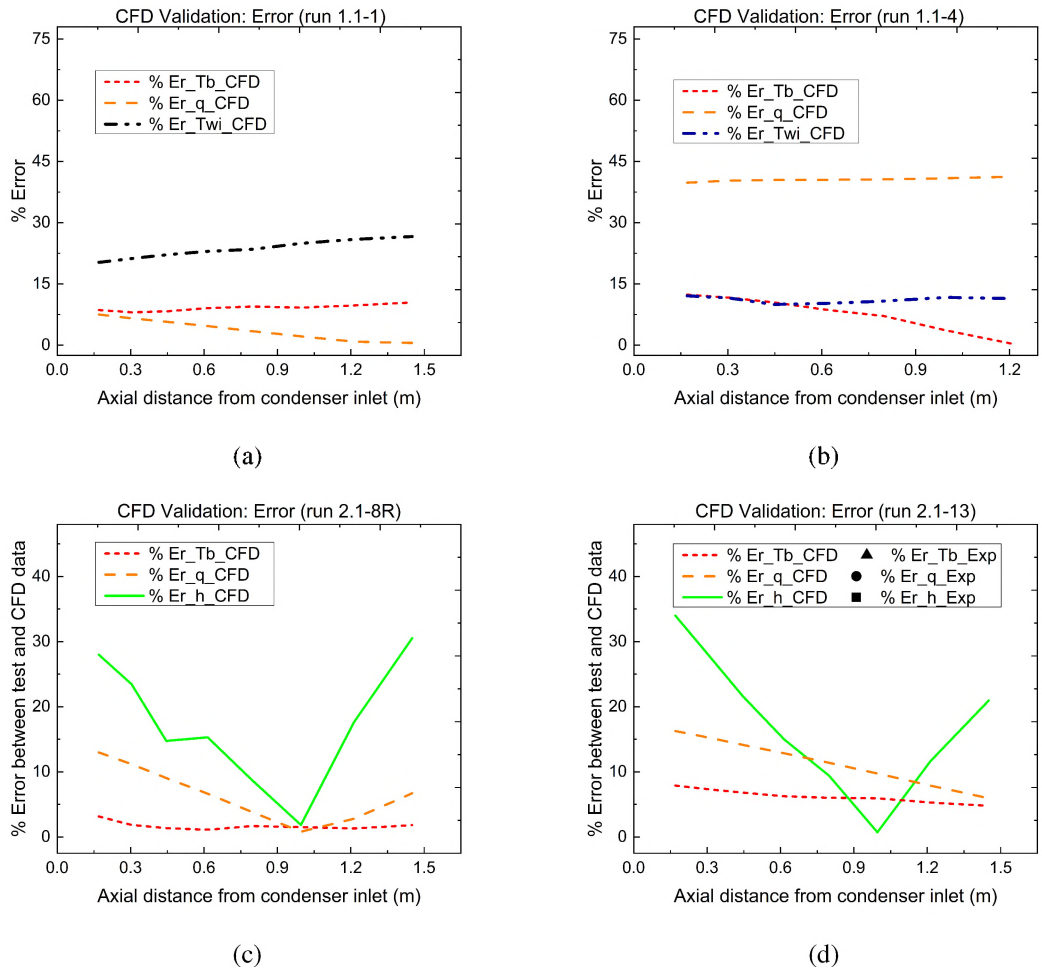

Figure 7.20. CFD validation error of Tb, q, and h for: (a) run 1.1-1, (b) run 1.1-4, (c) run 2.1-8R, and (d) run 2.1-13

7.2.2. Scaled Simulation Results. This study used Kuhn's test as the reference case. Kuhn used a 2-inch steam condenser tube with a 3-inch annular coolant tube. Based on the reference geometry, scaled-up and scaled-down geometries were prepared in the CAD, and used in the CFD simulation. The inlet mass flow rates for steam and water were scaled, keeping the same Reynolds number (Re). The scaled simulation results (the coolant bulk temperatures, heat flux, HTC, and Nu) are presented in Figure 7.21, Figure 7.22, Figure 7.23, and Figure 7.24, respectively.

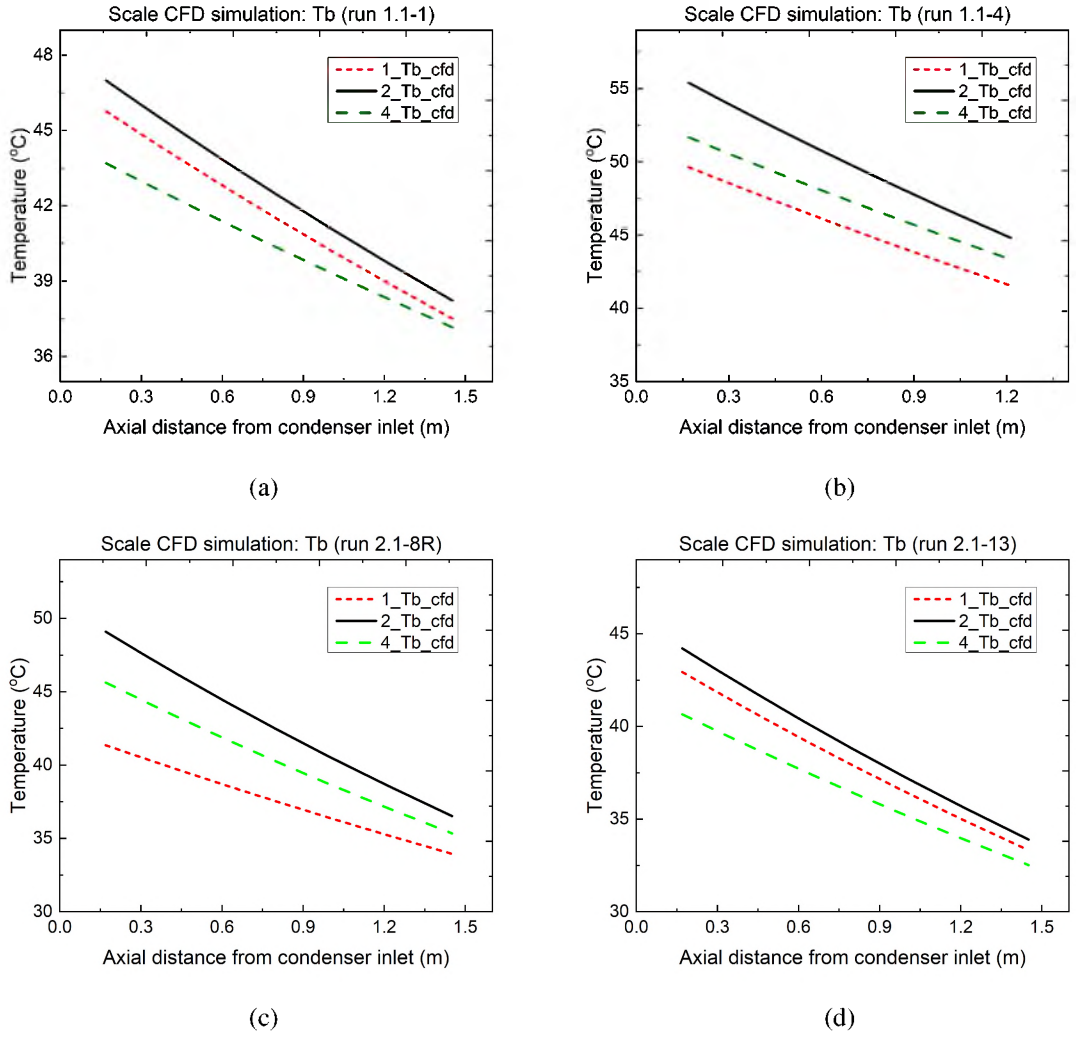

Figure 7.21. CFD scaling assessment results, Tb: (a) run 1.1-1, (b) run 1.1-4, (c) run 2.1-8R, and (d) run 2.1-13

The other boundary conditions were kept the same as in the reference test case—the boundary conditions for the scaled simulation are presented in Table 2 and 1. The scaled simulation results of the coolant Tb and heat flux showed that the reference case simulations exhibited higher Tb values than the scaled simulations; however, Tb from scaled simulations were inconsistent.

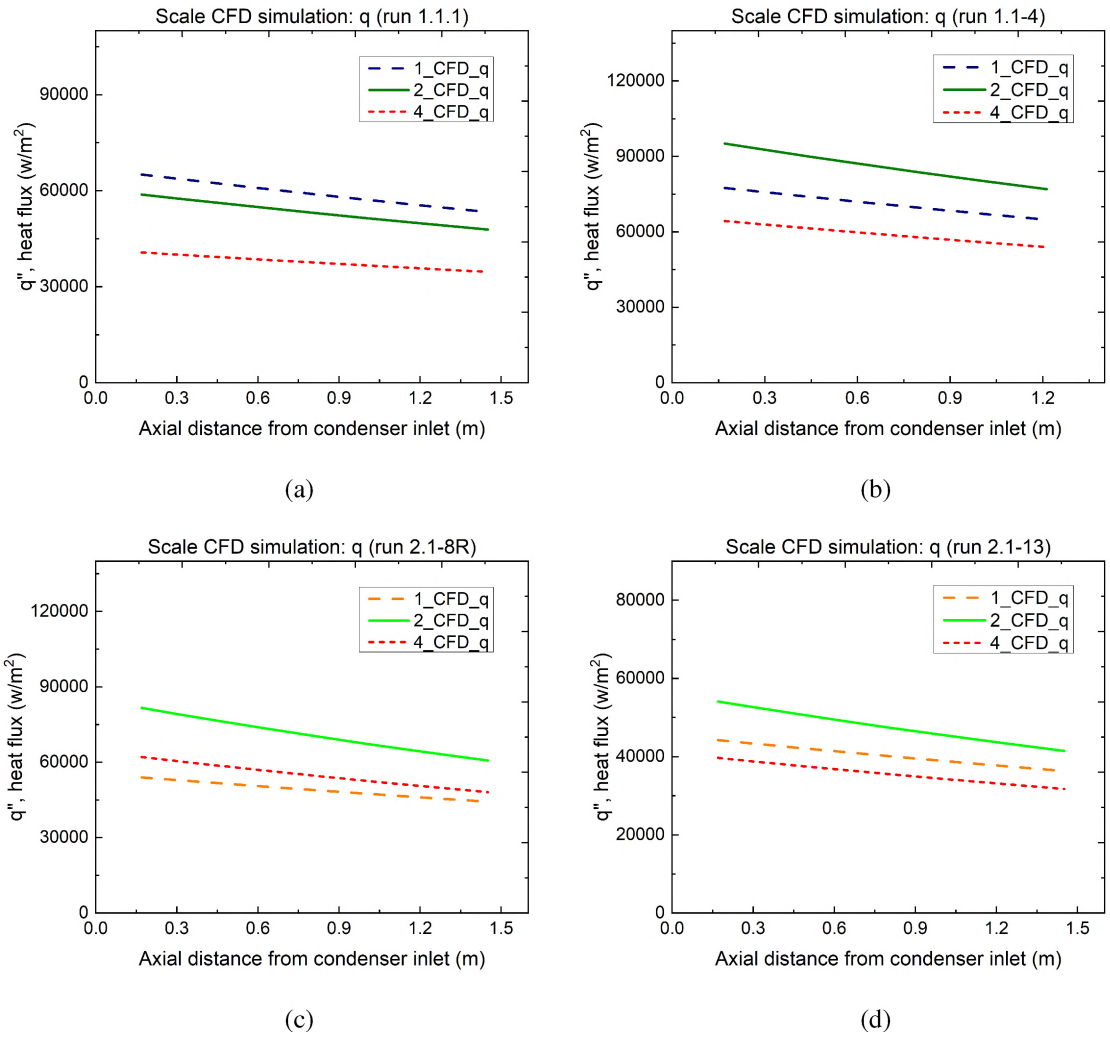

Figure 7.22. CFD scaling assessment results, q: (a) run 1.1-1, (b) run 1.1-4, (c) run 2.1-8R, and (d) run 2.1-13

The scaled simulations were compared with the non-dimensional parameters: Reynolds number (Re) and Nusselts number (Nu). Re represented the flow dynamics (laminar or turbulent); whereas, Nu represented the heat transfer performance between convection and conduction.

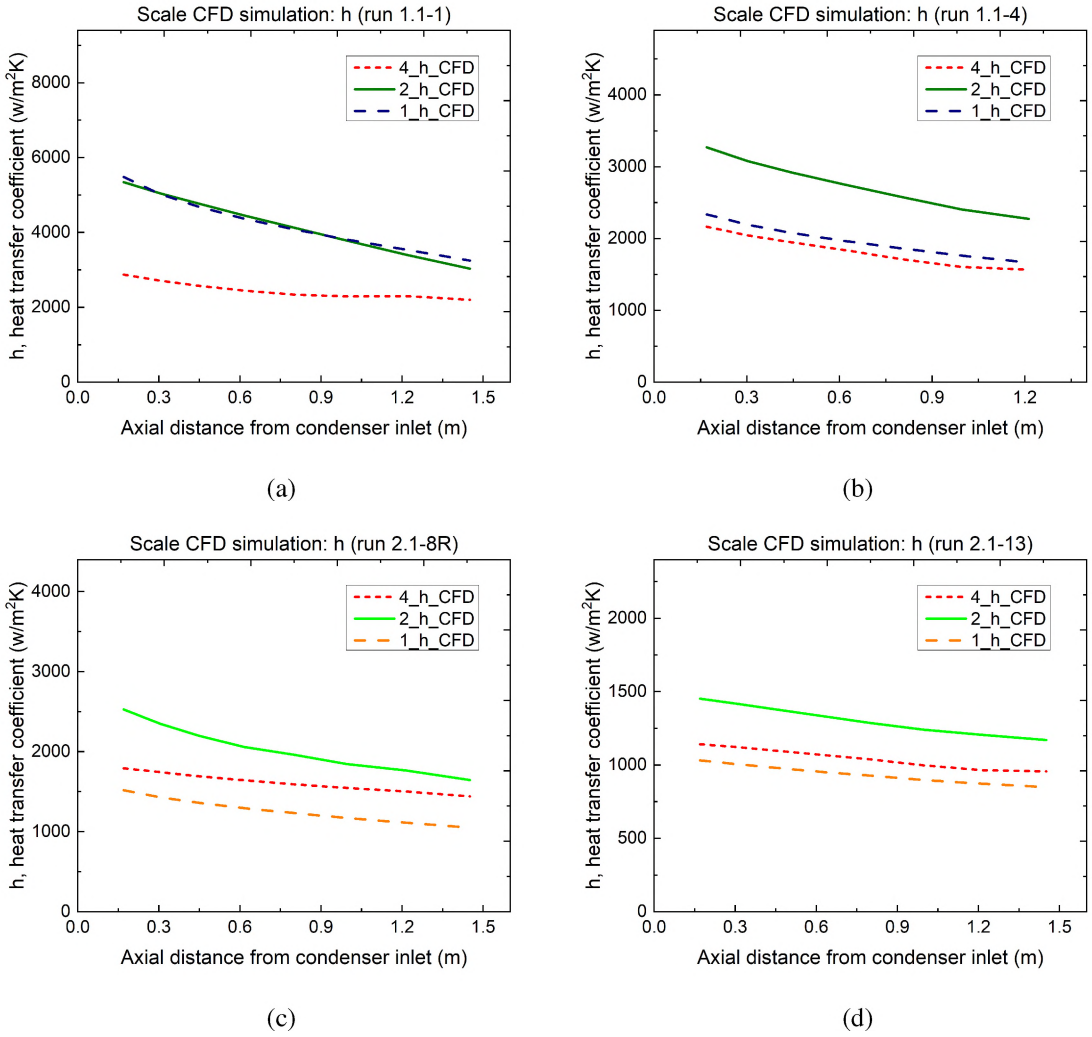

Figure 7.23. CFD scaling assessment results, h: (a) run 1.1-1, (b) run 1.1-4, (c) run 2.1-8R, and (d) run 2.1-13

Results showed: (a) HTCs for the reference simulation were equal to or higher form those of scaled simulations, and values ranged from 0.5-8 kW/m^{2}K; (b) HTCs for the scaled-up model had a higher value than that of the scaled-down model, (c) HTCs for

the low-pressure steam were higher than those from high-pressure steam, (d) simulated Nu values were consistent for both test cases; however, they were not consistent in scaled simulation results. Therefore, scaled test data were required to validate the CFD results.

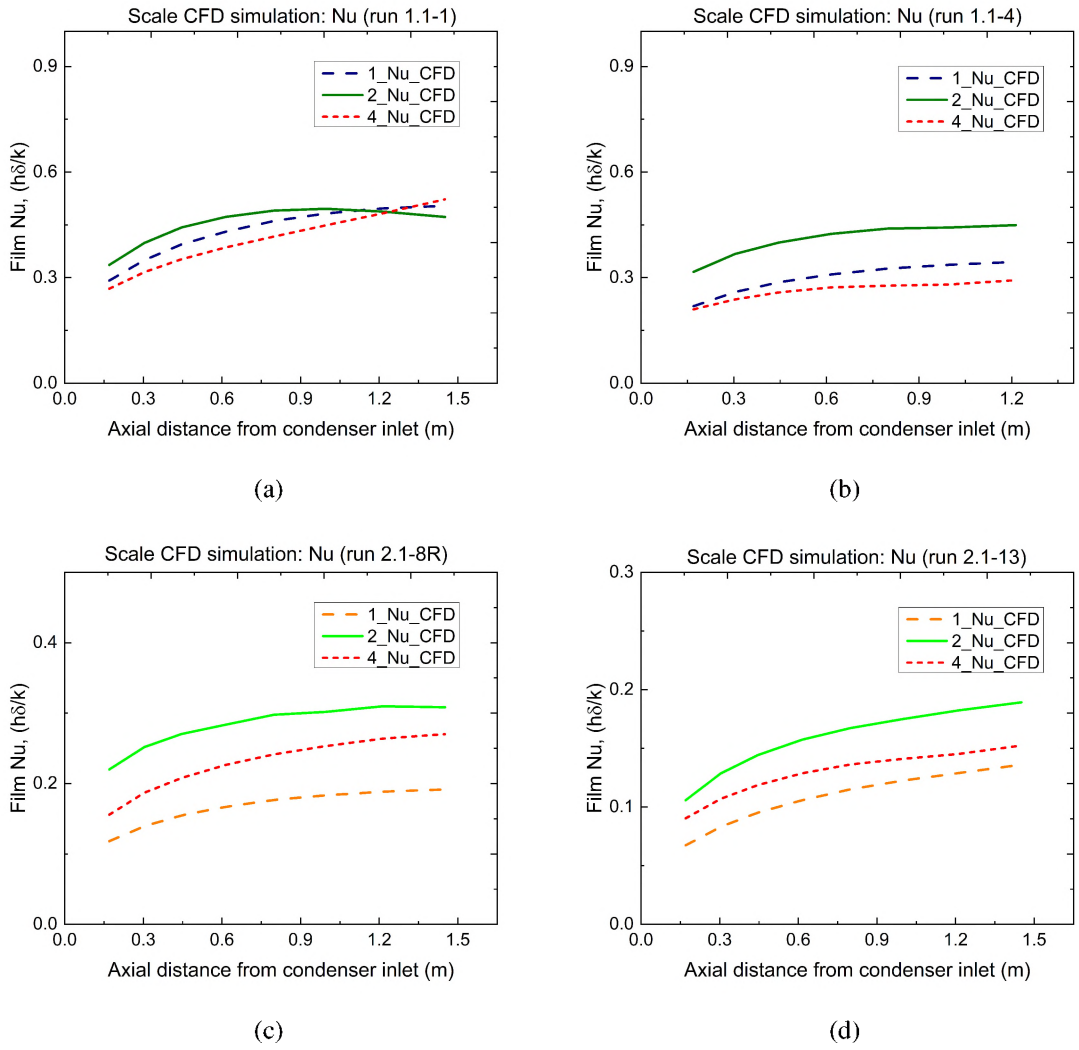

Figure 7.24. CFD scaling assessment results, Nu: (a) run 1.1-1, (b) run 1.1-4, (c) run 2.1-8R, and (d) run 2.1-13

7.2.3. Discussion About Scaled CFD Results. This study used conjugate heat transfer between the gas mixture and the annular coolant with real geometries. Therefore, little to no approximation and assumption were needed for the prediction of wall temperatures, surface heat fluxes, and HTC at the tube wall was required, which was directly obtained from the CFD simulations.

Results showed that heat transfer in the coolant was the limiting factor. The condensing wall heat flux had a high distribution variance and was not suitable for simple polynomial fit. Results had similar trends but HTC data was underpredicted. The turbulence intensity and eddy viscosity ratios improved the agreement.

The density of the gas-mixture increased radially. The axial velocity at the mixture-film interface was not negligible, which was expected for the longer condenser tubes with high mass flow rates. Simulation covered wide ranges of the test conditions: mass flows, pressures, and condenser tube diameters. The prediction for heat flux from the bulk coolant temperature was preferable and similar to the test data reduction method.

Based on simulation results, seed number density from 1000 to 5000 for steam condensation in the presence of air was recommended. This recommended value was 1000 to 10000 for the pure steam case. A detailed parametric study and uncertainty quantification for different types and volume concentration of non-condensable gases (like helium, nitrogen, air) were conducted to fill this gap.

The test data showed inconsistencies in condensing wall temperatures and heat flux profiles, specifically at the axial middle part of the test section, which caused deviations in the validation results. These inconsistencies would reduced using scaled test data.

Overall, this study's findings provided a primary assessment of the scaling effects and the challenges of CFD models to simulate the steam condensation for the reactor applications. It was recommended to validate scaled simulations with scaled test datasets to check the local behavior and species transport and to check for the complete modeling competencies.

7.3. PARAMETRIC STUDY AND MODEL SCALE EVALUATION

The previously discussed scaled simulation results provided a primary assessment of the scaling distortion, but the computational models had to be evaluated for the reactor physics parameters. The local physics parameter and steam-NCG mixture compositions are critical for reactor containment safety during a fuel failure accident case that releases hydrogen gas. These release hydrogen mixes with steam and air, which varied in accident cases, made a research gap in the reactor design safety. A comprehensive CHT parametric CFD study was performed to fill this research gap.

7.3.1. Parametric CFD Modeling Results. The scope of the parametric study covered NCG mass fractions of 0-40% for air and helium mixtures. The total mass fraction of NCG was kept at 40%; however, the percentage of air and helium varied. The helium mass fractions were 0%, 5%, 10%, 20%, and 40%. Therefore, the corresponding air mass fractions were 40%, 35%, 30%, 20%, and 0%. Helium was a substitute for hydrogen in the simulations because both gases exhibit similar thermal-transport properties (National Research Council, 2000). Hydrogen gas generates from the reactor core only if there is a fuel clad failure accident, which is beyond the design basis accident (BDBA). The steam and NCG (mostly air, and helium) percentages (molar fraction) were anticipated to be 60% and 0.4-40%, and helium (substitute for hydrogen) concentrations in the NCG mixture was 0–50% by volume (i.e. approximately 0-20% of the total mixture) for AP600 containment under postulated accident conditions Anderson *et al.* (1998). However, the MELCOR severe accident analysis for passive SMR showed the hydrogen concentration of 10% in the reactor core Li *et al.* (2017).

The multi-component gases, multiphase mixtures, and fluid film condensation models were applied with associated turbulence models. This parametric study used three boundary conditions—constant wall temperature (case: cont.T), curve-fit temperature (case:

fit.T), and mixed convective boundary conditions (case: combo)—for the condensing tube outer wall side. Condensing wall boundary conditions (temperature and heat flux) verification is shown in Figure 7.25.

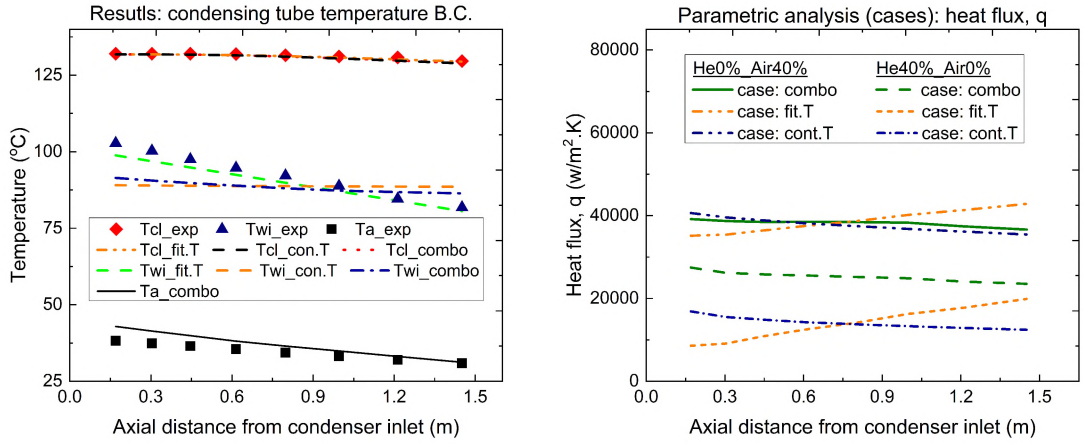

(a) (b)

Figure 7.25. Condensing wall boundary conditions verification: (a) temperature, and (b) heat flux

Simulation results showed that steam centerline temperatures, heat flux, and film thickness for He0%-Air40% simulation were identical in three cases (case: cont.T, case: fit.T, and case: combo). However, heat flux and film thickness results for simulation of He40%-Air0% were less than that of He0%-Air40% by factors of: (a) 1.65-1.75 for case: combo, and (b) 2.5-2.75 for case: fit.T and case: cont.T.

These simulation results showed that the prediction capabilities degraded with increasing helium percentages in the He-Air mixture of 40% with steam. The actual reactor containment system speculated a helium mixture of 5-10% maximum that provided conservative parametric simulation prediction capabilities. These heat flux values exhibited that case combo—mixed convective boundary condition—was the best choice for heat flux estimations.

The parametric simulation results of film HTC were calculated from the simulated temperature difference between the condensing wall (Twi), the interface (Tint), and the heat fluxes. The heat flux value for the combo (mixed convective boundary) case was approximated from the coolant bulk temperature distribution. Contrarily, the experimental heat flux values were used for curve fit temperature and constant temperature cases. The film HTC was estimated for different cases within the simulation parametric ranges, as shown in Figure 7.26.

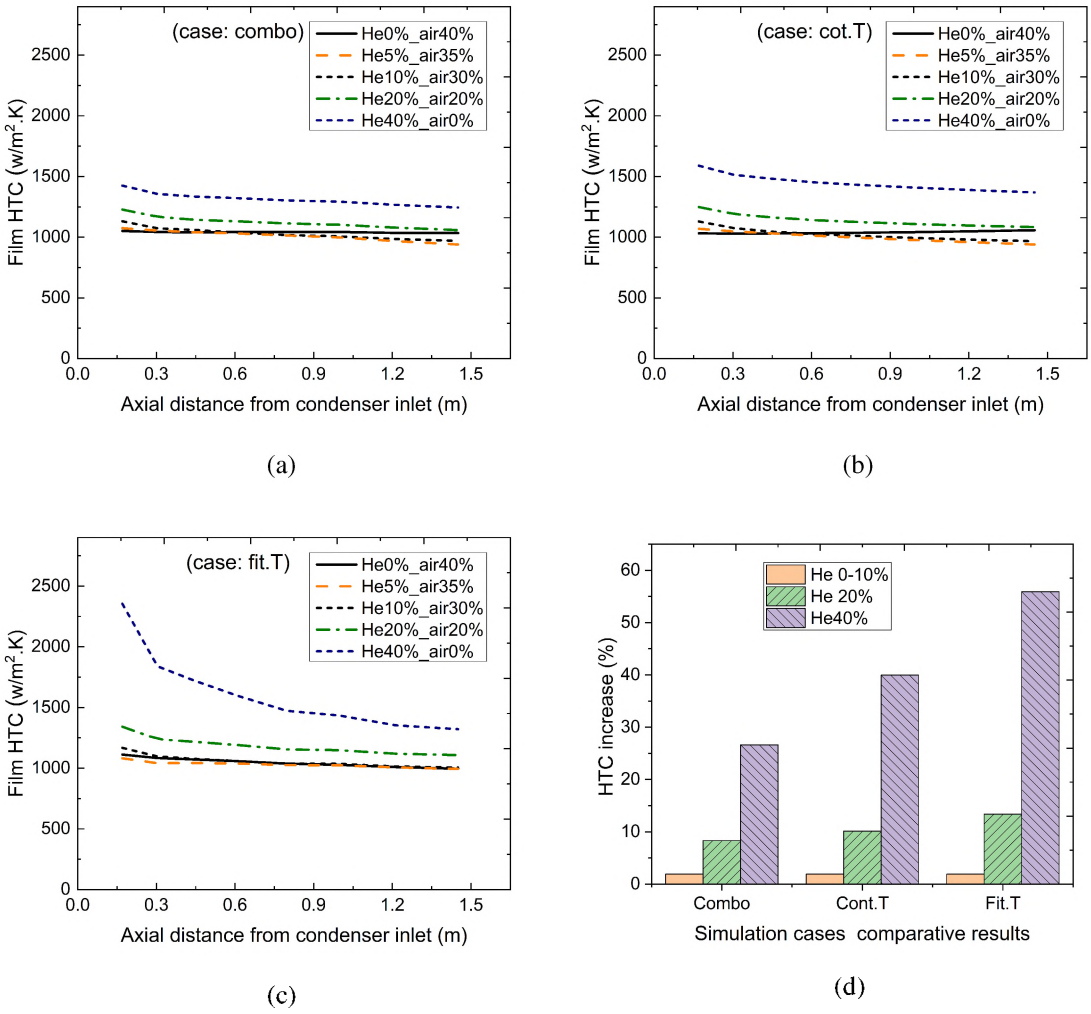

Figure 7.26. Parametric study of film HTC for case: (a) combo, (b) cont.T, and (c) fit.T, and (d) comparison

The film HTC result showed an approximately identical value (approximately 1030± 20 W/m^2 K) for the helium mixes of 0% to 10%; there was a 2% increase and a consistent trend. However, for the constant temperature and curve-fit temperature cases, the HTC value increased for increased helium percentages (20% to 40%).

Simulation cases results for film HTC compared with 0% or no helium simulation cases (He0%-Air40%), as illustrated in Figure 7.26 (d), exhibited that approximately 2% of HTC increased the helium percentages of up to 10%. However, the increased value of HTC for 20% helium and 40% helium cases ranged 8-13% and 26-57%, which were not realistic reactor accident cases. SMR postulate accidents condition the hydrogen (substituted by helium) percentage within 10% (Li *et al.*, 2017), and for a large reactor like AP600, it was up to 20% (Anderson *et al.*, 1998).

The following findings and conclusions were made based on the parametric simulation results:

(a) Although in a reactor containment, hydrogen (substituted by helium) ranged from 0-10% of the steam-gas mixture; parametric simulations were conducted for broader ranges, thereby keeping conservative design and analysis for reactor design extended safety margins.

(b) The developed simulation models showed consistent temperature changes, heat fluxes, and mole fractions with helium levels ranging 0-10% for the actual reactor containment helium fraction. For helium percentages between 10-20%, results were still satisfactory with moderate deviations in the result trends.

(c) The comparative HTC values exhibited that within 10% of the helium mixture, the change in HTC was 2% for all simulation wall boundary cases. Thus, the value of HTC increased with an increase in the helium mixture composition.

(d) The mixed convective boundary case was the best choice; however, the constant temperature and curve-fit temperature boundary conditions were also comparable for helium compositions up to 20%.

7.3.2. CHT Models Scale Evaluation Results. Le's (2012) physics-based CHT model was evaluated using Kuhn (1995) test cases (run1.1-1 and run1.1-4) for pure steam, as shown in Figure 7.27 and Figure 7.28.

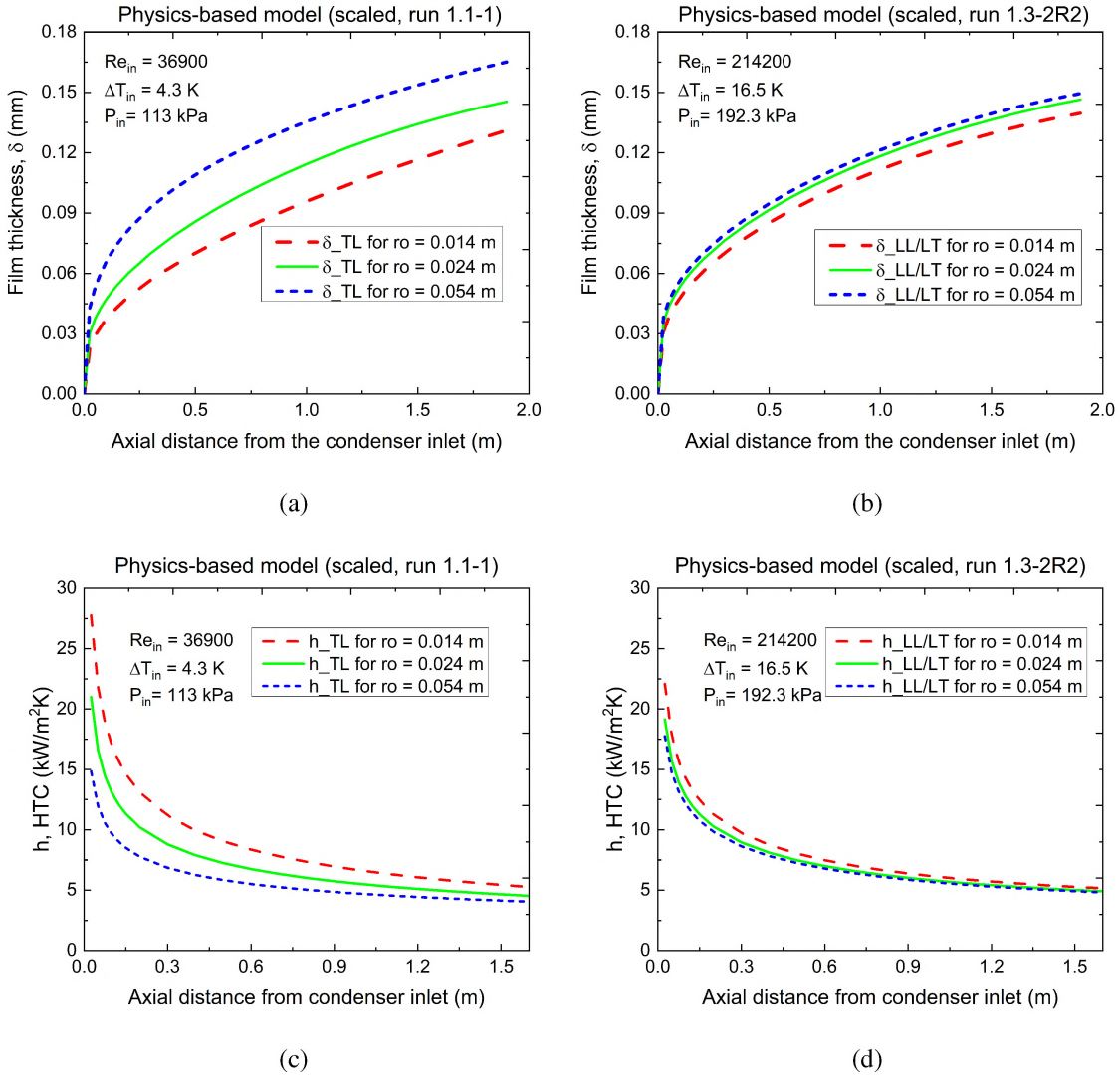

Figure 7.27. Physics based CHT model's scaled results for UCB Kuhn's tests (run1.1-1 and run1.3-2R2) data: (a)-(b) δ, and (c)-(d) h

Results for both test cases were similar; however, film thickness and HTC values for run 1.3-2R2 showed fewer scaling effects compared to Nu. This was because the flow modes differed. Run 1.1-1 provided better prediction for turbulent vapor-mixture cases (i.e., TT or TL), and run 1.3-2R2 provided better prediction for laminar vapor-mixture cases (i.e., LL or LT).

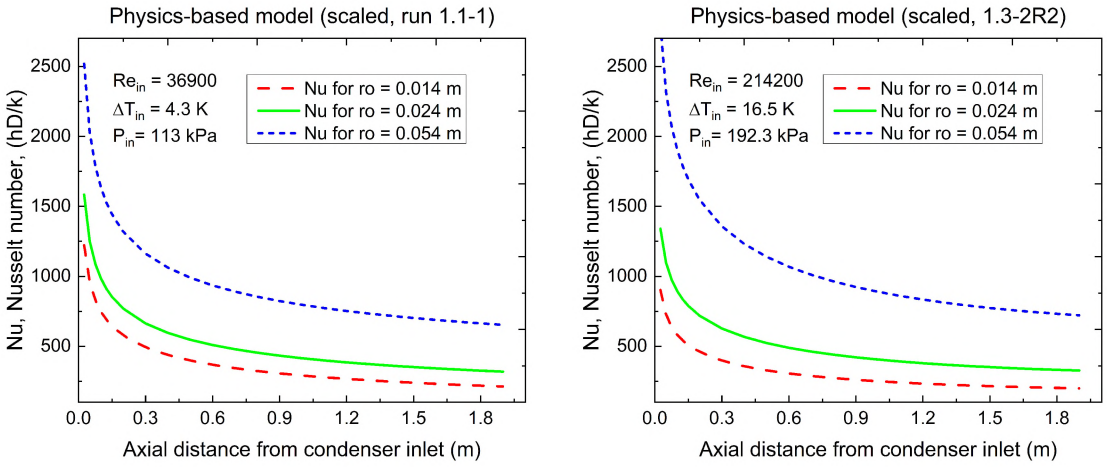

(a) (b)

Figure 7.28. Physics based CHT model's scaled results for UCB Kuhn's tests (run1.1-1 and run1.3-2R2) data:(e)-(f) Nu

Depending on the test case and complexity of the physics conditions, such as turbulence effects, and recirculating effects made challenges in predicting scaling effects for parameters like film thickness and HTC. However, Nu exhibited scaling effects in both test cases due to its non-dimensionality. Findings like these could be useful in predicting the scaling effect when the vapor-mixture region consists of different flow modes (e.g., turbulence and laminar flow).

8. CONCLUSIONS

Nuclear reactor systems are designed and analyzed with safety in mind. Advanced SMR systems target a higher safety margin than conventional commercial large-scale nuclear reactors with passive and inherent safety features. SMR systems are designed with steam condensation in the PCCS, which plays a critical role in removing reactor heat in case of a steam release accident. Review of relevant literature showed that there was an unmet need for experimental data required for designing and licensing PCCS of SMRs. This study addressed this gap by presenting an advanced scaled modular test facility design, setup, and testing with computational model evaluation and simulation validation. Tests data were collected for a wide range of operating conditions in keeping the parameters of interest. The simulations were performed for pure steam, steam-NCG mixtures, and varying pressure conditions. The simulation results showed that the present-day software package must be validated using a scaled test data matrix. New test databases were prepared with geometric, fluid, and test cases. Testing data, CFD results, and model evaluation results allow for better benchmarking and evaluation of the CHT models. These understanding and findings would support improving safety in advanced nuclear reactor systems design, analysis, and licensing. In addition, these findings were equally applicable to nuclear and non-nuclear advanced cooling applications for complex engineering systems.

APPENDIX A.

DERIVATION OF NUSSELT'S EQUATION

The x-momentum equation

$$u\frac{\partial u}{\partial x} + v\frac{\partial u}{\partial y} = -\frac{1}{\rho}\frac{dp_\infty}{dx} - g + \nu\frac{\partial^2 u}{\partial y^2} \tag{1}$$

Considering free stream at u = 0, we get $\frac{dp_\infty}{dx} = -\rho_\infty g$ and above equation simplifies to-

$$\frac{\partial^2 u}{\partial y^2} = -\frac{g}{\mu_l}(\rho_l - \rho_v) \tag{2}$$

Now, using Nassult's approximations $u(0) = 0$ and $\partial u/\partial y|_{y=\delta} = 0$, the film axial velocity and the mass flow rate per unit width, $\Gamma(x)$ are as follows-

$$u(y) = \frac{g(\rho_l - \rho_v)\delta^2}{\mu_l}\left[\frac{y}{\delta} - \frac{1}{2}\left(\frac{y}{\delta}\right)^2\right] \tag{3}$$

$$\frac{m(x)}{b} = \int_0^{\delta(x)} \rho_l u(y) dy = \frac{\rho_l(\rho_l - \rho_v) g\delta^3}{3\mu} \equiv \Gamma(x) \tag{4}$$

As the condensation takes place at the free surface, so the latent heat conducts through the condensate layer. Now, as per Fourier's law the surface heat flux is obtained as-

$$q_s'' = h_{fg}\frac{d\Gamma}{dx} = k\frac{T_{sat} - T_s}{\delta} \tag{5}$$

$$\frac{d\Gamma}{dx} = k\frac{T_{sat} - T_s}{\delta h_{fg}} \tag{6}$$

Now, differentiating the $\Gamma(x)$ with x and combining it with the above two equations the axial condensate film thickness $\delta(x)$ is as follows-

$$\delta(x) = \left[\frac{4k_l\mu_l(T_{sat} - T_s)x}{g\rho_l(\rho_l - \rho_v)h_{fg}}\right]^{1/4} \tag{7}$$

Later, inclusion of thermal advection effects by a latent heat of vaporization term, Rohsenow (1956) modified the h_{fg} in the Nusselt's derived condensate film thickness. Rohsenow recommended to use modified $h'_{fg} = h_{fg} + 0.68c_{p,l}\,(T_{sat} - T_s)$ or $h_{fg}(1 + 0.68Ja)$. Then, the local and average HTC h(x) and $\bar{h}$ for laminar flow are expressed as

$$h(x) = \frac{k_l}{\delta} = \left[\frac{g\rho_l\,(\rho_l - \rho_v)\,k_l^3 h'_{fg}}{4\mu\,(T_{sat} - T_w)\,x}\right]^{1/4} \tag{8}$$

$$\bar{h}_L = 0.943\left[\frac{g\rho_l\,(\rho_l - \rho_v)\,k_l^3 h'_{fg}}{4\mu\,(T_{sat} - T_w)\,L}\right]^{1/4} \tag{9}$$

Here, all liquid properties should be evaluated at the film temperature $T_f = (T_{st} + T_2)\,/2$ and ρ_v and h_{fg} evaluated at T_{sat}. Finally, the laminar film condensate average Nusselt number, $\overline{Nu}$ is estimated as follows-

$$\overline{Nu}_L = \frac{\bar{h}_L L}{k_l} = 0.943\left[\frac{g\rho_l\,(\rho_l - \rho_v)\,h'_{fg}L^3}{4\mu k_l\,(T_{sat} - T_w)}\right]^{1/4} \tag{10}$$

This relations are also valid for condensation on the inner or outer surface of a vertical tube of radius R (whenever, $R \gg \delta$). Besides, for inclined surfaces this relation will use $g\cos\theta$ instead of g. Where θ is the angle between the vertical and the surface. Then the Reynolds number, $Re_\Gamma \equiv \frac{4\Gamma_z}{\mu}$ can be simplified with the assumption $\rho_l \gg \rho_v$ as follows-

$$Re_\Gamma \equiv \frac{4\Gamma_z}{\mu} = \frac{4g\rho_l\,(\rho_l - \rho_v)\,\delta^3}{3\mu_l^2} = \frac{4g\rho_l^2\delta^3}{3\mu_l^2} \tag{11}$$

Finally, the average modified Nusselt number, $\overline{Nu} = \frac{\bar{h}_L\left(v_l^2/g\right)^{1/3}}{k_l}$ are as follows-

$$\begin{aligned}
\overline{Nu} &= 1.47Re_\delta^{-1/3} \quad \text{for} \quad Re_\delta \leqslant 30 \\
\overline{Nu} &= \frac{Re_\delta}{1.08Rc_\delta^{1.22} - 5.2} \quad \text{for} \quad 30 \leqslant Re_\delta \leqslant 1800 \\
\overline{Nu} &= \frac{Re_\delta}{8750 + 58\,Pr_l^{-0.5}\left(Re_\delta^{0.75} - 253\right)} \quad \text{for} \quad Re_8 \geq 1800
\end{aligned} \tag{12}$$

APPENDIX B.

PYTHON CODE FOR DATA REDUCTION

1. SAMPLE PYTHON CODE FOR DATA REDUCTION

1.1. PYTHON CODE: TEST DATA PRIMARY CLEANING

```
#This code filters the steady-state test data from the DAQ signals and stores it
     in a specific folder

import numpy as np
import matplotlib.pyplot as plt
from tqdm import tqdm
import glob
import os

# reading the files from a folder using glob, getting only the file names,
    sorting them

names = os.listdir('/home/palash/PhD_Thesis/CHT_test/raw_Test_data/
    CHT_Test_2inch_st_N2/ss')

names.sort()

print(names)

for i, item in enumerate(names):
    df = pd.read_csv('/home/palash/PhD_Thesis/CHT_test/raw_Test_data/
    CHT_Test_2inch_st_N2/ss/{}/Excel Waveform Data.txt'.format(item), sep="\t",
    skiprows=26, error_bad_lines=False)

    print(df)

    df.to_csv('/home/palash/PhD_Thesis/CHT_test/Test_Data_summary/2inch_st_N2/SS
    /{}.txt'.format(item), sep="\t", index=False)

    print(names[i])

print('Done')
```

1.2. PYTHON CODE: TEST DATA AVERAGE AND STD CALCULATION

```
# This code calculates the average and standard deviation from steady-state data with associated variables

import pandas as pd
import numpy as np
import matplotlib.pyplot as plt
from tqdm import tqdm
import glob
import os

# reading the files from a folder using glob, getting only the file names, sorting them

names = [os.path.basename(x) for x in glob.glob('/home/palash/PhD_Thesis/CHT_test/Test_Data_summary/2inch_st_N2/SS/*.txt')]

names.sort()
print(names)

# creating empty data frame and variable matrix

my_df_avg = pd.DataFrame()
my_df_std = pd.DataFrame()
my_var = []

# reading the files with names, using enumerate to keep the indexing

for i, item in enumerate(names):
    df = pd.read_csv('/home/palash/PhD_Thesis/CHT_test/Test_Data_summary/2inch_st_N2/SS/{}'.format(item), sep='\t')
    var_names = list(df.columns.values)

    for j, column in enumerate(df):

        col1 = str(item).split('.txt')[0].replace('run', '')
        col2 = str(item).split('.txt')[0].replace('run', '')

```

```
        if j == 0:
            var_time = df[column].max()
            my_df_avg.at[j, col1] = var_time
            my_df_std.at[j, col1] = var_time

        else:
            var_avg = df[column].mean()
            var_std = df[column].std()

            my_df_avg.at[j, col1] = var_avg
            my_df_std.at[j, col2] = var_std

    print('not done')

my_df_avg['variable'] = var_names
my_df_std['variable'] = var_names


#changing the variable name

df['New_var_name'] = pd.read_csv('/home/palash/PhD_Thesis/CHT_test/New_var_name.
    txt')
my_df_avg['variable'] = df['New_var_name']
my_df_std['variable'] = df['New_var_name']
list1 = list(my_df_avg)

print(list1)

print(my_df_avg)


my_df_avg.to_csv('/home/palash/PhD_Thesis/CHT_test/Test_Data_summary_solution/2
    inch_st_N2_avg.csv', float_format='%.3f', index=False)
my_df_std.to_csv('/home/palash/PhD_Thesis/CHT_test/Test_Data_summary_solution/2
    inch_st_N2_std.csv', float_format='%.3f', index=False)

print('Done')
```

2. SAMPLE (DRAFT) PYTHON CODE FOR CHT CALCULATION

```
# This code calculates CHT using steady-state test data and other parameters of interest

import pandas as pd
import numpy as np
import matplotlib.pyplot as plt
from tqdm import tqdm
from scipy import interpolate
from scipy.interpolate import CubicSpline
from scipy.interpolate import interp1d
from scipy.optimize import curve_fit
import glob
import os
from matplotlib import pyplot as plt  # to save figure
from pyXSteam.XSteam import XSteam # adding steam table
steamTable = XSteam(XSteam.UNIT_SYSTEM_MKS) # pressure in bar, temp deg C


# normalized value:
def norm(data):
    return ((data) - min(data)) / (max(data) - min(data))

# exponential curve fit:
def func(x, a, c, d):
    return a*np.exp(-c*x)+d

# for using different markers in a plot need to import itertools
import itertools

markers = itertools.cycle([ '*', 'o',  's', 'h', 'd', 'p', '+', '.', '1', 'D', 'H', 'v', '^'])
linestyle = itertools.cycle(['--', '-.', '-', ':'])


# Checking the file's name in a folder or a directory
names = [os.path.splitext(os.path.basename(x))[0] for x in
```

```
128         glob.glob('/home/palash/PhD_Thesis/CHT_test/Test_data_z_graph/4in_N2_1.
    csv')]
129 names.sort()
130 print(names)
131
132 # creating a panda data frame
133 df = pd.DataFrame()
134 df1 = pd.DataFrame()
135 df2 = pd.DataFrame()
136 df3 = pd.DataFrame() # to record calculated data
137 df4 = pd.DataFrame() # to record calculated data
138 df5 = pd.DataFrame() # to record calculated data
139
140 # Reading multiple csv files from a folder and plotting together
141 for i, item in enumerate(names):
142     df = pd.read_csv('/home/palash/PhD_Thesis/CHT_test/Test_data_z_graph/4
    in_N2_1.csv'.format(item))
143
144     print(df)
145
146     col_name = df.columns.values
147
148     #RTD temperature bias (C)
149     T_bias = (0, -2, 0, +2.5, 0.6339, -0.3222, -0.919,
150               1.0139, 0.65, -0.175, 0.66, 0.371, 0.305, -0.9224, -0.0154, -1.5,
    -0.8,
151               0.455, -0.0398, 0.02305, -0.4, -1.5, -0.471, -0.212, -0.35,
    -0.336, 0,
152               1.0139, 0.851, 1.402, 0.650, 1.464, 1.394, 0.194, 1.0425, 0.0314,
    0.0716,
153               0.564, -0.456, 0.528, 0.0739, -0.147, -0.641, -1.942, -1.443,
154               0.1621, 22.568, 0.004286, -0.002678, 0.12307, 1.3745, 0, 0, 0, 0,
    0, 0)
155
156     df1 = pd.DataFrame(T_bias, columns=['T_bias'])
157     df = df.iloc[:, :-1]  # removing the last column i.e., the variable column
158     # organizing RTD that were misplaced
159     df.iloc[7] = df.iloc[27] #replacing the 3_Ta_1 value by the 5_Ta_1 (new bias
     1.0139)
```

```
160     df.iloc[26] = df.iloc[44]  # replacing the 4_Two_10 value by the 6_Two_10 (
        new bias )
161     df.iloc[20] = df.iloc[39]  # replacing the 4_Two_4 value by the 6_Two_4 (new
         bias )
162 
163     # removing the bias error from all the columns
164     df2 = df.add(df1['T_bias'], axis=0)
165 
166     print(df2)
167     # print(len(df1))
168 
169     # data processing: removing bias error, and making Ta and Two data set
170     i = 0
171     while i < (len(df.columns)-1):
172         df = df.dropna()
173 
174         # raw data without bias removal
175         Ta_01 = df.iloc[7:17, [i]]
176         Two_01 = df.iloc[17:27, [i]]
177         Ta_02 = df.iloc[27:37, [i]]
178         Two_02 = df.iloc[37:47, [i]]
179 
180         # data after bias removal
181         x1 = df2.iloc[7:17, [i]]
182         x2 = df2.iloc[17:27, [i]]
183         y1 = df2.iloc[27:37, [i]]
184         y2 = df2.iloc[37:47, [i]]
185         x3 = df2.iloc[6:18, [i]]
186 
187         loc = np.array([0.25, 0.39, 0.53, 0.67, 0.83, 0.99, 1.17, 1.36, 1.56,
        1.77])
188         loc_x = np.array([0.12, 0.25, 0.39, 0.53, 0.67, 0.83, 0.99, 1.17, 1.36,
        1.56, 1.77])
189         loc_all = np.array([0.12, 0.25, 0.39, 0.53, 0.67, 0.83, 0.99, 1.17,
        1.36, 1.56, 1.77, 2.69])
190         loc_q = np.array([0.25, 0.39, 0.53, 0.67, 0.83, 0.99, 1.17, 1.36, 1.56,
        1.77, 2.69])
```

```
191         L = 2.69-0.12  # for water side L =2.44 m, at steam side = 2.69 m, water
    outlet at 0.12m and steam inlet at -0.2 m, measurements ware taken from the
    cooling water outlet to the inlet
192
193         print(loc.round(decimals=3))
194
195         # preparing 1D column np data
196         x1 = np.asarray(x1).squeeze()
197         y1 = np.asarray(y1).squeeze()
198         x2 = np.asarray(x2).squeeze()
199         y2 = np.asarray(y2).squeeze()
200         x3 = np.asarray(x3).squeeze()
201         print(x1)
202
203         # preparing 1D column empty np data series: expected shape all are (10,)
204         a = np.zeros(x1.shape)
205         b = np.zeros(y1.shape)
206         c = np.zeros(x2.shape)
207         d = np.zeros(y2.shape)
208         Tb = np.zeros(x1.shape)
209         Twi = np.zeros(x1.shape)
210         h_fg = np.zeros(x1.shape)
211         h_st = np.zeros(x1.shape)
212         h_col = np.zeros(x1.shape)
213         h_total = np.zeros(x1.shape)
214         Nu_col = np.zeros(x1.shape)
215         Nu_film = np.zeros(x1.shape)
216         Nu_exp = np.zeros(x1.shape)
217         q_raw = np.zeros(Tb.shape)
218         q_1 = np.zeros(q_raw.shape)
219         q_2 = np.zeros(x3.shape)
220         Tw_out = df2.iloc[4, [i]].values #.values will make df to ndarray
221         Tw_in = df2.iloc[1, [i]].values # for test from august
222         Tcond_out = df2.iloc[3, [i]].values
223         Tst_in = df2.iloc[2, [i]].values
224         Tw_out_df = df2.iloc[4, [i]]
225         Tw_in_df = df2.iloc[1, [i]]
226         Tcond_out_df = df2.iloc[3, [i]]
227         Tst_in_df = df2.iloc[2, [i]]
```

```
228
229         print(Tcond_out)
230         print(Tst_in)
231
232         ### using the manual log test data
233
234         m = df2.iloc[51, [i]].values  # mass flow rate (gpm)
235         #m = np.asarray(m1).squeeze()*0.063 # mass flow rate (kg/s)
236         c_p = 4.18  # for temperature 30 to 50 C this value found same
237         di = 4.26*0.0254 # steam tube pipe dia in m
238         do = 4.5*0.0254
239         A = ((m*0.063)*c_p /(3.142 * (di))).round(decimals=4)  # m*c_p/(pi*Di),
    here 4 inch 10 sch pipe OD =4.5 in, ID = 4.26*0.0254 m
240         B = (di*0.5)*(np.log(4.5/4.26))/(16.2*1000) #ri*ln(do/di)/kw, here kw is
     16.2 w/m.K at 100 deg C for ss 304 and 306
241
242         print("mass flow rate",m)
243         print ("B=", B)
244
245         ### adding tex box for mass flow rate and pressure info
246         st_flow = df2.iloc[48, [i]]*(60*60*0.001) # g/s to kg/hr
247         st_vel = st_flow * (1/60/60) / (3.142 * ((di / 2) ** 2))
248         st_pr = df2.iloc[47, [i]]*100+100 # convert to kpa
249         water_flow = df2.iloc[51, [i]] *0.063*3600  # convert to kg/hr
250         water_dp = df2.iloc[49, [i]] * 100  # convert to kpa
251         NCG_flow = df2.iloc[56, [i]] * 0.07344  # convert l/m to kg/hr
252         NCG_fraction = st_flow/NCG_flow
253
254         for j, val in enumerate(x1):
255             # moving average to get smooth curve (fist and last data point not
    included)
256             if j > 0 and j < len(x1) - 1:
257                 a[j] = (x1[j - 1] + x1[j] + x1[j + 1]) / 3
258                 b[j] = (y1[j - 1] + y1[j] + y1[j + 1]) / 3
259
260             else:
261                 a[j] = val
262                 b[j] = val
263             #print(j)
```

```
264
265         for j, val in enumerate(x2):
266
267             # moving average to get smooth curve (fist and last data point not
    included)
268             if j > 0 and j < len(x2) - 1:
269                 c[j] = (x2[j - 1] + x2[j] + x2[j + 1]) / 3
270                 #d[j] = (y2[j - 1] + y2[j] + y2[j + 1]) / 3
271             else:
272                 c[j] = val
273                 # d[j] = val
274
275         n = 3
276         Tb = 3*c/(2*(n+2))+(2*n+1)*a/(2*(n+2))
277
278         Tb_1_raw = np.append(Tb, Tw_in)
279         Tb_all_raw = np.append(Tw_out, Tb_1_raw)
280
281         #curve fit: exponential
282
283         Ta_popt, Ta_pcov = curve_fit(func, loc, a, p0=(1, 1e-2, 1), maxfev=3000)
      #
284         Two_popt, Two_pcov = curve_fit(func, loc, c, p0=(1.2, 1e-2, 1), maxfev
    =3000)  #
285         Tb_popt, Tb_pcov = curve_fit(func, loc, Tb, p0=(1.2, 1e-2, 1), maxfev
    =3000)  #
286
287         x_fit = np.linspace(min(loc), max(loc), 50)
288         x_fit_all = np.linspace(min(loc_all), max(loc_all), 50)
289
290         Tb_fit = func(x_fit, *Tb_popt)
291         #Tb_fit_all = func(x_fit_all, *Tb_all_popt)
292
293         y_fit_Ta = func(x_fit, *Ta_popt)
294         y_fit_Two = func(x_fit, *Two_popt)
295         y_fit_Tb = func(x_fit, *Tb_popt)
296         f_Tb = interp1d(x_fit, y_fit_Tb)
297         f_Ta = interp1d(x_fit, y_fit_Ta)
298         f_Two = interp1d(x_fit, y_fit_Two)
```

```
299         Tb_fit = f_Tb(loc)
300         Ta_fit = f_Ta(loc)
301         Two_fit = f_Two(loc)
302         #fiting the in and out temperature
303         Tw_in_fit = 0.3*Tw_in+0.7*Tb_fit[-1:]
304         Tw_out_fit = 1 * Tw_out + 0 * Tb_fit[0]
305         Tw_std = 1
306 
307         for j, val in enumerate(Tb_fit):
308 
309             # moving average to get smooth curve (fist and last data point not
    included)
310             if j > 0 and j < len(Tb_fit)-1:
311                 q_1[j] = A*((Tb_fit[j-1] - Tb_fit[j]) / (loc[j] - loc[j-1]) + (
    Tb_fit[j] - Tb_fit[j+1]) / (loc[j+1] - loc[j]))/2
312 
313             else:
314                 q_1[0] = A*1.05*((Tb_fit[0] - Tb_fit[1]) / (loc[1] - loc[0]))
315                 q_1[j] = A*((Tb_fit[j-1] - Tb_fit[j]) / (loc[j] - loc[j-1]))
316 
317         ### ----------------------------------
318         h_fg = np.zeros(x1.shape)
319         h_fg_mod = np.zeros(x1.shape)
320         m_con_x = np.zeros(x1.shape)
321         m_con_pw_x = np.zeros(x1.shape)
322         m_st_x = np.zeros(x1.shape)   ### axial steam flow
323 
324         x_quality = np.zeros(x1.shape) ### steam quality or void fraction
325         P_sat_x = np.zeros(x1.shape) ## steam saturation partial pressure in bar
326         T_sat_x = np.zeros(x1.shape)  ## steam saturation temperature in deg C
327 
328         d_lam = np.zeros(x1.shape)
329         d_lam_fo = np.zeros(x1.shape)
330         k_film = np.zeros(x1.shape)
331         Re_fo = np.zeros(x1.shape)
332         h_cond = np.zeros(x1.shape)
333         h_film = np.zeros(x1.shape)
334         h_film_Nu = np.zeros(x1.shape)
335         h_Nu = np.zeros(x1.shape) ## for degradation factor calcuation
```

```
336         DF = np.zeros(x1.shape) ## degradation factor, ratio of h_exp/h_Nu
337         T_film = np.zeros(x1.shape)
338         T_int = np.zeros(x1.shape)
339         T_st_avg = np.zeros(x1.shape)
340 
341         Twi = Two_fit + B * q_1
342         #cp_f = steamTable.CpL_t(Tst_in)
343 
344         for j, val in enumerate(Twi):
345                 #h_fg[j] = steamTable.h_pt(1, T_st_avg[j])
346                 h_fg[j] = steamTable.hV_t(Tst_in)-steamTable.hL_t(Tst_in)
347                 h_fg_mod[j]  = h_fg[j]  + (3 / 8) * steamTable.CpL_t(Twi[j]) *
    Twi[j]
348                 m_con_x[j]= 3.142 * di * q_1[j] * (loc_x[j+1] - loc_x[j]) /
    h_fg_mod[j] * 60 * 60  # condensate flow rate
349 
350         m_con = m_con_x.cumsum(axis = 0)   # cumalative condensate flow rate (kg
    /hr)
351         m_con_pw = m_con/ (3.142 * di)  # cumalative condensate flow rate per
    width (kg/hr/m)
352 
353         for j, val in enumerate(Twi):
354             ### using Nusselts approximation
355             m_con_pw_x[j] = m_con[j] / (3.142 * di)  # condensate flow rate per
    width
356 
357             m_st_x[j] = st_flow - m_con[j]
358             x_quality [j] = (st_flow - m_con[j]) / st_flow  ## void fraction or
    steam quality x = (m(total) - m(cond)) /mtotal
359             P_sat_x[j] = (st_pr * x_quality[j])*0.01  ## steam partial pressure
    in Bar, 100 kpa = 1 bar
360             T_sat_x [j] = steamTable.tsat_p(P_sat_x[j])
361             T_film [j] = T_sat_x[j] - 3/4 * abs(T_sat_x[j] - Twi [j])
362             T_int[j] = 0.5*(T_sat_x[j]+T_film[j])
363 
364             d_lam[j] = (4 * loc[j] * steamTable.tcL_t(T_film[j]) * steamTable.
    my_pt(1, T_film[j]) * (T_sat_x[j] - Twi[j])) / (
```

```
365                     9.81 * h_fg_mod[j] * steamTable.rhoL_t(T_film[j]) * (
steamTable.rhoL_t(T_film[j]) - steamTable.rhoV_t(T_film[j]))) ** (0.25)  #
need to update Tst_in to Tsb
366         d_lam_fo[j] = (3 * m_con[j]/(3.142 * di) * (1 / 60 / 60) *
steamTable.my_pt(1, T_film[j]) / (
367                     9.81 * steamTable.rhoL_t(T_film[j]) * (steamTable.rhoL_t
(T_film[j]) - steamTable.rhoV_t(T_sat_x[j])))) ** (1 / 3)
368
369
370         Re_fo[j] = m_con_pw[j]/steamTable.my_pt(1, T_film[j])  ## Re_f =
Gamma/mu or 4*Gamma/mu (when considering hydraulic diameter
371
372         h_cond[j] = q_1[j]/(T_sat_x[j] - T_int[j])
373         h_film[j] = q_1[j] / (T_int[j] - Twi[j])
374         k_film[j] = steamTable.tcL_t(T_film[j])
375         h_Nu[j] = steamTable.tcL_t(T_film[j]) / (d_lam[j] * 1000)  ## devide
 by 1000 to get kW/m2.K
376         h_film_Nu[j] = steamTable.tcL_t(T_film[j]) / (d_lam_fo[j] * 1000)  #
# devide by 1000 to get kW/m2.K
377         h_film_L = 0.943 * h_film[9] * ((loc[9] / 2.69) ** (0.25))
378         Nu_film[j] = h_film[j]*1000* (d_lam_fo[j] /steamTable.tcL_t(T_film[j
]))
379
380     cp_f = steamTable.CpL_t(Tst_in)
381     h_exp = q_1 / (T_sat_x - Twi)
382     h_col = q_1 /(Two_fit - Tb_fit)
383     Nu_col = h_col * 1000 * ((do-di) / 0.66)   # hD/k, water k at 70-80 deg
C
384
385     h_vapor_film = 1/(1/h_cond + 1/h_film)  #modified
386     h_overall = 1/(1/h_vapor_film + 1/h_col)  #modified
387     Nu_exp = h_exp *1000 * d_lam_fo / k_film
388
389     DF = h_exp/h_film_Nu
390
391
392     ### ----------------------------------
393
```

```
394         plt.figure(num=None, figsize=(10, 10), dpi=90, facecolor='w', edgecolor=
    'k') # fixing the size of the figures
395         plt.subplot(3, 2, 2)
396         plt.errorbar(loc, q_1*0.1, yerr= 0.1, marker=next(markers), linestyle=
    next(linestyle), linewidth=1.5, label = 'q (kW/$\mathrm{m^2}$) (x10)')
397         plt.errorbar(loc, h_exp, yerr=0.04 * h_exp, marker='h', color='black',
    markerfacecolor='black', linestyle='-', linewidth=2.5,
398                      label='h_exp (kW/$\mathrm{m^2}$.K)')
399         plt.errorbar(loc, h_film, yerr=0, marker=next(markers), linestyle=next(
    linestyle), linewidth=1.5, label='h_film (kW/$\mathrm{m^2}$.K)')
400         plt.xlabel('Axial distance from cooling water outlet, L (m)')
401         plt.ylabel('Axial q, h')
402         plt.legend(loc='upper right', labelspacing=0.5, fontsize=8, fancybox=
    True, framealpha=0.5)
403         plt.subplots_adjust(hspace=.35)
404         plt.subplot(3, 2, 3)
405         plt.errorbar(loc, Nu_film*10, yerr=0.05 * Nu_film, marker=next(markers),
     linestyle=next(linestyle), linewidth=1.5, label='Nu_film (x0.1)')
406         plt.errorbar(loc, Nu_col*0.1, yerr= 0.1, marker=next(markers), linestyle
    =next(linestyle), linewidth=1.5, label = 'Nu_coolant (x10)')
407         plt.errorbar(loc, DF*10, yerr= 0.1*DF, marker=next(markers), linestyle=
    next(linestyle), linewidth=1.5, label = 'DF (x0.1)')
408 
409         #plt.title('Test data: A-run '+col_name[i])
410         plt.xlabel('Axial distance from cooling water outlet, L (m)')
411         plt.ylabel('Axial Nu')
412         plt.legend(loc='upper right', labelspacing=0.5, fontsize=8, fancybox=
    True, framealpha=0.5)
413         plt.subplots_adjust(hspace=.35)
414         plt.subplot(3, 2, 4)
415         plt.errorbar(loc, m_con, yerr=0.1*m_con, marker=next(markers), linestyle
    =next(linestyle), linewidth=1.5, label='cond. flow rate (kg/hr)')
416         plt.errorbar(loc, m_st_x, yerr=0.01 * m_st_x, marker=next(markers),
    linestyle=next(linestyle), linewidth=1.5, label='steam flow rate (kg/hr)')
417         plt.errorbar(loc, d_lam_fo * 200000, yerr=0.1 * d_lam_fo, marker=next(
    markers), linestyle=next(linestyle),
418                      linewidth=2, label='film_delta (mm, x0.0005)')
419 
420         plt.xlabel('Axial distance from cooling water outlet, L (m)')
```

```
421         plt.ylabel('Axial mixture flows and delta')
422         plt.legend(loc='upper right', labelspacing=0.5, fontsize=8, fancybox=
    True, framealpha=0.5)
423 
424         plt.subplots_adjust(hspace=.35)
425         plt.subplot(3, 2, 5)
426         plt.errorbar(loc, T_sat_x , yerr=0.01 * T_sat_x, marker=next(markers),
    linestyle=next(linestyle), linewidth=1.5, label='saturation T (deg C)')
427         plt.errorbar(loc, T_film , yerr=0.01 * T_film, marker=next(markers),
    linestyle=next(linestyle), linewidth=1.5, label='film T (deg C)')
428         plt.errorbar(loc, T_int , yerr=0.01 * T_int, marker=next(markers),
    linestyle=next(linestyle), linewidth=1.5, label='interface T (deg C)')
429 
430         plt.xlabel('Axial distance from cooling water outlet, L (m)')
431         # plt.ylabel('Axial film thickness rate')
432         plt.ylabel('Axial vapor-mixture T')
433         plt.legend(loc='upper right', labelspacing=0.5, fontsize=8, fancybox=
    True, framealpha=0.5)
434 
435         plt.subplots_adjust(hspace=.35)
436 
437         plt.subplot(3, 2, 6)
438         plt.errorbar(loc, x_quality*10, yerr=0.1 * x_quality, marker=next(
    markers), linestyle=next(linestyle), linewidth=1.5, label='steam quality, x
    (%, x10)')
439         plt.errorbar(loc, P_sat_x * 10, yerr=0.1 * P_sat_x, marker=next(markers)
    , linestyle=next(linestyle), linewidth=1.5, label='steam pressure, P (bar,
    x0.1)')
440         plt.xlabel('Axial distance from cooling water outlet, L (m)')
441         plt.ylabel('Axial steam: quality and Pr')
442         plt.legend(loc='upper right', labelspacing=0.5, fontsize=8, fancybox=
    True, framealpha=0.5)
443 
444         plt.subplots_adjust(hspace=.35)
445 
446         plt.subplot(3, 2, 1) # the x-axis value need to correct
447         plt.errorbar(loc, Twi, yerr=1.5, linestyle='None', marker='D', label='
    Twi')
```

```
448         plt.errorbar(loc, a, yerr= 1.5, linestyle= 'None', marker='*', label = '
    Ta_raw')
449         plt.errorbar(loc, c, yerr= 1.5, linestyle= 'None', marker='o', label = '
    Two_raw')
450 
451         plt.errorbar(loc, Tb_fit, yerr= 1.5, marker='D', linestyle='--',
    linewidth=1.5, label = 'Tb_cal')
452 
453         plt.errorbar(2.44, Tw_in_fit, yerr= 2, marker='P', color = 'blue', label
     = 'Tw_in')
454         plt.errorbar(0, Tw_out_fit, yerr= 2, marker='X', color = 'magenta',
    label = 'Tw_out')
455         plt.errorbar(3, Tcond_out, yerr= 2.5, marker='h', color = 'purple',
    label = 'Tc_out')
456         plt.errorbar(-0.2, Tst_in, yerr= 2, marker='s', color = 'red', label = '
    Tst_in')
457 
458         plt.plot([], [], ' ', marker= '|', label="error bar")
459 
460         plt.legend(loc='upper right', labelspacing=0.5, fontsize=8,
    bbox_to_anchor=(0.9, .98), fancybox=True, framealpha=0.5)
461         plt.title('Test data: A-run '+col_name[i])
462         plt.xlabel('Axial distance from cooling water outlet, L (m)')
463         plt.ylabel('Axial T distribution, T (deg C)')
464 
465 
466         ### adding tex box for mass flow rate and pressure info
467 
468         textstr = '\n'.join((
469             r'steam_flow=%.2f kg/hr'% (st_flow,),
470             r'steam_pr=%.2f kpa' % (st_pr, ),
471             r'water_flow=%.2f kg/hr' % (water_flow, ),
472             r'water_dp=%.2f kpa'% (water_dp,),
473             r'NCG_flow=%.2f kg/hr' % (NCG_flow,)))
474             # r'NCG_mf=%.2f ' % (NCG_fraction,)))
475 
476         # these are matplotlib.patch.Patch properties
477         props = dict(boxstyle='round', facecolor='white', alpha=0.5)
478 
```

```
        # place a text box in upper left in axes coords
        plt.text(0.25, 102, textstr, fontsize=9, verticalalignment='top', bbox=
    props)
        plt.show()

        ### saving file block ------------------

        df_list = '4" steam+N2: A-run ' + col_name[i]
        print(df_list)

        ### test boundary conditions (BCs) save to file
        BCs = pd.MultiIndex.from_tuples(
                zip(['steam_flow=', 'steam_pr', 'Tst_in', 'Tcond_out', '
    water_flow', 'Tw_inlet', 'Tw_outlet','NCG_flow', '% NCG'], ['("kg/hr")',  '(
    kpa)', '(C)', '(C)','("kg/hr")', '(C)', '(C)','("kg/hr")', '%']))
        BCs_a = pd.concat([st_flow, st_pr, Tst_in_df, Tcond_out_df, water_flow,
    Tw_in_df, Tw_out_df, NCG_flow, NCG_fraction], axis=1)
        print(BCs_a.values)
        df4 = pd.DataFrame(BCs_a.values, columns=BCs)
        ### ----------------------------------------

        df5 = pd.DataFrame(
            {'Loc': loc, 'Ta': a, 'Two': c, 'Tb_fit': Tb_fit, 'Twi': Twi, 'Tsat'
    : T_sat_x, 'q': q_1, 'delta1': d_lam_fo*1000,'delta2': d_lam*1000, 'm_cond':
     m_con, 'h_exp': h_exp,})

        ### mode='a' used to add new df data to exiting same file
        df4.to_csv('/home/palash/PhD_Thesis/CHT_test/Test_data_z_graph/
    Final_Test_file/4_in_N2/{}.csv'.format(df_list), sep=',',
                   float_format='%.3f', index=False)  # saving file with file
    name
        df5.to_csv('/home/palash/PhD_Thesis/CHT_test/Test_data_z_graph/
    Final_Test_file/4_in_N2/{}.csv'.format(df_list), sep=',', mode='a',
                   float_format='%.3f', index=False)  # saving file with file
    name
        ## --------------------------------
        i = i + 1
print('Done')
```

APPENDIX C.

DATA AVAILABILITY AND PUBLICATIONS

1. TEST DATA AVAILABILITY

Sample test data using three test sections for steam, steam-He, and steam-N2 are presented in this report. The total test dataset that supports the findings of this study is available from the PI, Dr. Joshua P. Schlegel (e-mail: schlegelj@mst.edu), upon reasonable request. The definition and unit used in test data tables are presented in Table 1. The selected test data are presented in Table 2-10.

Table 1. Definition and unit used in test data table

Symbol	Definition and units
Vapor-mix	
Flow	steam flow, (kg/hr)
Pin	inlet vapor-mix pressure, (kPa)
Tst_in	inlet vapor-mix temperature, (°C)
T_out	outlet condensate-vapor-mix temperature, (°C)
Coolant (water)	
Flow	water flow, (kg/hr)
Tw_in	inlet coolant (water) temperature, (°C)
Tw_out	outlet coolant (water) temperature, (°C)
NCG	
Flow	NCG, (kg/hr)
MF	NCG mass fraction, (%)
He	Helium gas
N2	Nitrogen gas
Axial parameters	
loc	axial location (position) from cooling water outlet, (m)
MF	NCG mass fraction, (%)
Ta	measured, coolant adiabatic wall temperature, (°C)
Two	measured, condenser tube outer wall temperature, (°C)
Tb,fit	calculated, coolant axial bulk temperature, (°C)
Twi	calculated, condenser tube inner wall temperature, (°C)
Tsb	calculated, vapor-mix bulk temperature, (°C)
q	calculated, condenser tube wall heat flux, (kW/m^2)
delta1	film thickness without interfacial effects, (mm)
delta2	estimated film thickness, (mm)
m_cond	condensate mass flow rate, (kg/hr)
h_exp	local heat transfer coefficient, q/(Tsb-Twi), ($kW/m^2 \cdot K$)

Table 2. Test data for 4" test section and pure steam tests

A-run 0.3

	Vapor-mix				Water			NCG		
	Flow	Pin	Tst_in	T_out	Flow	Tw_in	Tw_out	Flow	MF	
	59.6	117.9	104.5	102.3	680.4	49.1	75.7	0.0	0	
loc	Ta	Two	Tb, fit	Twi	Tsb	q	delta1	delta2	m_cond	h_exp
0.25	68.4	74.5	69.7	74.3	103.3	29.31	0.057	0.018	2.0	1.011
0.39	65.5	72.8	68.1	72.7	102.3	27.39	0.072	0.028	4.0	0.925
0.53	63.7	71.1	66.4	71.3	101.3	26.36	0.082	0.040	5.9	0.879
0.67	62.5	69.7	64.9	70.1	100.3	25.33	0.091	0.051	7.7	0.839
0.83	61.3	68.9	63.2	69.0	99.2	24.27	0.098	0.064	9.7	0.803
0.99	59.2	68.2	61.5	68.0	98.1	23.19	0.105	0.077	11.7	0.771
1.17	56.7	67.7	59.8	67.2	96.9	22.09	0.111	0.091	13.7	0.743
1.36	54.0	66.5	58.0	66.4	95.6	20.97	0.117	0.105	15.8	0.717
1.56	51.9	65.7	56.3	65.8	94.3	19.84	0.122	0.119	17.9	0.695
1.77	50.2	64.9	54.5	65.2	92.9	19.29	0.127	0.132	20.0	0.696

A-run 0.3R4

	Vapor-mix				Water			NCG		
	Flow	Pin	Tst_in	T_out	Flow	Tw_in	Tw_out	Flow	MF	
	47.4	109.4	102.4	101.4	680.4	53.4	76.7	0.0	0	
loc	Ta	Two	Tb, fit	Twi	Tsb	q	delta1	delta2	m_cond	h_exp
0.25	68.9	75.5	70.3	75.4	101.1	26.25	0.055	0.015	1.8	1.021
0.39	66.0	73.9	68.8	73.9	100.0	24.38	0.069	0.025	3.5	0.936
0.53	64.4	72.6	67.4	72.7	98.9	23.16	0.079	0.034	5.2	0.885
0.67	63.4	71.5	66.0	71.7	97.8	21.95	0.087	0.044	6.8	0.842
0.83	62.5	70.8	64.6	70.8	96.6	20.75	0.094	0.054	8.5	0.805
0.99	60.7	70.2	63.2	70.1	95.4	19.53	0.100	0.064	10.1	0.771
1.17	58.5	69.9	61.7	69.5	94.2	18.30	0.105	0.075	11.8	0.741
1.36	56.2	69.0	60.3	68.9	92.9	17.07	0.110	0.085	13.5	0.713
1.56	54.4	68.5	58.8	68.5	91.5	15.86	0.115	0.094	15.2	0.689
1.77	53.1	68.0	57.5	68.2	90.1	15.27	0.119	0.103	16.8	0.696

A-run 0.5

	Vapor-mix				Water			NCG		
	Flow	Pin	Tst_in	T_out	Flow	Tw_in	Tw_out	Flow	MF	
	55.0	116.1	104.3	103.3	680.4	42.9	81.2	0.0	0	
loc	Ta	Two	Tb, fit	Twi	Tsb	q	delta1	delta2	m_cond	h_exp
0.25	73.4	80.2	74.8	79.7	103.0	24.92	0.053	0.013	1.7	1.073
0.39	70.5	78.6	73.3	78.6	102.0	23.47	0.067	0.021	3.4	1.002
0.53	68.8	77.2	72.0	77.5	101.1	22.95	0.077	0.030	5.0	0.974
0.67	67.9	76.0	70.6	76.5	100.2	22.43	0.085	0.038	6.7	0.947
0.83	67.0	75.1	69.1	75.4	99.1	21.88	0.092	0.048	8.5	0.922
0.99	65.2	74.3	67.6	74.3	98.0	21.31	0.099	0.058	10.2	0.898
1.17	62.9	73.8	65.9	73.2	96.8	20.71	0.105	0.069	12.2	0.876
1.36	60.7	72.5	64.3	72.0	95.5	20.09	0.111	0.080	14.2	0.856
1.56	58.7	71.0	62.6	70.9	94.1	19.46	0.116	0.092	16.2	0.838
1.77	57.2	69.3	60.8	69.8	92.6	19.14	0.122	0.105	18.3	0.838

Table 2. Test data for 4" test section and pure steam tests (cont.)

A-run 0.9

	Vapor-mix				Water			NCG		
	Flow	Pin	Tst_in	T_out	Flow	Tw_in	Tw_out	Flow	MF	
	69.1	166.6	113.5	111.4	1701.0	51.9	71.6	0.0	0	
loc	Ta	Two	Tb, fit	Twi	Tsb	q	delta1	delta2	m_cond	h_exp
0.25	63.6	70.2	65.2	70.2	112.9	53.83	0.070	0.026	3.7	1.263
0.39	61.6	68.7	64.0	68.5	111.1	49.58	0.089	0.041	7.3	1.163
0.53	60.3	67.3	62.8	67.4	109.4	46.28	0.101	0.056	10.7	1.100
0.67	59.4	66.3	61.7	66.7	107.8	43.09	0.111	0.070	13.9	1.047
0.83	58.7	66.0	60.6	66.1	106.0	39.94	0.119	0.085	17.3	1.002
0.99	57.2	65.9	59.5	65.8	104.2	36.83	0.126	0.099	20.4	0.959
1.17	55.5	66.1	58.4	65.5	102.2	33.75	0.133	0.113	23.6	0.920
1.36	53.6	65.7	57.4	65.4	100.3	30.75	0.139	0.125	26.7	0.882
1.56	52.4	65.3	56.4	65.3	98.3	27.87	0.144	0.137	29.6	0.847
1.77	51.4	64.7	55.4	65.3	96.1	26.47	0.149	0.146	32.5	0.858

A-run 30.2

	Vapor-mix				Water			NCG		
	Flow	Pin	Tst_in	T_out	Flow	Tw_in	Tw_out	Flow	MF	
	33.8	104.5	101.5	90.4	680.4	53.4	77.1	0.0	0	
loc	Ta	Two	Tb, fit	Twi	Tsb	q	delta1	delta2	m_cond	h_exp
0.25	69.1	75.8	70.7	75.8	99.2	28.04	0.056	0.014	1.9	1.194
0.39	66.5	74.2	69.1	74.1	97.6	25.74	0.071	0.022	3.7	1.098
0.53	64.9	72.9	67.6	72.9	95.9	23.86	0.080	0.031	5.5	1.034
0.67	63.8	71.7	66.3	71.9	94.4	22.06	0.088	0.038	7.1	0.981
0.83	62.7	71.0	64.8	71.0	92.6	20.30	0.095	0.046	8.8	0.939
0.99	60.8	70.4	63.5	70.4	90.9	18.57	0.101	0.053	10.3	0.903
1.17	58.9	70.0	62.1	69.8	89.1	16.87	0.106	0.059	11.9	0.875
1.36	56.7	69.4	60.8	69.4	87.3	15.23	0.110	0.064	13.4	0.853
1.56	55.2	69.0	59.5	69.1	85.4	13.67	0.114	0.068	14.8	0.838
1.77	54.1	68.8	58.4	68.9	83.5	12.92	0.118	0.069	16.2	0.886

A-run 40.2

	Vapor-mix				Water			NCG		
	Flow	Pin	Tst_in	T_out	Flow	Tw_in	Tw_out	Flow	MF	
	41.5	105.5	101.8	96.4	680.4	46.6	76.5	0.0	0	
loc	Ta	Two	Tb, fit	Twi	Tsb	q	delta1	delta2	m_cond	h_exp
0.25	66.1	75.0	68.4	74.9	99.9	25.33	0.054	0.015	1.7	1.014
0.39	63.5	73.7	66.9	73.6	98.7	23.15	0.068	0.024	3.4	0.922
0.53	62.0	72.5	65.6	72.5	97.6	21.25	0.078	0.033	4.9	0.848
0.67	61.1	71.5	64.3	71.6	96.5	19.45	0.085	0.042	6.3	0.781
0.83	60.3	70.7	63.1	70.7	95.4	17.70	0.091	0.052	7.8	0.718
0.99	58.8	69.9	61.9	70.0	94.3	16.01	0.096	0.062	9.1	0.659
1.17	57.2	69.5	60.7	69.3	93.1	14.37	0.101	0.072	10.5	0.603
1.36	55.5	68.7	59.6	68.7	92.0	12.80	0.105	0.083	11.7	0.549
1.56	54.2	68.2	58.6	68.2	90.9	11.33	0.109	0.093	12.9	0.499
1.77	53.4	67.8	57.6	67.8	89.9	10.62	0.113	0.103	14.1	0.483

Table 3. Test data for 4" test section and steam-He tests

A-run 1.1N1

	Vapor-mix				Water			NCG		
	Flow	Pin	Tst_in	T_out	Flow	Tw_in	Tw_out	Flow	MF	
	32.7	114.1	97.0	89.6	680.4	44.2	69.6	19.1	1.7	
loc	Ta	Two	Tb, fit	Twi	Tsb	q	delta1	delta2	m_cond	h_exp
0.25	64.9	67.8	65.4	67.7	101.4	31.85	0.059	0.022	2.1	0.945
0.39	62.3	65.8	63.6	65.7	99.4	29.56	0.075	0.035	4.3	0.878
0.53	60.6	64.0	61.9	63.9	97.3	28.05	0.087	0.048	6.3	0.840
0.67	59.2	62.1	60.2	62.4	95.3	26.56	0.095	0.060	8.2	0.808
0.83	58.2	60.7	58.5	60.8	92.9	25.06	0.103	0.075	10.3	0.782
0.99	55.8	59.4	56.8	59.5	90.4	23.56	0.110	0.088	12.3	0.761
1.17	53.8	58.5	55.0	58.2	87.7	22.04	0.117	0.101	14.3	0.748
1.36	51.1	57.3	53.3	57.1	84.7	20.52	0.123	0.112	16.4	0.744
1.56	49.6	56.1	51.6	56.0	81.4	19.04	0.129	0.120	18.3	0.751
1.77	47.9	54.9	49.9	55.2	77.7	18.31	0.134	0.124	20.3	0.812

A-run 1.1N2

	Vapor-mix				Water			NCG		
	Flow	Pin	Tst_in	T_out	Flow	Tw_in	Tw_out	Flow	MF	
	34.1	112.2	97.1	88.8	680.4	43.8	68.4	17.3	2.0	
loc	Ta	Two	Tb, fit	Twi	Tsb	q	delta1	delta2	m_cond	h_exp
0.25	63.0	66.6	63.8	66.5	101.1	30.70	0.059	0.022	2.1	0.886
0.39	60.6	64.5	62.0	64.5	99.2	28.39	0.075	0.036	4.1	0.818
0.53	58.9	62.8	60.4	62.8	97.4	26.73	0.086	0.050	6.1	0.774
0.67	57.6	61.0	58.8	61.4	95.5	25.11	0.094	0.063	7.9	0.735
0.83	56.6	59.8	57.1	59.9	93.4	23.49	0.102	0.079	9.8	0.701
0.99	54.4	58.6	55.6	58.7	91.3	21.88	0.109	0.093	11.7	0.670
1.17	52.5	57.9	53.9	57.5	89.0	20.27	0.115	0.108	13.5	0.643
1.36	50.1	56.7	52.3	56.5	86.6	18.68	0.121	0.122	15.4	0.621
1.56	48.7	55.6	50.8	55.6	84.0	17.14	0.126	0.134	17.2	0.603
1.77	47.2	54.5	49.3	54.8	81.2	16.39	0.131	0.144	19.0	0.622

A-run 1.1N3

	Vapor-mix				Water			NCG		
	Flow	Pin	Tst_in	T_out	Flow	Tw_in	Tw_out	Flow	MF	
	34.4	110.6	97.2	88.4	680.4	43.3	67.8	15.8	2.2	
loc	Ta	Two	Tb, fit	Twi	Tsb	q	delta1	delta2	m_cond	h_exp
0.25	61.7	65.9	62.6	65.7	100.8	29.76	0.058	0.023	2.0	0.849
0.39	59.2	63.9	60.9	63.9	99.0	27.48	0.074	0.037	4.0	0.782
0.53	57.6	62.2	59.3	62.3	97.2	25.78	0.085	0.051	5.9	0.737
0.67	56.3	60.5	57.8	60.8	95.5	24.13	0.093	0.065	7.6	0.696
0.83	55.4	59.3	56.2	59.4	93.5	22.50	0.101	0.080	9.5	0.660
0.99	53.3	58.2	54.7	58.2	91.6	20.87	0.107	0.095	11.2	0.625
1.17	51.6	57.5	53.1	57.1	89.5	19.25	0.114	0.111	13.0	0.594
1.36	49.2	56.3	51.6	56.0	87.3	17.66	0.119	0.127	14.8	0.566
1.56	47.9	55.2	50.2	55.1	85.0	16.13	0.124	0.141	16.4	0.541
1.77	46.6	54.0	48.8	54.4	82.5	15.38	0.129	0.154	18.1	0.547

Table 3. Test data for 4" test section and steam-He tests (cont.)

A-run 1.1N4

	Vapor-mix				Water			NCG		
	Flow	Pin	Tst_in	T_out	Flow	Tw_in	Tw_out	Flow	MF	
	34.8	109.7	97.2	88.3	680.4	42.8	67.4	14.7	2.4	
loc	Ta	Two	Tb, fit	Twi	Tsb	q	delta1	delta2	m_cond	h_exp
0.25	60.9	65.6	62.0	65.4	100.6	29.54	0.058	0.023	2.0	0.841
0.39	58.4	63.6	60.3	63.6	98.8	27.25	0.074	0.037	4.0	0.774
0.53	56.8	61.9	58.7	62.0	97.1	25.52	0.085	0.051	5.8	0.727
0.67	55.6	60.3	57.2	60.6	95.4	23.84	0.093	0.065	7.5	0.684
0.83	54.7	59.0	55.6	59.2	93.5	22.18	0.101	0.081	9.4	0.646
0.99	52.7	57.9	54.1	58.0	91.7	20.53	0.107	0.096	11.1	0.609
1.17	51.0	57.2	52.6	56.8	89.6	18.89	0.113	0.113	12.9	0.576
1.36	48.7	56.0	51.1	55.8	87.5	17.28	0.119	0.129	14.6	0.545
1.56	47.4	54.8	49.7	54.8	85.3	15.74	0.124	0.145	16.2	0.517
1.77	46.1	53.7	48.4	54.0	82.9	14.99	0.128	0.158	17.9	0.518

A-run 1.1N5

	Vapor-mix				Water			NCG		
	Flow	Pin	Tst_in	T_out	Flow	Tw_in	Tw_out	Flow	MF	
	34.4	108.9	97.2	88.2	680.4	42.5	67.3	14.0	2.5	
loc	Ta	Two	Tb, fit	Twi	Tsb	q	delta1	delta2	m_cond	h_exp
0.25	60.4	65.3	61.6	65.2	100.3	29.76	0.059	0.023	2.0	0.848
0.39	58.0	63.4	59.9	63.4	98.6	27.42	0.074	0.037	4.0	0.779
0.53	56.4	61.7	58.3	61.7	96.8	25.62	0.085	0.051	5.8	0.730
0.67	55.2	60.0	56.8	60.3	95.1	23.87	0.093	0.065	7.6	0.686
0.83	54.3	58.7	55.2	58.9	93.2	22.15	0.101	0.081	9.4	0.646
0.99	52.2	57.6	53.7	57.7	91.3	20.45	0.107	0.097	11.1	0.608
1.17	50.5	56.9	52.2	56.5	89.2	18.76	0.113	0.113	12.9	0.574
1.36	48.2	55.7	50.8	55.5	87.1	17.11	0.119	0.129	14.6	0.541
1.56	47.0	54.6	49.3	54.6	84.9	15.53	0.124	0.144	16.2	0.512
1.77	45.8	53.5	48.0	53.8	82.5	14.76	0.128	0.158	17.8	0.513

A-run 1.1N6

	Vapor-mix				Water			NCG		
	Flow	Pin	Tst_in	T_out	Flow	Tw_in	Tw_out	Flow	MF	
	34.7	108.4	97.3	88.1	680.4	42.2	67.3	13.2	2.6	
loc	Ta	Two	Tb, fit	Twi	Tsb	q	delta1	delta2	m_cond	h_exp
0.25	60.1	65.3	61.3	65.1	100.2	30.00	0.059	0.023	2.0	0.856
0.39	57.7	63.3	59.6	63.3	98.4	27.62	0.075	0.037	4.0	0.785
0.53	56.1	61.6	58.0	61.6	96.7	25.77	0.085	0.051	5.9	0.734
0.67	54.9	59.8	56.5	60.2	95.0	23.98	0.094	0.065	7.6	0.688
0.83	53.9	58.6	54.9	58.7	93.1	22.22	0.101	0.081	9.5	0.647
0.99	51.9	57.5	53.5	57.5	91.2	20.47	0.108	0.097	11.2	0.607
1.17	50.1	56.8	51.9	56.3	89.2	18.75	0.114	0.114	12.9	0.571
1.36	47.9	55.6	50.5	55.3	87.1	17.07	0.119	0.130	14.6	0.537
1.56	46.7	54.4	49.1	54.4	84.9	15.46	0.124	0.146	16.2	0.506
1.77	45.5	53.3	47.8	53.6	82.6	14.68	0.129	0.159	17.8	0.506

Table 4. Test data for 4" test section and steam-N2 tests

A-run 0.9N0a

	Vapor-mix				Water			NCG		
	Flow	Pin	Tst_in	T_out	Flow	Tw_in	Tw_out	Flow	MF	
	59.8	150.4	103.5	107.4	737.1	51.4	78.6	13.2	4.5	
loc	Ta	Two	Tb, fit	Twi	Tsb	q	delta1	delta2	m_cond	h_exp
0.25	69.1	76.9	71.0	76.9	110.1	38.33	0.061	0.019	2.6	1.154
0.39	66.1	75.0	69.0	74.8	108.8	35.16	0.077	0.031	5.1	1.036
0.53	64.0	73.1	67.1	73.1	107.5	32.54	0.088	0.044	7.5	0.946
0.67	62.5	71.3	65.4	71.6	106.2	30.02	0.097	0.057	9.7	0.867
0.83	61.2	69.9	63.6	70.1	104.9	27.57	0.104	0.072	12.0	0.794
0.99	59.2	68.9	61.9	68.9	103.6	25.16	0.111	0.087	14.0	0.726
1.17	57.1	68.2	60.2	67.8	102.2	22.81	0.117	0.103	16.2	0.663
1.36	54.8	66.9	58.5	66.9	100.9	20.54	0.122	0.120	18.2	0.604
1.56	52.9	65.9	57.0	66.0	99.5	18.39	0.126	0.137	20.1	0.549
1.77	51.4	65.3	55.6	65.4	98.2	17.35	0.131	0.154	22.0	0.529

A-run 0.9N0d

	Vapor-mix				Water			NCG		
	Flow	Pin	Tst_in	T_out	Flow	Tw_in	Tw_out	Flow	MF	
	59.0	150.4	100.8	105.3	737.1	43.7	78.5	11.2	5.3	
loc	Ta	Two	Tb, fit	Twi	Tsb	q	delta1	delta2	m_cond	h_exp
0.25	72.1	76.8	73.2	76.8	109.9	45.2	0.065	0.019	3.0	1.369
0.39	69.0	74.2	70.8	74.0	108.2	42.2	0.082	0.032	6.1	1.232
0.53	66.8	71.5	68.5	71.4	106.5	40.3	0.094	0.046	9.0	1.149
0.67	64.9	68.9	66.3	69.2	104.9	38.5	0.104	0.06	11.8	1.08
0.83	63.3	66.7	63.9	67.0	103.0	36.7	0.113	0.077	14.8	1.02
0.99	60.3	65.0	61.7	65.1	101.0	34.8	0.121	0.094	17.7	0.967
1.17	57.6	63.6	59.2	63.2	98.9	32.9	0.129	0.112	20.8	0.922
1.36	54.4	61.8	56.8	61.5	96.6	31.0	0.136	0.131	23.9	0.884
1.56	52.1	60.1	54.4	60.1	94.1	29.1	0.142	0.15	26.9	0.853
1.77	49.3	58.5	52.1	58.8	91.4	28.1	0.149	0.166	30.0	0.86

A-run 0.9N1

	Vapor-mix				Water			NCG		
	Flow	Pin	Tst_in	T_out	Flow	Tw_in	Tw_out	Flow	MF	
	58.7	150.4	100.4	104.8	737.1	45.8	76.2	11.0	5.3	
loc	Ta	Two	Tb, fit	Twi	Tsb	q	delta1	delta2	m_cond	h_exp
0.25	70.5	74.7	71.5	74.7	109.9	44.2	0.064	0.021	3.0	1.257
0.39	67.5	72.3	69.2	72.1	108.3	41.0	0.082	0.034	5.9	1.136
0.53	65.3	70.0	66.9	69.9	106.7	38.9	0.094	0.048	8.8	1.058
0.67	63.4	67.7	64.8	68.0	105.1	36.7	0.103	0.063	11.4	0.991
0.83	61.7	65.9	62.6	66.1	103.3	34.6	0.112	0.08	14.3	0.931
0.99	58.8	64.5	60.4	64.5	101.5	32.4	0.12	0.097	17.0	0.877
1.17	56.2	63.4	58.2	63.0	99.5	30.3	0.127	0.115	19.8	0.83
1.36	53.2	61.8	56.0	61.7	97.4	28.1	0.133	0.133	22.6	0.787
1.56	51.0	60.5	53.8	60.6	95.3	26.0	0.139	0.151	25.3	0.749
1.77	48.5	59.5	51.8	59.6	93.0	25.0	0.145	0.168	28.0	0.748

Table 4. Test data for 4" test section and steam-N2 tests (cont.)

A-run 0.9N4

	Vapor-mix				Water			NCG		
	Flow	Pin	Tst_in	T_out	Flow	Tw_in	Tw_out	Flow	MF	
	56.5	140.4	99.2	103.9	737.1	52.5	77.1	8.8	6.4	
loc	Ta	Two	Tb, fit	Twi	Tsb	q	delta1	delta2	m_cond	h_exp
0.25	68.9	75.5	70.5	75.5	108.0	37.3	0.061	0.019	2.5	1.145
0.39	66.0	73.7	68.6	73.5	106.7	34.1	0.077	0.031	5.0	1.028
0.53	64.0	71.9	66.7	71.8	105.4	31.4	0.088	0.044	7.2	0.937
0.67	62.6	70.1	65.1	70.4	104.1	28.9	0.096	0.056	9.3	0.857
0.83	61.4	68.8	63.3	69.1	102.8	26.4	0.104	0.071	11.5	0.783
0.99	59.4	67.9	61.7	68.0	101.5	24.0	0.11	0.085	13.5	0.714
1.17	57.3	67.4	60.1	67.0	100.1	21.6	0.115	0.101	15.5	0.651
1.36	55.0	66.3	58.5	66.1	98.8	19.3	0.12	0.117	17.4	0.591
1.56	53.3	65.4	57.1	65.4	97.5	17.2	0.125	0.133	19.2	0.535
1.77	52.0	64.6	55.7	64.8	96.2	16.2	0.129	0.149	20.9	0.515

A-run 0.9N8

	Vapor-mix				Water			NCG		
	Flow	Pin	Tst_in	T_out	Flow	Tw_in	Tw_out	Flow	MF	
	60.1	140.4	100.1	104.9	737.1	45.8	76.7	5.9	10.2	
loc	Ta	Two	Tb, fit	Twi	Tsb	q	delta1	delta2	m_cond	h_exp
0.25	71.0	75.1	72.0	75.1	107.9	43.3	0.064	0.019	2.9	1.322
0.39	68.1	72.8	69.7	72.6	106.4	40.3	0.081	0.032	5.8	1.193
0.53	65.8	70.5	67.5	70.4	104.9	38.4	0.093	0.045	8.6	1.114
0.67	64.0	68.2	65.4	68.5	103.4	36.5	0.103	0.059	11.2	1.047
0.83	62.3	66.4	63.2	66.7	101.6	34.6	0.112	0.075	14.1	0.989
0.99	59.4	65.2	61.0	65.1	99.9	32.6	0.119	0.091	16.8	0.938
1.17	56.7	64.1	58.8	63.7	98.0	30.7	0.126	0.108	19.7	0.893
1.36	53.6	62.5	56.5	62.4	96.0	28.7	0.133	0.125	22.5	0.855
1.56	51.3	61.2	54.3	61.3	93.9	26.8	0.139	0.141	25.3	0.822
1.77	48.7	60.4	52.2	60.4	91.7	25.8	0.145	0.156	28.1	0.827

A-run 0.9N10

	Vapor-mix				Water			NCG		
	Flow	Pin	Tst_in	T_out	Flow	Tw_in	Tw_out	Flow	MF	
	58.7	140.4	99.4	104.3	737.1	50.6	76.8	4.4	13.3	
loc	Ta	Two	Tb, fit	Twi	Tsb	q	delta1	delta2	m_cond	h_exp
0.25	69.0	75.2	70.5	75.2	108.1	38.0	0.061	0.019	2.5	1.157
0.39	66.1	73.3	68.5	73.1	106.7	35.0	0.078	0.032	5.1	1.043
0.53	64.1	71.4	66.6	71.4	105.4	32.7	0.089	0.044	7.4	0.961
0.67	62.6	69.7	64.9	69.9	104.1	30.4	0.097	0.057	9.6	0.889
0.83	61.2	68.3	63.0	68.5	102.7	28.2	0.105	0.072	12.0	0.824
0.99	59.0	67.3	61.3	67.4	101.4	26.0	0.112	0.087	14.1	0.764
1.17	56.7	66.7	59.5	66.3	100.0	23.8	0.118	0.103	16.4	0.708
1.36	54.2	65.5	57.8	65.4	98.5	21.7	0.123	0.119	18.5	0.655
1.56	52.4	64.6	56.2	64.6	97.1	19.7	0.128	0.135	20.5	0.606
1.77	50.7	63.9	54.6	64.0	95.6	18.7	0.133	0.151	22.6	0.592

Table 5. Test data for 2" test section and pure steam tests

C-run 0.4R4

	Vapor-mix				Water			NCG		
	Flow	Pin	Tst_in	T_out	Flow	Tw_in	Tw_out	Flow	MF	
	40.5	111.2	103.5	101.1	907.2	47.1	63.0	0.0	0.0	
loc	Ta	Two	Tb, fit	Twi	Tsb	q	delta1	delta2	m_cond	h_exp
0.25	61.4	67.7	63.8	67.7	101.2	61.3	0.074	0.022	2.0	1.832
0.39	61.0	65.7	62.5	65.2	99.6	58.1	0.095	0.035	4.1	1.688
0.53	61.2	62.7	61.2	63.1	98.0	57.6	0.109	0.05	6.1	1.649
0.67	60.0	60.9	60.0	61.3	96.3	57.1	0.121	0.065	8.1	1.629
0.83	59.2	59.0	58.5	59.6	94.3	56.5	0.132	0.081	10.4	1.627
0.99	56.2	58.6	57.1	58.2	92.2	55.9	0.142	0.097	12.7	1.645
1.17	54.4	57.5	55.6	56.9	89.7	55.3	0.152	0.113	15.2	1.689
1.36	51.7	56.3	53.9	55.9	86.8	54.7	0.162	0.126	17.9	1.766
1.56	50.7	55.0	52.2	55.0	83.5	54.0	0.171	0.136	20.6	1.892
1.77	49.9	53.7	50.5	54.3	79.6	53.6	0.18	0.14	23.5	2.115

C-run 0.5

	Vapor-mix				Water			NCG		
	Flow	Pin	Tst_in	T_out	Flow	Tw_in	Tw_out	Flow	MF	
	56.4	132.6	110.7	105.1	907.2	50.1	65.6	0.0	0.0	
loc	Ta	Two	Tb, fit	Twi	Tsb	q	delta1	delta2	m_cond	h_exp
0.25	63.2	71.2	66.2	71.2	106.7	54.9	0.07	0.022	1.8	1.545
0.39	63.3	69.1	65.1	68.4	105.7	52.4	0.09	0.037	3.7	1.403
0.53	64.0	65.4	63.9	66.0	104.7	52.8	0.104	0.053	5.6	1.366
0.67	63.0	63.6	62.8	64.2	103.6	53.2	0.116	0.07	7.5	1.349
0.83	62.3	61.7	61.4	62.5	102.3	53.6	0.127	0.089	9.6	1.345
0.99	59.1	61.9	60.1	61.1	100.9	54.0	0.137	0.108	11.9	1.356
1.17	57.3	60.7	58.6	59.9	99.3	54.5	0.146	0.128	14.4	1.384
1.36	54.5	59.6	56.9	59.0	97.5	55.0	0.156	0.148	17.0	1.429
1.56	53.4	58.2	55.2	58.3	95.4	55.5	0.165	0.166	19.9	1.494
1.77	52.9	56.9	53.4	57.7	93.1	55.8	0.173	0.181	22.9	1.576

C-run 0.7

	Vapor-mix				Water			NCG		
	Flow	Pin	Tst_in	T_out	Flow	Tw_in	Tw_out	Flow	MF	
	48.3	126.8	104.3	101.6	907.2	50.2	65.1	0.0	0.0	
loc	Ta	Two	Tb, fit	Twi	Tsb	q	delta1	delta2	m_cond	h_exp
0.25	63.4	70.2	65.9	70.1	105.3	55.0	0.071	0.022	1.8	1.565
0.39	63.2	68.1	64.8	67.6	104.1	52.4	0.09	0.036	3.7	1.434
0.53	63.6	65.0	63.6	65.5	102.9	52.4	0.104	0.052	5.5	1.401
0.67	62.6	63.3	62.5	63.7	101.6	52.5	0.116	0.068	7.4	1.384
0.83	61.9	61.4	61.1	62.1	100.1	52.5	0.127	0.086	9.5	1.381
0.99	58.9	61.4	59.8	60.8	98.6	52.6	0.136	0.103	11.6	1.392
1.17	57.3	60.3	58.3	59.6	96.7	52.6	0.146	0.122	14.0	1.42
1.36	54.6	59.2	56.8	58.7	94.6	52.7	0.155	0.139	16.6	1.467
1.56	53.6	57.9	55.1	57.9	92.2	52.7	0.164	0.155	19.3	1.538
1.77	52.8	56.7	53.4	57.3	89.5	52.7	0.172	0.167	22.1	1.639

Table 5. Test data for 2" test section and pure steam tests (cont.)

C-run 0.7R1

	Vapor-mix				Water			NCG		
	Flow	Pin	Tst_in	T_out	Flow	Tw_in	Tw_out	Flow	MF	
	36.4	116.3	102.4	100.1	907.2	50.1	64.3	0.0	0.0	
loc	Ta	Two	Tb, fit	Twi	Tsb	q	delta1	delta2	m_cond	h_exp
0.25	62.9	69.6	65.3	69.6	102.4	57.1	0.072	0.021	1.9	1.741
0.39	62.6	67.5	64.2	67.0	100.8	54.0	0.092	0.034	3.8	1.598
0.53	62.9	64.4	63.0	64.8	99.1	53.3	0.106	0.048	5.7	1.556
0.67	61.9	62.7	61.8	63.1	97.4	52.6	0.117	0.062	7.5	1.535
0.83	61.2	60.9	60.5	61.5	95.3	51.8	0.128	0.078	9.6	1.535
0.99	58.3	60.8	59.2	60.3	93.1	51.0	0.137	0.092	11.7	1.553
1.17	56.7	59.8	57.8	59.2	90.5	50.2	0.147	0.105	14.0	1.6
1.36	54.2	58.7	56.3	58.3	87.6	49.3	0.156	0.116	16.3	1.682
1.56	53.3	57.6	54.8	57.6	84.2	48.3	0.164	0.124	18.8	1.816
1.77	52.6	56.5	53.2	57.1	80.3	47.9	0.172	0.125	21.4	2.061

C-run 0.8

	Vapor-mix				Water			NCG		
	Flow	Pin	Tst_in	T_out	Flow	Tw_in	Tw_out	Flow	MF	
	56.2	126.9	108.8	103.7	907.2	45.5	63.7	0.0	0.0	
loc	Ta	Two	Tb, fit	Twi	Tsb	q	delta1	delta2	m_cond	h_exp
0.25	62.5	68.8	64.9	68.7	105.2	70.9	0.077	0.023	2.3	1.946
0.39	62.0	66.5	63.4	66.1	103.9	67.0	0.099	0.038	4.7	1.774
0.53	61.9	63.5	61.9	63.8	102.5	66.0	0.114	0.054	7.1	1.705
0.67	60.5	61.5	60.5	61.9	101.2	64.9	0.126	0.071	9.4	1.653
0.83	59.5	59.4	58.9	60.0	99.6	63.8	0.138	0.091	12.0	1.613
0.99	56.3	58.8	57.3	58.4	97.9	62.7	0.148	0.111	14.6	1.586
1.17	54.5	57.4	55.6	56.9	96.0	61.4	0.158	0.132	17.4	1.573
1.36	51.7	56.0	53.7	55.6	93.8	60.2	0.168	0.153	20.3	1.574
1.56	50.6	54.5	51.9	54.5	91.5	58.8	0.177	0.173	23.3	1.591
1.77	49.4	53.1	50.0	53.6	88.8	58.2	0.185	0.191	26.5	1.649

C-run 0.9

	Vapor-mix				Water			NCG		
	Flow	Pin	Tst_in	T_out	Flow	Tw_in	Tw_out	Flow	MF	
	55.4	126.9	108.8	104.1	907.2	46.8	64.2	0.0	0.0	
loc	Ta	Two	Tb, fit	Twi	Tsb	q	delta1	delta2	m_cond	h_exp
0.25	62.7	69.4	65.2	69.3	105.2	66.7	0.076	0.023	2.2	1.857
0.39	62.2	67.1	63.8	66.6	104.0	63.2	0.097	0.038	4.4	1.693
0.53	62.4	63.9	62.4	64.4	102.7	62.7	0.111	0.054	6.7	1.634
0.67	61.1	62.0	61.0	62.4	101.4	62.1	0.124	0.071	8.9	1.594
0.83	60.2	59.9	59.5	60.6	99.8	61.6	0.135	0.09	11.4	1.568
0.99	57.0	59.5	57.9	59.0	98.2	60.9	0.145	0.109	13.9	1.556
1.17	55.1	58.2	56.2	57.6	96.3	60.3	0.155	0.13	16.7	1.559
1.36	52.3	56.9	54.5	56.4	94.2	59.6	0.165	0.15	19.6	1.578
1.56	51.1	55.4	52.6	55.4	91.8	58.9	0.174	0.169	22.6	1.618
1.77	50.0	54.0	50.7	54.6	89.2	58.5	0.183	0.185	25.7	1.693

Table 6. Test data for 2" test section and steam-He tests

C-run 2.1

	Vapor-mix				Water			NCG		
	Flow	Pin	Tst_in	T_out	Flow	Tw_in	Tw_out	Flow	MF	
	31.7	116.0	102.7	95.9	907.2	46.9	61.2	11.0	2.9	
loc	Ta	Two	Tb, fit	Twi	Tsb	q	delta1	delta2	m_cond	h_exp
0.25	59.6	66.1	61.9	66.1	102.0	60.0	0.074	0.023	2.0	1.673
0.39	59.0	64.0	60.6	63.5	100.0	56.4	0.094	0.038	4.0	1.542
0.53	59.2	61.0	59.4	61.3	98.0	54.9	0.109	0.054	5.9	1.496
0.67	58.2	59.2	58.2	59.5	95.9	53.4	0.12	0.069	7.8	1.469
0.83	57.5	57.3	56.9	57.9	93.4	51.9	0.131	0.085	9.9	1.463
0.99	54.7	57.0	55.6	56.6	90.8	50.3	0.14	0.099	12.0	1.475
1.17	53.3	56.1	54.2	55.5	87.6	48.6	0.15	0.113	14.2	1.516
1.36	50.8	55.0	52.8	54.6	84.1	46.9	0.158	0.123	16.5	1.595
1.56	50.0	53.9	51.4	53.9	80.0	45.2	0.167	0.127	18.8	1.737
1.77	49.3	52.9	49.9	53.4	75.0	44.3	0.175	0.122	21.1	2.048

C-run 2.2

	Vapor-mix				Water			NCG		
	Flow	Pin	Tst_in	T_out	Flow	Tw_in	Tw_out	Flow	MF	
	32.4	115.9	102.1	95.2	907.2	47.7	61.4	9.5	3.4	
loc	Ta	Two	Tb, fit	Twi	Tsb	q	delta1	delta2	m_cond	h_exp
0.25	59.7	66.1	62.0	66.1	102.0	59.4	0.074	0.023	1.9	1.654
0.39	59.2	64.0	60.7	63.5	100.1	55.7	0.094	0.038	3.9	1.52
0.53	59.3	61.0	59.5	61.3	98.2	54.0	0.108	0.054	5.8	1.466
0.67	58.3	59.3	58.3	59.6	96.2	52.4	0.119	0.069	7.7	1.432
0.83	57.6	57.5	57.1	58.1	93.8	50.6	0.13	0.085	9.7	1.416
0.99	54.9	57.3	55.8	56.9	91.4	48.9	0.139	0.1	11.7	1.416
1.17	53.5	56.3	54.5	55.8	88.5	47.0	0.148	0.114	13.9	1.439
1.36	51.1	55.4	53.1	55.0	85.3	45.1	0.157	0.125	16.1	1.491
1.56	50.4	54.3	51.7	54.4	81.6	43.2	0.165	0.132	18.3	1.585
1.77	49.7	53.4	50.3	53.9	77.3	42.3	0.172	0.131	20.5	1.801

C-run 2.4

	Vapor-mix				Water			NCG		
	Flow	Pin	Tst_in	T_out	Flow	Tw_in	Tw_out	Flow	MF	
	33.5	115.8	101.7	95.0	907.2	48.5	61.9	7.3	4.6	
loc	Ta	Two	Tb, fit	Twi	Tsb	q	delta1	delta2	m_cond	h_exp
0.25	60.2	66.7	62.5	66.7	102.1	57.9	0.073	0.023	1.9	1.637
0.39	59.8	64.6	61.3	64.1	100.3	54.4	0.093	0.038	3.8	1.5
0.53	60.0	61.6	60.1	61.9	98.5	53.0	0.107	0.053	5.7	1.448
0.67	59.0	59.9	59.0	60.2	96.6	51.5	0.118	0.068	7.5	1.415
0.83	58.3	58.0	57.7	58.7	94.4	50.0	0.129	0.085	9.5	1.4
0.99	55.6	57.9	56.5	57.5	92.1	48.5	0.138	0.1	11.5	1.4
1.17	54.2	57.0	55.1	56.5	89.4	46.8	0.147	0.114	13.7	1.422
1.36	51.7	56.1	53.8	55.6	86.4	45.2	0.155	0.126	15.8	1.47
1.56	51.0	55.0	52.4	55.0	83.0	43.5	0.163	0.134	18.0	1.556
1.77	50.4	54.0	51.0	54.5	79.0	42.6	0.171	0.135	20.3	1.74

Table 6. Test data for 2" test section and steam-He tests (cont.)

C-run 2.6

	Vapor-mix				Water			NCG		
	Flow	Pin	Tst_in	T_out	Flow	Tw_in	Tw_out	Flow	MF	
	31.3	115.6	101.1	94.7	907.2	49.2	62.4	5.5	5.7	
loc	Ta	Two	Tb, fit	Twi	Tsb	q	delta1	delta2	m_cond	h_exp
0.25	60.7	67.0	62.9	67.0	102.0	56.4	0.072	0.023	1.8	1.614
0.39	60.2	65.0	61.7	64.4	100.1	53.0	0.092	0.037	3.7	1.486
0.53	60.4	62.0	60.6	62.4	98.2	51.6	0.106	0.052	5.5	1.44
0.67	59.5	60.4	59.5	60.7	96.3	50.2	0.117	0.066	7.3	1.413
0.83	58.9	58.6	58.2	59.2	93.9	48.8	0.128	0.082	9.3	1.406
0.99	56.2	58.5	57.0	58.1	91.5	47.3	0.137	0.096	11.2	1.415
1.17	54.7	57.6	55.7	57.1	88.6	45.7	0.146	0.109	13.3	1.451
1.36	52.3	56.7	54.4	56.3	85.3	44.1	0.154	0.119	15.4	1.518
1.56	51.6	55.7	53.0	55.7	81.7	42.5	0.162	0.124	17.6	1.635
1.77	51.1	54.7	51.7	55.2	77.3	41.7	0.169	0.122	19.8	1.886

C-run 2.8

	Vapor-mix				Water			NCG		
	Flow	Pin	Tst_in	T_out	Flow	Tw_in	Tw_out	Flow	MF	
	29.9	115.5	101.0	94.5	907.2	46.4	62.1	3.7	8.1	
loc	Ta	Two	Tb, fit	Twi	Tsb	q	delta1	delta2	m_cond	h_exp
0.25	60.8	66.6	62.9	66.6	101.7	61.7	0.074	0.023	2.0	1.757
0.39	60.2	64.6	61.6	64.1	99.6	57.9	0.095	0.037	4.1	1.634
0.53	60.2	61.8	60.4	62.1	97.3	56.2	0.109	0.051	6.1	1.593
0.67	59.2	60.1	59.1	60.4	95.0	54.5	0.121	0.065	8.0	1.571
0.83	58.4	58.2	57.8	58.8	92.3	52.7	0.132	0.08	10.1	1.573
0.99	55.7	57.8	56.5	57.5	89.3	50.9	0.141	0.092	12.2	1.596
1.17	54.1	56.8	55.1	56.3	85.8	49.0	0.15	0.104	14.4	1.658
1.36	51.8	55.7	53.7	55.3	81.8	47.0	0.159	0.11	16.7	1.775
1.56	51.1	54.5	52.2	54.5	77.1	45.1	0.168	0.111	19.0	1.995
1.77	50.3	53.5	50.8	53.9	71.4	44.1	0.176	0.099	21.3	2.527

C-run 2.9

	Vapor-mix				Water			NCG		
	Flow	Pin	Tst_in	T_out	Flow	Tw_in	Tw_out	Flow	MF	
	34.6	115.9	102.9	96.4	907.2	45.9	61.2	2.2	15.7	
loc	Ta	Two	Tb, fit	Twi	Tsb	q	delta1	delta2	m_cond	h_exp
0.25	59.9	65.8	62.0	65.8	102.0	64.5	0.076	0.024	2.1	1.781
0.39	59.2	63.6	60.6	63.2	100.1	60.5	0.097	0.039	4.3	1.643
0.53	59.1	60.8	59.3	61.1	98.1	58.6	0.111	0.054	6.3	1.587
0.67	58.0	59.1	58.1	59.4	96.0	56.8	0.123	0.069	8.4	1.549
0.83	57.2	57.2	56.7	57.7	93.6	54.8	0.134	0.086	10.6	1.529
0.99	54.4	56.7	55.3	56.4	91.1	52.9	0.143	0.101	12.7	1.524
1.17	52.9	55.7	53.9	55.2	88.2	50.8	0.153	0.116	15.1	1.544
1.36	50.4	54.6	52.4	54.3	84.8	48.7	0.162	0.128	17.4	1.593
1.56	49.6	53.5	50.9	53.5	81.1	46.6	0.17	0.135	19.8	1.686
1.77	48.8	52.4	49.4	52.8	76.7	45.5	0.178	0.135	22.2	1.909

Table 7. Test data for 2" test section and steam-N2 tests

C-run 3

	Vapor-mix				Water			NCG		
	Flow	Pin	Tst_in	T_out	Flow	Tw_in	Tw_out	Flow	MF	
	31.8	111.4	103.0	97.1	907.2	49.6	62.3	14.7	2.2	
loc	Ta	Two	Tb, fit	Twi	Tsb	q	delta1	delta2	m_cond	h_exp
0.25	60.7	66.7	62.9	66.8	100.9	57.0	0.073	0.022	1.9	1.668
0.39	60.3	64.7	61.7	64.2	99.1	53.5	0.092	0.036	3.8	1.535
0.53	60.5	61.9	60.5	62.2	97.2	52.1	0.106	0.051	5.6	1.486
0.67	59.5	60.2	59.4	60.5	95.3	50.6	0.118	0.065	7.4	1.457
0.83	58.8	58.5	58.2	59.1	93.0	49.1	0.128	0.08	9.4	1.447
0.99	56.1	58.3	57.0	57.9	90.6	47.5	0.137	0.094	11.3	1.454
1.17	54.6	57.4	55.6	56.9	87.7	45.9	0.146	0.107	13.4	1.488
1.36	52.3	56.5	54.3	56.1	84.5	44.2	0.155	0.117	15.6	1.554
1.56	51.6	55.5	52.9	55.5	80.9	42.5	0.163	0.122	17.7	1.669
1.77	51.1	54.5	51.6	55.0	76.7	41.6	0.17	0.12	19.9	1.919

C-run 3.1

	Vapor-mix				Water			NCG		
	Flow	Pin	Tst_in	T_out	Flow	Tw_in	Tw_out	Flow	MF	
	30.7	111.4	102.6	96.8	907.2	49.4	62.4	12.9	2.4	
loc	Ta	Two	Tb, fit	Twi	Tsb	q	delta1	delta2	m_cond	h_exp
0.25	60.7	66.9	63.0	66.9	101.0	54.8	0.072	0.022	1.8	1.611
0.39	60.5	64.9	61.8	64.4	99.1	51.6	0.091	0.036	3.6	1.484
0.53	60.7	62.0	60.7	62.4	97.2	50.3	0.105	0.05	5.4	1.442
0.67	59.7	60.4	59.6	60.7	95.3	49.1	0.116	0.065	7.1	1.419
0.83	59.1	58.7	58.4	59.3	93.0	47.8	0.127	0.08	9.1	1.417
0.99	56.4	58.6	57.2	58.1	90.6	46.4	0.136	0.093	11.0	1.432
1.17	54.9	57.8	56.0	57.2	87.7	45.0	0.145	0.105	13.0	1.475
1.36	52.6	56.8	54.6	56.4	84.4	43.6	0.153	0.115	15.1	1.554
1.56	52.0	55.8	53.3	55.8	80.7	42.1	0.161	0.119	17.3	1.689
1.77	51.5	54.8	51.9	55.4	76.4	41.3	0.169	0.116	19.5	1.971

C-run 3.4

	Vapor-mix				Water			NCG		
	Flow	Pin	Tst_in	T_out	Flow	Tw_in	Tw_out	Flow	MF	
	38.5	111.5	103.6	97.4	907.2	46.3	60.0	7.3	5.2	
loc	Ta	Two	Tb, fit	Twi	Tsb	q	delta1	delta2	m_cond	h_exp
0.25	58.4	64.7	60.7	64.8	101.2	59.5	0.074	0.024	2.0	1.633
0.39	58.0	62.6	59.4	62.1	99.6	55.9	0.094	0.04	3.9	1.491
0.53	58.1	59.6	58.2	60.0	98.0	54.4	0.109	0.056	5.9	1.43
0.67	57.0	57.9	57.1	58.2	96.4	52.9	0.12	0.073	7.8	1.386
0.83	56.4	56.1	55.8	56.7	94.5	51.3	0.131	0.091	9.8	1.357
0.99	53.6	55.8	54.5	55.5	92.5	49.7	0.14	0.109	11.9	1.34
1.17	52.1	55.0	53.1	54.4	90.2	47.9	0.149	0.126	14.1	1.338
1.36	49.7	53.9	51.7	53.5	87.7	46.2	0.158	0.142	16.3	1.352
1.56	49.0	52.9	50.3	52.9	84.9	44.4	0.166	0.156	18.6	1.385
1.77	48.3	51.9	48.9	52.4	81.8	43.5	0.173	0.165	20.9	1.479

Table 7. Test data for 2" test section and steam-N2 tests (cont.)

C-run 3.5

	Vapor-mix				Water			NCG		
	Flow	Pin	Tst_in	T_out	Flow	Tw_in	Tw_out	Flow	MF	
	42.2	115.7	105.4	99.7	907.2	47.2	61.6	5.5	7.7	
loc	Ta	Two	Tb, fit	Twi	Tsb	q	delta1	delta2	m_cond	h_exp
0.25	59.8	66.6	62.3	66.6	102.4	57.6	0.073	0.023	1.9	1.608
0.39	59.5	64.4	61.1	63.9	101.0	54.5	0.093	0.039	3.8	1.469
0.53	59.9	61.3	59.9	61.7	99.6	53.9	0.107	0.055	5.7	1.423
0.67	58.8	59.5	58.7	59.9	98.1	53.2	0.119	0.071	7.6	1.394
0.83	58.1	57.7	57.4	58.3	96.4	52.5	0.13	0.09	9.8	1.381
0.99	55.1	57.6	56.1	57.0	94.5	51.8	0.139	0.108	11.9	1.381
1.17	53.6	56.6	54.6	55.9	92.4	51.0	0.149	0.126	14.2	1.399
1.36	51.0	55.5	53.1	55.0	89.9	50.2	0.158	0.143	16.7	1.436
1.56	50.1	54.2	51.5	54.3	87.2	49.4	0.166	0.157	19.2	1.498
1.77	49.4	53.1	49.9	53.7	84.1	48.9	0.175	0.167	21.8	1.609

C-run 3.6

	Vapor-mix				Water			NCG		
	Flow	Pin	Tst_in	T_out	Flow	Tw_in	Tw_out	Flow	MF	
	40.0	115.7	104.8	99.7	907.2	48.4	62.7	3.7	10.9	
loc	Ta	Two	Tb, fit	Twi	Tsb	q	delta1	delta2	m_cond	h_exp
0.25	60.7	67.5	63.2	67.5	102.4	57.2	0.072	0.022	1.9	1.64
0.39	60.5	65.4	62.0	64.8	100.9	54.2	0.092	0.037	3.8	1.5
0.53	60.9	62.2	60.9	62.6	99.4	53.6	0.107	0.053	5.7	1.456
0.67	59.8	60.4	59.7	60.8	97.8	53.0	0.118	0.069	7.6	1.432
0.83	59.1	58.6	58.4	59.2	96.0	52.3	0.129	0.086	9.7	1.425
0.99	56.2	58.5	57.1	58.0	94.0	51.6	0.139	0.103	11.8	1.433
1.17	54.6	57.5	55.6	56.9	91.7	50.9	0.148	0.119	14.1	1.463
1.36	52.0	56.4	54.1	56.0	89.1	50.2	0.157	0.134	16.6	1.516
1.56	51.1	55.3	52.6	55.3	86.1	49.4	0.166	0.146	19.1	1.602
1.77	50.4	54.1	50.9	54.8	82.7	49.0	0.174	0.152	21.7	1.753

C-run 3.8

	Vapor-mix				Water			NCG		
	Flow	Pin	Tst_in	T_out	Flow	Tw_in	Tw_out	Flow	MF	
	39.8	115.7	104.4	99.6	907.2	49.3	63.4	2.6	15.5	
loc	Ta	Two	Tb, fit	Twi	Tsb	q	delta1	delta2	m_cond	h_exp
0.25	61.3	68.0	63.8	68.1	102.4	56.0	0.072	0.022	1.8	1.632
0.39	61.2	66.0	62.7	65.4	100.9	53.1	0.092	0.036	3.7	1.494
0.53	61.6	62.8	61.5	63.3	99.5	52.5	0.106	0.052	5.6	1.452
0.67	60.5	61.1	60.4	61.5	97.9	52.0	0.117	0.067	7.4	1.429
0.83	59.8	59.3	59.1	59.9	96.1	51.4	0.128	0.084	9.5	1.422
0.99	56.9	59.2	57.8	58.7	94.2	50.8	0.138	0.1	11.6	1.431
1.17	55.3	58.3	56.4	57.6	91.9	50.1	0.147	0.117	13.9	1.461
1.36	52.8	57.2	54.9	56.7	89.3	49.4	0.156	0.131	16.3	1.515
1.56	51.9	56.0	53.3	56.0	86.4	48.7	0.164	0.142	18.7	1.601
1.77	51.2	54.8	51.8	55.5	83.1	48.3	0.172	0.149	21.3	1.75

Table 8. Test data for 1" test section and pure steam tests

B-run 2.0R1

	Vapor-mix				Water			NCG		
	Flow	Pin	Tst_in	T_out	Flow	Tw_in	Tw_out	Flow	MF	
	47.5	109.4	102.9	101.8	907.2	43.6	56.7	0.0	0.0	
loc	Ta	Two	Tb, fit	Twi	Tsb	q	delta1	delta2	m_cond	h_exp
0.25	55.6	60.2	57.1	60.1	101.2	96.7	0.088	0.028	1.6	2.357
0.39	55.1	58.2	56.0	58.0	100.1	91.6	0.113	0.046	3.3	2.174
0.53	54.5	56.0	55.0	56.4	99.1	90.5	0.13	0.065	4.9	2.12
0.67	53.6	55.0	54.0	55.2	98.0	89.3	0.143	0.084	6.5	2.086
0.83	53.0	53.9	52.9	54.1	96.8	88.1	0.156	0.105	8.3	2.068
0.99	51.2	54.1	51.8	53.4	95.5	86.9	0.168	0.125	10.1	2.064
1.17	49.4	53.0	50.6	52.8	94.0	85.5	0.179	0.146	12.1	2.075
1.36	47.3	52.3	49.3	52.3	92.4	84.1	0.189	0.166	14.2	2.1
1.56	46.0	51.5	47.9	52.0	90.6	82.7	0.198	0.186	16.3	2.141
1.77	44.9	51.8	46.6	51.8	88.7	82.0	0.208	0.203	18.6	2.22

B-run 2.0R2

	Vapor-mix				Water			NCG		
	Flow	Pin	Tst_in	T_out	Flow	Tw_in	Tw_out	Flow	MF	
	53.3	109.4	103.3	102.1	907.2	45.2	57.7	0.0	0.0	
loc	Ta	Two	Tb, fit	Twi	Tsb	q	delta1	delta2	m_cond	h_exp
0.25	55.4	61.2	57.3	61.1	101.4	83.3	0.084	0.027	1.4	2.068
0.39	55.3	59.4	56.4	59.0	100.6	79.5	0.107	0.045	2.8	1.912
0.53	54.9	57.0	55.6	57.5	99.8	79.8	0.123	0.064	4.3	1.886
0.67	54.0	56.1	54.7	56.3	99.0	80.1	0.137	0.082	5.7	1.879
0.83	53.4	55.0	53.6	55.4	98.0	80.4	0.149	0.103	7.4	1.888
0.99	51.9	55.6	52.6	54.7	96.9	80.8	0.16	0.123	9.0	1.911
1.17	50.1	54.5	51.5	54.1	95.8	81.1	0.171	0.144	10.9	1.95
1.36	48.1	53.8	50.2	53.8	94.4	81.6	0.182	0.165	12.9	2.005
1.56	46.7	53.0	48.9	53.5	93.0	82.0	0.192	0.186	15.1	2.076
1.77	45.7	53.2	47.6	53.3	91.4	82.2	0.201	0.204	17.3	2.16

B-run 2.1

	Vapor-mix				Water			NCG		
	Flow	Pin	Tst_in	T_out	Flow	Tw_in	Tw_out	Flow	MF	
	59.4	109.4	104.5	102.7	907.2	46.8	59.0	0.0	0.0	
loc	Ta	Two	Tb, fit	Twi	Tsb	q	delta1	delta2	m_cond	h_exp
0.25	55.6	62.7	58.0	62.7	101.6	71.3	0.079	0.026	1.2	1.834
0.39	56.0	60.8	57.2	60.4	101.0	68.7	0.101	0.043	2.4	1.694
0.53	55.8	58.3	56.5	58.8	100.3	70.2	0.117	0.062	3.7	1.69
0.67	54.8	57.4	55.7	57.7	99.7	71.8	0.13	0.08	5.0	1.709
0.83	54.2	56.3	54.8	56.8	98.9	73.5	0.142	0.1	6.5	1.745
0.99	53.1	57.1	53.8	56.2	98.0	75.4	0.153	0.12	8.1	1.8
1.17	51.1	56.1	52.7	55.7	97.1	77.5	0.165	0.141	9.9	1.873
1.36	49.4	55.6	51.5	55.4	96.0	79.8	0.175	0.162	11.8	1.967
1.56	47.8	54.7	50.2	55.2	94.7	82.3	0.185	0.182	14.0	2.082
1.77	46.8	54.8	48.8	55.1	93.3	83.6	0.195	0.201	16.2	2.185

Table 8. Test data for 1" test section and pure steam tests (cont.)

B-run 3.2

	Vapor-mix				Water			NCG		
	Flow	Pin	Tst_in	T_out	Flow	Tw_in	Tw_out	Flow	MF	
	59.0	117.4	104.3	103.2	907.2	44.3	57.3	0.0	0.0	
loc	Ta	Two	Tb, fit	Twi	Tsb	q	delta1	delta2	m_cond	h_exp
0.25	55.2	61.3	57.2	61.2	103.4	89.5	0.086	0.029	1.5	2.122
0.39	55.2	59.3	56.3	59.0	102.6	85.3	0.109	0.047	3.0	1.953
0.53	54.7	56.7	55.3	57.3	101.9	85.5	0.126	0.067	4.6	1.917
0.67	53.6	55.7	54.4	56.0	101.0	85.6	0.14	0.086	6.1	1.901
0.83	52.9	54.6	53.3	55.0	100.1	85.7	0.153	0.109	7.9	1.9
0.99	51.5	55.2	52.2	54.2	99.1	85.8	0.164	0.13	9.7	1.914
1.17	49.6	54.1	51.0	53.7	97.9	86.0	0.175	0.153	11.7	1.943
1.36	47.5	53.4	49.7	53.3	96.7	86.2	0.186	0.176	13.8	1.985
1.56	46.0	52.5	48.3	53.0	95.3	86.3	0.196	0.198	16.0	2.04
1.77	44.9	52.6	46.8	52.8	93.8	86.4	0.205	0.219	18.4	2.109

B-run 1.1

	Vapor-mix				Water			NCG		
	Flow	Pin	Tst_in	T_out	Flow	Tw_in	Tw_out	Flow	MF	
	25.6	108.4	102.2	101.6	907.2	49.8	61.3	0.0	0.0	
loc	Ta	Two	Tb, fit	Twi	Tsb	q	delta1	delta2	m_cond	h_exp
0.25	57.6	64.5	60.1	64.5	100.6	68.9	0.078	0.024	1.1	1.91
0.39	58.3	62.7	59.3	62.3	99.2	65.8	0.099	0.039	2.3	1.783
0.53	58.1	60.3	58.6	60.7	97.7	66.3	0.115	0.054	3.5	1.792
0.67	57.1	59.4	57.8	59.6	96.2	66.8	0.127	0.069	4.7	1.829
0.83	56.4	58.4	57.0	58.8	94.3	67.4	0.139	0.084	6.1	1.899
0.99	55.3	59.1	56.1	58.3	92.3	68.0	0.15	0.097	7.5	1.999
1.17	53.6	58.3	55.2	57.9	89.9	68.6	0.16	0.109	9.1	2.148
1.36	52.2	57.8	54.1	57.6	87.0	69.3	0.17	0.118	10.8	2.361
1.56	50.9	57.1	53.0	57.5	83.7	70.1	0.18	0.122	12.6	2.676
1.77	50.0	57.2	51.8	57.4	79.7	70.5	0.19	0.119	14.5	3.158

B-run 1.2

	Vapor-mix				Water			NCG		
	Flow	Pin	Tst_in	T_out	Flow	Tw_in	Tw_out	Flow	MF	
	37.8	108.4	103.9	102.8	907.2	45.1	58.6	0.0	0.0	
loc	Ta	Two	Tb, fit	Twi	Tsb	q	delta1	delta2	m_cond	h_exp
0.25	56.9	61.8	58.6	61.8	100.7	95.6	0.088	0.026	1.6	2.459
0.39	56.6	59.9	57.6	59.6	99.4	90.2	0.112	0.043	3.2	2.27
0.53	56.2	57.7	56.6	58.0	98.1	88.6	0.129	0.06	4.8	2.21
0.67	55.2	56.6	55.6	56.8	96.7	86.8	0.142	0.077	6.4	2.174
0.83	54.5	55.4	54.5	55.7	95.1	85.0	0.155	0.096	8.2	2.158
0.99	52.8	55.6	53.4	55.0	93.5	83.2	0.166	0.113	9.9	2.157
1.17	51.1	54.6	52.2	54.4	91.6	81.2	0.176	0.131	11.8	2.178
1.36	49.1	54.0	51.0	53.9	89.6	79.1	0.186	0.147	13.7	2.218
1.56	48.0	53.2	49.8	53.6	87.3	77.0	0.196	0.161	15.7	2.283
1.77	47.0	53.4	48.5	53.4	84.8	76.0	0.204	0.172	17.8	2.416

Table 9. Test data for 1" test section and steam-He tests

B-run 1.6

	Vapor-mix				Water			NCG		
	Flow	Pin	Tst_in	T_out	Flow	Tw_in	Tw_out	Flow	MF	
	17.4	106.3	96.8	79.5	907.2	42.8	52.3	1.8	9.5	
loc	Ta	Two	Tb, fit	Twi	Tsb	q	delta1	delta2	m_cond	h_exp
0.25	49.8	55.8	51.8	55.8	98.8	91.6	0.088	0.031	1.5	2.134
0.39	49.6	53.8	50.8	53.5	96.0	84.0	0.112	0.049	3.0	1.976
0.53	49.2	51.6	49.9	51.8	93.2	77.7	0.128	0.067	4.4	1.877
0.67	48.4	50.5	49.1	50.6	90.4	71.7	0.141	0.083	5.7	1.802
0.83	48.0	49.3	48.2	49.7	87.2	65.8	0.152	0.099	7.1	1.755
0.99	46.8	49.4	47.4	49.0	83.9	60.1	0.161	0.112	8.3	1.722
1.17	45.5	48.7	46.6	48.5	80.2	54.5	0.17	0.122	9.6	1.723
1.36	44.1	48.3	45.8	48.2	76.1	49.0	0.178	0.127	10.8	1.759
1.56	43.6	47.8	45.0	48.0	71.6	43.9	0.185	0.126	11.9	1.858
1.77	43.4	47.8	44.4	47.9	66.4	41.4	0.192	0.114	13.0	2.238

B-run 2.7

	Vapor-mix				Water			NCG		
	Flow	Pin	Tst_in	T_out	Flow	Tw_in	Tw_out	Flow	MF	
	20.4	107.0	96.7	89.8	907.2	46.9	57.0	6.6	3.1	
loc	Ta	Two	Tb, fit	Twi	Tsb	q	delta1	delta2	m_cond	h_exp
0.25	54.6	60.1	56.5	60.2	99.4	91.0	0.087	0.027	1.5	2.323
0.39	54.5	58.3	55.5	57.9	97.0	84.3	0.11	0.043	3.0	2.155
0.53	54.1	56.1	54.6	56.3	94.7	79.5	0.126	0.059	4.4	2.072
0.67	53.2	55.0	53.8	55.2	92.3	74.9	0.139	0.074	5.8	2.015
0.83	52.7	53.8	52.8	54.2	89.6	70.3	0.15	0.089	7.2	1.988
0.99	51.4	54.0	52.0	53.6	86.8	65.7	0.16	0.101	8.6	1.978
1.17	49.9	53.2	51.1	53.1	83.5	61.0	0.169	0.111	10.0	2.004
1.36	48.4	52.9	50.2	52.7	80.0	56.5	0.178	0.117	11.4	2.072
1.56	47.7	52.3	49.3	52.5	76.1	52.0	0.185	0.118	12.7	2.205
1.77	47.4	52.3	48.5	52.4	71.5	49.8	0.193	0.111	14.0	2.597

B-run 3.5

	Vapor-mix				Water			NCG		
	Flow	Pin	Tst_in	T_out	Flow	Tw_in	Tw_out	Flow	MF	
	23.9	107.3	99.6	95.6	907.2	48.3	59.4	3.7	6.5	
loc	Ta	Two	Tb, fit	Twi	Tsb	q	delta1	delta2	m_cond	h_exp
0.25	56.5	62.7	58.7	62.8	99.8	88.5	0.085	0.025	1.5	2.391
0.39	56.7	60.9	57.8	60.5	97.9	82.7	0.108	0.04	3.0	2.211
0.53	56.4	58.5	56.9	58.8	95.9	79.5	0.124	0.056	4.4	2.141
0.67	55.4	57.4	56.0	57.6	94.0	76.4	0.137	0.07	5.8	2.098
0.83	54.9	56.1	55.1	56.6	91.6	73.1	0.149	0.085	7.3	2.085
0.99	53.6	56.4	54.1	55.9	89.3	69.8	0.159	0.098	8.7	2.091
1.17	51.8	55.5	53.2	55.3	86.5	66.5	0.169	0.11	10.2	2.133
1.36	50.3	55.1	52.2	54.9	83.4	63.0	0.178	0.119	11.8	2.212
1.56	49.5	54.4	51.2	54.7	80.0	59.6	0.186	0.123	13.3	2.35
1.77	49.1	54.4	50.3	54.5	76.1	57.9	0.194	0.121	14.9	2.677

Table 9. Test data for 1" test section and steam-He tests (cont.)

B-run 4.2

	Vapor-mix				Water			NCG		
	Flow	Pin	Tst_in	T_out	Flow	Tw_in	Tw_out	Flow	MF	
	29.1	107.8	99.2	96.3	907.2	46.1	62.8	7.0	4.2	
loc	Ta	Two	Tb, fit	Twi	Tsb	q	delta1	delta2	m_cond	h_exp
0.25	59.1	66.2	61.7	66.2	100.2	90.1	0.085	0.022	1.5	2.642
0.39	59.7	64.3	60.8	63.9	98.7	84.7	0.108	0.036	3.0	2.436
0.53	59.5	61.7	59.9	62.1	97.1	82.6	0.124	0.051	4.5	2.362
0.67	58.4	60.4	58.9	60.7	95.4	80.4	0.137	0.065	5.9	2.314
0.83	57.8	58.9	57.9	59.4	93.5	78.2	0.149	0.08	7.5	2.293
0.99	56.4	59.0	57.0	58.4	91.5	75.9	0.16	0.094	9.1	2.293
1.17	54.6	57.8	55.9	57.5	89.1	73.5	0.17	0.108	10.8	2.324
1.36	53.1	57.1	54.8	56.8	86.5	71.0	0.179	0.12	12.5	2.389
1.56	52.3	56.1	53.7	56.3	83.7	68.5	0.188	0.129	14.3	2.502
1.77	51.9	55.7	52.6	55.9	80.4	67.2	0.197	0.133	16.1	2.743

B-run 5.3

	Vapor-mix				Water			NCG		
	Flow	Pin	Tst_in	T_out	Flow	Tw_in	Tw_out	Flow	MF	
	48.1	113.5	103.4	99.8	907.2	43.3	56.9	7.7	6.2	
loc	Ta	Two	Tb, fit	Twi	Tsb	q	delta1	delta2	m_cond	h_exp
0.25	56.4	60.5	57.8	60.6	101.9	129.9	0.097	0.028	2.2	3.145
0.39	55.5	58.5	56.4	58.2	100.5	120.0	0.124	0.046	4.3	2.836
0.53	54.8	56.3	55.2	56.4	99.2	112.8	0.142	0.065	6.4	2.634
0.67	53.7	54.9	53.9	54.9	97.9	105.7	0.155	0.084	8.3	2.462
0.83	53.1	53.3	52.6	53.7	96.4	98.7	0.168	0.105	10.3	2.31
0.99	50.9	53.1	51.4	52.7	95.0	91.8	0.179	0.126	12.2	2.171
1.17	49.1	52.0	50.2	52.0	93.5	84.8	0.189	0.148	14.2	2.044
1.36	46.9	51.4	48.9	51.4	91.9	78.0	0.198	0.17	16.1	1.924
1.56	46.1	50.7	47.7	51.0	90.3	71.4	0.206	0.191	18.0	1.812
1.77	45.6	50.8	46.6	50.7	88.7	68.1	0.213	0.212	19.8	1.792

B-run 5.9

	Vapor-mix				Water			NCG		
	Flow	Pin	Tst_in	T_out	Flow	Tw_in	Tw_out	Flow	MF	
	38.8	117.3	101.7	99.5	907.2	43.2	56.8	3.7	10.6	
loc	Ta	Two	Tb, fit	Twi	Tsb	q	delta1	delta2	m_cond	h_exp
0.25	56.6	60.5	57.9	60.6	102.4	134.2	0.098	0.029	2.2	3.205
0.39	55.6	58.4	56.5	58.2	100.7	124.0	0.125	0.047	4.5	2.918
0.53	54.8	56.2	55.2	56.3	98.9	116.5	0.143	0.065	6.6	2.734
0.67	53.7	54.8	53.9	54.8	97.1	109.1	0.157	0.083	8.5	2.579
0.83	53.0	53.3	52.6	53.6	95.2	101.8	0.17	0.103	10.6	2.447
0.99	50.8	52.9	51.3	52.6	93.2	94.6	0.181	0.122	12.6	2.327
1.17	49.0	51.8	50.0	51.8	91.1	87.3	0.191	0.142	14.6	2.223
1.36	46.7	51.2	48.7	51.2	88.9	80.2	0.201	0.16	16.6	2.13
1.56	45.9	50.5	47.5	50.7	86.5	73.4	0.209	0.177	18.5	2.049
1.77	45.3	50.6	46.4	50.4	84.0	70.0	0.217	0.19	20.4	2.082

Table 10. Test data for 1" test section and steam-N2 tests

B-run 5.2

	Vapor-mix				Water			NCG		
	Flow	Pin	Tst_in	T_out	Flow	Tw_in	Tw_out	Flow	MF	
	35.7	109.6	101.1	98.1	907.2	52.3	62.3	11.0	3.2	
loc	Ta	Two	Tb, fit	Twi	Tsb	q	delta1	delta2	m_cond	h_exp
0.25	58.2	65.9	60.9	66.1	101.2	77.2	0.08	0.023	1.3	2.201
0.39	58.9	64.2	60.1	63.5	100.1	72.5	0.102	0.038	2.6	1.981
0.53	58.6	61.5	59.3	61.8	99.0	70.3	0.118	0.054	3.8	1.89
0.67	57.6	60.4	58.5	60.6	97.9	68.2	0.13	0.069	5.1	1.83
0.83	57.0	59.2	57.7	59.8	96.7	66.0	0.141	0.086	6.4	1.789
0.99	56.1	59.8	56.9	59.3	95.4	63.7	0.15	0.101	7.7	1.761
1.17	54.4	59.2	56.0	58.9	94.0	61.3	0.159	0.117	9.2	1.746
1.36	53.0	58.9	55.1	58.7	92.5	58.9	0.168	0.132	10.6	1.74
1.56	52.0	58.4	54.1	58.5	90.9	56.4	0.175	0.146	12.0	1.741
1.77	51.6	58.2	53.2	58.4	89.2	55.2	0.183	0.158	13.5	1.793

B-run 5.4

	Vapor-mix				Water			NCG		
	Flow	Pin	Tst_in	T_out	Flow	Tw_in	Tw_out	Flow	MF	
	32.2	109.7	100.2	97.7	907.2	48.6	59.3	10.1	3.2	
loc	Ta	Two	Tb, fit	Twi	Tsb	q	delta1	delta2	m_cond	h_exp
0.25	55.7	63.1	58.3	63.2	100.9	90.6	0.086	0.025	1.5	2.406
0.39	56.1	61.1	57.3	60.6	99.4	84.5	0.109	0.042	3.0	2.175
0.53	55.7	58.5	56.4	58.8	98.0	81.1	0.125	0.059	4.5	2.065
0.67	54.6	57.3	55.5	57.5	96.6	77.7	0.138	0.075	5.9	1.986
0.83	54.0	56.0	54.5	56.6	95.0	74.2	0.149	0.093	7.4	1.93
0.99	52.9	56.4	53.6	55.9	93.3	70.6	0.159	0.109	8.9	1.887
1.17	51.1	55.7	52.6	55.5	91.5	67.0	0.169	0.125	10.4	1.859
1.36	49.5	55.4	51.7	55.2	89.6	63.3	0.177	0.14	12.0	1.842
1.56	48.5	54.8	50.7	55.0	87.5	59.7	0.185	0.153	13.5	1.836
1.77	48.1	54.7	49.7	54.9	85.3	57.9	0.192	0.164	15.1	1.905

B-run 5.5

	Vapor-mix				Water			NCG		
	Flow	Pin	Tst_in	T_out	Flow	Tw_in	Tw_out	Flow	MF	
	30.1	109.7	100.2	97.7	907.2	51.1	61.2	8.1	3.7	
loc	Ta	Two	Tb, fit	Twi	Tsb	q	delta1	delta2	m_cond	h_exp
0.25	57.1	64.8	59.8	65.0	100.9	80.1	0.082	0.024	1.3	2.227
0.39	57.8	63.0	58.9	62.4	99.6	75.0	0.104	0.039	2.7	2.016
0.53	57.4	60.3	58.1	60.6	98.2	72.6	0.119	0.055	4.0	1.929
0.67	56.3	59.2	57.3	59.5	96.9	70.1	0.132	0.07	5.2	1.873
0.83	55.8	58.0	56.5	58.6	95.3	67.5	0.143	0.087	6.6	1.838
0.99	54.9	58.6	55.6	58.0	93.7	64.9	0.153	0.102	8.0	1.818
1.17	53.1	58.0	54.7	57.6	91.9	62.2	0.162	0.116	9.4	1.814
1.36	51.7	57.6	53.8	57.4	90.0	59.4	0.17	0.13	10.8	1.822
1.56	50.7	57.1	52.9	57.3	87.9	56.6	0.178	0.141	12.3	1.845
1.77	50.3	56.9	51.9	57.2	85.7	55.2	0.185	0.15	13.8	1.936

Table 10. Test data for 1" test section and steam-N2 tests (cont.)

B-run 5.8

	Vapor-mix				Water			NCG		
	Flow	Pin	Tst_in	T_out	Flow	Tw_in	Tw_out	Flow	MF	
	52.9	109.8	103.0	100.6	907.2	45.2	57.7	5.1	10.3	
loc	Ta	Two	Tb, fit	Twi	Tsb	q	delta1	delta2	m_cond	h_exp
0.25	55.2	61.8	57.5	61.9	101.2	114.0	0.093	0.027	1.9	2.901
0.39	55.1	59.7	56.3	59.2	100.1	105.7	0.118	0.044	3.8	2.584
0.53	54.5	57.1	55.1	57.3	99.1	100.0	0.135	0.063	5.6	2.393
0.67	53.2	55.7	54.0	55.9	98.1	94.4	0.149	0.082	7.3	2.238
0.83	52.6	54.3	52.9	54.7	96.9	88.8	0.161	0.103	9.2	2.105
0.99	51.1	54.4	51.8	53.9	95.8	83.2	0.171	0.123	10.9	1.986
1.17	49.2	53.4	50.6	53.3	94.6	77.6	0.181	0.145	12.7	1.878
1.36	47.3	53.0	49.5	52.9	93.4	72.0	0.189	0.167	14.4	1.776
1.56	46.3	52.4	48.4	52.6	92.2	66.5	0.197	0.188	16.2	1.68
1.77	45.8	52.4	47.3	52.4	90.9	63.9	0.204	0.209	17.9	1.658

B-run 5.9

	Vapor-mix				Water			NCG		
	Flow	Pin	Tst_in	T_out	Flow	Tw_in	Tw_out	Flow	MF	
	49.4	109.8	102.6	100.7	907.2	49.3	60.7	2.9	16.8	
loc	Ta	Two	Tb, fit	Twi	Tsb	q	delta1	delta2	m_cond	h_exp
0.25	56.7	64.7	59.5	64.8	101.3	92.7	0.086	0.024	1.5	2.539
0.39	57.3	62.7	58.5	62.1	100.4	86.6	0.109	0.041	3.1	2.261
0.53	56.8	59.9	57.6	60.2	99.5	83.4	0.125	0.058	4.6	2.123
0.67	55.7	58.6	56.7	58.9	98.6	80.2	0.138	0.075	6.0	2.021
0.83	55.0	57.3	55.7	57.8	97.5	77.0	0.15	0.094	7.6	1.939
0.99	54.0	57.8	54.7	57.2	96.5	73.6	0.16	0.112	9.2	1.872
1.17	52.0	56.9	53.7	56.7	95.4	70.2	0.169	0.131	10.8	1.814
1.36	50.4	56.5	52.6	56.4	94.2	66.7	0.178	0.15	12.4	1.763
1.56	49.3	56.0	51.6	56.2	93.0	63.2	0.186	0.169	14.0	1.717
1.77	48.9	55.9	50.6	56.1	91.7	61.5	0.193	0.186	15.7	1.725

B-run 6.1

	Vapor-mix				Water			NCG		
	Flow	Pin	Tst_in	T_out	Flow	Tw_in	Tw_out	Flow	MF	
	44.8	109.9	102.2	100.1	907.2	53.4	63.8	14.7	3.0	
loc	Ta	Two	Tb, fit	Twi	Tsb	q	delta1	delta2	m_cond	h_exp
0.25	59.3	67.5	62.2	67.7	101.4	80.2	0.081	0.022	1.3	2.378
0.39	60.2	65.7	61.4	65.0	100.5	75.3	0.103	0.037	2.7	2.117
0.53	59.9	62.8	60.6	63.2	99.6	73.1	0.119	0.052	4.0	2.004
0.67	58.7	61.6	59.8	61.9	98.8	70.9	0.131	0.067	5.3	1.928
0.83	58.1	60.4	58.9	61.1	97.7	68.7	0.142	0.084	6.7	1.873
0.99	57.3	61.2	58.0	60.5	96.7	66.4	0.151	0.1	8.0	1.832
1.17	55.4	60.4	57.1	60.1	95.6	64.0	0.161	0.116	9.5	1.803
1.36	54.0	60.0	56.1	59.9	94.4	61.5	0.169	0.132	11.0	1.781
1.56	52.9	59.5	55.2	59.7	93.2	59.0	0.177	0.148	12.5	1.765
1.77	52.5	59.5	54.2	59.7	91.9	57.8	0.184	0.162	14.1	1.794

2. SIMULATION TEST CASES

The simulation test conditions were taken from the UCB Kuhn's test database (Kuhn, 1995). The test data table symbols w, T, P, q, h, and DF were for mass flow rate, temperature, pressure, heat flux, HTC, and degradation factor. Subscripts s, c, and g were for steam, coolant, and NCG. The selected Kuhn's test cases are presented in Figures 1 and 2.

Run 2.1-8R

Ws = 51.2 Kg/hr Pinlet = 413.1 KPa Wc = 925.1 Kg/hr Tc,i = 27.5 °C
Wg = 8.870 Kg/hr Tinlet = 145.3 °C Tc,o = 52.5 °C

Loc	Ta	Tb	Tb,fit	Two	Tw	Twi	Tsb	Tcl	q"	Wcond
17.0	45.2	50.7	50.3	104.0	105.8	114.1	140.8	144.8	.938E+05	4.01
30.4	43.0	48.5	48.6	102.0	103.7	111.6	140.6	144.6	.891E+05	6.97
44.6	41.4	46.7	46.9	98.6	100.2	107.7	140.3	144.4	.842E+05	9.92
61.5	39.3	44.8	45.0	98.9	100.4	107.4	139.9	144.2	.789E+05	13.23
79.8	37.6	43.2	43.1	97.4	98.8	105.4	139.5	143.7	.734E+05	16.55
99.6	35.8	41.2	41.1	94.0	95.3	101.4	139.0	143.1	.680E+05	19.83
121.3	33.9	39.1	39.2	90.0	91.2	96.8	138.4	142.4	.624E+05	23.10
145.1	32.2	37.2	37.2	86.2	87.3	92.5	137.7	141.7	.569E+05	26.35

Loc	Ref	Delta1	Delta2	Xgb	Psb	Remix	shear	shear*	hexp	DF
17.0	32.1	.842E-04	.755E-04	.105	369.9	.256E+05	.185E+00	.108E+01	.351E+04	.430
30.4	54.9	.102E-03	.938E-04	.111	367.3	.242E+05	.161E+00	.937E+00	.307E+04	.455
44.6	75.6	.115E-03	.108E-03	.118	364.4	.226E+05	.139E+00	.793E+00	.258E+04	.434
61.5	100.9	.127E-03	.121E-03	.127	360.7	.211E+05	.118E+00	.668E+00	.243E+04	.449
79.8	123.8	.138E-03	.133E-03	.137	356.4	.194E+05	.976E-01	.548E+00	.215E+04	.431
99.6	142.5	.148E-03	.144E-03	.149	351.4	.177E+05	.795E-01	.434E+00	.181E+04	.390
121.3	158.2	.158E-03	.155E-03	.164	345.4	.161E+05	.632E-01	.333E+00	.150E+04	.347
145.1	171.7	.167E-03	.165E-03	.182	338.1	.145E+05	.489E-01	.249E+00	.126E+04	.309

Run 2.1-13

Ws = 50.1 Kg/hr Pinlet = 412.6 KPa Wc = 758.3 Kg/hr Tc,i = 26.4 °C
Wg =32.800 Kg/hr Tinlet = 131.8 °C Tc,o = 49.3 °C

Loc	Ta	Tb	Tb,fit	Two	Tw	Twi	Tsb	Tcl	q"	Wcond
17.0	42.9	48.0	47.5	95.8	97.0	102.8	132.2	132.0	.646E+05	2.72
30.4	41.4	46.4	46.1	93.5	94.7	100.3	131.8	132.0	.621E+05	4.75
44.6	39.9	44.8	44.6	90.9	92.1	97.5	131.3	132.0	.595E+05	6.80
61.5	38.1	43.0	43.0	88.5	89.6	94.7	130.7	131.9	.566E+05	9.11
79.8	36.5	41.3	41.3	86.3	87.3	92.2	130.0	131.5	.536E+05	11.48
99.6	34.9	39.6	39.5	83.2	84.2	88.8	129.2	131.1	.505E+05	13.87
121.3	33.1	37.6	37.7	79.4	80.3	84.6	128.4	130.8	.473E+05	16.30
145.1	31.2	35.6	35.9	76.9	77.8	81.8	127.4	129.6	.441E+05	18.79

Loc	Ref	Delta1	Delta2	Xgb	Psb	Remix	shear	shear*	hexp	DF
17.0	19.0	.767E-04	.662E-04	.301	288.5	.338E+05	.231E+00	.124E+01	.220E+04	.246
30.4	32.6	.929E-04	.829E-04	.310	284.7	.328E+05	.214E+00	.113E+01	.197E+04	.268
44.6	45.6	.105E-03	.960E-04	.320	280.6	.318E+05	.197E+00	.103E+01	.176E+04	.272
61.5	59.6	.117E-03	.109E-03	.332	275.6	.306E+05	.180E+00	.920E+00	.157E+04	.271
79.8	73.1	.127E-03	.119E-03	.345	270.1	.295E+05	.163E+00	.820E+00	.142E+04	.265
99.6	85.2	.137E-03	.130E-03	.360	264.1	.283E+05	.147E+00	.722E+00	.125E+04	.252
121.3	95.6	.147E-03	.140E-03	.376	257.4	.271E+05	.132E+00	.626E+00	.108E+04	.235
145.1	106.6	.155E-03	.150E-03	.394	249.9	.260E+05	.117E+00	.544E+00	.967E+03	.223

Figure 1. Kuhn's Test cases: steam-NCG

Run 1.1-1

Ws = 60.2 Kg/hr Pinlet = 113.9 KPa Wc = 999.8 Kg/hr Tc,i = 31.5 °C
Wg = .000 Kg/hr Tinlet = 138.8 °C Tc,o = 52.0 °C

Loc	Ta	Tb	Tb,fit	Two	Tw	Twi	Tsb	Tcl	q"	Wcond
17.0	47.5	51.4	51.0	93.0	94.1	99.0	103.3	136.8	.547E+05	2.16
30.4	46.0	50.0	50.1	92.3	93.3	98.2	103.3	136.5	.540E+05	3.84
44.6	45.1	49.0	49.1	91.1	92.1	96.9	103.3	136.0	.532E+05	5.58
61.5	44.0	48.1	47.9	91.3	92.3	97.0	103.3	135.4	.523E+05	7.63
79.8	42.8	46.9	46.7	90.6	91.6	96.2	103.3	134.7	.514E+05	9.81
99.6	41.1	45.3	45.4	89.4	90.4	94.9	103.3	133.9	.504E+05	12.11
121.3	39.8	44.0	44.0	88.9	89.9	94.4	103.3	133.1	.493E+05	14.58
145.1	38.4	42.7	42.5	88.7	89.6	94.0	103.3	132.5	.481E+05	17.23

Loc	Ref	Delta1	Delta2	Xgb	Psb	Remix	shear	shear*	hexp	DF
17.0	14.4	.721E-04	.514E-04	.000	113.9	.328E+05	.567E+00	.294E+01	.128E+05	1.351
30.4	25.5	.874E-04	.663E-04	.000	113.9	.319E+05	.538E+00	.278E+01	.105E+05	1.346
44.6	36.8	.992E-04	.783E-04	.000	113.9	.309E+05	.508E+00	.261E+01	.831E+04	1.210
61.5	50.4	.110E-03	.898E-04	.000	113.9	.298E+05	.474E+00	.244E+01	.833E+04	1.345
79.8	64.5	.120E-03	.100E-03	.000	113.9	.286E+05	.439E+00	.225E+01	.727E+04	1.279
99.6	79.1	.129E-03	.111E-03	.000	113.9	.274E+05	.404E+00	.206E+01	.603E+04	1.141
121.3	94.9	.137E-03	.120E-03	.000	113.9	.260E+05	.368E+00	.187E+01	.551E+04	1.110
145.1	111.9	.145E-03	.130E-03	.000	113.9	.245E+05	.331E+00	.168E+01	.515E+04	1.097

Run 1.1-4

Ws = 60.2 Kg/hr Pinlet = 405.2 KPa Wc = 1086.6 Kg/hr Tc,i = 33.4 °C
Wg = .000 Kg/hr Tinlet = 148.0 °C Tc,o = 66.2 °C

Loc	Ta	Tb	Tb,fit	Two	Tw	Twi	Tsb	Tcl	q"	Wcond
17.0	58.2	63.2	63.1	113.6	116.6	130.4	144.1	147.7	.158E+06	6.77
30.4	55.9	61.0	60.6	112.1	115.0	128.5	144.1	147.6	.155E+06	11.94
44.6	53.5	58.5	58.1	109.4	112.2	125.4	144.1	146.4	.151E+06	17.24
61.5	50.1	55.4	55.1	109.4	112.1	124.9	144.1	144.9	.146E+06	23.40
79.8	46.8	52.5	52.0	109.7	112.4	124.7	144.1	145.0	.141E+06	29.86
99.6	42.5	48.6	48.8	110.3	112.9	124.8	144.1	145.1	.136E+06	36.62
121.3	38.2	44.7	45.4	110.0	112.5	123.9	144.1	145.0	.131E+06	43.71

Loc	Ref	Delta1	Delta2	Xgb	Psb	Remix	shear	shear*	hexp	DF
17.0	63.5	.962E-04	.829E-04	.000	405.2	.282E+05	.283E+00	.186E+01	.116E+05	1.614
30.4	111.0	.116E-03	.105E-03	.000	405.2	.255E+05	.238E+00	.155E+01	.989E+04	1.673
44.6	158.2	.132E-03	.122E-03	.000	405.2	.228E+05	.195E+00	.126E+01	.804E+04	1.542
61.5	214.2	.146E-03	.139E-03	.000	405.2	.195E+05	.150E+00	.971E+00	.759E+04	1.612
79.8	273.2	.159E-03	.153E-03	.000	405.2	.161E+05	.108E+00	.699E+00	.729E+04	1.680
99.6	335.1	.170E-03	.166E-03	.000	405.2	.125E+05	.681E-01	.440E+00	.705E+04	1.738
121.3	398.6	.180E-03	.179E-03	.000	405.2	.877E+04	.296E-01	.191E+00	.648E+04	1.698

Run 1.3-2R2

Ws = 39.0 Kg/hr Pinlet = 192.3 KPa Wc = 927.3 Kg/hr Tc,i = 29.6 °C
Wg = .000 Kg/hr Tinlet = 135.5 °C Tc,o = 54.2 °C

Loc	Ta	Tb	Tb,fit	Two	Tw	Twi	Tsb	Tcl	q"	Wcond
17.0	48.8	53.9	52.7	104.6	105.9	112.0	119.0	134.7	.689E+05	2.81
30.4	47.2	52.4	51.4	103.5	104.8	110.8	119.0	134.3	.682E+05	4.99
44.6	45.5	50.7	50.1	102.5	103.8	109.8	119.0	134.1	.674E+05	7.27
61.5	43.9	49.2	48.5	101.6	102.9	108.8	119.0	133.8	.665E+05	9.95
79.8	41.9	47.4	46.9	101.1	102.4	108.2	119.0	133.6	.655E+05	12.81
99.6	39.8	45.3	45.1	99.8	101.0	106.7	119.0	133.3	.645E+05	15.84
121.3	37.3	43.0	43.2	98.9	100.1	105.7	119.0	133.1	.633E+05	19.11
145.1	34.8	40.6	41.1	98.2	99.4	104.9	119.0	132.8	.621E+05	22.63

Loc	Ref	Delta1	Delta2	Xgb	Psb	Remix	shear	shear*	hexp	DF
17.0	21.7	.755E-04	.663E-04	.000	192.3	.201E+05	.197E+00	.113E+01	.986E+04	1.085
30.4	38.3	.916E-04	.830E-04	.000	192.3	.189E+05	.178E+00	.102E+01	.837E+04	1.117
44.6	55.5	.104E-03	.963E-04	.000	192.3	.176E+05	.159E+00	.905E+00	.732E+04	1.109
61.5	75.6	.116E-03	.109E-03	.000	192.3	.162E+05	.138E+00	.784E+00	.653E+04	1.100
79.8	97.0	.126E-03	.120E-03	.000	192.3	.146E+05	.118E+00	.666E+00	.608E+04	1.116
99.6	119.1	.135E-03	.130E-03	.000	192.3	.129E+05	.973E-01	.548E+00	.526E+04	1.039
121.3	143.0	.144E-03	.140E-03	.000	192.3	.111E+05	.772E-01	.433E+00	.478E+04	1.007
145.1	168.7	.153E-03	.150E-03	.000	192.3	.914E+04	.575E-01	.322E+00	.442E+04	.986

Figure 2. Kuhn's Test cases: pure steam

3. PUBLICATIONS

The published/submitted/probable journal titles are as follows:

1. P. K. Bhowmik, J. P. Schlegel*, V. Kalra, C. Mills, S. Usman, "Design of condensation heat transfer experiment to evaluate scaling distortion in small modular reactor safety analysis," Journal of Nuclear Engineering and Radiation Science, 7 (3), 031406.

2. P. K. Bhowmik, J. P. Schlegel*, V. Kalra, S. Hong, S. Usman, S. Alam, "CFD validation of condensation heat transfer in scaled down small modular reactor applications. Part 1: pure steam," Experimental and Computational Multiphase Flow (In press).

3. P. K. Bhowmik, J. P. Schlegel*, V. Kalra, S. Hong, S. Usman, S. Alam, "CFD validation of condensation heat transfer in scaled down small modular reactor applications. Part 2: Part 2: steam with non-condensable gas," Experimental and Computational Multiphase Flow (In press).

4. P. K. Bhowmik, J. P. Schlegel*, "Parametric study of condensation heat transfer in small modular reactor system: multi-component gas mixtures," (Submitted to Experimental and Computational Multiphase Flow).

5. P. K. Bhowmik, J. P. Schlegel*, S. Revankar, "State-of-the-art and review of condensation heat transfer for small modular reactor application. Part-1: Experimental studies.," (Submitted to Int. J. Heat and Mass Transfer).

6. P. K. Bhowmik, J. P. Schlegel*, Scott Ormiston, "State-of-the-art and review of condensation heat transfer for small modular reactor application. Part-2: Computational studies.," (In preparation).

7. P. K. Bhowmik, J. P. Schlegel*, et al. "Steam condensation experiments to evaluate scaling distortion in small modular reactor safety analysis. Part I: Scaled Test with Pure Steam," (In preparation).

8. P. K. Bhowmik, J. P. Schlegel*, "Steam condensation experiments to evaluate scaling distortion in small modular reactor safety analysis. Part II: with N2 and He as Non-condensable gases," (In preparation).

9. P. K. Bhowmik, J. P. Schlegel*, et al., "Assessment of condensation heat transfer models to evaluate scaling distortion in small modular reactor safety analysis," (In preparation).

10. P. K. Bhowmik, J. P. Schlegel*, et al., "System code capabilities in nuclear reactor passive safety:RELAP, MELCOR, and GOTHIC," (In preparation).

REFERENCES

Indicators for Nuclear Power Development, number NG-T-4.5 in Nuclear Energy Series, INTERNATIONAL ATOMIC ENERGY AGENCY, Vienna, 2015, ISBN 978-92-0-107115-6.

'Energy-United Nations Sustainable Development Goals (SDG),' 2019, [Online; accessed 24-December-2019].

'Nuclear Power by Number,' Technical report, Nuclear Energy Institute Inc., 1201 F Street, NW Washington, DC 20004, March 2019.

Ağlar, F., 'Assessment of the relap5/mod3. 3 code for condensation in the presence of air using experimental data and theoretical model,' Annals of Nuclear Energy, 2013, **60**, pp. 329–340.

Ağlar, F. and Tanrikut, A., 'A new heat transfer correlation for condensation in the presence of air and its implementation into relap5/mod3. 3,' Nuclear Technology, 2008, **161**(3), pp. 286–298.

Ahmed, F., Ara, N., Deshpande, V., Mollah, A., and Bhowmik, P., 'CFD validation with optimized mesh using benchmarking data of pebble-bed high-temperature reactor,' Progress in Nuclear Energy, 2021, **134**, p. 103653.

Akaki, H., Kataoka, Y., and Murase, M., 'Measurement of condensation heat transfer coefficient inside a vertical tube in the presence of noncondensable gas,' Journal of nuclear science and technology, 1995, **32**(6), pp. 517–526.

Alam, S. B., Kumar, D., Almutairi, B., Bhowmik, P. K., Goodwin, C., and Parks, G. T., 'Small modular reactor core design for civil marine propulsion using micro-heterogeneous duplex fuel. part i: Assembly-level analysis,' Nuclear Engineering and Design, 2019, **346**, pp. 157–175.

Ambrosini, W., Forgione, N., Manfredini, A., and Oriolo, F., 'On various forms of the heat and mass transfer analogy: Discussion and application to condensation experiments,' Nuclear Engineering and Design, 2006, **236**(9), pp. 1013–1027.

Ambrosini, W., Forgione, N., Merli, F., Oriolo, F., Paci, S., Kljenak, I., Kostka, P., Vyskocil, L., Travis, J., Lehmkuhl, J., *et al.*, 'Lesson learned from the sarnet wall condensation benchmarks,' Annals of nuclear energy, 2014, **74**, pp. 153–164.

Anderson, M. H., Herranz, L. E., and Corradini, M. L., 'Experimental analysis of heat transfer within the ap600 containment under postulated accident conditions,' Nuclear Engineering and Design, 1998, **185**(2-3), pp. 153–172.

András Cserháti, 'The Future of Nuclear Energy?' 2017, vice president of the Hungarian Nuclear Society.[Online; accessed 24-December-2019].

Araki, H., Kataoka, Y., and Murase, M., 'Measurement of condensation heat transfer coefficient inside a vertical tube in the presence of noncondensable gas,' Journal of Nuclear Science and Technology, 1995, **32**(6), pp. 517–526.

Banerjee, S. and Hassman, Y., 'Relap5/mod3 simulation of steam condensation in the presence of noncondensible gases under natural circulation conditions,' Transactions of the American Nuclear Society, 1993, **69**, pp. 269–271.

Bhowmik, P. K., 'Nanofluid operation and valve engineering of super for small unit passive enclosed reactor,' 2016.

Bhowmik, P. K., Schlegel, J., Kalra, V., Alam, S., Hong, S., and Usman, S., 'CFD validation of condensation heat transfer in scaled-down small modular reactor applications, part 1: pure steam,' Experimental and Computational Mulitphase Flow, 2021a, **In press**.

Bhowmik, P. K., Schlegel, J., Kalra, V., Alam, S., Hong, S., and Usman, S., 'CFD validation of condensation heat transfer in scaled-down small modular reactor applications, part 2: steam and non-condensable gas,' Experimental and Computational Mulitphase Flow, 2021b, **In press**.

Bhowmik, P. K., Schlegel, J. P., Kalra, V., Mills, C., and Usman, S., 'Design of condensation heat transfer experiment to evaluate scaling distortion in small modular reactor safety analysis,' Journal of Nuclear Engineering and Radiation Science, 2021c, **7**(3), p. 031406.

Bhowmik, P. K., Shamim, J. A., Chen, X., and Suh, K. Y., 'Rod bundle thermal-hydraulics experiment with water and water-al2o3 nanofluid for small modular reactor,' Annals of Nuclear Energy, 2021d, **150**, p. 107870.

Bhowmik, P. K. and Suh, K. Y., 'Flow mapping using 3d full-scale CFD simulation and hydrodynamic experiments of an ultra-supercritical turbine's combined valve for nuclear power plant,' International Journal of Energy and Environmental Engineering, 2021, pp. 1–17.

Bian, H., Sun, Z., Ding, M., and Zhang, N., 'Local phenomena analysis of steam condensation in the presence of air,' Progress in Nuclear Energy, 2017, **101**, pp. 188–198.

Bian, H., Sun, Z., Zhang, N., Meng, Z., and Ding, M., 'A preliminary assessment on a two-phase steam condensation model in nuclear containment applications,' Annals of Nuclear Energy, 2018, **121**, pp. 615–625.

Blangetti, F., Krebs, R., and Schlunder, E., 'Condensation in vertical tubes–experimental results and modeling,' 1982, **1**(2).

Bocanegra, R., Jimenez, G., and Fernández-Cosials, M. K., 'Development of a pwr-w gothic 3d model for containment accident analysis,' Annals of Nuclear Energy, 2016, **87**, pp. 547–560.

Boyer, B. D., Parlatan, Y., Slovik, G. C., and Rohatgi, U. S., 'An assessment of relap5 mod3. 1.1 condensation heat transfer modeling with giraffe heat transfer tests,' Technical report, Brookhaven National Lab., Upton, NY (United States); Nuclear Regulatory . . . , 1995.

Brooks, C. S., Fullmer, W. D., and Lietwiler, C. D., 'Assessment of relap5/mod3. 3 for subcooled boiling, flashing and condensation in a vertical annulus,' in '16th International Topical Meeting on Nuclear Reactor Thermal Hydraulics, NURETH 2015,' American Nuclear Society, 2015 pp. 7261–7271.

Butterworth, D., 'Film condensation of pure vapor,' Heat Exchanger Design Handbook, 1983, **2**, pp. 6–2.

Carelli, M., Petrovic, B., Mycoff, C., Trucco, P., Ricotti, M. E., and Locatelli, G., 'Economic comparison of different size nuclear reactors,' Cancún, Quintana Roo, México, del, 2007, **1**, pp. 1–5.

Chen, S., Gerner, F., and Tien, C., 'General film condensation correlations,' Experimental Heat Transfer, 1987, **1**(2), pp. 93–107.

Cheng, X., Bazin, P., Cornet, P., Hittner, D., Jackson, J., Jimenez, J. L., Naviglio, A., Oriolo, F., and Petzold, H., 'Experimental data base for containment thermalhydraulic analysis,' Nuclear engineering and design, 2001, **204**(1-3), pp. 267–284.

Choi, K. Y., Park, H. S., Kim, S. J., No, H. C., and Bang, Y. S., 'Assessment and improvement of condensation models in relap5/mod3. 2,' Nuclear technology, 1998, **124**(2), pp. 103–117.

Chun, K. and Seban, R., 'Heat transfer to evaporating liquid films,' 1971.

Colburn, A. P., 'Problems in design and research on condensers of vapours and vapour mixtures,' Proceedings of the Institution of Mechanical Engineers, 1951, **164**(1), pp. 448–458.

Colburn, A. P. and Hougen, O. A., 'Design of cooler condensers for mixtures of vapors with noncondensing gases,' Industrial & Engineering Chemistry, 1934, **26**(11), pp. 1178–1182.

Corradini, M. L., 'Turbulent condensation on a cold wall in the presence of a noncondensable gas,' Nuclear technology, 1984, **64**(2), pp. 186–195.

Corradini, M. L., 'Fundamentals of multiphase flow,' Available on: http://wins. engr. wisc. edu/teaching/mpfBook/node26. html, 1997.

Crawley, F. and Tyler, B., *HAZOP: Guide to best practice*, Elsevier, 2015.

Dalkilic, A. and Wongwises, S., 'Intensive literature review of condensation inside smooth and enhanced tubes,' International Journal of Heat and Mass Transfer, 2009, **52**(15-16), pp. 3409–3426.

De la Rosa, J., Escriva, A., Herranz, L., Cicero, T., and Munoz-Cobo, J., 'Review on condensation on the containment structures,' Progress in Nuclear Energy, 2009, **51**(1), pp. 32–66.

Dehbi, A., Golay, M., and Kazimi, M., 'Condensation experiments in steam-air and steam-air-helium mixtures under turbulent natural convection,' in 'National Conference of Heat Transfer, AIChE Symp. Ser,' volume 87, 1991 pp. 19–28.

Dehbi, A. and Guentay, S., 'A model for the performance of a vertical tube condenser in the presence of noncondensable gases,' Nuclear Engineering and Design, 1997, **177**(1-3), pp. 41–52.

Dehbi, A., Janasz, F., and Bell, B., 'Prediction of steam condensation in the presence of noncondensable gases using a CFD-based approach,' Nuclear Engineering and Design, 2013, **258**, pp. 199–210.

Dehbi, A. A., *The effects of noncondensable gases on steam condensation under turbulent natural convection conditions*, Ph.D. thesis, Massachusetts Institute of Technology, 1991.

Dunjó, J., Fthenakis, V., Vílchez, J. A., and Arnaldos, J., 'Hazard and operability (hazop) analysis. a literature review,' Journal of hazardous materials, 2010, **173**(1-3), pp. 19–32.

Fillo, J., 'Condensation wall heat transfer in presence of noncondensable gas,' Technical report, American Society of Mechanical Engineers, New York, NY, 1985.

Fu, W., Li, X., Wu, X., and Corradini, M. L., 'Numerical investigation of convective condensation with the presence of non-condensable gases in a vertical tube,' Nuclear Engineering and Design, 2016, **297**, pp. 197–207.

Fu, W., YOON, D., Corradini, M. L., and Anderson, M. H., 'Assessment of the melcor and relap5-3d code for condensation in the presence of noncondensable gas,' Proc. Int. Topl. Mtg. Nuclear Reactor Thermal Hydraulics 2015, 2015.

Fullmer, W. D., Kumar, V., and Brooks, C. S., 'Validation of relap5/mod3. 3 for subcooled boiling, flashing and condensation in a vertical annulus,' Progress in Nuclear Energy, 2016, **93**, pp. 205–217.

Ganguli, A. A., Dahikar, S. K., Gandhi, M. S., Joshi, J. B., and Vijayan, P. K., 'Heat transfer and flow pattern in co-current downward steam condensation in vertical pipes-ii: Comparison with published work,' The Canadian Journal of Chemical Engineering, 2013, **91**(5), pp. 974–991.

George, T. L. and Singh, A., 'Separate effects tests for gothic condensation and evaporative heat transfer models,' Nuclear Engineering and Design, 1996, **166**(3), pp. 403–411.

Ghiaasiaan, S., Kamboj, B., and Abdel-Khalik, S., 'Two-fluid modeling of condensation in the presence of noncondensables in two-phase channel flows,' Nuclear science and engineering, 1995, **119**(1), pp. 1–17.

Goodykoontz, J. H. and Dorsch, R. G., 'Local heat-transfer coefficient for condensation of steam in vertical down-flow within a 5/8-inch-diameter tube,' Technical Report TN D-3326, National Aeronautics and Space Administration (NASA), Lewis Research Center, Cleveland, Ohio, 1966.

Goodykoontz, J. H. and Dorsch, R. G., 'Local heat-transfer coefficient and static pressure for condensation of high-velocity steam within a tube,' Technical Report TN D-3953, National Aeronautics and Space Administration (NASA), Lewis Research Center, Cleveland, Ohio, 1967.

Hassan, Y. A. and Raja, L. L., 'Analysis of experiments for steam condensation in the presence of non-condensable gases using the relap5/mod3 code,' Nuclear technology, 1993, **104**(1), pp. 76–88.

Houkema, M., Siccama, N., à Nijeholt, J. L., and Komen, E., 'Validation of the CFX4 CFD code for containment thermal-hydraulics,' Nuclear Engineering and Design, 2008, **238**(3), pp. 590–599.

Huang, J., Zhang, J., and Wang, L., 'Review of vapor condensation heat and mass transfer in the presence of non-condensable gas,' Applied thermal engineering, 2015, **89**, pp. 469–484.

Huhtiniemi, I. K. and Corradini, M. L., 'Condensation in the presence of noncondensable gases,' Nuclear Engineering and Design, 1993, **141**(3), pp. 429–446.

IAEA, 'Advances in small modular reactor technology developments,' 2018.

IEA, 'CO2 status report—the latest trends in energy and emissions in 2018,' International Energy Agency, 2019.

Incropera, F. P., Lavine, A. S., Bergman, T. L., and DeWitt, D. P., *Fundamentals of heat and mass transfer*, Wiley, 2007.

Jang, Y.-J., Choi, D.-J., Lee, Y.-G., and Kim, S., 'Experimental study of condensation heat transfer in the presence of noncondensable gas on the vertical tube,' 2015.

Jehee Lee, H. K. C. K. W. L. M. K. C., Chi-Jin Choi, 'Assessment of the wall film condensation model with non-condensable gas in relap5 and trace for vertical tube and plate geometries,' Technical report, NUREG/IA-0491, IAR, U.S. Nuclear Regulatory Commission, 2019.

Jiang, X., Studer, E., and Kudriakov, S., 'A simplified model of passive containment cooling system in a CFD code,' Nuclear Engineering and Design, 2013, **262**, pp. 579–588.

Kataoka, I., 'Review of thermal-hydraulic researches in severe accidents in light water reactors,' Journal of Nuclear Science and Technology, 2013, **50**(1), pp. 1–14.

Kim, M. H. and Corradini, M., 'Modeling of condensation heat transfer in a reactor containment,' Nuclear Engineering and Design, 1990, **118**(2), pp. 193–212.

Kim, S. J., 'Turbulent film condensation of high pressure steam in a vertical tube of passive secondary condensation system,' 2000.

Kletz, T. A., 'Hazop—past and future,' Reliability Engineering & System Safety, 1997, **55**(3), pp. 263–266.

Kletz, T. A., *HAZOP and HAZAN: identifying and assessing process industry hazards*, IChemE, 1999.

Kuhn, S., Peterson, P., and Schrock, V., 'Determination of the local heat flux in condensation experiments,' Experimental Heat Transfer An International Journal, 1996, **9**(2), pp. 149–163.

Kuhn, S. Z., *Investigation of Heat Transfer from Condensing Steam-Gas Mixtures and Turbulent Films Flowing Downward Inside a Vertical Tube*, Ph.D. thesis, University of California, Berkeley, UMI, 300 North Zeeb Road, Ann Arbor, MI 48103, 1995.

Kutateladze, S., 'Semi-empirical theory of film condensation of pure vapours,' International Journal of Heat and Mass Transfer, 1982, **25**(5), pp. 653–660.

Labuntsov, D., 'Heat transfer in film condensation of pure steam on vertical surfaces and horizontal tubes,' Teploenergetika, 1957, **4**(7), pp. 72–79.

Le, Q., 'Physically based closed-form solutions for film condensation of pure vapors in vertical tubes,' 2012.

Lee, H., Kharangate, C. R., Mascarenhas, N., Park, I., and Mudawar, I., 'Experimental and computational investigation of vertical downflow condensation,' International Journal of Heat and Mass Transfer, 2015, **85**, pp. 865–879.

Lee, K. Y., *The Effects of Noncondensable Gas on Steam Condensation in a Vertical Tube of Passive Residual Heat Removal System*, Ph.D. thesis, Department of Mechanical Engineering, Pohang University of Science and Technology, Pohang, Korea, 2007.

Lee, K. Y. and Kim, M. H., 'Experimental and empirical study of steam condensation heat transfer with a noncondensable gas in a small-diameter vertical tube,' Nuclear Engineering and Design, 2008, **238**(1), pp. 207–216.

Lee, U.-J. and Park, G.-C., 'Experimental study on hydrogen behavior at a subcompartment in the containment building,' Nuclear Engineering and Design, 2002, **217**, pp. 41–47.

Li, J.-D., 'CFD simulation of water vapour condensation in the presence of non-condensable gas in vertical cylindrical condensers,' International journal of heat and mass transfer, 2013, **57**(2), pp. 708–721.

Li, L., Kim, T. W., Zhang, Y., Revankar, S. T., Tian, W., Su, G., and Qiu, S., 'Melcor severe accident analysis for a natural circulation small modular reactor,' Progress in Nuclear Energy, 2017, **100**, pp. 197–208.

Lin, A., Chen, Y.-S., and Yuann, Y.-R., 'Kuosheng mark iii containment analyses using gothic,' Nuclear Engineering and Design, 2013, **263**, pp. 255–262.

Liu, H., Todreas, N., and Driscoll, M., 'An experimental investigation of a passive cooling unit for nuclear plant containment,' Nuclear Engineering and Design, 2000, **199**(3), pp. 243–255.

Martín, Valdepeñas, J., Jimenez, M., Martin-Fuertes, F., and Benitez, J. F., 'Comparison of film condensation models in presence of non-condensable gases implemented in a CFD code,' Heat and mass transfer, 2005, **41**(11), pp. 961–976.

Minkowycz, W. and Sparrow, E., 'Condensation heat transfer in the presence of noncondensables, interfacial resistance, superheating, variable properties, and diffusion,' International Journal of Heat and Mass Transfer, 1966, **9**(10), pp. 1125–1144.

Mishra, A. A. and Girimaji, S. S., 'Intercomponent energy transfer in incompressible homogeneous turbulence: multi-point physics and amenability to one-point closures,' Journal of Fluid Mechanics, 2013, **731**, pp. 639–681.

Moghanaki, S. K. and Rahgoshay, M., 'Pressurizer modeling: Using different thermodynamic models and comparing results with relap code results,' Applied Mechanics and Materials, 2013, **423**, pp. 1444–1448.

Moon, Y., Park, H., and Bang, Y., *Assessment of RELAP5/MOD3. 2 for reflux condensation experiment*, Citeseer, 2000.

Mullin, E. M., 'High pressure condensation in an smr containment,' 2015.

Munoz-Cobo, J., Herranz, L., Sancho, J., Tkachenko, I., and Verdu, G., 'Turbulent vapor condensation with noncondensable gases in vertical tubes,' International Journal of Heat and Mass Transfer, 1996, **39**(15), pp. 3249–3260.

Nguyen, V. and Trinh, H., 'Assessment of steam condensation model with the presence of non-condensable gas in a vertical tube using relap5 mod 3.2 code and mit exp. data,' Nuclear Science and Technology (Hanoi), 2014, **4**(3), pp. 7–18.

NuScale, 'Passive Safety Systems, NuScale power LLC,' 2019, [Online; accessed 24-December-2019].

Nusselt, W., 'Die oberflachenkondensation des wasserdamphes,' Z. Vereins desutscher Ininuere, 1916.

Ogg, D. G., *Vertical downflow condensation heat transfer in gas-steam mixtures*, University of California, Berkeley, 1991.

Oh, S. and Revankar, S., 'Boundary layer analysis for steam condensation in a vertical tube with noncondensable gases,' Int. J. Heat Ex, 2005, **6**, pp. 93–124.

Oh, S. T., Seungmin & Revankar, 'Experimental and theoretical investigation of film condensation with noncondensable gas,' International Journal of Heat and Mass Transfer, 2006, **49**(15-16), pp. 2523–2534.

Othmer, D. F., 'The condensation of steam,' Industrial & Engineering Chemistry, 1929, **21**(6), pp. 576–583.

Padmanaban, A., 'Film thickness measurements in falling annular films,' 2006.

Papini, D., Grgić, D., Cammi, A., and Ricotti, M. E., 'Analysis of different containment models for iris small break loca, using gothic and relap5 codes,' Nuclear engineering and design, 2011, **241**(4), pp. 1152–1164.

Park, H. S., *Steam condensation heat transfer in the presence of noncondenables in a vertical tube of passive containment cooling system*, Ph.D. thesis, Department of Nuclear Engineering, Korea Advanced Institute of Science and Technology (KAIST), Taejon, Korea, 1999.

Park, H. S. and No, H. C., 'A condensation experiment in the presence of noncondensables in a vertical tube of a passive containment cooling system and its assessment with relap5/mod3. 2,' Nuclear Technology, 1999a, **127**(2), pp. 160–169.

Park, H. S. and No, H. C., 'A condensation experiment in the presence of noncondensables in a vertical tube of a passive containment cooling system and its assessment with relap5/mod3.2,' Nuclear Technology, 1999b, **127**(2), pp. 160–169.

Park, J. Y., 'Assessments of ucb-kuhn condensation tests by various thermal-hydraulic codes,' 2015.

Peterson, P., 'Theoretical basis for the uchida correlation for condensation in reactor containments,' Nuclear Engineering and Design, 1996, **162**(2-3), pp. 301–306.

Peterson, P., Schrock, V., and Kageyama, T., 'Diffusion layer theory for turbulent vapor condensation with noncondensable gases,' Journal of Heat Transfer, 1993, **115**(4), pp. 998–1003.

PRIS, 'International Atomic Energy Agency, "Power reactor information system," PRIS,' 2019, [Online; accessed 24-December-2019].

Punetha, M. and Khandekar, S., 'A CFD based modelling approach for predicting steam condensation in the presence of non-condensable gases,' Nuclear Engineering and Design, 2017, **324**, pp. 280–296.

Ravva, S. R., Iyer, K. N., Gupta, S., and Gaikwad, A. J., 'Implementation and validation of the condensation model for containment hydrogen distribution studies,' Nuclear Engineering and Design, 2014, **270**, pp. 34–47.

Revankar, S. T., Zhou, W., and Henderson, G., 'Experimental and thermalhydraulic code assessment of the transient behavior of the passive condenser system in an advanced boiling water reactor,' Technical report, Purdue Univ., West Lafayette, IN (United States), 2008.

Rohsenow, W., 'Effect of vapor velocity on laminar and turbulent film condensation,' Transactions of ASME, 1956, pp. 1645–1648.

Rohsenow, W. M., 'A method of correlating heat transfer data for surface boiling of liquids,' Technical report, Cambridge, Mass.: MIT Division of Industrial Cooporation,[1951], 1951.

Rosner, R. and Goldberg, S., 'Small modular reactors–key to future nuclear power generation in the us,' Energy Policy Institute at Chicago, The University of Chicago, Chicago, 2011.

Sato, T. and Kojima, Y., 'Variations of a passive safety containment for a bwr with active and passive safety systems,' Nuclear Engineering and Design, 2007, **237**(1), pp. 74–86.

Schulz, T. L., 'Westinghouse ap1000 advanced passive plant,' Nuclear Engineering and Design, 2006, **236**(14-16), pp. 1547–1557.

Shah, M. M., 'A general correlation for heat transfer during film condensation inside pipes,' International Journal of heat and mass transfer, 1979, **22**(4), pp. 547–556.

Shamim, J. A., Bhowmik, P. K., Xiangyi, C., and Suh, K. Y., 'A new correlation for convective heat transfer coefficient of water–alumina nanofluid in a square array subchannel under pwr condition,' Nuclear Engineering and Design, 2016, **308**, pp. 194–204.

Sharma, P. K., Gera, B., Singh, R., and Vaze, K., 'Computational fluid dynamics modeling of steam condensation on nuclear containment wall surfaces based on semiempirical generalized correlations,' Science and Technology of Nuclear Installations, 2012, **2012**.

Shmerler, J. and Mudawwar, I., 'Local heat transfer coefficient in wavy free-falling turbulent liquid films undergoing uniform sensible heating,' International journal of heat and mass transfer, 1988, **31**(1), pp. 67–77.

Shulyak, N., 'Westinghouse small modular reactor: taking proven technology to the next level,' in 'INPRO Dialogue Forum on Nuclear Energy Innovations: Common User Considerations for Small and Medium-sized Nuclear Power Reactors,' 2011 .

Shumway, R. W., 'Assessment of mit and ucb wall condensation tests and of the pre-release relap5/mod3. 2 code condensation models,' Technical report, Lockheed Idaho Technologies Co., 1995.

Siddique, M., *The effects of noncondensable gases on steam condensation under forced convection conditions*, Ph.D. thesis, Department of Nuclear Engineering, Massachusetts Institute of Technology (MIT), 77 Massachusetts Ave, Cambridge, MA 02139, 1992.

Siddique, M., Golay, M. W., and Kazimi, M. S., 'Theoretical modeling of forced convection condensation of steam in a vertical tube in the presence of a noncondensable gas,' Nuclear technology, 1994, **106**(2), pp. 202–215.

Slaughterbeck, D., 'Review of heat transfer coefficients for condensing steam in a containment building following a loss-of-coolant accident.' Technical report, Idaho Nuclear Corp., Idaho Falls, 1970.

Smith, M. C. and Wright, R. F., 'Westinghouse small modular reactor passive safety system response to postulated events,' June 2012.

Soliman, M., Schuster, J., and Berenson, P., 'A general heat transfer correlation for annular flow condensation,' Journal of Heat Transfer, 1968, **90**(2), pp. 267–274.

Sparrow, E. and Eckert, E., 'Effects of superheated vapor and noncondensable gases on laminar film condensation,' AIChE Journal, 1961, **7**(3), pp. 473–477.

Su, J., Fan, L., and Gao, L., 'Review of steam condensation heat transfer under containment cooling system condition,' Atomic Energy Science and Technology, 2016, **50**(11), pp. 1956–1966.

Su, J., Sun, Z., and Zhang, D., 'Numerical analysis of steam condensation over a vertical surface in presence of air,' Annals of Nuclear Energy, 2014, **72**, pp. 268–276.

Tagami, T., 'Interim report on safety assessments and facilities establishment project for june 1965, no. 1,' Japanese Atomic Energy Research Agency, 1965.

Tanrikut, A. and Yesin, O., *In-Tube Steam Condensation in the Presence of Air*, Office of Nuclear Regulatory Research, US Nuclear Regulatory Commission, 2000.

Tusar, M. H., Bhowmik, P. K., Salam, B., Ahamed, J. U., and Kim, J. K., 'Convective heat transfer and friction factor characteristics of helical strip inserted annuli at turbulent flow,' International Journal of Heat and Mass Transfer, 2021, **176**, p. 121422.

Uchida, H., Oyama, A., and Togo, Y., 'Evaluation of post-incident cooling systems of light water power reactors,' Technical report, Tokyo Univ., 1964.

Vierow, K., 'Enhancement of nuclear power plant safety by condensation-driven passive heat removal systems,' Thermal Engineering in Power Systems, 2008, **22**, p. 141.

Vierow, K. and Schrock, V., 'Condensation in a natural circulation loop with noncondensable gases, 1,' in 'Proceedings of the international conference on multiphase flows' 91-Tsukuba,' 1991 .

Vierow, K. M., 'Behavior of steam-air systems condensing in cocurrent vertical downflow,' MS Thesis, Univ. of California, Berkeley, 1990.

Wang, C.-Y. and Tu, C.-J., 'Effects of non-condensable gas on laminar film condensation in a vertical tube,' International Journal of Heat and Mass Transfer, 1988, **31**(11), pp. 2339–2345.

Wang, X., Chang, H., and Corradini, M., 'A CFD study of wave influence on film steam condensation in the presence of non-condensable gas,' Nuclear Engineering and Design, 2016, **305**, pp. 303–313.

Whalley, P. B., 'Boiling, condensation, and gas-liquid flow,' 1987.

Wu, Q. and Corradini, M., 'Integral reactor containment condensation model and experimental validation,' Technical report, Battelle Energy Alliance, LLC, Idaho Falls, ID (United States), 2016.

Yadav, M. K., Khandekar, S., and Sharma, P. K., 'An integrated approach to steam condensation studies inside reactor containments: A review,' 2016, doi: 10.1016/j.nucengdes.2016.01.004.

Yuann, R., Schrock, V., Chen, X., *et al.*, 'Numerical modeling of condensation from vapor-gas mixtures for forced down flow inside a tube,' Technical report, 1995.

Yuann, R. Y., *Condensation from vapor-gas mixture for forced downflow inside a tube*, Ph.D. thesis, University of California, Berkeley, 1993.

Zhou, W., Wolf, B., and Revankar, S., 'Assessment of relap5/mod3. 3 condensation models for the tube bundle condensation in the pccs of esbwr,' Nuclear Engineering and Design, 2013, **264**, pp. 111–118.

Zschaeck, G., Frank, T., and Burns, A., 'CFD modelling and validation of wall condensation in the presence of non-condensable gases,' Nuclear Engineering and Design, 2014, **279**, pp. 137–146.

VITA

In July 2021, Palash Kumar Bhowmik received his PhD in Nuclear Engineering from Missouri University of Science and Technology. His doctoral research on scaling, experiments, and simulations of condensation heat transfer for advanced nuclear reactor's safety. He received his MSc in Nuclear Engineering from Seoul National University, South Korea in February 2016, a BSc in Electrical and Electronics Engineering from Chittagong University of Engineering and Technology, Bangladesh in August 2008, and an MBA from the University of Science and Technology Chittagong, Bangladesh in July 2013. He worked in the TRIGA MARK-II research reactor, petroleum oil refinery, and thermal power plant. He worked on the advanced reactor passive safety system at THEMES (Thermal-Hydraulics Experiment, Modeling, and Engineering Simulation) Laboratory under the guidance of Dr. Joshua P. Schlegel. Mr. Bhowmik's research theme was ATOMS (Advanced Thermo-nuclear Operation Modeling and Simulations). He served as president of the council of a graduate students at Missouri S&T in 2017-2018. He was the founding president of the Bangladesh Student Association at Missouri S&T. He became an member of the Institute of Electrical and Electronics Engineers (IEEE), American Society of Mechanical Engineers (ASME), and American Society of Nuclear Engineers (ANS) during his time at Missouri S&T.